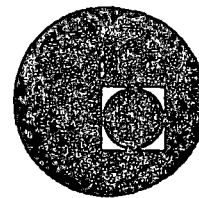


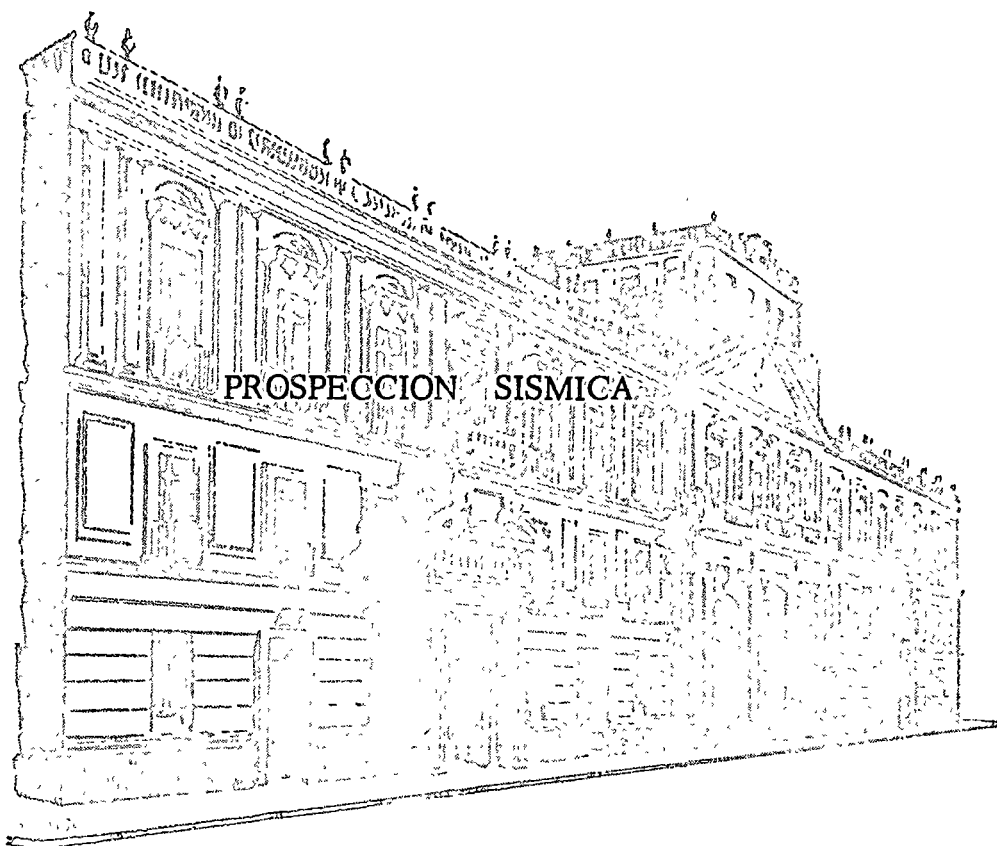


centro de educación continua
división de estudios superiores
facultad de ingeniería, unam



III CURSO INTERNACIONAL DE INGENIERIA SISMICA

ANALISIS DINAMICO DE ESTRUCTURAS ESPECIALES



M. EN I. BELSAY MARTINEZ R.

ALFONSO TORRES DE OJEDA

Director de la Oficina de Estudios e Investigaciones Científicas

Ministerio de Educación y Ciencia



CONSEJO DE INVESTIGACIONES CIENTÍFICAS

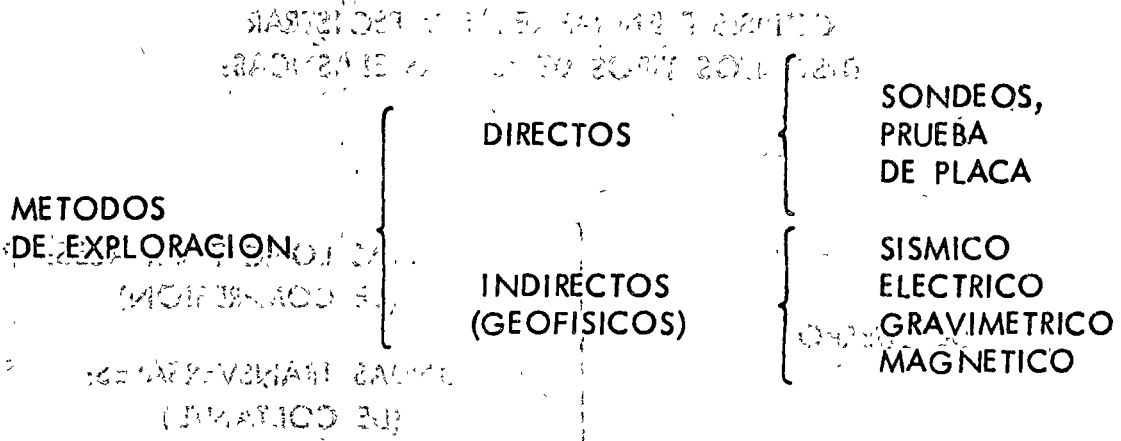
INSTITUTO NACIONAL DE ESTADÍSTICA

SECRETARÍA DE ESTADO

SECRETARÍA DE ESTADO

SECCION DE METODOS DE PROSPECCION

METODOS DE PROSPECCION SISMICA



LOS METODOS GEOFISICOS SE HAN APLICADO EN LA DETECCION DE:

- MINERALES
- PETROLEO
- AGUA

EN ING. CIVIL SE APLICAN EN:

- CONSTRUCCION DE VIAS TERRESTRES
- TRAZO DE TUBERIAS, CANALES, TUNELES, ETC.
- DISEÑO DE AEROPUERTOS
- DISEÑO DE CIMENTACIONES, ETC.

LOS METODOS ELECTRICO Y SISMICO SON LOS MAS EMPLEADOS

EL METODO SISMICO ES MAS CONFIABLE

CONSISTE EN GENERAR Y REGISTRAR
DISTINTOS TIPOS DE ONDAS ELASTICAS:

DE CUERPO	}	ONDAS LONGITUDINALES: P	
		(DE COMPRESION)	.
DE SUPERFICIE	}	ONDAS TRANSVERSALES: S	
		(DE CORTANTE)	
		ONDAS DE RAYLEIGH: R	
		ONDAS DE LOVE: L	

PRINCIPALES CARACTERISTICAS:

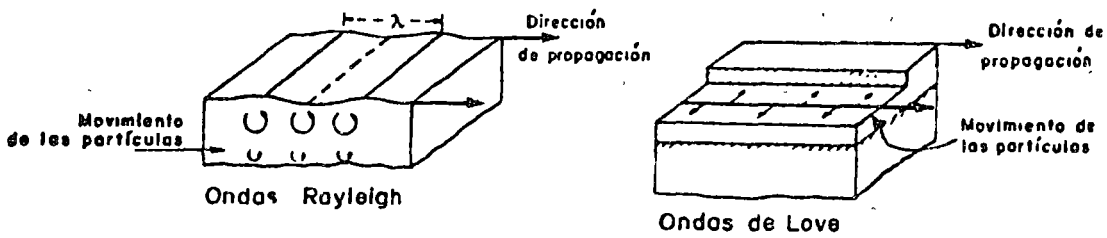
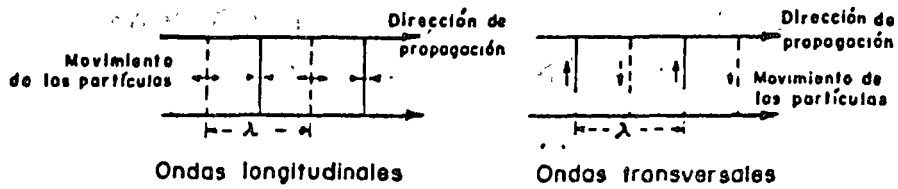
$$v_p = \sqrt{\frac{\lambda + 2G}{\rho}} \quad v_s = \sqrt{\frac{G}{\rho}} \quad \Rightarrow v_p > v_s$$

λ = CONSTANTE DE LAME

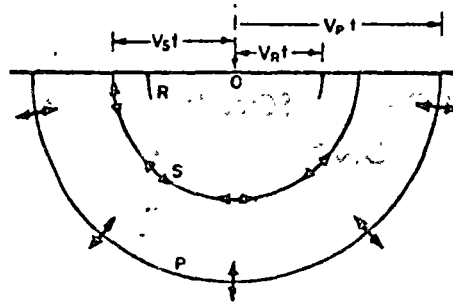
G = MODULO (DINAMICO) DE RIGIDEZ
AL CORTANTE

ρ = DENSIDAD DEL MATERIAL

SOLIDO ELASTICO, HOMOGENEO E
ISOTROPO



a) Movimientos de las partículas de un sólido producidas en la propagación de ondas elásticas



b) Frentes de los impulsos de las ondas P, S y R después de su iniciación en el punto "O"

Características de las ondas elásticas en un sólido

- LAS ONDAS S SE POLARIZAN EN DOS PLANOS:
ONDAS SH Y SV

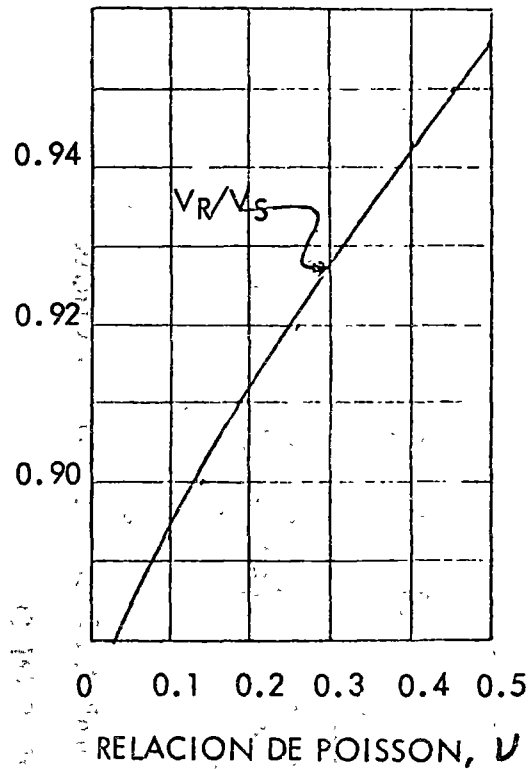
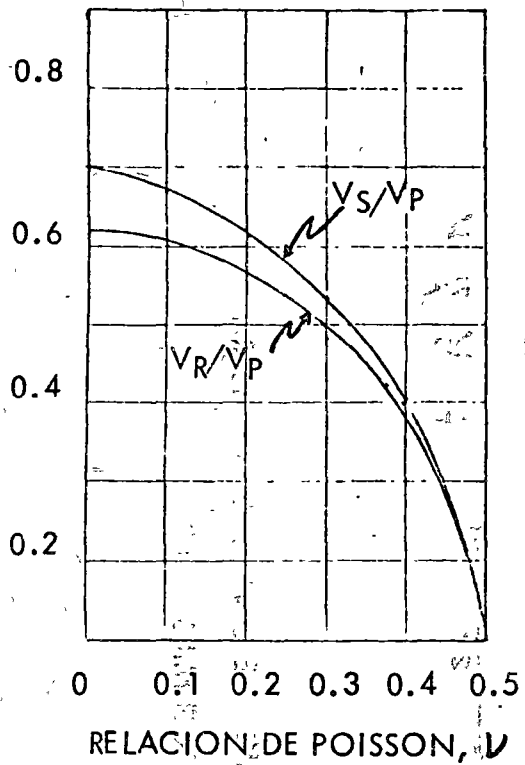
- LAS ONDAS R SE PROPAGAN EN UN SEMIESPACIO.
SU AMPLITUD DISMINUYE CON LA PROFUNDIDAD.

$$V_R < V_S$$

- LAS ONDAS L SE PRESENTAN CUANDO UN ESTRATO
(V_{S1}) SE APOYA EN UN SEMIESPACIO (V_{S2}).

$$\text{SI } V_{S1} < V_{S2} \quad \Rightarrow \quad V_{S1} < V_L < V_{S2}$$

- LAS ONDAS L SON DISPERSIVAS, I.E. V_L CRECE
CON LA LONG. DE ONDA.
- LAS ONDAS S SE APLICAN EN EL ANALISIS DINAMICO
DE ESTRUCTURAS.
- SON DE GRAN INTERES EN DISEÑO SISMICO.



V_P ONDA LONGITUDINAL

V_S ONDA TRANSVERSAL

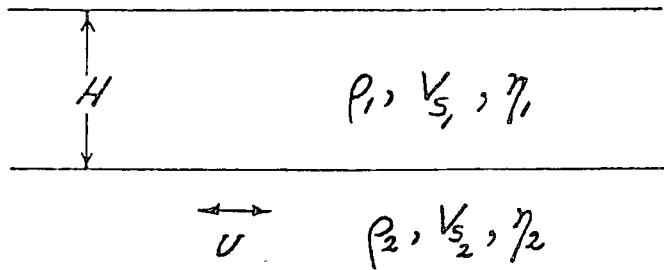
V_R ONDA DE RAYLEIGH

RELACION ENTRE LAS VELOCIDADES DE PROPAGACION

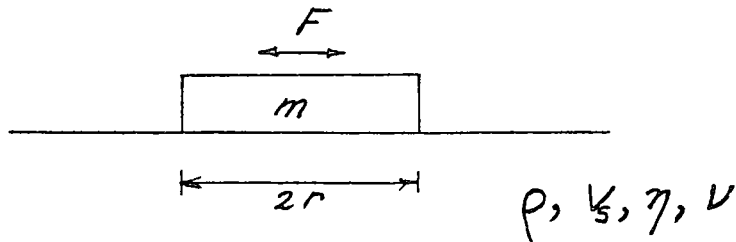
DE LAS ONDAS SISMICAS Y LA RELACION DE POISSON

ALGUNAS APLICACIONES DE LAS ONDAS TRANSVERSALES
AL ANALISIS ESTRUCTURAL

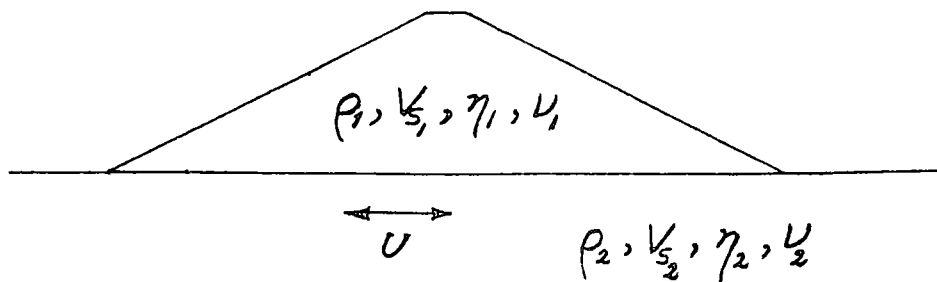
- A) RESPUESTA SISMICA DE UN ESTRATO APOYADO EN UN SEMIESPACIO



- B) RESPUESTA DINAMICA DE UNA ZAPATA CIRCULAR APOYADA EN UN SEMIESPACIO



- C) RESPUESTA SISMICA DE UNA PRESA DE TIERRA APOYADA EN UN SEMIESPACIO



POR LA PRESENCIA DE UNA INTERFASE LAS ONDAS SISMICAS SE REFLEJAN Y SE REFRACTAN

LEYES DE LA REFLEXION:

1. LA ONDA INCIDENTE, LA ONDA REFLEJADA Y LA NORMAL A LA SUPERFICIE EN EL PUNTO DE INCIDENCIA ESTAN CONTENIDAS EN EL MISMO PLANO.
2. EL ANGULO DE INCIDENCIA ES IGUAL AL ANGULO DE REFLEXION.

LEYES DE LA REFRACCION:

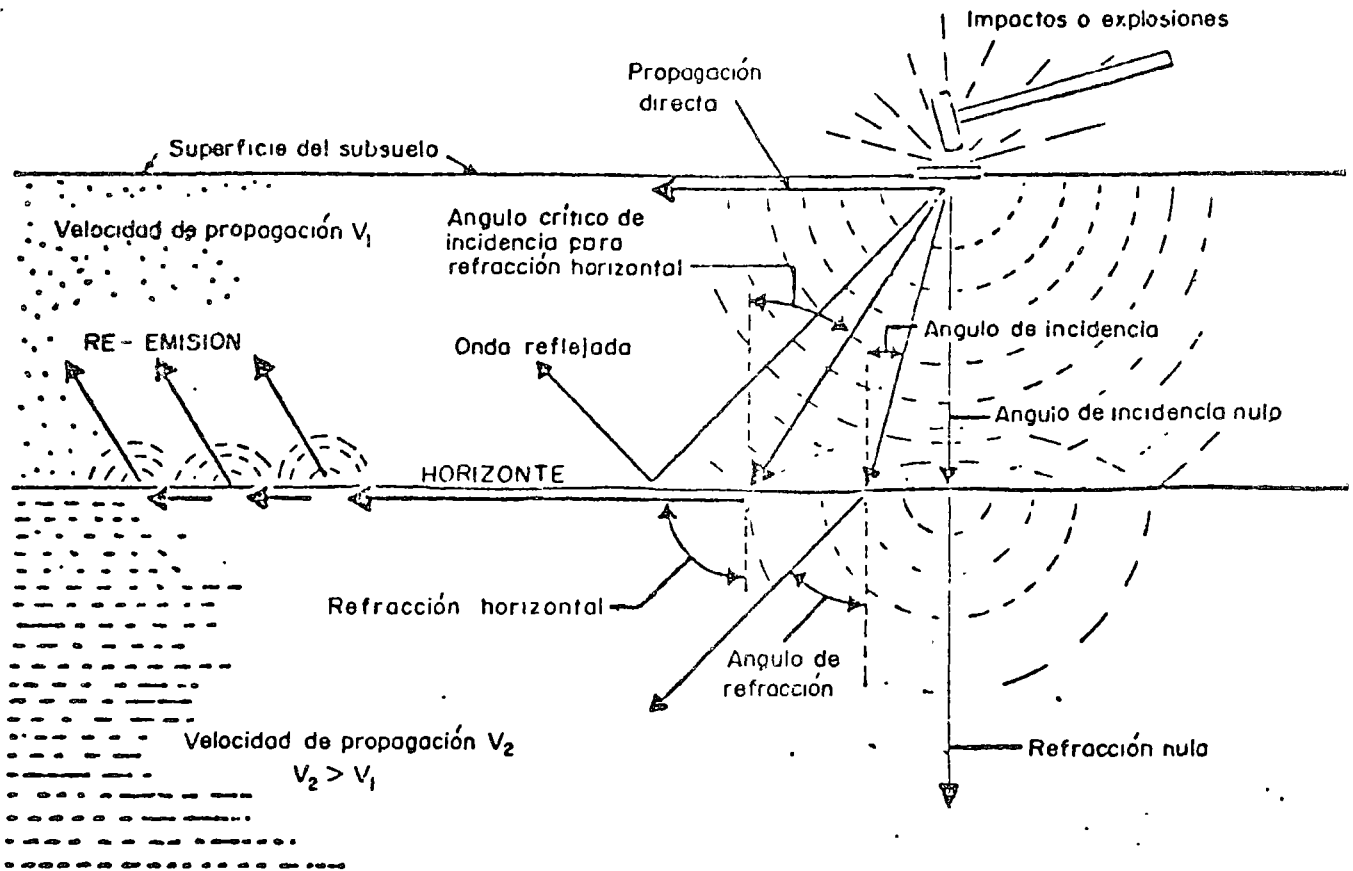
1. LA ONDA INCIDENTE, LA ONDA REFRACTADA Y LA NORMAL A LA SUPERFICIE EN EL PUNTO DE INCIDENCIA ESTAN CONTENIDAS EN EL MISMO PLANO.
2. LA RELACION ENTRE EL SENO DEL ANGULO DE INCIDENCIA Y EL SENO DEL ANGULO DE REFRACCION ES CONSTANTE (LEY DE SNELL).

PARA MEDIR ONDAS P SE TIENEN DOS METODOS:

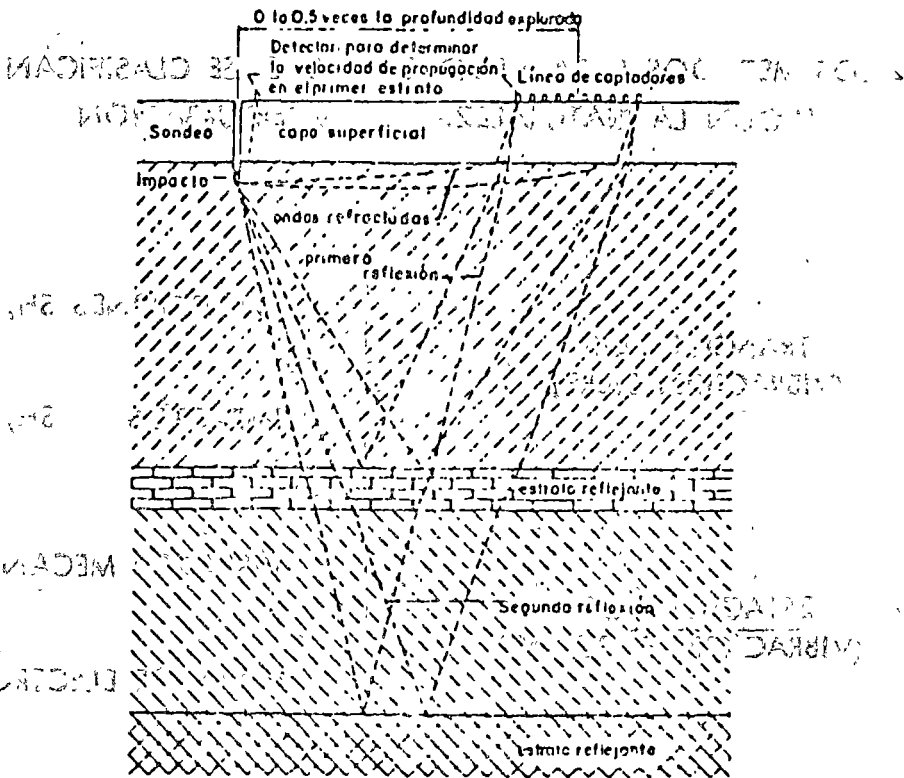
REFLEXION (EXPLORACION PROFUNDA, $H > 600$ m)

REFRACCION (EXPLORACION SOMERA, $H < 100$ m)

EL METODO DE REFRACCION ES APLICABLE CUANDO LA DENSIDAD CRECE CON LA PROFUNDIDAD

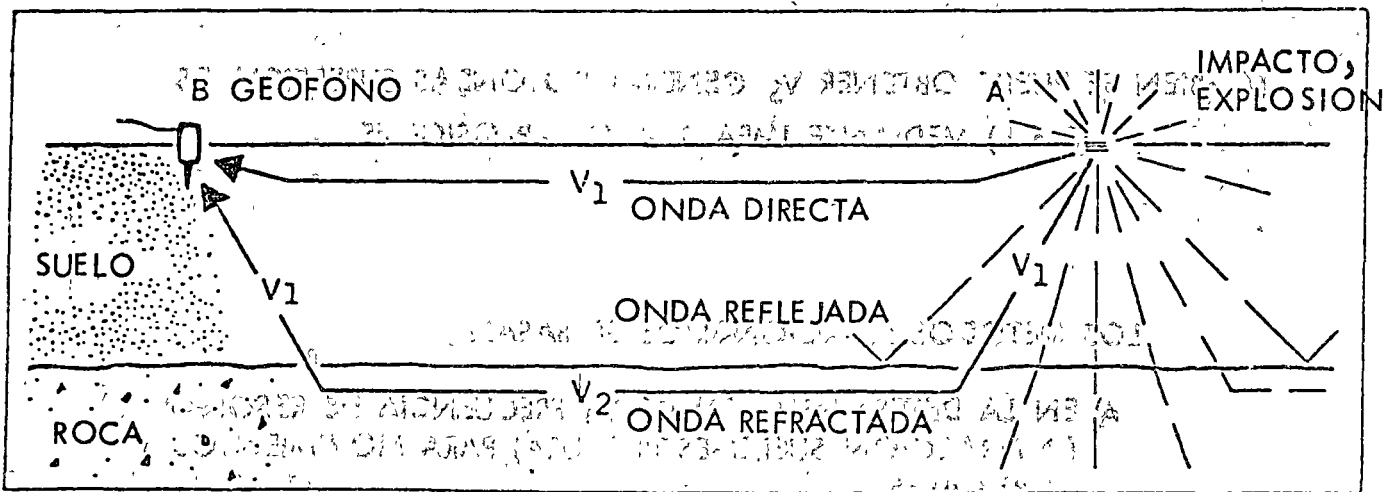


Trayectorias de las ondas elásticas en un medio estratificado.



PRINCIPIO DEL METODO DE REFLEXION

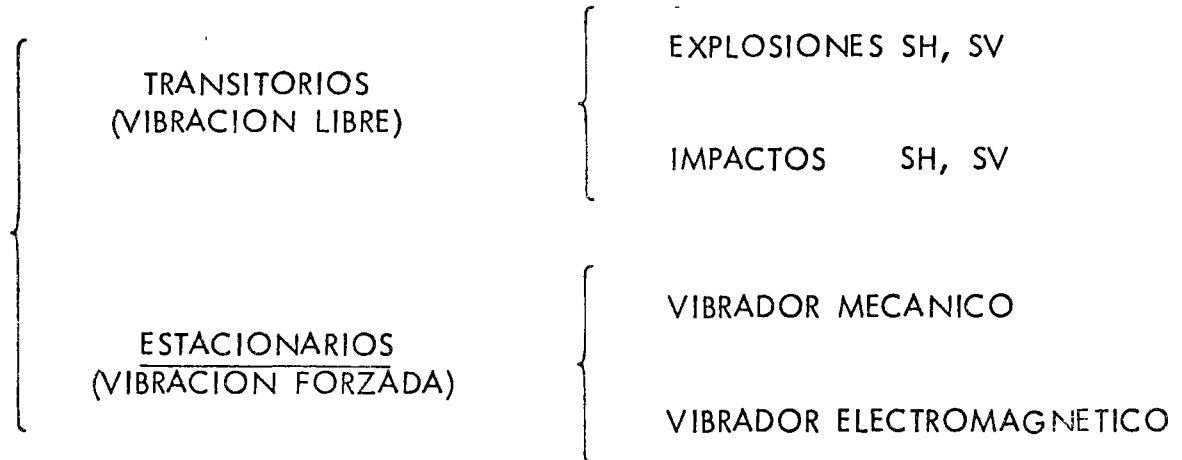
COLOCAR LOS CAPTADORES (GEOFONOS) CON LOS TIEMPOS DE LLEGADA A LAS ONDAS EN LA VELOCIDAD DE PROPAGACION EN UNAS 25 DETERMINADAS 25 DETERMINADAS



PRINCIPIO DEL METODO DE REFRACCION

ALTA O NO TIENE UNAS

LOS METODOS PARA MEDIR ONDAS S SE CLASIFICAN
SEGUN LA NATURALEZA DE LA PERTURBACION



LA VELOCIDAD DE PROPAGACION DE LAS ONDAS S SE DETERMINA
CON LOS TIEMPOS DE LLEGADA Y LAS DISTANCIAS A LAS QUE SE
COLOCAN LOS CAPTADORES (GEOFONOS)

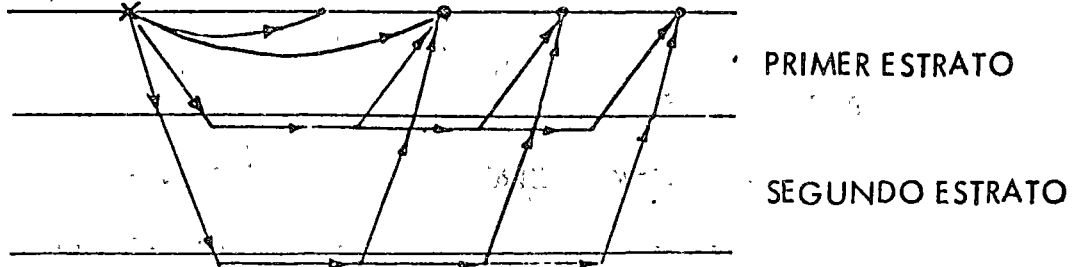
TAMBIEN SE PUEDE OBTENER V_S GENERANDO ONDAS SUPERFICIALES
(R o L) MEDIANTE IMPACTOS O EXPLOSIONES

LOS METODOS ESTACIONARIOS SE BASAN

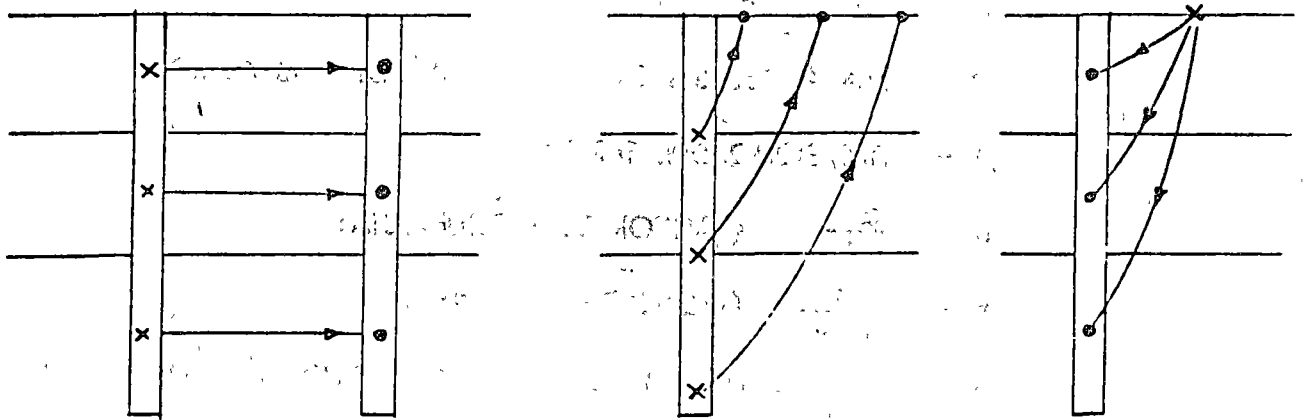
- A) EN LA DETERMINACION DE LA FRECUENCIA DE RESONANCIA
(INTERACCION SUELO-ESTRUCTURA) PARA MOVIMIENTOS
VERTICALES
- B) EN LA OBSERVACION DE LAS ONDAS DE RAYLEIGH (ONDAS
SUPERFICIALES)

METODOS TRANSITORIOS

A) PROSPECCION HORIZONTAL (REFRACCION)



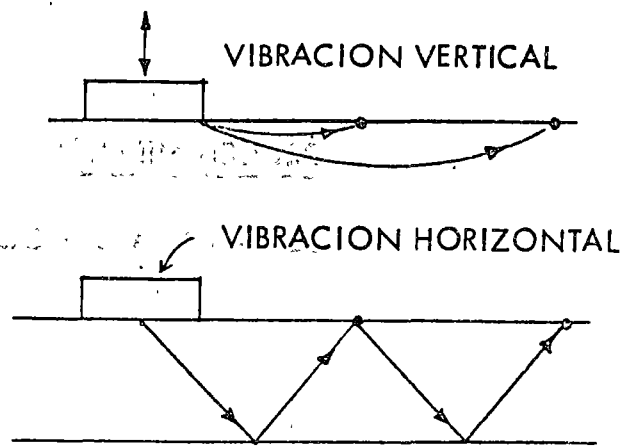
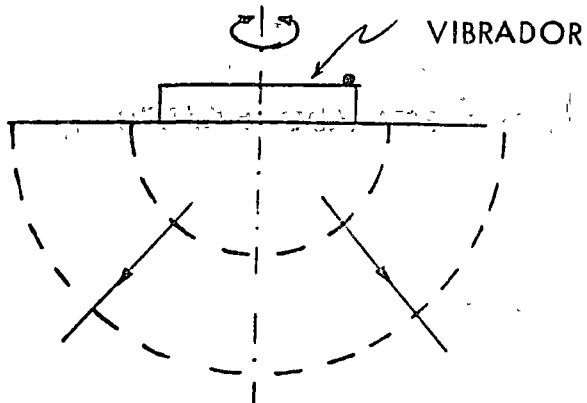
B) PROSPECCION VERTICAL (ONDAS DIRECTAS)



x IMPACTOS O EXPLOSIONES

• GEOFONOS

METODOS ESTACIONARIOS



A) METODO DE LA FRECUENCIA DE RESONANCIA

PARAMETROS

 ω = FRECUENCIA CIRCULAR DE RESONANCIA

F = AMPLITUD DE LA EXCITACION A LA FRECUENCIA DE RESONANCIA

U = AMPLITUD DE LA BASE DEL VIBRADOR, A LA FRECUENCIA DE RESONANCIA

r = RADIO DE LA CIMENTACION

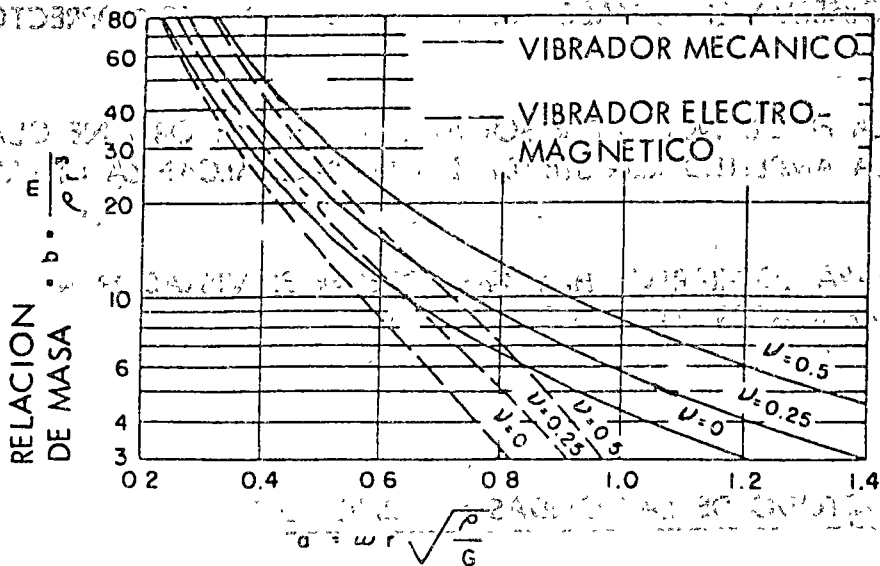
m = MASA DEL SISTEMA CIMENTACION-VIBRADOR

 ρ = DENSIDAD DEL TERRENO $a = \frac{\omega r}{V_s}$ (FACTOR DE FRECUENCIA) $b = \frac{m}{\rho r^3}$ (RELACION DE MASA) $A_m = \frac{\omega^2 \rho r^3}{F} U$ (FACTOR DE AMPLITUD PARA UN VIBRADOR MECANICO) $A_e = \frac{V_s^2 \rho r}{F} U$ (FACTOR DE AMPLITUD PARA UN VIBRADOR ELECTROMAGNETICO)PROCEDIMIENTOSE CALCULA b Y CON UN VALOR DE \hat{v} ESTIMADO SE CALCULA a

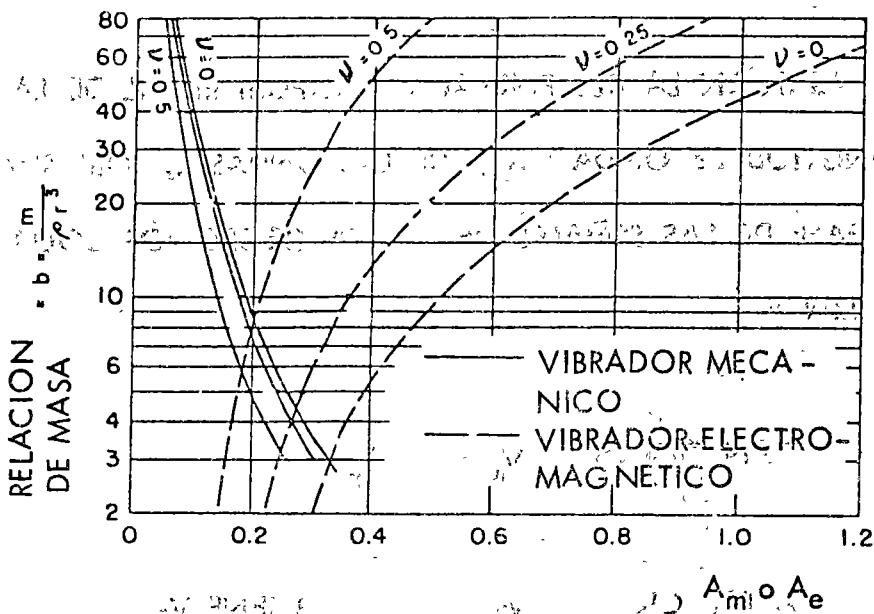
$$\Rightarrow V_s = \frac{\omega r}{a}$$

CON b Y V_s SE OBTIENE A_m O A_e EN EL PRIMER CASO $U = \frac{F A_m}{\omega^2 \rho r^3}$ EN EL SEGUNDO $U = \frac{F A_e}{V_s^2 \rho r}$

PROCEDIMIENTO PARA EL CALCULO DE V_s
 POR EL METODO DE LA RESONANCIA



$$\frac{V_s}{a} = \frac{\omega_r}{a}$$



De $A_m = \frac{\omega^2 \rho r^3}{F} U$ se obtiene U

De $A_e = \frac{V_s^2 \rho r}{F} U$ se obtiene U

- SE COMPARAN U CALCULADO Y U MEDIDO, Y SE OBSERVA SI EL VALOR SUPUESTO DE ν ES CORRECTO
- LA FRECUENCIA DE RESONANCIA ω SE OBTIENE CUANDO LA AMPLITUD REGISTRADA EN LA BASE ALCANZA UN MAXIMO
- PARA LOGRARLO, HAY QUE OPERAR EL VIBRADOR A DIFERENTES FRECUENCIAS

B) METODO DE LAS ONDAS SUPERFICIALES

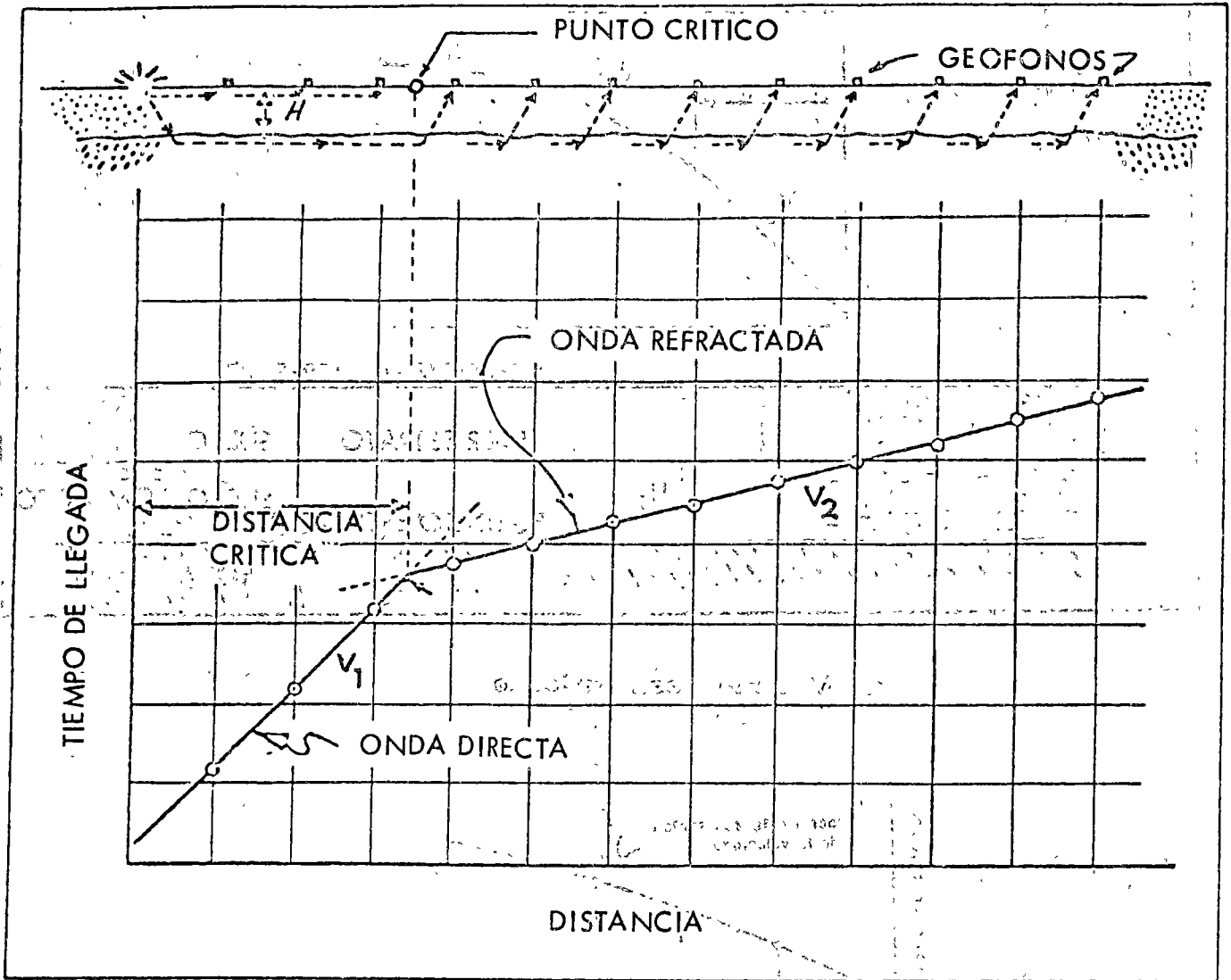
ONDAS R VIBRACION VERTICAL

ONDAS L VIBRACION HORIZONTAL

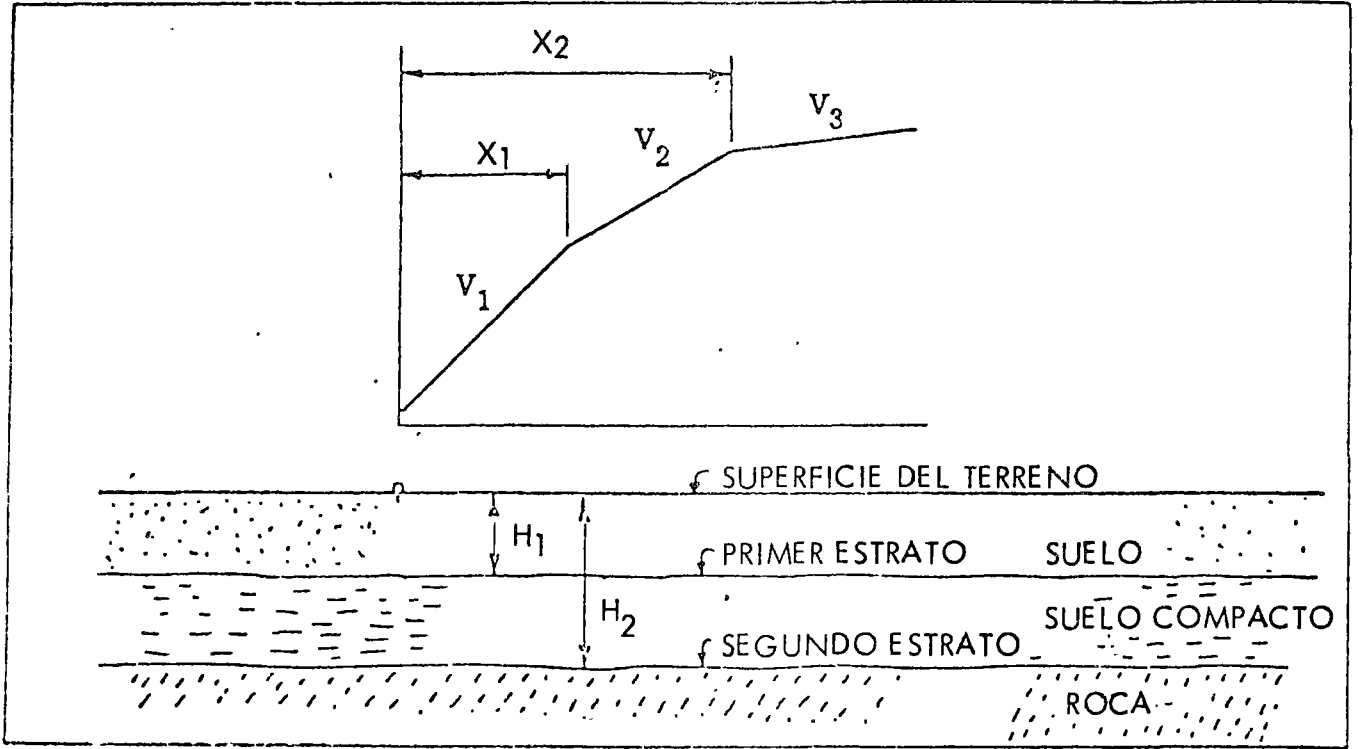
SE BASAN EN LA DETERMINACION EXPERIMENTAL DE LA LONGITUD DE ONDA (λ) DE LAS ONDAS R, OBSERVANDO LA FASE DE LAS SEÑALES DE VARIOS GEOFONOS COLOCADOS EN LINEA

ENTONCES
$$V_R = \frac{\omega}{2\pi} \lambda$$

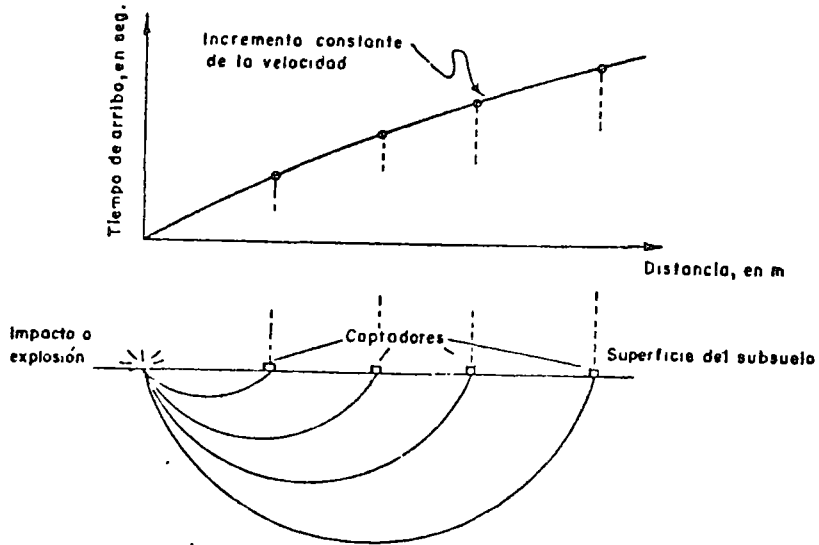
DE LA RELACION V_R / V_S SE OBTIENE V_S



GRAFICA DISTANCIA-TIEMPO PARA UN SOLO ESTRATO

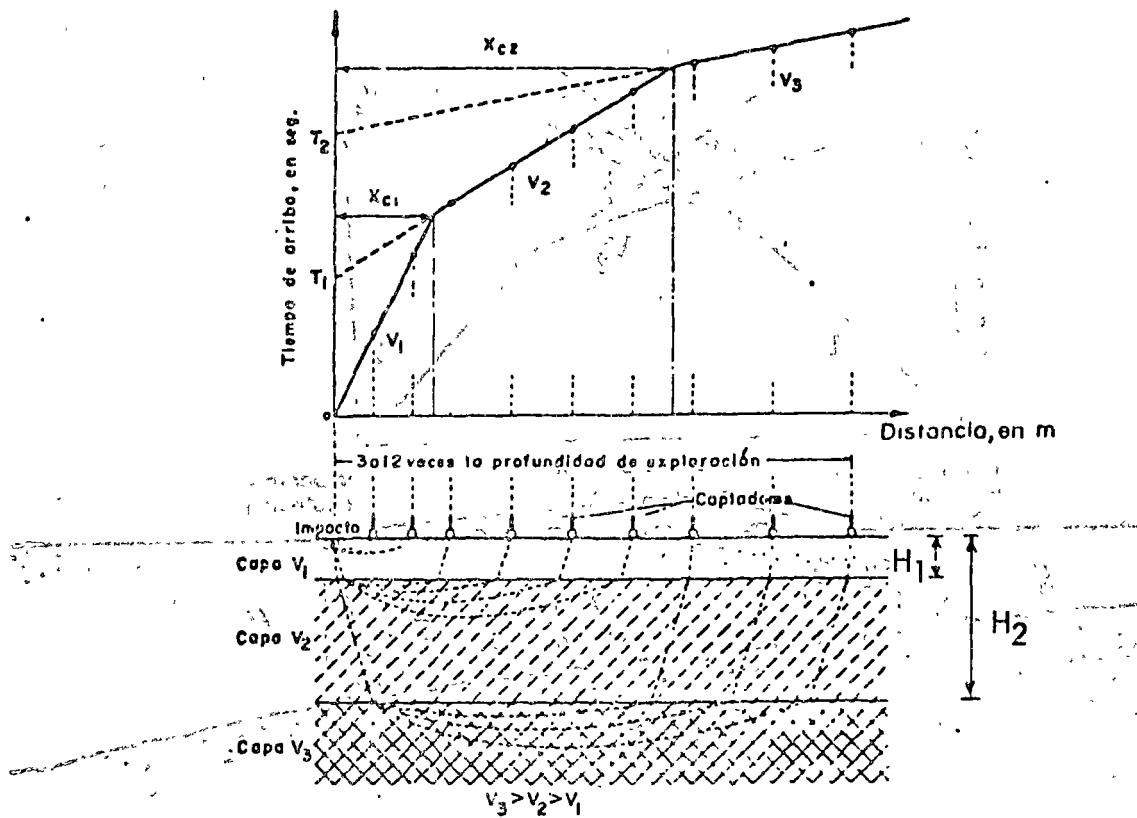


a) Material estratificado



b) Material homogéneo

Gráficas distancia - tiempo de llegada en prospección horizontal



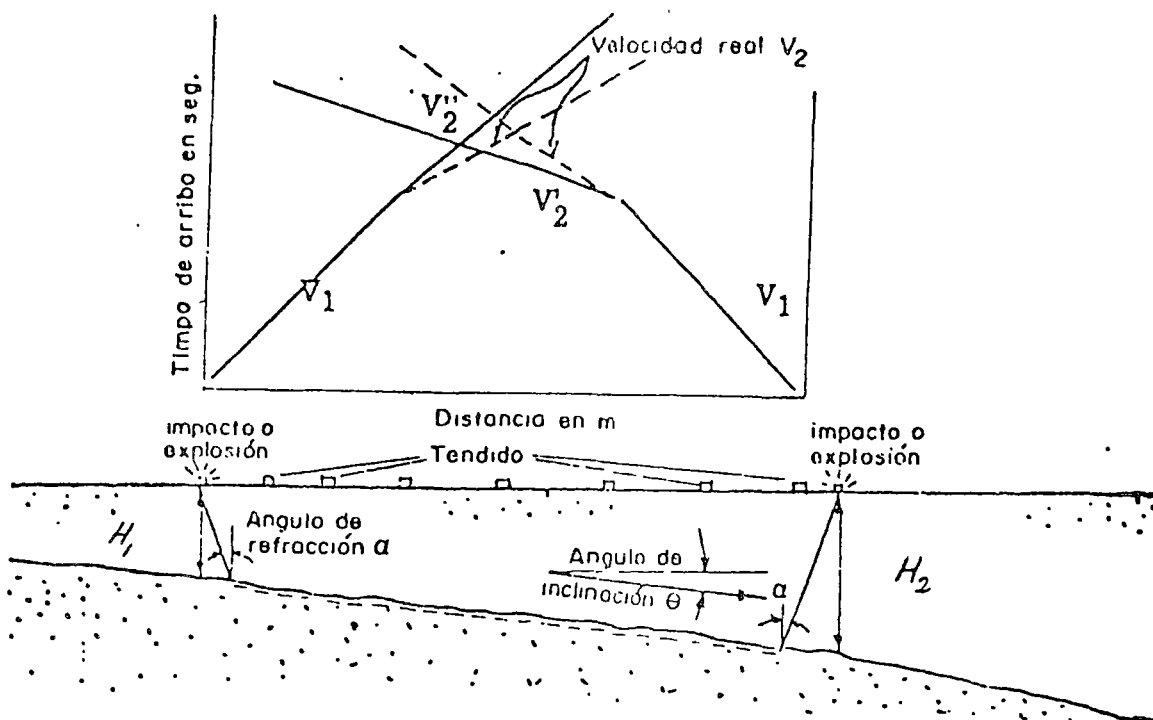
PROFUNDIDAD DEL PRIMER ESTRATO:

$$H_1 = \frac{x_{C1}}{2} \sqrt{\frac{v_2 - v_1}{v_2 + v_1}}$$

PROFUNDIDAD DEL SEGUNDO ESTRATO:

$$H_2 = H_1(1 - R) + \frac{x_{C2}}{2} \sqrt{\frac{v_3 - v_2}{v_3 + v_2}}$$

		VALORES DE R					
VALORES DE v_3/v_2	1.1	.39	.17	.12	.06	.03	.02
	1.5	.56	.31	.21	.12	.07	.03
	2	.60	.34	.24	.15	.08	.04
	3	.63	.36	.26	.16	.09	.04
	5	.64	.37	.26	.16	.09	.05
	10	.64	.38	.27	.17	.11	.05
		1.1	1.5	2	3	5	10
		VALORES DE v_2/v_1					



ANGULO DE INCLINACION $\theta = \frac{1}{2} \left[\text{sen}^{-1} \left(\frac{V_1}{V_2'} \right) - \text{sen}^{-1} \left(\frac{V_1}{V_2''} \right) \right]$

GRAFICA DISTANCIA - TIEMPO DE LLEGADA
 PARA UN ESTRATO INCLINADO

BOGOTÁ 15 DE JUNIO DE 1964

COMUNICACION

AGUSTO

MATERIALES TÍPICOS CORRESPONDIENTES A DIVERSOS RANGOS DE VELOCIDAD DE ONDAS P.

Velocidades de propagación
(en m/seg)

MATERIAL

160 - 560	Suelos superficiales, tierras vegetales, fangos, pantanos.
430 - 930	Arena seca, gravas finas.
900 - 1160	Gravas medianas, gravas con arcilla.
1000 - 1160	Gravas húmedas, tillitas compactadas, rellenos, estratos arcillosos.
1330 - 2660	Lutitas, pizarras, areniscas, gravas cementadas, granitos alterados
3000 - o más	Roca sana, sin intemperismo o fracturamiento.

(c)

RELACION ENTRE LOS PRINCIPALES PARAMETROS ELASTICOS

DINAMICOS Y V_S, V_P

- SE TENIA

$$V_P = \sqrt{\frac{\lambda + 2G}{\rho}} \quad (1) \quad V_S = \sqrt{\frac{G}{\rho}} \quad (2)$$

- DE (1) Y (2)

$$\left(\frac{V_P}{V_S}\right)^2 = \frac{\lambda + 2G}{G} = \alpha^2 \quad (3)$$

- DE LA TEORIA DE ELASTICIDAD

$$\lambda = \frac{E}{(1 + \nu)(1 - 2\nu)} \quad (4) \quad \frac{\lambda + 2G}{\lambda} = \frac{1 - \nu}{\nu} \quad (5)$$

- COMBINANDO (3) Y (5)

$$\alpha^2 G = \frac{\lambda(1 - \nu)}{\nu} \quad (6)$$

- SUSTITUYENDO (4) EN (6) Y RECORDANDO

$$G = \frac{E}{2(1 + \nu)} \quad (7)$$

- SE OBTIENE

$$\alpha^2 = \frac{2(1 - \nu)}{1 - 2\nu} \quad (8)$$

- DESPEJANDO ν

$$\nu = \frac{2 - (V_P/V_S)^2}{2[1 - (V_P/V_S)^2]} \quad (9)$$

- ADEMÁS, DE (2):

$$G = \frac{V_p^2}{V_s^2} \rho \quad (10)$$

- ENTONCES, DE (7)

$$E = 2G (1 + \nu) \quad (11)$$

- SUSTITUYENDO (9) Y (10) EN (11) SE OBTIENE

$$E = \frac{3 V_p^2 - 4 V_s^2}{(V_p/V_s)^2 - 1} \rho \quad (12)$$

- EN LAS ECS ANTERIORES

ν = RELACION DE POISSON

G = MODULO DE RIGIDEZ

E = MODULO DE ELASTICIDAD

V_p = VELOCIDAD DE PROPAGACION

DE LAS ONDAS LONGITUDINALES

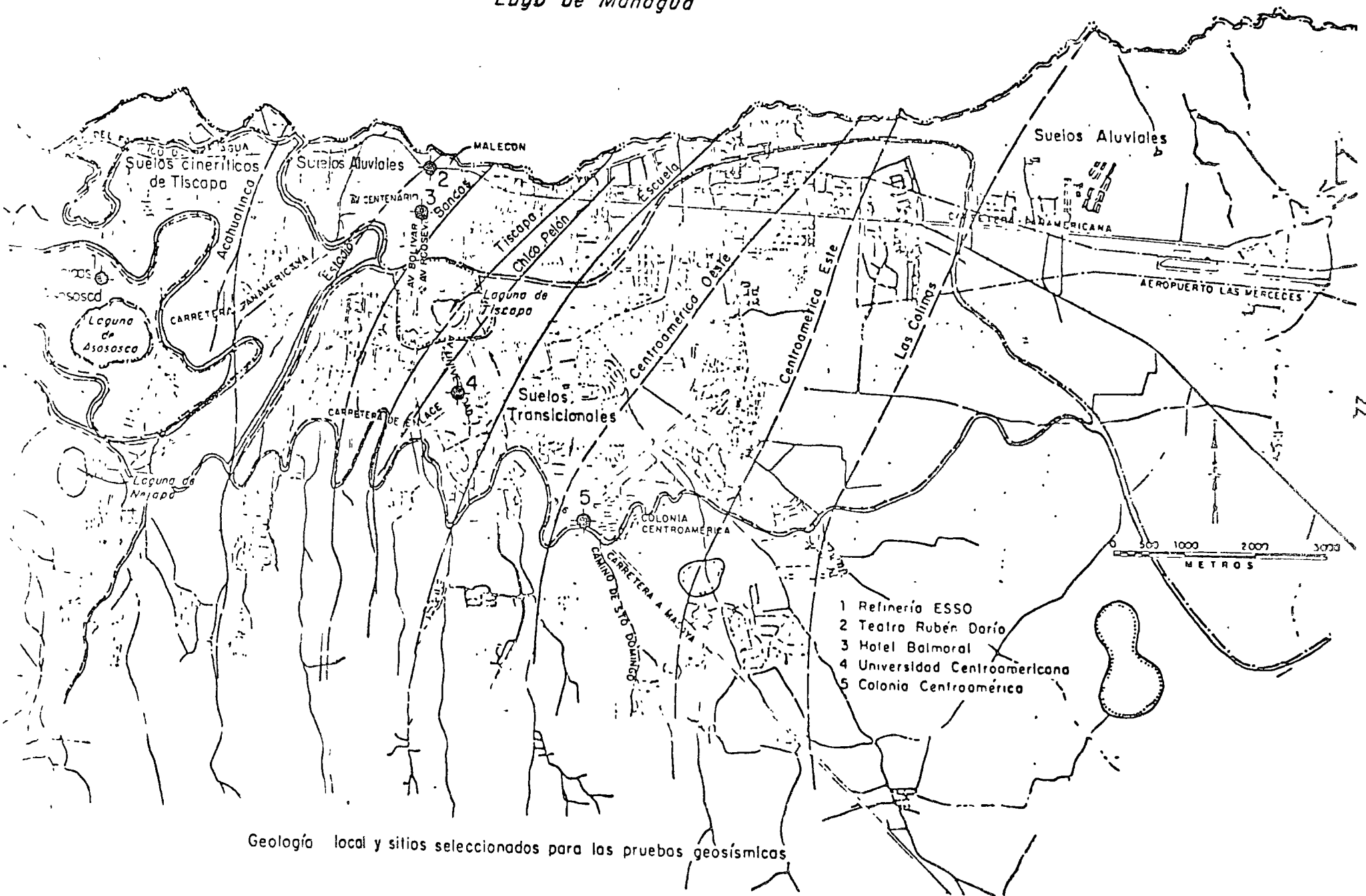
V_s = VELOCIDAD DE PROPAGACION

DE LAS ONDAS TRANSVERSALES

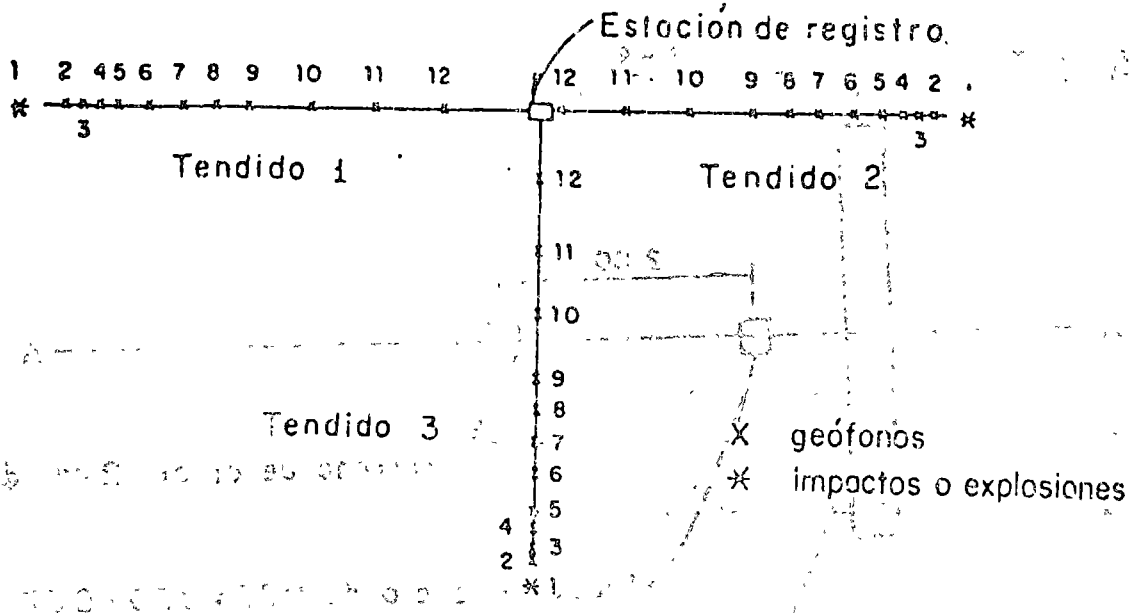
ρ = DENSIDAD DEL MATERIAL

} DINAMICOS

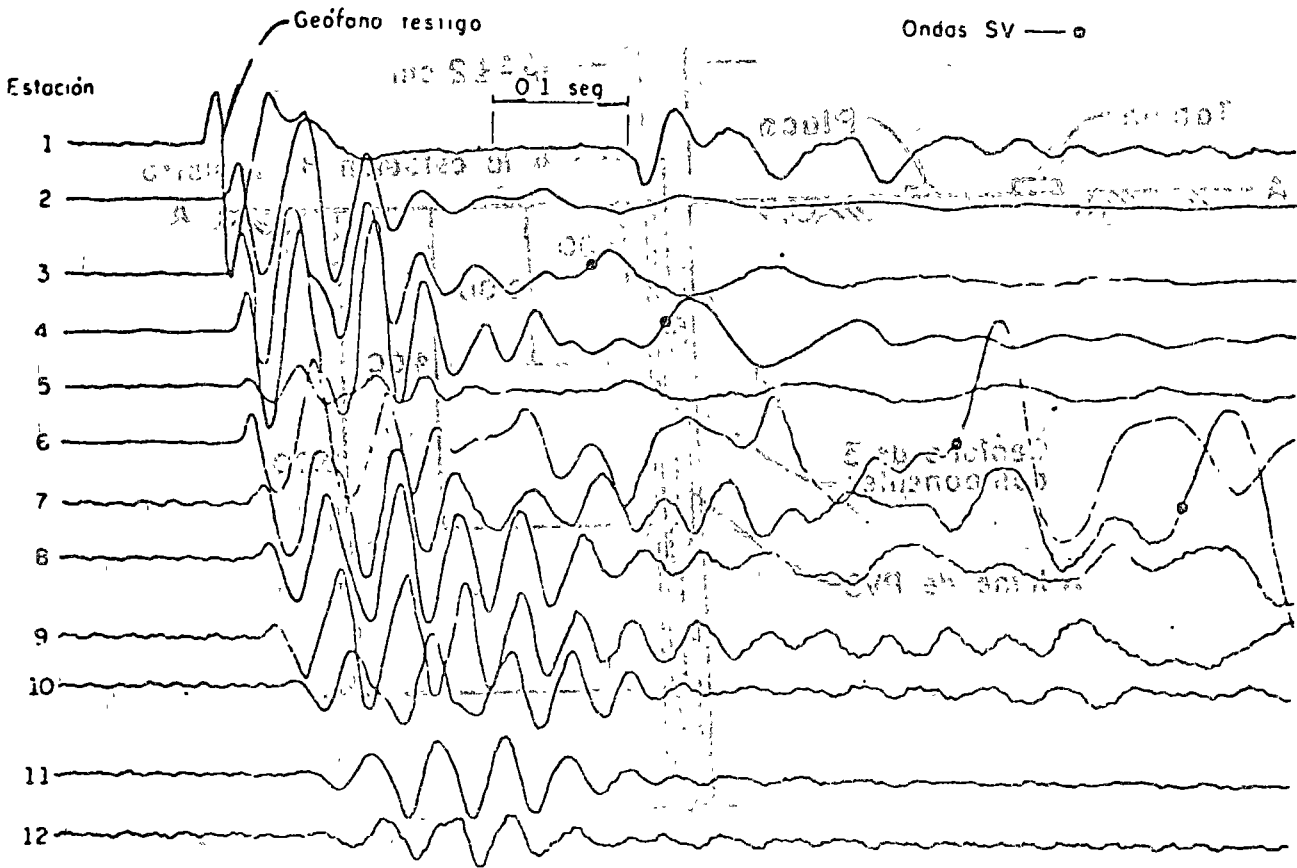
Lago de Managua



Geología local y sitios seleccionados para las pruebas geosísmicas

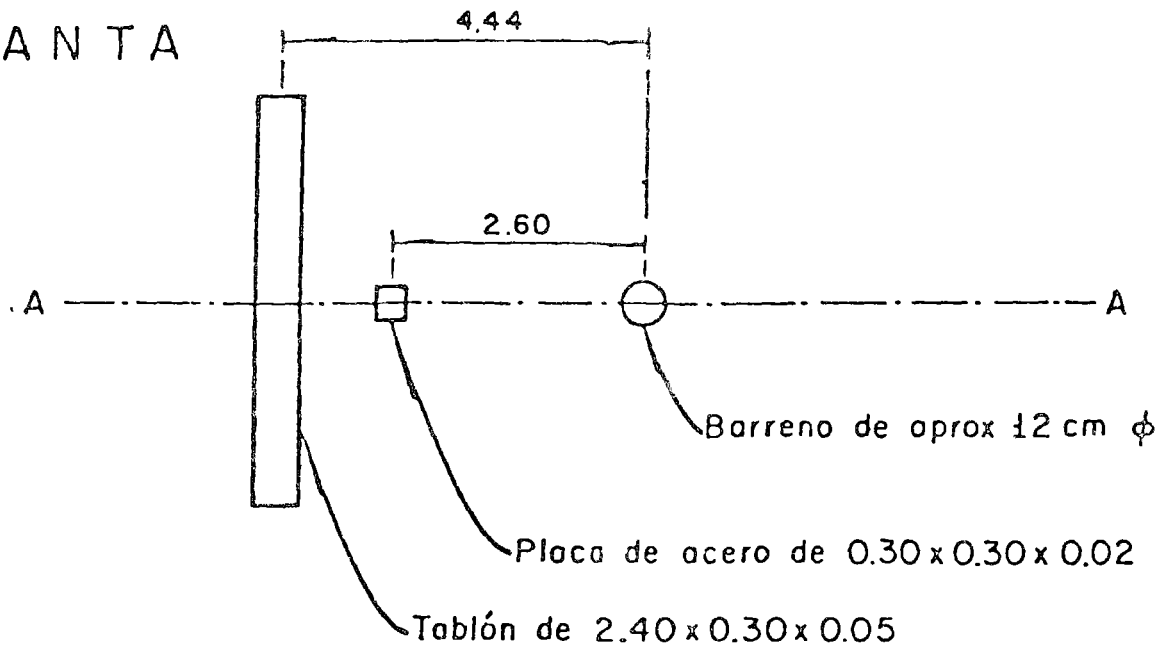


Líneas de prospección horizontal en el área por explorar



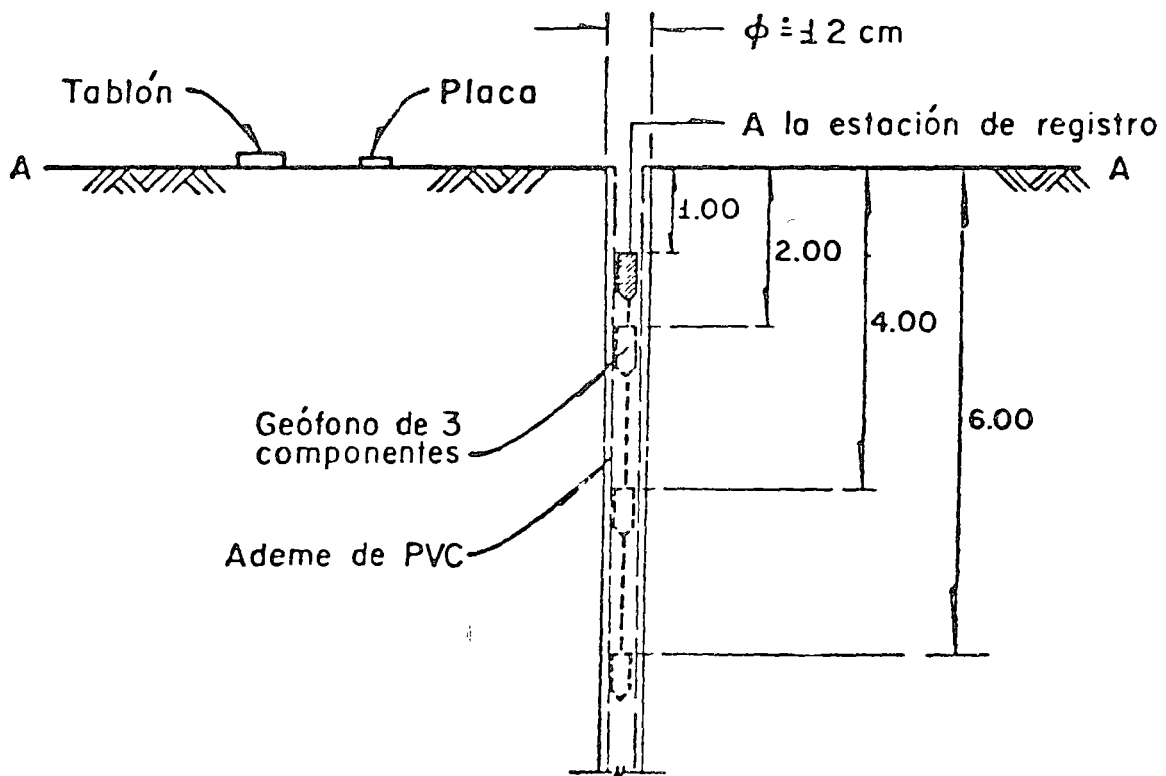
Registro típico de ondas longitudinales generadas mediante explosiones

P L A N T A

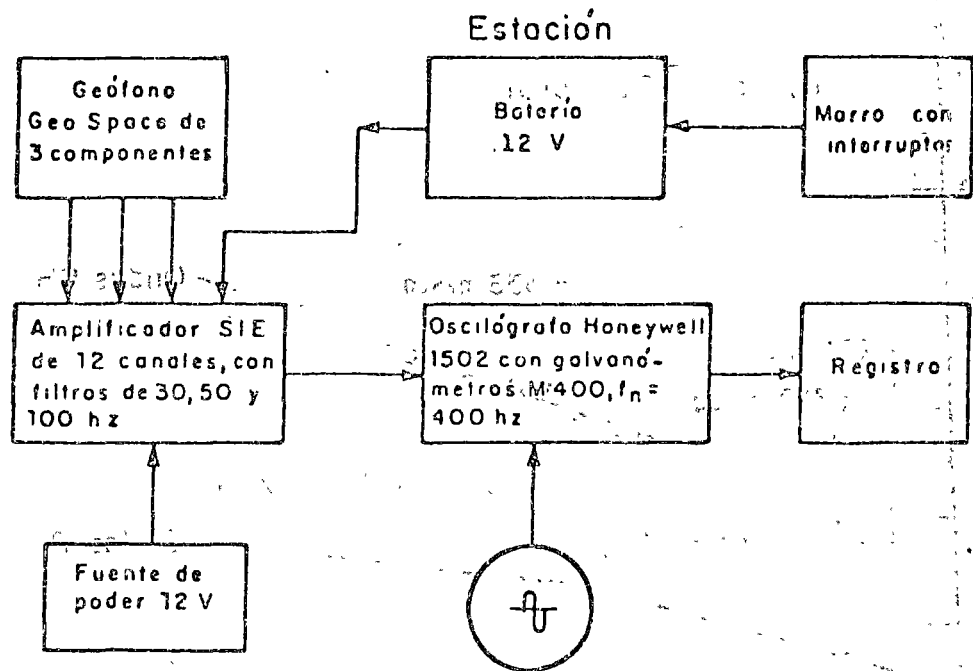


E L E V A C I O N

Acotaciones en m



Posición del geófono y de las fuentes de excitación en el barreno \perp

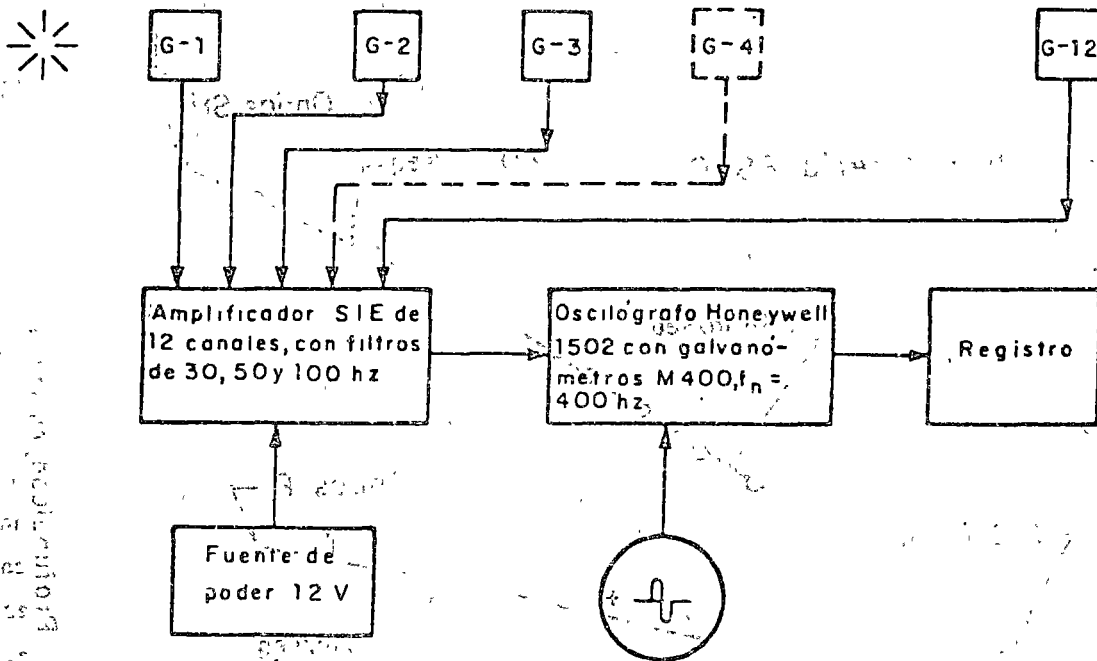


a) Prospección vertical

Explosión

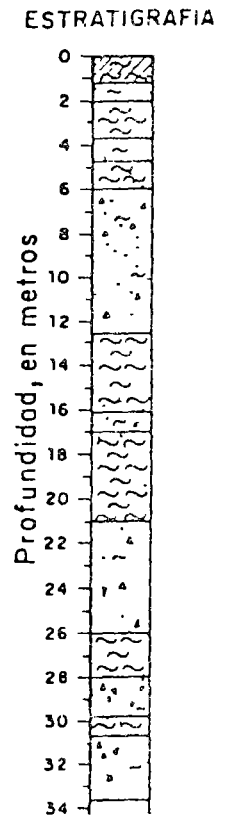
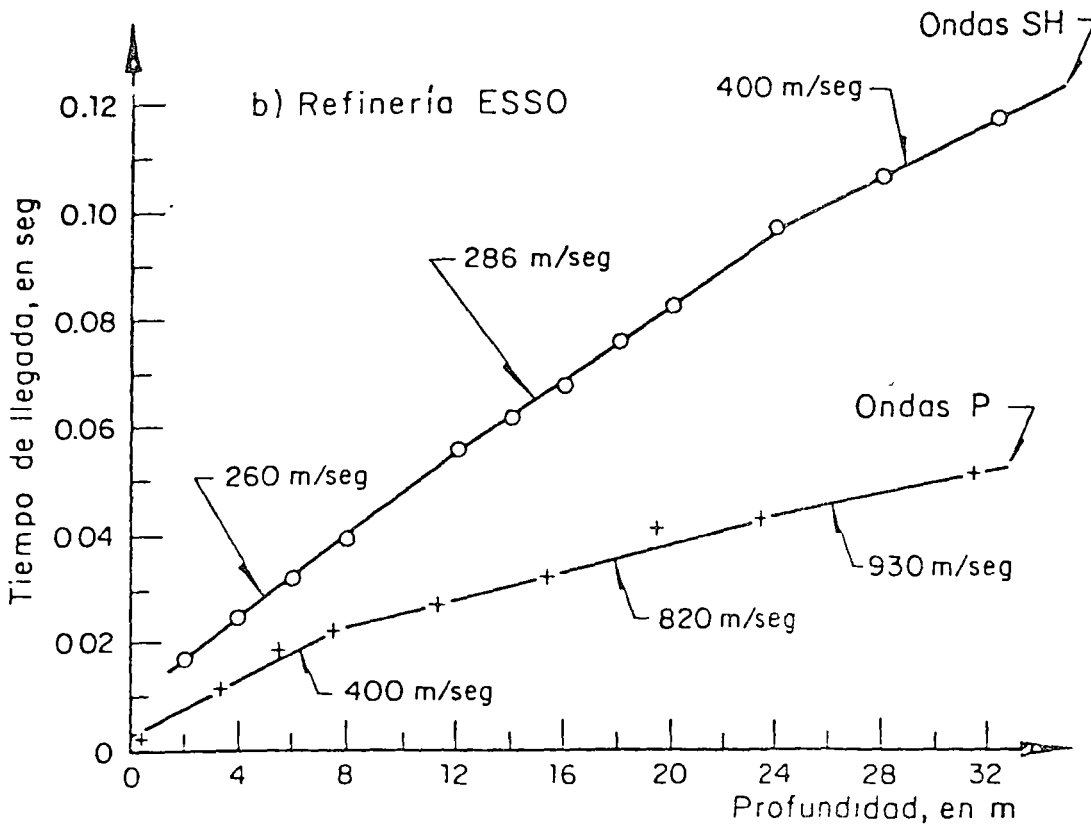
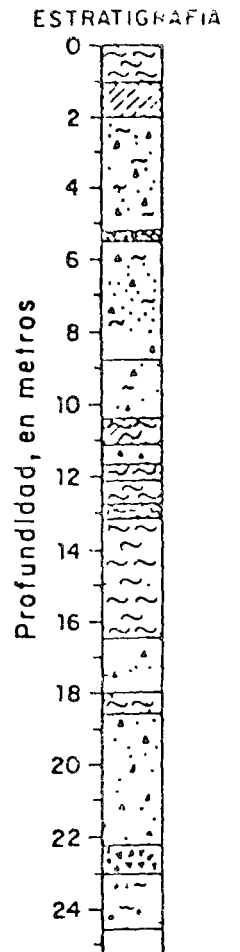
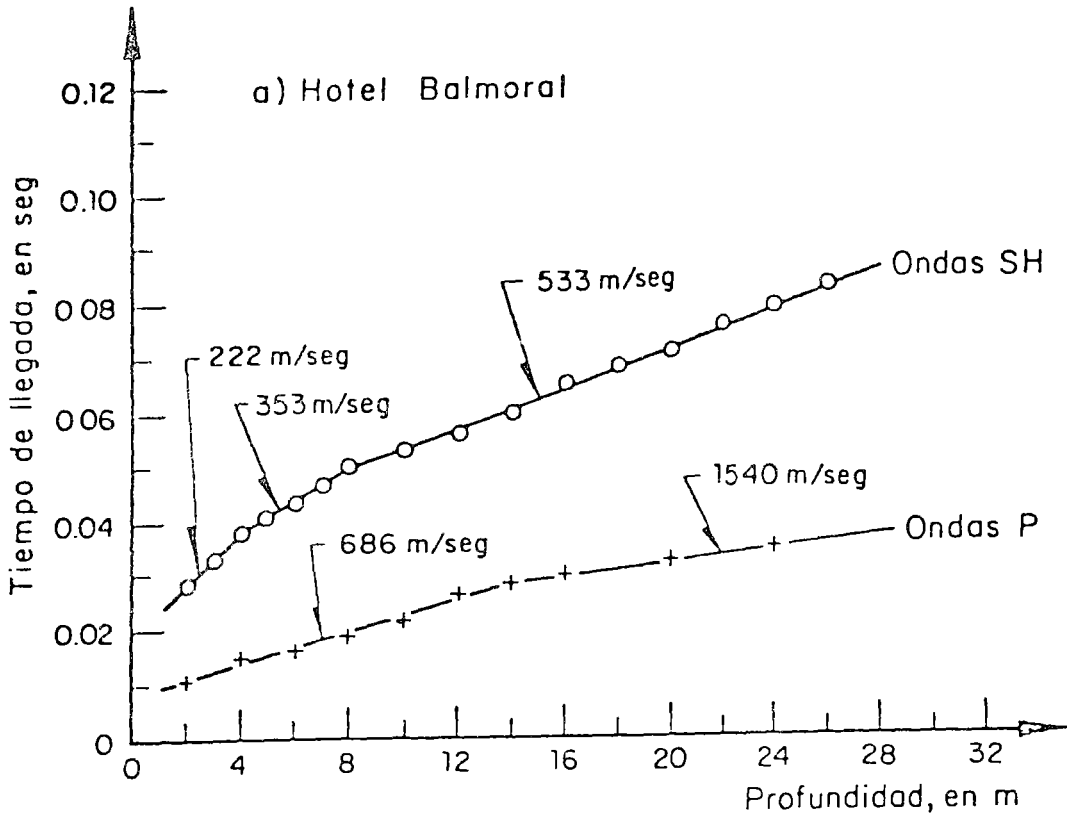
Tendido

Testigo

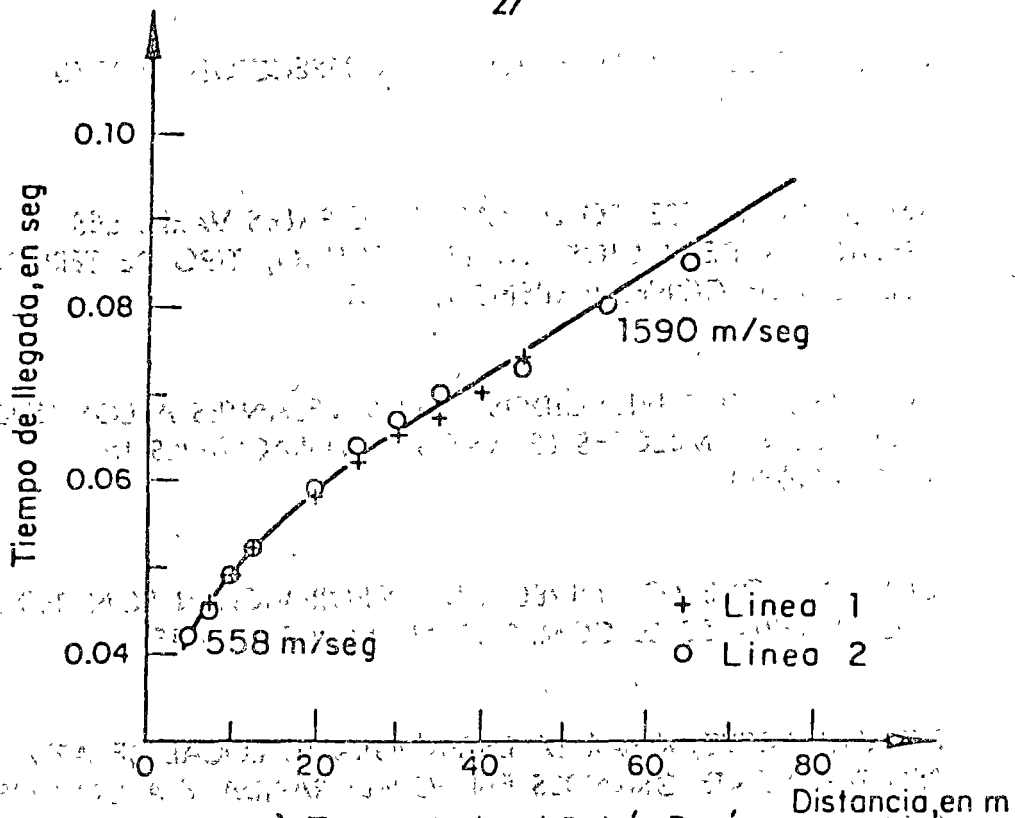


b) Prospección horizontal

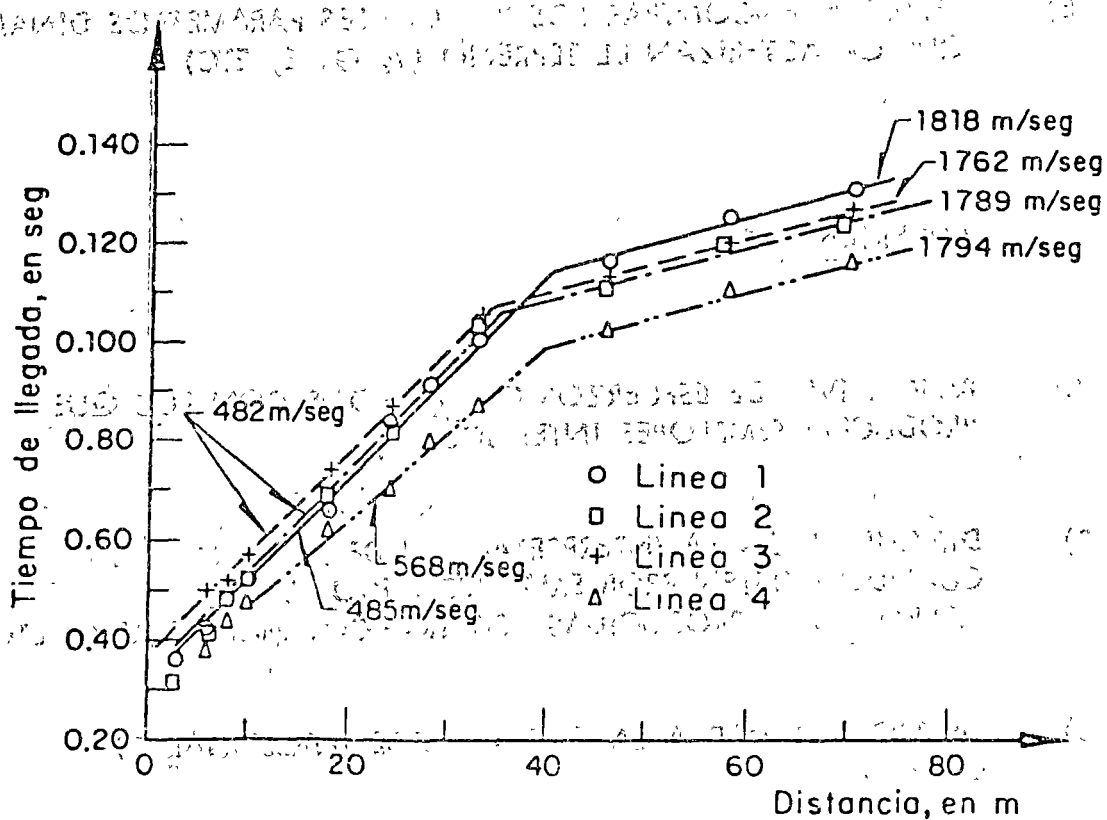
Diagramas de la instrumentación empleada en las pruebas geosísmicas



Gráficas profundidad-tiempo de llegada de ondas transver-sales (SH) y longitudinales (P)



a) Teatro Nacional Rubén Darío



b) Universidad Centroamericana

VENTAJAS DE LOS METODOS DE PROSPECCION SISMICA

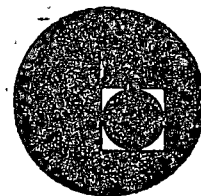
- A) INCLUYEN EL EFECTO DE LAS PRINCIPALES VARIABLES (RELACION DE VACIOS, NIVEL FREATICO, TIPO DE TERRENO, PRESION DE CONFINAMIENTO, ETC)
- B) LOS ESFUERZOS INDUCIDOS SON SEMEJANTES A LOS QUE PRODUCEN TEMBLORES LEJANOS O VIBRACIONES DE MAQUINARIA
- C) DEBIDO A QUE LOS NIVELES DE DEFORMACION SON REDUCIDOS, LOS MATERIALES SE COMPORTAN ELASTICAMENTE
- D) PERMITEN DETERMINAR LA ESTRATIGRAFIA LOCAL DE AREAS RELATIVAMENTE GRANDES EN FORMA RAPIDA Y A UN COSTO MENOR
- E) PERMITEN ENCONTRAR LOS PRINCIPALES PARAMETROS DINAMICOS QUE CARACTERIZAN EL TERRENO (ν , G, E, ETC)

ADVERTENCIAS

- A) BAJO NIVEL DE ESFUERZOS COMPARADOS CON LOS QUE PRODUCEN TEMBLORES INTENSOS
- B) DIFICULTAD EN LA INTERPRETACION DE LOS REGISTROS CUANDO EXISTEN PROBLEMAS DE RUIDO LOCAL (VIBRACIONES PRODUCIDAS POR TRAFICO, MAQUINARIA, ETC)
- C) LA PROFUNDIDAD A LA QUE SE PUEDE INVESTIGAR ES LIMITADA



centro de educación continua
división de estudios superiores
facultad de ingeniería, unam



ANALISIS DINAMICO DE ESTRUCTURAS ESPECIALES



DR. JACOBO BIELAK

AGOSTO DE 1977.

JOURNAL OF THE ENGINEERING MECHANICS DIVISION

MODAL ANALYSIS FOR BUILDING-SOIL INTERACTION

By Jacobo Bielak,¹ A. M. ASCE

INTRODUCTION

Compliance of the soil foundation has become recognized as a potentially important factor in design of earthquake resistant structures. Several methods have consequently been developed in recent years to analyze the dynamic response of structures supported on flexible soils, including applications of Fourier analysis (3,7,8,17), Laplace transform techniques (2,7), Foss's method (7), the finite element method (4,5,14,16) and direct step-by-step numerical integration (11).

Modal superposition has perhaps been the most widely used technique in the transient analysis of time invariant linear systems. This method, however, is not rigorously applicable to the study of soil-structure interaction because the foundation stiffness and damping coefficients are frequency dependent, and therefore, the building-foundation system does not possess classical normal modes. Application of the superposition method to interaction studies nevertheless remains desirable, provided the resulting loss in accuracy is not too great. This approach makes the required calculations equivalent to those for one-degree-of-freedom damped oscillators, along with giving physical insight into the dynamics of building-foundation systems. Moreover, the response of many structures is often dominated by only one or a few modal components. Even for complex systems of this type, analysis via modal superposition can be particularly effective, as only a few terms need be considered.

Various approximate methods of superposition for the interaction problem have been recently proposed (9,10,12,13,15).

The methods have differed in the way in which modal damping is calculated: Roesset, Whitman, and Dobry (13); Novak (9,10); and Rainer (12) assigned weighted values of damping based on the energy ratio criterion due to Jacobsen

¹Note.—Discussion open until March 1, 1977. To extend the closing date one month, a written request must be filed with the Editor of Technical Publications, ASCE. This paper is part of the copyrighted Journal of the Engineering Mechanics Division, Proceedings of the American Society of Civil Engineers, Vol. 102, No. EM5, October, 1976. Manuscript was submitted for review for possible publication on February 9, 1976.

¹Research Prof., Inst. de Ingeniería, Universidad Nacional Autónoma de México, México, D. F., México.

(6) for evaluation of equivalent modal damping in composite elastic and inelastic structures, whereas Tsai (15) calculated the modal damping by matching the exact and normal modal solutions of the amplitude transfer function for a certain structural location. While the latter method ensures that the peak values of the steady-state response coincide for the exact and modal analyses at a given location, it requires that the exact solution be obtained before the modal damping can be evaluated. Also, the resulting damping coefficient does not differentiate between individual sources of energy dissipation.

The present paper proposes an alternative expression for the modal damping in the system. This approximation is obtained as a formal extension of the classical method of modal analysis which is also equivalent to the energy ratio criterion proposed by Jacobsen. By making use of the modal shapes of the fixed-base superstructure modal damping in the system is expressed as a weighted sum of the critical damping ratios of the superstructure plus an additional term representing the energy dissipated by the soil.

For single-story buildings the degree of accuracy achieved by the method proposed herein is studied by comparing the expression for the effective damping ratio with that found previously from an exact solution. Several examples are used to illustrate the applicability of the modal method to multistory structures supported on viscoelastic soils. Results obtained by this method are compared with exact solutions in the frequency domain, and the individual contributions of the soil and structure to the overall modal damping of the building-soil system are evaluated as well.

ANALYSIS OF SYSTEM

Assuming linear behavior of soil and structure, the equations of motion of building-foundation systems can be written as

$$M_o u + C_o(\omega) \dot{u} + K_o(\omega) u = P \quad (1)$$

when subjected to steady-state harmonic excitation, in which M_o , C_o , and K_o = mass, damping, and stiffness matrices, ω = circular frequency of excitation, and u and P are displacement and steady-state disturbance vectors, respectively. Eq. 1 governs the oscillations resulting from forces applied directly to the structure as well as those produced by the ground motion.

Matrices C_o and K_o include elements that describe the time invariant damping and stiffness properties of the superstructure, and additional elements that refer to the same properties evaluated at the interface between building and soil. These elements can be evaluated using an analytical approach for the case of a simple foundation such as a rigid disk resting on the surface of a viscoelastic half space (18) or stratum, or by the finite element method if the soil and foundation models are more complex (16). Since the resulting functions vary with the frequency of excitation it becomes clear that the matrices C_o and K_o also will be frequency dependent.

Although Eq. 1 refers to the steady-state response of the system, the transient excitation can also be readily described by this expression if Eq. 1 is interpreted as the Fourier transformed version of the governing equation. The vector, P , must then be regarded as the Fourier transform of the transient excitation

$P(t)$. With this interpretation the transient response may be obtained by taking the inverse transform of Eq. 1.

In this study an alternative modal method for the analysis of the transient response will be presented. It will be assumed that the frequency dependent elements in $K_o(\omega)$ do not vary significantly with ω over the interval of interest, and may be approximated by a constant value corresponding to the fundamental resonance frequency of the building-foundation system, since the fundamental-mode contribution is usually the most significant one to the total response. The variation of $C_o(\omega)$ with frequency is more rapid and, therefore, will be considered explicitly in the analysis.

Approximate Modal Method of Superposition. Let \tilde{X}_j be the j th orthogonal mode and $\tilde{\omega}_j$ the corresponding natural circular frequency of the undamped building-foundation system. These quantities are defined by the eigenvalue problem

$$K_o(\tilde{\omega}_j) \tilde{X}_j = \tilde{\omega}_j^2 M_o \tilde{X}_j \quad (2)$$

which can be solved either directly or by the partition or modal synthesis techniques (4,7,15,16).

Now suppose that Eq. 1 admits a solution of the form

$$u(t) = \sum_{j=1}^N \tilde{X}_j q_j(t) \quad (3)$$

in which the sum is over the total number of independent degrees-of-freedom of the structure-foundation system, and $q_j(t)$ are the generalized coordinates of the problem.

Substituting this solution into Eq. 1, premultiplying the result by the transpose of \tilde{X}_k and neglecting the terms containing the product $\tilde{X}_k^T C_o \tilde{X}_j$, for k not equal to j , the following equation is obtained

$$q_j(t) + 2\tilde{\omega}_j \tilde{\eta}_j q_j(t) + \tilde{\omega}_j^2 q_j(t) = \tilde{p}_j(t), \quad j = 1, 2, \dots, N \quad (4)$$

$$\text{in which } \tilde{\omega}_j^2 = \frac{\tilde{X}_j^T K_o(\tilde{\omega}_j) \tilde{X}_j}{\tilde{X}_j^T M_o \tilde{X}_j} \quad (5)$$

$$2\tilde{\eta}_j \tilde{\omega}_j = \frac{\tilde{X}_j^T C_o(\tilde{\omega}_j) \tilde{X}_j}{\tilde{X}_j^T M_o \tilde{X}_j} \quad (6)$$

$$\tilde{p}_j(t) = \frac{\tilde{X}_j^T p(t)}{\tilde{X}_j^T M_o \tilde{X}_j} \quad (7)$$

Note that K_o is taken to be a constant matrix for all values of frequency. The matrix, C_o , on the other hand, is assigned the value of the natural frequency of the mode in question for the calculation of the corresponding modal damping. Successive approximations are required to obtain the fundamental mode shape and natural frequency as $K_o(\tilde{\omega}_j)$ is not known at the outset. With $K_o(\tilde{\omega}_j)$ established, the remaining modes and natural frequencies can be determined as for a constant matrix. No iterations are needed to calculate $\tilde{\eta}_j$.

The method just described does not provide a rigorous solution to Eq. 1 because the two assumptions required for its exact applicability—that K_o

be independent of frequency and $C_o(\omega)$ orthogonal with respect to the normal modes—are not satisfied in general. Yet transfer functions corresponding to steady-state response of building-foundation systems generally resemble those obtained for linear systems with time invariant properties having classical normal modes. It is, therefore, expected that the modal superposition method can produce sufficiently accurate approximations from an engineering standpoint, especially if the structure itself admits normal mode decomposition.

Modal Damping in Terms of Soil and Structural Properties — The overall damping for a given mode of the building-foundation system is a composite value made up of the energy dissipated by the structure and energy losses from internal friction and wave radiation into the foundation medium. In the structure itself, damping is usually specified as damping ratios for the structural modes while energy dissipation in the soil is measured by the coefficients of equivalent frequency-dependent dampers related to the imaginary part of the impedance functions between the building foundation and surrounding soil. It is desirable to find an expression for the overall damping in the system in terms of these quantities. This is accomplished by introducing the modal configurations of the fixed-base superstructure in the expression for $\tilde{\eta}_j$.

As an illustration, consider the building-foundation system in Fig. 1. It consists of a linear viscously damped n -story structure with one degree-of-freedom per floor, resting on the surface of a homogeneous linear viscoelastic half space. For fixed-base response, the superstructure has a stiffness matrix, \mathbf{K} , a mass matrix, \mathbf{M} , and a damping matrix, \mathbf{C} , such that the superstructure admits decomposition into classical normal modes. The structural base is assumed to be a rigid plate of radius a and negligible thickness, and no slippage is allowed between base and soil. Formulated thus, the building-foundation system has $n + 2$ significant degrees-of-freedom, i.e. horizontal translation of each floor mass, horizontal translation of the base mass, and rotation of the system in the plane of motion.

Assuming small displacements and steady-state periodic excitation, the equations of motion of the building-foundation model shown in Fig. 1 can be expressed as

$$\begin{bmatrix} \mathbf{M} & \mathbf{M}_b \\ \mathbf{M}_b^T & \mathbf{M}_{bb} \end{bmatrix} \begin{Bmatrix} \mathbf{v} \\ \mathbf{v}_b \end{Bmatrix} + \begin{bmatrix} \mathbf{C} & \mathbf{0} \\ \mathbf{0} & \mathbf{C}_{bb}(\omega) \end{bmatrix} \begin{Bmatrix} \mathbf{v} \\ \mathbf{v}_b \end{Bmatrix} + \begin{bmatrix} \mathbf{K} & \mathbf{0} \\ \mathbf{0} & \mathbf{K}_{bb}(\omega) \end{bmatrix} \begin{Bmatrix} \mathbf{v} \\ \mathbf{v}_b \end{Bmatrix} = -\mathbf{f}_g(t) \quad (8)$$

In these equations, $\mathbf{v} = \{v_j\}$, a column vector, $v_j =$ horizontal displacement of the superstructure at the j th floor relative to the base mass, excluding rotations, $\mathbf{v}_b^T = (v_o, h_1\phi)$, vector of the base mass generalized displacements, $v_o =$ translation of the base mass relative to the free field motion, $\phi =$ rotation of the base mass, $v_g =$ free-field surface displacement, $h_j =$ height of the j th story above base mass, and

$$\mathbf{M}_b^T = \begin{bmatrix} m_1 m_2 & m_n \\ m_1 \frac{m_2 h_2}{h_1} & \frac{m_n h_n}{h_1} \end{bmatrix}, \quad \mathbf{M}_{bb} = \begin{bmatrix} \sum_{i=1}^n m_i + m_o & \sum_{i=1}^n \frac{m_i h_i}{h_1} \\ \sum_{i=1}^n \frac{m_i h_i}{h_1} & \sum_{i=1}^n \frac{m_i h_i^2}{h_1^2} + \frac{I}{h_1^2} \end{bmatrix} \quad (9)$$

and $\mathbf{f}^T = (m_1, m_2, \dots, m_n, (\sum_{i=1}^n m_i + m_o), (\sum_{i=1}^n m_i h_i / h_1))$, the effective forcing vector, $m_j =$ mass of the j th floor, $m_o =$ base mass, and $I =$ centroidal moment of inertia of the base and top masses. The displacement, $h_1\phi$ is used

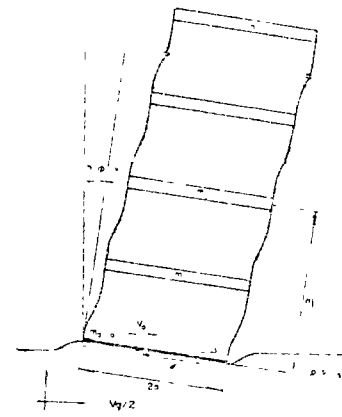


FIG 1—Model of Building-Foundation System

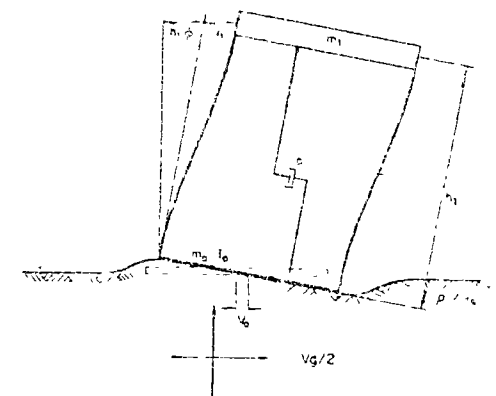


FIG 2—Single-Story Building Foundation System

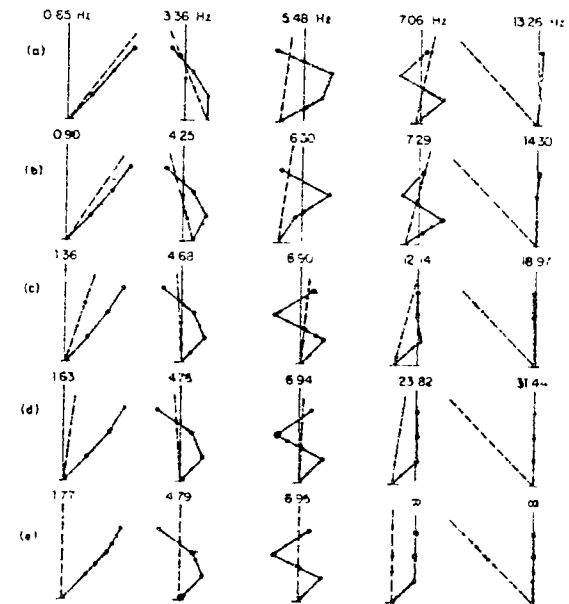


FIG 3—Mode Shapes and Undamped Natural Frequencies of Flexible Base Structure and Fixed-Base Structure, Dashed Curves Represent Base Rotation (a) $V_g = 100$ m/s, (b) $V_g = 150$ m/s, (c) $V_g = 300$ m/s, (d) $V_g = 600$ m/s, (e) Rigid Soil

as a measure of the base mass rotation in order to arrive at a set of homogeneous variables. This results in matrices and vectors having elements of the same dimensions.

Matrices $C_{bb}(\omega)$ and $K_{bb}(\omega)$ appearing in the system damping and stiffness matrices consist of terms representing the imaginary and real parts, respectively, of the frequency dependent dynamic stiffness of the foundation medium at the interface with the structural base. These terms can be interpreted as the damping and stiffness coefficients of equivalent frequency-dependent dampers and springs. In this representation, the springs account for the flexibility of the soil, whereas the dashpots account for the effect of energy dissipated by radiation and internal friction of the soil material.

The modal damping for the system under study can be obtained from Eq. 6 since Eq. 8 is of the form of Eq. 1. To find an expression for $\bar{\eta}_j$ in terms of the usual structural and soil properties, let the modal configuration, \bar{X}_j , of the building-foundation system be partitioned into its structural components, the corresponding vector being denoted by Y_j , and the corresponding base mass rigid body displacement, represented by $Z_j^T = \langle (v_o)_j, (h_1\phi)_j \rangle$;

$$\bar{X}_j^T = \langle Y_j^T, Z_j^T \rangle; \quad j = 1, 2, \dots, N \quad (10)$$

Vector Y_j may be expressed as a linear combination of modal configurations X_i of the fixed-base structure, for the set of these vectors, X_j , is a basis for the superstructure displacements, v . Thus

$$Y_j = \sum_{i=1}^n \alpha_{ij} X_i \quad (11)$$

in which $\alpha_{ij} = \frac{X_i^T M Y_j}{X_i^T M X_i}$ (12)

The corresponding expression for $\bar{\eta}_j$ is obtained by substituting Eqs. 10-12 into Eq. 6 and making use of the orthogonality of fixed-base modal configurations X_i with respect to the mass matrix, M :

$$\bar{\eta}_j = \sum_{k=1}^n \beta_{kj} \eta_k + \lambda_j; \quad j = 1, 2, \dots, N \quad (13)$$

in which $\beta_{kj} = \frac{(X_k^T M Y_j)^2}{(X_k^T M X_k)(\bar{X}_j^T M_o \bar{X}_j)} \frac{\omega_k}{\omega_j}$ (14)

$$\lambda_j = \frac{1}{2\omega_j} \frac{Z_j^T C_{rr}(\omega_j) Z_j}{\bar{X}_j^T M_o \bar{X}_j} \quad (15)$$

and ω_j and η_j are, respectively, the natural circular frequency and damping ratio of the j th mode of the fixed-base superstructure. Eq. 13 shows that all the structural modes contribute to the overall damping of a given mode. Coefficients β_{kj} measure the contributions of the various modal fractions of critical damping of the superstructure, and λ_j gives the damping ratio due to the energy dissipated by the soil. From Eq. 14 it follows, however, that β_k will be small for $k \neq j$ whenever the structural configuration of a given mode of the building-foundation system does not depart appreciably from the corresponding modal shape of the fixed-base superstructure.

The expression for $\bar{\eta}_j$ given by Eq. 13 was obtained for the structure shown

in Fig. 1. It is clear from the derivation of this equation that the formula is equally applicable to any linear superstructure having classical normal modes provided its base can be idealized as a rigid body. If the building foundation is not rigid, and therefore experiences differential settlements, the off-diagonal damping and stiffness matrices in Eq. 8 will not vanish; the expression for $\bar{\eta}_j$ will include an additional term representing the energy dissipated in the superstructure as a result of the relative displacements of the foundation. Because of the equivalence for linear systems between the modal method of analysis and the corresponding modal damping factor derived from the energy ratio criterion (1), Eq. 13 includes special cases rules (9,13) obtained for various specialized systems on the basis of this energy criterion.

APPLICATIONS

The steady-state response to sinusoidal excitation of some idealized building-foundation systems will next be examined to test the validity of the modal method previously developed. In addition to numerical examples, formulas for some of the more important parameters of response for single story structure-foundation systems will be presented and compared with those obtained earlier (7) from an exact solution.

Single-Story Structure on Viscoelastic Half Space.—For the first example, an idealized single-story interaction system will be considered, as shown in Fig. 2. The single-story structure of height h_1 is linear, viscously damped, and has a base mass resting on the surface of the half space with density ρ , shear modulus G , Poisson's ratio ν , and linear hysteretic damping coefficient D , defined as $1/4\pi$ times the ratio of the energy dissipated per cycle by a soil specimen under a steady-state harmonic motion, to the maximum strain energy stored in the specimen. Coefficient D is independent of the excitation frequency. For fixed-base response, the structure has stiffness k_1 , mass m_1 , undamped natural circular frequency $\omega_1 = (k_1/m_1)^{1/2}$, dashpot coefficient c_1 , and damping ratio $\eta_1 = c_1/(2m_1\omega_1)$.

The equations of motion of the system under study are given by Eq. 8 with n equal to unity. Matrices M , C , and K must be replaced with scalars m_1 , c_1 , and k_1 , respectively, and the displacement vector, v , has only one component,

v_1 . An explicit solution for the resulting version of Eq. 8 may be obtained under the assumption that the effect of the base mass, m_o , and centroidal moment of inertia I_o of the base and top masses on the response is small and may be neglected.

Another approximation frequently introduced in the analysis of the vibration of building-foundation systems resting on the surface of the ground is to neglect the coupling terms in the matrices, $C_{bb}(\omega)$ and $K_{bb}(\omega)$, which appear in Eq. 8, because they are generally small compared to the corresponding diagonal terms. Thus it is customary to assume that $C_{bb}(\omega)$ and $K_{bb}(\omega)$ are diagonal matrices of the form

$$C_{bb}(\omega) = \begin{bmatrix} c_{11}(\omega) & 0 \\ 0 & c_{\phi\phi}(\omega) \end{bmatrix} \dots \dots \dots (16)$$

$$\text{and } \mathbf{K}_{bb}(\omega) = \begin{bmatrix} k_{11}(\omega) & 0 \\ 0 & k_{\phi\phi}(\omega) \end{bmatrix} \quad (17)$$

Functions c_{11} , $c_{\phi\phi}$, and k_{11} , $k_{\phi\phi}$ represent the damping and stiffness coefficients of the equivalent frequency-dependent dampers and springs arising from the interaction force and moment between the base mass and the soil, and are given by

$$c_{11} = \frac{K_o a}{V_s} c_o^*(a_o, \nu, D); \quad c_{\phi\phi} = \frac{K_\phi a}{V_s h_1^2} c_\phi^*(a_o, \nu, D) \quad (18)$$

$$k_{11} = K_o k_o^*(a_o, \nu, D); \quad k_{\phi\phi} = \frac{K_\phi}{h_1^2} k_\phi^*(a_o, \nu, D) \quad (19)$$

in which K_j = static stiffness of the base mass in the direction, j , and

$$K_o = \frac{8Ga}{2 - \nu}; \quad K_\phi = \frac{8Ga^3}{3(1 - \nu)} \quad (20)$$

$V_s = (G/\rho)^{1/2}$ the shear wave velocity of the soil medium, and k_o^* and c_o^* = dimensionless real valued functions of Poisson's ratio, the loss ratio, D , and of the dimensionless frequency parameter, $a_o = \omega a/V_s$. Closed-form approximations for these functions are given in Ref. 18. (The notation, $\tan \delta$, is used for $2D$ in Ref. 18.)

With the first simplifying assumption described, the method of superposition leads to an explicit solution of Eq. 8, with only one associated mode. Thus, the eigenvalue problem

$$\mathbf{K}_o(\bar{\omega}_1) \bar{\mathbf{X}}_1 = \bar{\omega}_1^2 \mathbf{M}_o \bar{\mathbf{X}}_1 \quad (21)$$

which defines the natural frequency and modal shape of the single-story interaction system, has the closed-form solution

$$\frac{\bar{\omega}_1}{\omega_1} = \left[1 - \frac{k_1}{k_{11}(\bar{\omega}_1)} + \frac{k_1}{k_{\phi\phi}(\bar{\omega}_1)} \right]^{-1/2} \quad (22)$$

$$\text{and } \bar{\mathbf{X}}_1^T = \left\langle 1, \frac{k_1}{k_{11}(\bar{\omega}_1)}, \frac{k_1}{k_{\phi\phi}(\bar{\omega}_1)} \right\rangle \quad (23)$$

With this, the corresponding fraction of critical damping can be obtained immediately from Eq. 13

$$\bar{\eta}_1 = \left(\frac{\bar{\omega}_1}{\omega_1} \right)^3 \eta_1 + \frac{1}{2} \bar{\omega}_1^2 m_1 \left[\frac{c_{11}(\bar{\omega}_1)}{k_{11}^2(\bar{\omega}_1)} + \frac{c_{\phi\phi}(\bar{\omega}_1)}{k_{\phi\phi}^2(\bar{\omega}_1)} \right] \quad (24)$$

In the notation of Eq. 13, $\beta_{11} = (\bar{\omega}_1/\omega_1)^2$ for this problem. [Consideration of structural (frequency independent) damping would have led to an exponent of only two.] Since $\bar{\omega}_1/\omega_1 < 1$ for compliant soils, the contribution of the superstructure to the overall damping in the system can be considerably smaller than η_1 , even for relatively large values of $\bar{\omega}_1/\omega_1$.

Having specified the natural frequency and damping of an equivalent simple oscillator, the response of the interaction system to the earthquake motion,

$v_1(t)$ may be calculated from Eqs. 3 and 4. It remains to evaluate the effective excitation, $\hat{p}_1(t)$. Using Eq. 7 for this purpose and the impulse response function for the simple oscillator described by Eq. 3, the following solution is obtained for the system displacements: $\mathbf{u}^T(t) = (v_1(t), v_\phi(t), h_1 \phi(t))$:

$$\mathbf{u}(t) = -\frac{1}{\bar{\omega}_d} \bar{\mathbf{X}}_1 \int_0^t \exp[-\bar{\eta}_1 \bar{\omega}_1(t - \tau)] \sin[\bar{\omega}_d(t - \tau)] v_R^*(\tau) d\tau \quad (25)$$

$$\text{in which } \bar{\omega}_d = \bar{\omega}_1 (1 - \bar{\eta}_1^2)^{1/2} \quad (26)$$

$$\text{and } v_R^*(t) = \left(\frac{\bar{\omega}_1}{\omega_1} \right)^2 v_R(t) \quad (27)$$

Except for differences in notation, the result in Eqs. 22-27 is identical to that presented by Jennings and the writer (7). The earlier result was obtained from an exact solution by setting m_o , I_1 , and the off-diagonal terms in $\mathbf{C}_{bb}(\omega)$ and $\mathbf{K}_{bb}(\omega)$ equal to zero, as in the present analysis. In addition, only first-order soil and structural damping terms were retained in the expression for the overall damping in that solution.

The foregoing equations show that assuming the existence of uncoupled classical normal modes for the building-foundation system under study is equivalent to neglecting the second-order and higher-order soil and structural damping terms in the exact expression for the system damping coefficient. The error involved in this approximation is generally small.

To calculate the system displacements from the response of a one-degree-of-freedom oscillator resting on rigid ground, the original excitation has been replaced in Eq. 25 by an equivalent one with a factor $(\bar{\omega}_1/\omega_1)^2$. This replacement is not necessary in determining other response quantities; e.g., the maximum base shear, Q , of the interaction system is given by

$$Q = k_1 \hat{v}_1 = m_1 \omega_1^2 \hat{v}_1 \quad (28)$$

in which \hat{v}_1 = the peak value of $v_1(t)$. Let \hat{w}_1 be the maximum value of the relative displacement, $w_1(t)$, of a simple oscillator with circular natural frequency $\bar{\omega}_1$ and damping ratio $\bar{\eta}_1$ subjected to the original excitation, $v_R(t)$. Clearly, \hat{v}_1 and \hat{w}_1 are related by

$$\hat{v}_1 = \left(\frac{\bar{\omega}_1}{\omega_1} \right)^2 \hat{w}_1 \quad (29)$$

and therefore, Q may be expressed in terms of \hat{w}_1 as

$$Q = m_1 \bar{\omega}_1^2 \hat{w}_1 \quad (30)$$

This equation shows that the maximum base shear of the single-story building-foundation system shown in Fig. 2 is given directly in terms of the spectral value of the pseudoceleration of the simple oscillator corresponding to a base acceleration, $v_R(t)$.

The preceding analysis was developed for a direct model of a one-story building-foundation system. More generally, it may be viewed as the first-mode approximation of a multistory system. Approximate values of the fundamental frequency, $\bar{\omega}_1$, and damping factor $\bar{\eta}_1$ can be obtained from Eqs. 22-24, provided

the parameters, k_i , m_i , and h_i , are replaced with the corresponding modal parameters (7). With $\bar{\omega}_1$ and $\bar{\eta}_1$ determined, the approximate response of the fundamental mode can be calculated from

$$\langle v^T(t), v_o(t), h_1 \phi(t) \rangle = \frac{\sum_i m_i X_{i1}}{\sum_i m_i X_{i1}^2} \left(\frac{\bar{\omega}_1}{\omega_1} \right)^2 \left\langle X_{11}^T, \frac{k_1}{k_{v_1}(\bar{\omega}_1)} X_{11}, \frac{k_1}{k_{\phi\phi}(\bar{\omega}_1)} X_{11} \right\rangle w_1(t) \quad (31)$$

in which $w_1(t)$ is the previously defined relative displacement of the equivalent single-degree damped oscillator.

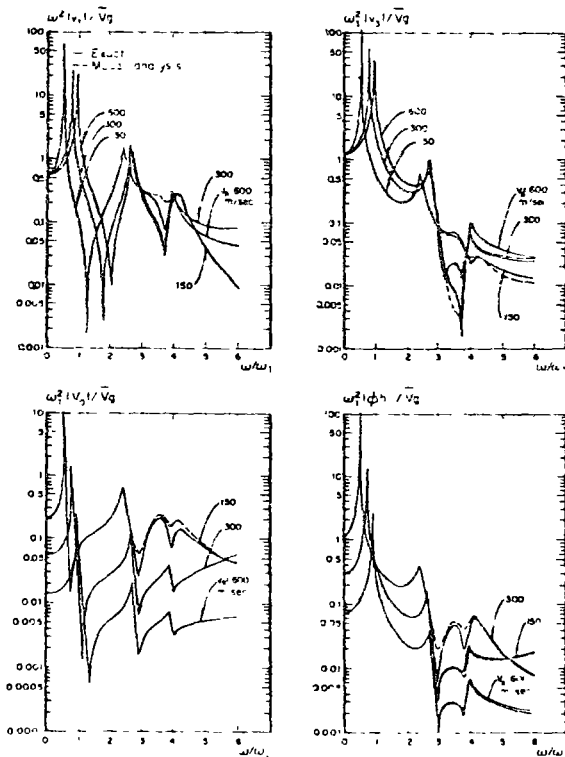


FIG 4—Amplification Ratios for Frequency Response of Three-Story Building-Foundation System ($D = 0$)

Multistory Structures on Viscoelastic Half Space—The steady-state response of an idealized three-story system of the type shown in Fig. 1 will be used to show the application of the analysis to multistory building foundation systems. To evaluate the accuracy attained by the modal approach, results will be compared

with those from an exact solution. Additional examples are provided in Ref. 1.

The structure has masses $m_i = 15,000$ kg (16.6 ton), base mass $m_o = 30,000$ kg (33.1 ton), story heights of 3.5 m (11.5 ft); and a circular base mat with radius of 1.75 m (5.75 ft). The corresponding natural frequencies and modal configurations are shown in the first three columns of Fig. 3(e). A uniform modal damping, $\bar{\eta}_j = 2\%$ critical ($j = 1, 2, 3$), has been assumed for the fixed-base structure.

The foundation soil has a unit mass of $2,000$ kg/m³ (125 pcf) and Poisson's

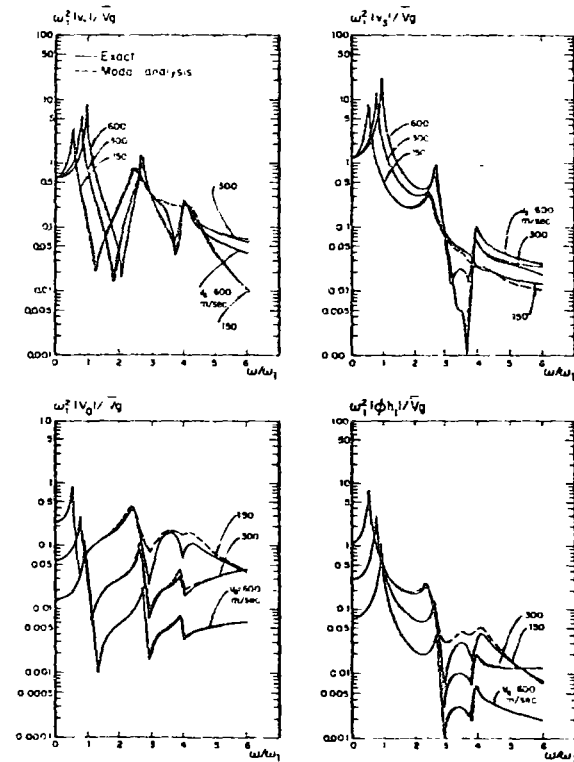


FIG 5—Amplification Ratios for Frequency Response of Three-Story Building-Foundation System ($D = 0.10$)

ratio, ν , of 0.45. Four different soil stiffnesses will be considered. In terms of the shear wave velocity, $V_s = 100$ m/s (328 fps), 150 m/s (492 fps), 300 m/s (984 fps), and 600 m/s (1,967 fps).

The response of the idealized structure to a steady-state acceleration, $\ddot{v}_g(t)$, of amplitude \bar{v}_g has been calculated for several soil conditions. Figs. 4 and 5 give frequency response curves for the amplitudes of v_1 , v_3 , $h_1 \phi$ and v_o , in dimensionless form for different values of V_s and the material damping factor, D . To assess the accuracy of the approximate analysis, two frequency response curves have been included in these figures, one obtained by the modal approach specified

TABLE 1—Modal Contribution to Effective Damping Three-Story Structure

V_s , in meters per second (feet per second) (1)	Mode number, i (system) (2)	Structural Contribution			Soil Contribution			Overall damping, $\bar{\eta}_i$ (8)
		Mode 1 (3)	Mode 2 (4)	Mode 3 (5)	Translation (6)	Rocking (7)		
600 (1,967)	1	1.57×10^{-2}	6.99×10^{-8}	4.11×10^{-9}	7.05×10^{-1}	1.43×10^{-2}	3.07×10^{-2}	
	2	3.53×10^{-5}	1.97×10^{-2}	2.26×10^{-8}	7.61×10^{-4}	5.00×10^{-4}	2.10×10^{-2}	
	3	2.13×10^{-5}	2.41×10^{-7}	1.99×10^{-2}	3.54×10^{-4}	7.35×10^{-5}	2.03×10^{-2}	
	4	1.01×10^{-5}	6.39×10^{-4}	1.70×10^{-4}	2.27×10^{-4}	4.13×10^{-5}	2.30×10^{-1}	
	5	5.12×10^{-2}	6.87×10^{-4}	9.84×10^{-5}	3.97×10^{-4}	9.92×10^{-2}	1.52×10^{-1}	
300 (984)	1	8.96×10^{-3}	2.85×10^{-7}	1.75×10^{-5}	2.07×10^{-1}	3.98×10^{-2}	5.08×10^{-2}	
	2	2.46×10^{-4}	1.86×10^{-2}	1.02×10^{-6}	5.09×10^{-1}	1.24×10^{-3}	2.51×10^{-2}	
	3	2.09×10^{-4}	1.79×10^{-5}	1.95×10^{-2}	2.75×10^{-1}	1.09×10^{-4}	2.26×10^{-2}	
	4	6.94×10^{-4}	1.80×10^{-3}	5.56×10^{-4}	2.17×10^{-1}	1.57×10^{-3}	2.22×10^{-1}	
	5	8.63×10^{-2}	1.13×10^{-1}	2.18×10^{-4}	1.22×10^{-1}	7.32×10^{-2}	1.62×10^{-1}	
150 (492)	1	2.63×10^{-3}	2.44×10^{-2}	1.57×10^{-8}	3.85×10^{-1}	7.12×10^{-2}	7.77×10^{-2}	
	2	3.59×10^{-4}	1.14×10^{-2}	3.34×10^{-5}	6.22×10^{-2}	2.80×10^{-3}	7.68×10^{-2}	
	3	1.56×10^{-5}	6.44×10^{-3}	5.42×10^{-1}	1.03×10^{-1}	3.47×10^{-4}	1.17×10^{-1}	
	4	5.77×10^{-6}	2.64×10^{-3}	1.45×10^{-2}	5.59×10^{-2}	1.22×10^{-3}	7.42×10^{-2}	
	5	1.15×10^{-1}	1.55×10^{-3}	3.91×10^{-4}	1.24×10^{-1}	4.25×10^{-2}	1.61×10^{-1}	
100 (328)	1	9.75×10^{-4}	1.20×10^{-7}	7.86×10^{-9}	4.55×10^{-1}	8.32×10^{-2}	8.87×10^{-2}	
	2	6.63×10^{-5}	2.88×10^{-3}	3.97×10^{-5}	1.59×10^{-1}	4.08×10^{-3}	1.66×10^{-1}	
	3	2.01×10^{-5}	1.69×10^{-2}	6.24×10^{-4}	5.38×10^{-2}	8.82×10^{-3}	7.34×10^{-2}	
	4	3.97×10^{-4}	8.10×10^{-4}	1.92×10^{-2}	6.76×10^{-3}	4.47×10^{-4}	2.76×10^{-2}	
	5	1.24×10^{-1}	1.70×10^{-1}	4.71×10^{-4}	9.31×10^{-4}	3.03×10^{-2}	1.57×10^{-1}	

Note: $D = 0.10$, $\eta_1 = 2 \times 10^{-2}$; $Q = 1, 2, 3$

by Eqs. 3-7 and 13 and the other by the exact method, the latter corresponds to the direct numerical solution of the system of algebraic equations obtained from Eq. 8 for each value of the exciting circular frequency, ω . Agreement between the two sets of curves is excellent even when effects of soil-structure interaction are highly pronounced. This suggests that no significant differences are to be expected in the response to earthquake motion of the system analyzed, as calculated by the modal method or by a more rigorous approach, such as that provided by the Fourier operational method (3,7,8,16).

Figs. 4 and 5 show the main effects of soil-structure interaction on the steady-state response of building-foundation systems. Interaction reduces the resonant frequencies from those of the structure on a rigid base, and the magnitude of the peak values of the response changes with respect to that of the building on rigid ground, reflecting the change in the critical damping ratio from η_1 to $\bar{\eta}_1$. These changes in natural frequency, effective amount of damping, and mode shapes, are shown in greater detail in Fig. 3 and Table 1.

Vibration modes and corresponding undamped natural circular frequencies of the three-story structure are shown in Fig. 3 for several values of V_s . The results show that the fundamental frequency is reduced considerably on soft soil, but that the remaining frequencies corresponding to the structural modes decrease more slowly. The two additional frequencies, which arise from the introduction of rocking and relative lateral motion of the base, decrease monotonically from infinity for decreasing V_s .

Five modal shapes are depicted in each case, three associated with the structural modes, and two additional ones, arising from the introduction of rigid body motion of the base. For the rigid case [Fig. 3(e)] the first three curves give the modal shapes of the superstructure and the others represent the limiting cases of the two additional modes, one corresponds to a lateral displacement and the other to a rotation of the base. The structural masses remain fixed for these two modes.

The remaining cases show the relative contribution of the structural deformation and of the base translation and rocking to the total mass displacements. For each value of V_s , the modal configurations are arranged in order of ascending frequency. In this arrangement the first three modes represent essentially perturbed versions of the corresponding rigid-base modes, provided the soil is relatively stiff. For soft soil a change occurs and a perturbed structural mode becomes associated with a higher frequency as shown in Fig. 3(b), where for $V_s = 150$ m/s the fourth mode shape is related to the third structural mode.

Table 1 presents the critical damping ratios, $\bar{\eta}_i$, of the three-story system, for $D = 0.10$. This table includes individual contributions of the structure and of the foundation damping elements to the composite damping in the system, as determined from Eq. 13. For a given mode of the system and value of V_s , the corresponding line in Table 1 yields the value of the soil damping due to rocking and lateral translation of the foundation base and of the individual structural modal damping contributions. Each term represents a fraction of critical damping, and the sum of these terms gives $\bar{\eta}_i$. Results in this table show that for the perturbed structural modes, the off-diagonal participation factors, β_{ki} , are significantly smaller than β_{ii} , suggesting that for practical applications the summation in Eq. 13 can be replaced with $\beta_{ii}\eta_i$. In this case, however, subscript i ranges only over the n values corresponding to the perturbed structural modes.

This simplification is not applicable to the two new modes for which β_{ij} ($k \neq j$) can exceed β_{jj} .

Participation factor β_{jj} remained in all cases below one for the examples considered in this study. Attempts to prove the validity of this observation for arbitrary structures were unsuccessful. However, it can be shown from Eq. 14 that β_{jj} always satisfies this condition and that $\omega_j/\bar{\omega}_j$ is an upper bound for β_{jj} .

Table 1, Figs. 4 and 5, and the additional results presented in Ref. 1 indicate that the contribution of the soil to the overall damping factor is strongly dependent upon the material damping, showing a definite increase for increasing values of D . This effect is predominant in rocking but is also present in the relative lateral translation of the base. System damping associated with the modal damping of the superstructure is, as expected, practically independent of D . For the multistory building-foundation systems used in the examples, however, soil-structure interaction produces a significant reduction on the fundamental mode contribution of the superstructure to the total damping $\bar{\eta}_1$, thus leading to a net reduction ($\bar{\eta}_1 < \eta_1$) when material damping is not included in the analysis. Net increases result for $D = 0.1$. The effects of these increases or reductions clearly affect the response of the system. Thus, in Figs. 4 and 5 it is seen that whereas the peak amplitude of the response grows for decreasing values of V_s for vanishing D , the opposite is true for $D = 0.10$.

SUMMARY AND CONCLUSIONS

A method of modal superposition has been presented for calculating the earthquake response of linear structures with foundation interaction. Modal damping in the system, $\bar{\eta}_1$, was determined by formally extending the classical method of modal analysis. To estimate the accuracy of the method suggested, analytical and numerical studies were performed. The first example concerned a single-story three-degree-of-freedom building-foundation system, which has substantial variation in the damping and stiffness of individual components. An explicit analytical solution for the earthquake response of the system was obtained by the modal method and compared with the results of an exact analysis; this showed that application of the approximate modal method of superposition is equivalent to neglecting the second order and higher-order soil and structural damping terms in the exact analysis. Numerical examples illustrate the applicability of the modal method to multistory structures supported on viscoelastic soils with hysteretic damping. Results of this method and those of an exact analysis are presented in the form of transfer functions. Excellent agreement is found between the two solutions.

From the cases studied it seems that the proposed modal method of analysis provides a sufficiently accurate technique for determining the response of linear building-foundation systems. The method should prove most useful when the response is dominated by only a few modal components.

In the development of the theory it was assumed that the stiffness matrix $K_{ij}(\omega)$ may be approximated by the constant value $K_{ij}(\bar{\omega}_j)$. This is reasonable whenever the soil stiffness components do not vary too rapidly with the excitation frequency or when the fundamental mode dominates the system response. If this is not the case the actual values of K_{ij} may have to be considered for

the evaluation of each natural frequency. Further comparative studies may be in order to determine the range of applicability of the method to a more general class of problems governed by Eq. 1 than the ones considered in this paper. Satisfactory results would be expected whenever the corresponding transfer functions have distinct peaks that resemble those obtained for time-invariant linear systems having classical normal modes.

ACKNOWLEDGMENTS

The numerical calculations reported in this paper were made by Víctor J. Palencia. His assistance is gratefully acknowledged. The writer also would like to thank Niels C. Lind and Emilio Rosenblueth for critical reading of the manuscript.

APPENDIX I—REFERENCES

1. Brelak, J., "Modal Analysis for Building-Soil Interaction," *Report E17*, Instituto de Ingeniería, Universidad Nacional Autónoma de México, México, D. F., July, 1975.
2. Castellani, A., "Foundation Compliance Effects on Earthquake Response Spectra," *Journal of the Soil Mechanics and Foundations Division, ASCE*, Vol. 96, No. SM4, Proc. Paper 7425, July, 1970, pp. 1335-1355.
3. Chopra, A. K., and Gutiérrez, J. A., "Earthquake Analysis of Multistory Buildings Including Foundation Interaction," *Earthquake Engineering and Structural Dynamics*, Vol. 3, 1974, pp. 65-77.
4. Chu, S. L., Agrawal, O. K., and Singh, S., "Finite Element Treatment of Soil-Structure Interaction Problem for Nuclear Power Plant Under Seismic Excitation," *Proceedings of the 2nd International Conference on Structural Mechanics in Reactor Technology*, Berlin, Germany, Sept., 1973.
5. Izenberg, J., and Ailham, S. A., "Interaction of Soil and Power Plants in Earthquakes," *Journal of the Power Division, ASCE*, Vol. 98, No. PO2, Proc. Paper 9242, Oct., 1972, pp. 273-291.
6. Jacobsen, L. S., "Damping in Composite Structures," *Proceedings of the 2nd World Conference on Earthquake Engineering*, Tokyo, Japan, Vol. 2, 1960, pp. 1029-1044.
7. Jennings, P. C., and Brelak, J., "Dynamics of Building-Soil Interaction," *Bulletin of the Seismological Society of America*, Vol. 63, 1973, pp. 9-48.
8. Liu, S. C., and Fagel, L. W., "Earthquake Interaction by Fast Fourier Transform," *Journal of the Engineering Mechanics Division, ASCE*, Vol. 97, No. EM4, Proc. Paper 8324, Aug., 1971, pp. 1223-1237.
9. Novak, M., "Effect of Soil on Structural Response to Wind and Earthquake," *Earthquake Engineering and Structural Dynamics*, Vol. 3, 1974, pp. 79-96.
10. Novak, M., "Additional Note on the Effect of Soil on Structural Response," *Earthquake Engineering and Structural Dynamics*, Vol. 3, 1975, pp. 312-315.
11. Parmelee, R. A., Perelman, D. S., and Lee, S. L., "Seismic Response of Multiple-story Structure on Flexible Foundations," *Bulletin of the Seismological Society of America*, Vol. 59, 1969, pp. 1061-1070.
12. Ramer, J. H., "Damping in Dynamic Structure-Foundation Interaction," *Canadian Geotechnical Journal*, Vol. 12, 1975, pp. 13-22.
13. Roesset, J. M., Whitman, R. V., and Dohy, R., "Modal Analysis for Structures with Foundation Interaction," *Journal of the Structural Division, ASCE*, Vol. 99, No. ST3, Proc. Paper 9603, Mar., 1973, pp. 399-416.
14. Seed, H. B., Lysmer, J., and Hwang, R., "Soil-Structure Interaction Analysis for Seismic Response," *Journal of the Geotechnical Engineering Division, ASCE*, Vol. 101, No. GT5, Proc. Paper 11318, May, 1975, pp. 439-457.
15. Tsai, N. C., "Modal Damping for Soil-Structure Interaction," *Journal of the Engineering Mechanics Division, ASCE*, Vol. 100, No. EM3, Proc. Paper 10603, Apr., 1974, pp. 323-341.

- 16 Vaish, A. K. and Chopra, A. K., "Earthquake Finite Element Analysis of Structure-Foundation Systems," *Journal of the Engineering Mechanics Division*, ASCE, Vol. 100, No. EM6, Proc. Paper 10990, Dec. 1974, pp. 1011-1016.
- 17 Veletsos, A. S. and Meek, J. W., "Dynamic Behavior of Building-Foundation Systems," *Earthquake Engineering and Structural Dynamics*, Vol. 3, 1974, pp. 121-138.
- 18 Veletsos, A. S. and Verbic, B., "Vibration of Viscoelastic Foundations," *Earthquake Engineering and Structural Dynamics*, Vol. 2, 1973, pp. 87-102.

APPENDIX II.—NOTATION

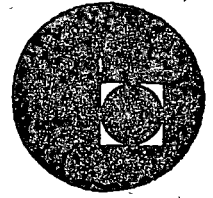
The following symbols are used in this paper

- a_o = dimensionless frequency parameter,
 \mathbf{C}, \mathbf{C}_o = damping matrices of fixed-base structure and structure-foundation system;
 \mathbf{C}_{bb} = damping matrix of foundation medium at interface with structural base,
 $c_1, c_{\psi}, c_{\phi\phi}$ = dashpot "constants";
 D = hysteretic damping ratio,
 \mathbf{K}, \mathbf{K}_o = stiffness matrices of fixed-base structure and structure-foundation system,
 \mathbf{K}_{bb} = stiffness matrix of foundation medium at interface with structural base,
 K_j = static stiffness of disk in j direction,
 $k_1, k_{\psi}, k_{\phi\phi}$ = spring "constants";
 k_j^v, c_j^v = dimensionless real-valued functions of ν , D , and a_o (17);
 \mathbf{M}, \mathbf{M}_o = mass matrices of fixed-base structure and foundation-structure system,
 m_o, m_i = mass of base and structural floor,
 Q = maximum base shear;
 q_j = generalized coordinates of problem (see Eq. 3);
 $\mathbf{u}, \mathbf{u}, \ddot{\mathbf{u}}$ = displacement, velocity, and acceleration vectors,
 V_s = shear wave velocity of soil,
 \mathbf{v} = displacement vector of superstructure,
 v_o = translation of base mass relative to free-field motion,
 $(v_o)_i$ = modal translation of base mass relative to free-field motion;
 \ddot{v}_g = input free-field acceleration,
 \ddot{v}_g^R = amplitude of free-field input acceleration;
 $\mathbf{X}_j, \tilde{\mathbf{X}}_i$ = modal shape of fixed-base structure and building-foundation system;
 \mathbf{Y}_i = modal displacement of superstructure,
 \mathbf{Z}_i = modal displacement of base mass,
 β_{ki} = weighting factor (see Eq. 13);
 $\eta_j, \bar{\eta}_k$ = critical damping ratio per mode of fixed-base structure and building-foundation system,
 λ_j = soil contribution to overall damping (see Eq. 13);
 ϕ = rocking of base,
 $(\phi)_i$ = modal base rocking,
 ω = circular frequency of excitation, and
 $\omega_j, \bar{\omega}_k$ = circular natural frequency of fixed-base structure and building-foundation system

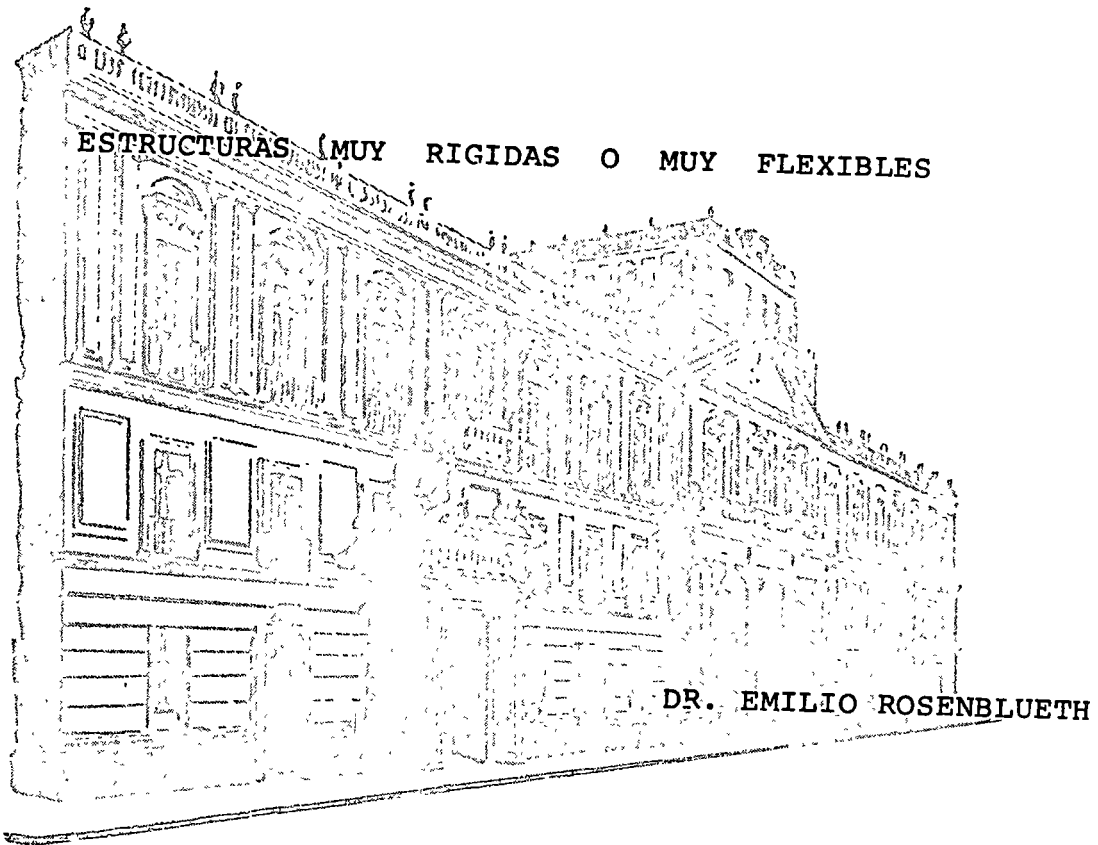




centro de educación continua
división de estudios superiores
facultad de ingeniería, unam

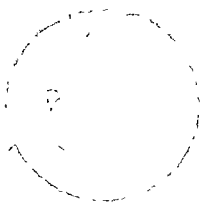


ANALISIS DINAMICO DE ESTRUCTURAS
ESPECIALES



JULIO_AGOSTO, 1977.

'edc



ALTERNATIVE DISPUTE RESOLUTION
CENTRE OF EXCELLENCE
FOR THE PROVINCE OF ONTARIO
AND TERRITORIES



ALTERNATIVE DISPUTE RESOLUTION
CENTRE OF EXCELLENCE

CIVIL ENGINEERING ABSTRACT

Approximate Design for Multicomponent Earthquakes, by Emilio Rosenblueth and Humberto Contreras. (EM) Using reasonable assumptions it is shown that a structure's survival under simultaneous action of several earthquake components corresponds to a response ellipsoid falling inside a failure surface. An approximate practical method is proposed to verify this condition. Method uses linear combination of responses to individual components.

APPROXIMATE DESIGN FOR MULTICOMPONENT EARTHQUAKES

KEY WORDS: Beams; bridges; buildings; chimneys; columns; design; dynamics; earthquakes; engineering mechanics; failure; pipelines; probability theory; safety; statistical analysis; stresses; structural engineering; towers; vibration.

Current design criteria intend to provide values of structural responses to a single component of a design earthquake, at a fixed exceedance probability. It is desirable to know whether a structure is safe, at that reliability level, under the combined effect of several simultaneous earthquake components. If the component accelerograms are idealized as zero-mean Gaussian processes and the structure behaves linearly, then structural responses associated with a given exceedance probability define an ellipsoid in the response space. In this space, points falling inside the failure surface (interaction surface) correspond to survival; those outside, to failure. A structure is safe, at the specified reliability level, if the corresponding ellipsoid falls entirely within the survival region. Computations to verify this condition are, however, quite awkward. An approximate method is developed which replaces computation of the ellipsoid coordinates with that of a linear combination of responses to individual components. Maximum possible errors introduced by the approximation are evaluated and found ordinarily to be acceptable.

REFERENCE: "Approximate Design for Multicomponent Earthquakes," Emilio Rosenblueth and Humberto Contreras, Journal of the Engineering Mechanics Division, ASCE, Vol. No. EM, Proc. Paper

APPROXIMATE DESIGN FOR MULTICOMPONENT EARTHQUAKES

Emilio Rosenblueth,¹ F. ASCE, and Humberto Contreras²

Introduction

It has been customary to design structures so that they resist the envelope of effects of the various components of earthquake motion as though these components acted one at a time. There is growing consciousness that design should recognize the simultaneous action of all the components. Such consciousness begins to be reflected in building code requirements and there is need to develop a practical procedure to fulfill these requirements. Emphasis is on practical, for rigorous criteria demand an unwarranted effort on the designer's part.

This paper is written under the assumption that the structure of interest has been analyzed for every component of motion deemed significant. In the simplest case such components include motion only along two orthogonal horizontal directions. For a structure founded on a rigid base in a strongly seismic area the number of significant components can be as high as six (three in translation and as many in rotation), and in a long structure on several supports (such as a bridge or a supported pipeline) this number can be much greater. Criteria for the combination of the various components, based on a stochastic treatment of the disturbances, are expounded and an approximate procedure is proposed which minimizes the maximum possible errors caused by the simplifications adopted.

The Three Translational Components at a Point

First consider two horizontal components, along axes X and Y , perpendicular to each other. Let S_X and S_Y denote the corresponding undamped intensities in Housner's sense (4), that is, the integrals of the respective spectral pseudo-

¹Prof. of Engng., Universidad Nacional Autónoma de México, Mexico, DF.

²Grad. Research Assist., Instituto de Ingeniería, Universidad Nacional Autónoma de México, Mexico, DF.

velocities in ft/sec (3.3 times the spectral pseudovelocities in m/sec), in the interval of periods of 0.1 to 2.4 sec, and let $S_X \leq S_Y$. It is known (5) that $E(S_X/S_Y)$ is an increasing function of $(S_X^2 + S_Y^2)^{1/2}$, where $E(\cdot)$ = expectation, and that when $(S_X^2 + S_Y^2)^{1/2} > 4.5$ the expected intensity ratio exceeds 0.9. Now, in view of the usual relations between spectral pseudovelocities and maximum ground velocity and between the latter and the modified Mercalli intensity (5), $(S_X^2 + S_Y^2)^{1/2} = 4.5$ corresponds to an intensity somewhat smaller than 5 in the latter scale. Consequently $E(S_X/S_Y)$ will almost always exceed 0.9 in cases of practical interest; indeed, S_X/S_Y will rarely lie below this value. The assumption that horizontal ground-motion intensity is independent of direction, as specified in all known building codes, simplifies the calculations and introduces no more than small errors on the safe side. It will accordingly be adopted.

Under some conditions it is important to take into account the vertical component of ground motion (8) and for slender structures the rotational components can be significant (9). In yet other structures additional components can demand attention.

It has been found that ordinarily there is correlation between orthogonal horizontal translational components (6). The correlation is nil, however, among three orthogonal directions, which may be called the motion's principal directions. This statement should be interpreted as follows. Let U, V, and W denote three orthogonal directions and u, v, and w the corresponding ground motions. For a given time interval 0, t, the variances and covariances of the ground acceleration are

$$\text{Var } \ddot{u} = \int_0^t \ddot{u}^2 d\tau \quad (1)$$

$$\text{Cov}(\ddot{u}, \ddot{v}) = \int_0^t \ddot{u}\ddot{v} d\tau \quad (2)$$

where dots denote time derivatives, and similarly for the other accelerations and pairs of these variables. Given t, there are three orthogonal directions such that the covariances of the accelerations are nil. Penzien and Watabe (6) have found

that after the first few seconds following the beginning of an earthquake, these directions vary little with τ and are oriented roughly as follows; one direction towards the earthquake epicenter; one vertically; and so the third is horizontal and perpendicular to the first direction.

Var \ddot{u} as defined in Eq. 1 is known as the Arias intensity (2) in the direction U when t equals the earthquake duration. It is closely related to the Housner and the modified Mercalli scales. Hence, the assumption $S_x \cong S_y$ amounts to $\text{Var } \ddot{x} \cong \text{Var } \ddot{y}$. Assuming that ground translation is the result of superimposing three orthogonal, stochastically independent motions, two of them horizontal and having equal Arias intensities, implies that there is no correlation between motions along any pair of orthogonal horizontal directions.

Ground accelerations are zero-mean processes, for their probability densities are assumed to be even functions. This, together with the foregoing results, lends weight to the assumption that for arbitrary group of three instants, t_1 , t_2 , and t_3 , ground accelerations $\ddot{x}(t_1)$, $\ddot{y}(t_2)$, and $\ddot{z}(t_3)$ along three orthogonal directions X , Y , and Z , of which the latter is vertical, are uncorrelated. Under these conditions the responses of any linear structure to these three disturbances are also uncorrelated. This statement follows immediately from the relation

$$r_{xi}(t) = \int_0^t \ddot{x}(\tau) \psi_{xi}(t - \tau) d\tau \quad (4)$$

where $r_{xi}(t)$ = i th structural response of interest (generalized force or generalized deformation) at time t due to the disturbance \ddot{x} , and ψ_{xi} = transfer function for response r_{xi} (5).

The state of the system or of any part thereof (even the state of any arbitrary cross section of a member in the system) at every instant t is defined by a set of responses $r_i(t)$, $i = 1, 2, \dots, n$, where $r_i(t) = r_{oi} + r_{xi}(t) + r_{yi}(t) + r_{zi}(t)$, and r_{oi} is the value of r_i due to gravity loads. When r_{xi} , r_{yi} , and r_{zi} are uncorrelated, the variance of $r_i(t)$ equals the sum of the corresponding variances. If the state

of the system is represented by vector $\underline{r}(t) = \{r_i(t)\}$ in an n-dimensional space in which each cartesian coordinate corresponds to one of the r_i 's, the point representing $E(\bar{r})$ lies at $\underline{r}_0 = \{r_{0i}\}$, for if \ddot{x} , \ddot{y} , and \ddot{z} are zero-mean processes so are r_{xi} , r_{yi} , and r_{zi} and hence so is r_i . The square roots of the covariances of vector $\underline{r}(t)$ define an ellipsoid in this space, with center at \underline{r}_0 . If the ground accelerograms are Gaussian processes, responses associated with any fixed exceedance probability are proportional to the corresponding standard deviations. Surfaces joining points of equal exceedance probability are then geometrically similar concentric ellipsoids, and their axes equal the root of the sum of squared responses to individual components.

This conclusion can be used as basis for solving the problem of analysis -- by finding out whether the ellipsoid for a prescribed exceedance probability lies inside the failure surface (more generally, whether it lies inside the surface associated with a given limit state) -- and of design -- by finding the structural parameters for which the limit-state surface of interest is tangent to or lies just outside the ellipsoid in question. Both tasks are excessively demanding. A simpler, approximate procedure will be developed subsequently.

Despite the foregoing remarks, on horizontal ground there must always be some measure of correlation between the vertical and every horizontal component, especially if the maximum responses occur near the end of the earthquake. The vertical and horizontal components of Rayleigh waves, for example, are perfectly correlated (5). If the different components excite different natural periods of vibration and the corresponding frequencies lie sufficiently wide apart, the squares of modal responses are additive, as are modal responses to a single component when, again, the natural frequencies are not too close to each other (5). In this case, then, responses to the different components are practically uncorrelated no matter the degree of correlation among the components.

If two or three correlated components excite the same natural modes one can compute the modal responses combining the effects of these components and taking

the correlations into account. A more difficult situation arises when the correlated components excite natural modes whose frequencies lie close to each other. This case will not be dealt with here.

Other Ground-Motion Components

The foregoing scheme carries over to other earthquake components under many practical situations. For example, the rotational component about a horizontal axis in Rayleigh waves of a given frequency is completely correlated with the horizontal component perpendicular to this axis, as it is with the vertical component. In Love waves of given frequency the rotational component about a vertical axis is completely correlated with the horizontal component perpendicular to the direction of wave travel (9). One can also expect some correlation, after appropriate time shifts, among the ground motions that excite the different piers of a bridge. In most cases of practical interest such correlations can be incorporated in the analysis and one is left with a structural system (or subsystem or critical section) whose response to gravity and earthquake, for any given exceedance probability, is defined in the space of vector R_0 by an ellipsoid with center at R_0 and with radii parallel to the coordinates, equal to $R_i = (\sum_{j=1}^m R_{ij}^2)^{1/2}$, where subscript i refers to each coordinate in the state space and subscript j refers to each of the m ground-motion components.

Failure Surfaces

For every structural-member section, structural subsystem, and system and for every given limit state there is a surface defined by $F(R) = 0$, called the failure surface, such that its interior, called the safe domain, contains all points associated with conditions in which the section, subsystem, or system does not enter the given limit state. At a prescribed level of probability, the section, subsystem, or structure does not enter the limit state if and only if the pertinent ellipsoid lies completely inside the safe domain.

Analyses described in the foregoing paragraphs imply linear behavior of the

structure. Rigorously, then, every section must behave linearly and hence every failure surface is a convex polyhedron. Consistently with building codes and established practice, though, one ought to be able to find generalized forces assuming linear behavior, modified in a crude manner to account for overall ductility, and to design or verify whether the structure or any of its parts enters a limit state by locally recognizing pronouncedly nonlinear behavior when the structure has appreciable ductility. Failure surfaces are then curved and in almost all cases convex.

The last statement merits some remarks, as the assumption that failure surfaces are convex plays a role in computing the maximum errors that can be introduced by the approximate method to be developed subsequently. Drucker (3) has shown that failure surfaces are convex if the coordinates of the state space are generalized forces and the stress-strain curves of the structure's constitutive materials do not have descending branches. The first requirement is important since failure surfaces are often nonconvex if one chooses external forces rather than generalized forces as coordinates when failure involves buckling of members made of nonlinear materials. The limitation can be disposed of by using forces at sections rather than external member-forces as coordinates to represent states of a structural member. The requirement that the stress-strain curve have everywhere non-negative slope is less restrictive, for practically all failure surfaces for structural-member sections are known to be convex even if the structural materials have a descending branch. Figs. 1 and 2 show typical failure "surfaces," respectively for a column section under longitudinal force and bending and for a reinforced concrete section under biaxial bending and a constant longitudinal compressive force.

In those exceptional cases when the failure surface is not convex, one can use the approximate procedure in this paper at the risk of introducing errors on the unsafe side greater than the bounds to be found subsequently, or one may resort to the more rigorous approach dealing directly with the state ellipsoid.

Approximate Procedure

In general the state ellipsoid (or response ellipsoid) has inclined axes and the failure surface does not admit simple description. The task of finding out whether the ellipsoid lies entirely within the safe domain and that of selecting a failure surface that will lie just outside the ellipsoid are excessively awkward for routine design. An approximate procedure will accordingly be expounded which replaces the ellipsoid with 2^n points, where n = number of ground-motion components. With what is usually a small sacrifice of accuracy the procedure will be simplified so that only 2^n points are needed. Sometimes, inspection will disclose that a single such point suffices.

The coordinates of these points will be chosen to be those of the vectors

$$\underline{R} = \underline{R}_0 + \sum_{i=1}^n \alpha_i \underline{R}_i \quad (3)$$

where the α 's are coefficients and \underline{R}_i = response to i th component of ground motion. The linear form of Eq. 3 is chosen for the sake of simplicity. Also for this sake the condition will be imposed that coefficients α_i not depend on the structure nor on the disturbance. In principle the α 's should be computed so that utility be maximized taking into account the relative frequencies with which different types of structures will be designed, the different types of earthquakes that will occur, the implications of the choice of the α 's on initial costs and failure rates, and the consequences of failure. Lacking this, the coefficients will be computed so that the maximum possible errors introduced in the amplitude of the seismic-response vector by Eq. 3 will be minimum under the assumption that failure surfaces are always convex. In what follows the term "error" will be taken to mean the difference between the length $\|\underline{R}\|$ of vector \underline{R} computed using Eq. 3 and the "exact" $\|\underline{R}\|$, divided by the "exact" $\|\underline{R}\|$. Quotation marks are used around the word exact chiefly because, consistently with current (1976) criteria, it is the distance in the response space between the origin and the point of tangency of the response ellipsoid, obtained from a linear analysis, and the failure surface, which ordi-

rarily corresponds to markedly nonlinear behavior.

Only positive values of α_i are of interest, for if \underline{R}_i is the maximum numerical value of the response to the i th component, both \underline{R}_i and $-\underline{R}_i$ must be represented in the state space (response space).

When a structure responds to a single ground-motion component, only α_1 is of interest. The error introduced by Eq. 3 is then nil if one chooses $\alpha_1 = 1$.

When $n = 2$, both α_1 and α_2 are of interest. The maximum error on the safe side, as a fraction of the actual response, obtains when $\underline{R}_0 = \underline{0}$, $\|\underline{R}_1\| = \|\underline{R}_2\|$, \underline{R}_1 is perpendicular to \underline{R}_2 , and the failure "surface" is circular. Then, with $\alpha_1 = 1$, $\|\underline{R}\| = \|\underline{R}_1\|$ while Eq. 3 gives $\|\underline{R}\| = (1 + \alpha_2^2)^{1/2} \|\underline{R}_1\|$. Maximum error on the unsafe side is found when $\underline{R}_0 = \underline{0}$, $\|\underline{R}_1\| = \|\underline{R}_2\|$, and \underline{R}_1 and \underline{R}_2 are colinear. Then, with $\alpha_1 = 1$, $\|\underline{R}\| = \|\underline{R}_1\| \sqrt{2}$ while Eq. 3 gives $\|\underline{R}\| = (1 + \alpha_2) \|\underline{R}_1\|$. (Fig. 3 depicts these extreme cases.) The value of α_2 satisfying the criterion adopted is found from equating the maximum errors on the safe and unsafe sides:

$$(1 + \alpha_2^2)^{1/2} - 1 = \frac{\sqrt{2} - (1 - \alpha_2)}{\sqrt{2}}$$

whence $\alpha_2 = 0.336$, with maximum errors of 5.5%. Values in Table 1 were obtained in like fashion.

Somewhat smaller values of α_i and much smaller errors are obtained when not all the \underline{R}_i 's are assumed equal. For example, when $\|\underline{R}_1\| = 2\|\underline{R}_2\|$ and $\underline{R}_i = \underline{0}$ for $i \geq 3$, choice of $\alpha_2 = 0.336$ gives a maximum error of 4.5% on the safe side and none on the unsafe side while $\alpha_2 = 0.222$ gives maximum errors of 0.6%. These results indicate that: 1) errors in Table 1 for large n are deceptively high, for rarely will all components produce comparable responses (errors are further reduced because the two principal horizontal intensities are not strictly equal), and 2) if all α_i 's are to be made equal for $i \geq 2$, so as to decrease the number of points requiring study in the state space, a value smaller than 0.336 will be in order, since it will often happen that only two components require consideration. A value

as low as 0.222 is not advisable because errors on the unsafe side are much more objectionable than those on the safe side. Accordingly it seems advisable to choose $\alpha_i = 0.3$ for $i \geq 2$. The last three columns in Table 1 contain results of this choice.

The approximate procedure developed here is applied as follows.

1. Compute the responses to gravity loads and to the n components of ground motion regarded as potentially significant. Let those responses be arranged into vectors $\underline{R} = \underline{R}_0$ and \underline{R}_i respectively, with $i = 1, 2, \dots, n$.
2. Obtain vectors $\underline{R} = \underline{R}_0 + \sum_{i=1}^n \alpha_i \underline{R}_i$, assigning plus and minus signs to $\alpha_i \underline{R}_i$, ordering the \underline{R}_i 's in all possible permutations, and giving the α_i 's the values in Table 1.
3. If the problem is one of analysis, find out whether all points fall within the failure surface. If the problem is one of design, assign the design parameters such values that the safe domain will contain all the points.

Solution of a problem of analysis is represented in Fig. 4. The section in question can be a beam subjected to bending moments in a vertical and a horizontal plane, caused by gravity forces and by two components of ground motion. The eight points shown in the figure correspond to $\alpha_1 = 1, \alpha_2 = 0.3$. One concludes that the beam is safe. Also shown is the ellipse for the combined effects. Ordinarily it would be unnecessary to explore all eight points.

Often the design may have to be done for two levels of earthquake intensity and the design parameters selected so that the low-intensity points found in the manner described fall inside all failure surfaces while the high-intensity points fall outside the failure surfaces for serviceability and nonstructural-damage limit states but inside the failure surface for collapse.

Towers and Chimney Stacks

It is advisable to increase the α_i 's for $i \geq 2$ in the analysis and design of towers and chimney stacks. A value of 0.5 is suggested in lieu of 0.3. This

recommendation stems from two considerations:

In towers having square or rectangular plan, supported on four equal columns, every given total vertical force defines a plane of responses M_x and M_y -- the overturning moments acting parallel to the sides of the base. -- The intersection of any such plane with the failure surface describes a rhombus. Thus the equation of the failure surface is $|M_x| + \alpha|M_y| = a$ a function of the total vertical force, where α is a constant. In square-plan towers on four equal legs, $\alpha = 1$. If $\alpha_i = 0.3$ for $i \geq 2$ were adopted and a tower were analyzed parallel to the sides of the base, errors of up to $(\sqrt{2} - 1.3)/\sqrt{2} = 8.1\%$ would be systematically introduced on the unsafe side, plus errors due to neglect of the vertical and other components of ground motion if these were neglected. With $\alpha_i = 0.5$ for $i \geq 2$ the error will lie on the safe side. The maximum error, when the entire disturbance consists of horizontal translations, would be $(1.5 - \sqrt{2})/\sqrt{2} = 6.1\%$ for a perfectly symmetrical structure, and if there are three orthogonal translational components producing statistically equal effects the maximum error in the ideal case of perfect symmetry would be $(1 + 0.5 + 0.5 - \sqrt{3})/\sqrt{3} = 15.5\%$. In view of considerations in the next paragraph, this figure will not be attained in practice and it is likely that errors will still lie on the unsafe side.

In structures nominally having radial symmetry, such as chimney stacks, an apparently insignificant asymmetry causes an appreciable degree of coupling between modes of vibration involving orthogonal, horizontal displacements. The phenomenon has been observed in free-vibration experiments with a real stack (5,10). Under small oscillations the superposition of effects is sufficiently important to believe that the coefficient 0.5 should lie closer to 0.7. However, pending in-depth studies of the question, regard for even minor hysteretic behavior lends weight to the recommended value 0.5 for design. The same conclusion applies to other lightly damped structures whose dynamic behavior in horizontal planes does not nominally depend on the direction of oscillation.

Examples

Both examples chosen to illustrate the procedure proposed concern a circular section of reinforced concrete columns in buildings. In both, only three translational components of ground motion will be taken into account assuming that the significant effects of the rotational components about horizontal axes has been incorporated in the computation of modal responses to the translational components because of complete correlation between both kinds of response.

Example 1. The aim is to design a column having circular cross-section to resist shear. In accordance with ACI 318-71 (1), in the range of interest the shear resistance is $V = V' + 0.001\sqrt{f'_c}N$, where V' = capacity that the member would have in the absence of longitudinal force, N = longitudinal compression, and f'_c = nominal compressive strength, in psi (if f'_c is in kg/cm^2 coefficient 0.001 becomes 0.0038). The failure surface in this range is as shown in Fig. 5 for $f'_c = 4000$ psi ($280 \text{ kg}/\text{cm}^2$). Let results of analysis be those in Table 2, in which the first subscript of V indicates the direction in which the shear acts and the second subscript identifies the ground-motion component producing the response; thus V_{xy} = shear in direction X due to ground accelerations in direction Y; the subscript of N indicates the component producing longitudinal force; positive V 's are directed toward the building's interior when seen from above; and positive N 's are compressions.

Fig. 6 shows a vertical and the horizontal projection of the vector resulting from applying the procedure described. The capacity required in shear if no axial force were acting was computed as follows for the combination $R_o + 0.3R_x + R_y + 0.3R_z$ (which governs the required concrete strength or column radius). It was found that $V' = 298$ kip (135 metric ton).

Actually other combinations were tried. With $R_o + R_x + 0.3R_y + 0.3R_z$, $V' = 253$ kip (115 ton); with $R_o + R_x + 0.3R_y - 0.3R_z$, $V' = 244$ kip (111 ton). Also shown in the figure are the projections of vector $R_o + 0.336R_x + R_y + 0.250R_z$,

for which $V' = 302$ kip (138 ton) and the ellipsoid giving the exact solution, $V' = 208$ kip (99 ton). In this case use of coefficients $\{\alpha_i\} = (1, 0.3, 0.3)$ involved an error of 43% in V' . The error was 45% with $\{\alpha_i\} = (1, 0.336, 0.250)$. These errors are larger than indicated in Table 1 because values in the table refer to the seismic-response vector, not to the required strength.

Example 2. It is desired to design the column under eccentric compression when the longitudinal forces acting on the section of interest are again those in Table 2 and the bending moments, in units of c ton-meters where $c = \text{constant}$, are numerically equal to the shears in the table. Say that in elevation the failure surfaces for different amounts of longitudinal reinforcement are as shown in Fig. 7. In horizontal planes these surfaces define circles.

From inspection it is evident that, if $\alpha_2 = \alpha_3 = 0.3$, there is need only to study combinations $\underline{R}_O + \underline{R}_x + 0.3\underline{R}_y + 0.3\underline{R}_z$, $\underline{R}_O + 0.3\underline{R}_x + \underline{R}_y + 0.3\underline{R}_z$, and $\underline{R}_O + 0.3\underline{R}_x + 0.3\underline{R}_y + \underline{R}_z$. The corresponding vector sums are shown in Fig. 7, where the radial section of the failure surfaces is rotated to coincide with plane $V_{x,N}$. The second combination is critical and the column requires 1.55% longitudinal reinforcement.

Conclusions

A procedure has been presented for combining the effects of various ground-motion components. The approach assumes that such effects are uncorrelated Gaussian processes or that correlations are taken into account in computing modal responses. A simple approximation is derived under the assumption that failure surfaces are convex. In most practical cases the simple procedure introduces errors smaller than about 4% in the magnitude of the seismic-response vector. The percentage error in the required resistance is, however, not bounded thereby, as found in Example 1.

In essence the simple procedure consists in finding in the state space the

points defined by vectors $\underline{R} = \underline{R}_0 + \sum_{i=1}^n \alpha_i \underline{R}_i$, where subscript 0 and i refer respectively to effects of gravity forces and of the ith component of ground motion, n is the number of potentially significant components, and vectors \underline{R}_i are taken with the most unfavorable sign combination and in the most unfavorable order. It is shown that $\alpha_1 = 1$. A further simplification consists in taking $\alpha_i = 0.3$ for $i \geq 2$. For towers and chimney stacks, though, it is suggested that α_i be taken as 0.5 for $i \geq 2$.

Acknowledgements

The simplified procedure was proposed early in 1975 (with $\alpha_i = 1/3$ for $i \geq 2$) by A. S. Veletsos of Rice University. Even earlier, N. M. Newmark proposed this procedure, with $\alpha_i = 0.4$ for $i \geq 2$. It has served as basis for tentative code requirements in the United States (being drafted by the Applied Technology Council) and in the Federal District of Mexico. The main ideas in the present paper were developed in Ref. 8. The writers are grateful to A. S. Veletsos, D. Veneziano and E. Rukos for their constructive criticisms.

Appendix I -- References

1. American Concrete Institute, "ACI Standard 318-71, Building Code Requirements for Reinforced Concrete," ACI, Detroit, Mich. 1971.
2. Arias, A., "A Measure of Earthquake Intensity," Seismic Design for Nuclear Power Plants, MIT Press, Ed. R. J. Hansen, 1970, 438-483.
3. Drucker, D. C., "A Definition of Stable Inelastic Material," Trans. ASME, Journal of Appl. Mechs., Vol. 26, 1969, 101-106.
4. Housner, G. W., "Spectrum Intensities of Strong-Motion Earthquake," Proc. Symp. Earthq. and Blast Effects Structures, C.M. Duke and M. Reigen, eds., University of California, Los Angeles, 1952, 21-36.
5. Newmark, N. M., and Rosenblueth, E., Fundamentals of Earthquake Engineering, Prentice-Hall, Inc., Englewood Cliffs, N.J., 1971.

6. Penzien, J., and Watabe, M., "Simulation of 3-Dimensional Earthquake Ground Motion," Bulletin of the International Institute of Seismology and Earthquake Engineering, Vol. 12, 1974, 103-115.
7. Rosenblueth, E., "Criterio Aproximado de Diseño ante Sismos de Varios Componentes," Fourth Natl. Conf. on Earthq. Engng., Oaxaca, Mexico, to be published in Ingeniería, Mexico, 1976.
8. Rosenblueth, E., "Efectos del Componente Vertical en Edificios Altos," Fourth Natl. Conf. on Earthq. Engng., Oaxaca, Mexico, to be published in Ingeniería, Mexico, 1976.
9. Rosenblueth, E., "Tall Buildings Under Five-Component Earthquake," Proc. ASCE, Journal of the Structural Division, Vol. 102, No. 2, February 1976, 453-459.
10. Yamamoto, S. and Suzuki, N., "Experimental and Theoretical Analysis of Response Against Earthquake of Tower Structures Having Non-Uniform Sections Governed by Bending Vibrations," Proc. Third World Conf. Earthq. Engng., Auckland and Wellington, New Zealand, 1965, 2.730-2.747.

Appendix II -- Notation

- c = constant affecting the bending moments in Example 2;
- $E(\cdot)$ = expectation of variable (\cdot);
- $F(\underline{R})$ = function defining a failure surface;
- i = subscript identifying a ground-motion component;
- j = subscript identifying a structural response;
- M = bending moment;
- N = axial force;
- m = number of structural responses defining the state of a system or of a part thereof;
- n = number of potentially significant ground-motion components;
- o = subscript identifying effects of gravity forces;
- \underline{R} = vector of maximum values of structural responses;

- R = element of \underline{R} , $= \max_t |r(t)|$;
- r = structural response at a given instant;
- S = Housner spectral intensity;
- t = time;
- X = horizontal coordinate;
- x = horizontal ground displacement;
- Y = horizontal coordinate;
- y = horizontal ground displacement;
- Z = vertical coordinate;
- z = vertical ground displacement;
- α = coefficient in the failure surfaces of towers;
- α_i = coefficient of the i th component of \underline{R} ;
- δ = Dirac delta function; and
- ψ = transfer function.

(mirrored text)

Symbol	Value	Unit
α	3.3	
α_1	1.0	
α_2	0.0	
α_3	3.1	
α_4	1.0	
α_5	0.0	
α_6	3.1	
α_7	1.0	
α_8	0.0	
α_9	3.1	
α_{10}	1.0	
α_{11}	0.0	
α_{12}	3.1	
α_{13}	1.0	
α_{14}	0.0	
α_{15}	3.1	
α_{16}	1.0	
α_{17}	0.0	
α_{18}	3.1	
α_{19}	1.0	
α_{20}	0.0	

Table 1. Values of α_i and maximum errors in amplitude of seismic-response vector

i or n	α_i	max error, %	α_i	max error safe side, %	max error unsafe side, %
1	1.000	0	1.0	0	0
2	0.336	5.5	0.3	4.4	8.1
3	0.250	8.4	0.3	8.6	7.6
4	0.206	10.4	0.3	12.7	5.0
5	0.179	11.8	0.3	16.6	1.6
6	0.160	13.0	0.3	20.4	-2.1
7	0.146	13.9	0.3	24.1	-5.8
8	0.135	14.7	0.3	27.7	-9.6
9	0.126	15.4	0.3	31.1	-13.3
10	0.118	16.0	0.3	34.5	-17.0

Table 2. Data for Example 1

Concept	Magnitude	kjp (ton)
V_{ox}	88	(40)
V_{oy}	88	(40)
N_o	2202	(1000)
V_{xx}	<u>+176</u>	(<u>+80</u>)
V_{xy}	<u>+44</u>	(<u>+20</u>)
N_x	<u>+440</u>	(<u>+200</u>)
V_{yx}	<u>+88</u>	(<u>+40</u>)
V_{yy}	<u>+220</u>	(<u>+100</u>)
N_y	<u>+440</u>	(<u>+200</u>)
V_{zx}	<u>+22</u>	(<u>+10</u>)
V_{zy}	<u>+44</u>	(<u>+20</u>)
N_z	<u>+440</u>	(<u>+200</u>)

Figure captions

1. Failure "surfaces" for moment-axial force in reinforced concrete column.
2. Failure "surface" for moment-axial force in reinforced concrete column under axial force.
3. Extreme errors in approximate procedure.
4. Beam under gravity forces and two seismic components.
5. Failure surface for circular column under shear and axial force.
6. Solution of Example 1: design under shear.
7. Solution of Example 2: design under eccentric compression.

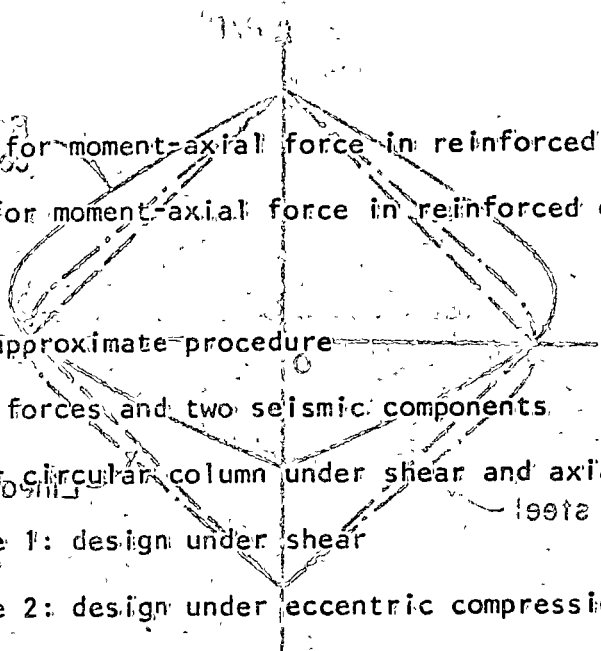


Fig. 1. Failure "surfaces" for moment-axial force in reinforced concrete column.

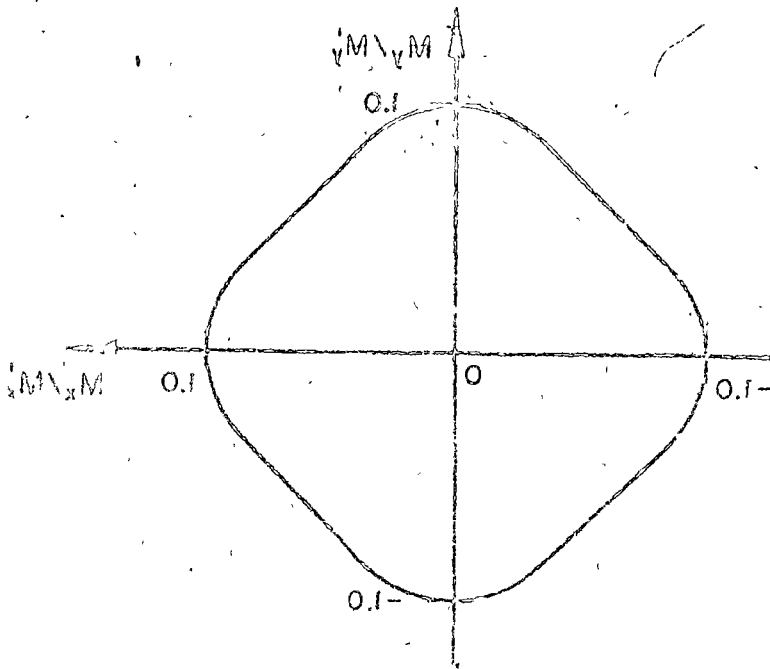


Fig. 2. Failure "surface" for moment-moment in reinforced concrete column under fixed axial force.

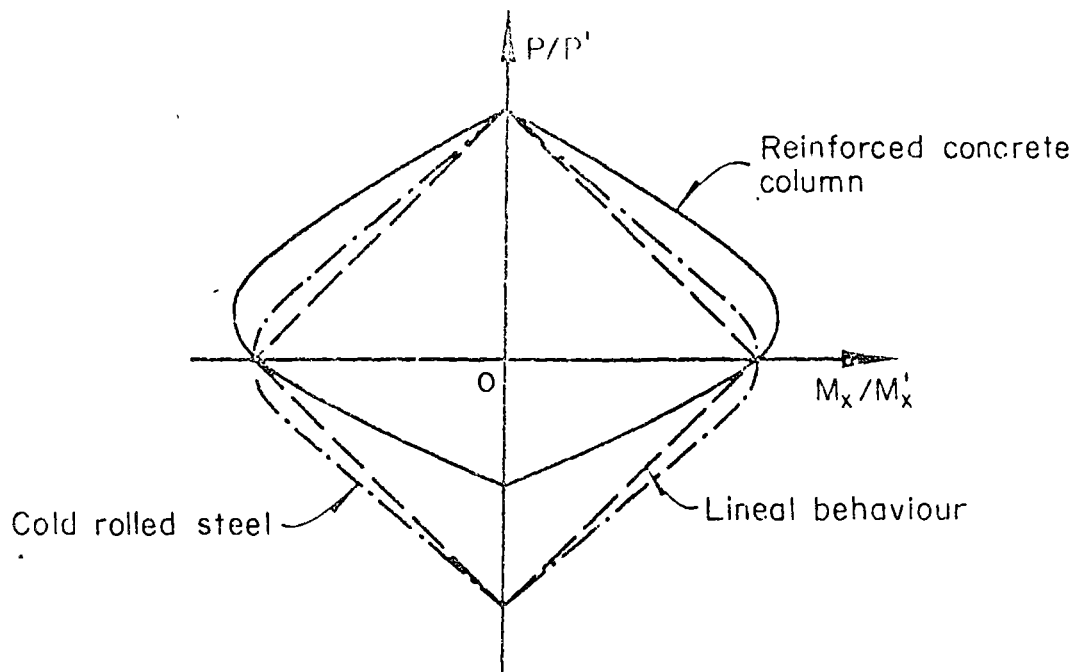


Fig 1. Failure "surfaces" for moment - axial force in reinforced concrete column

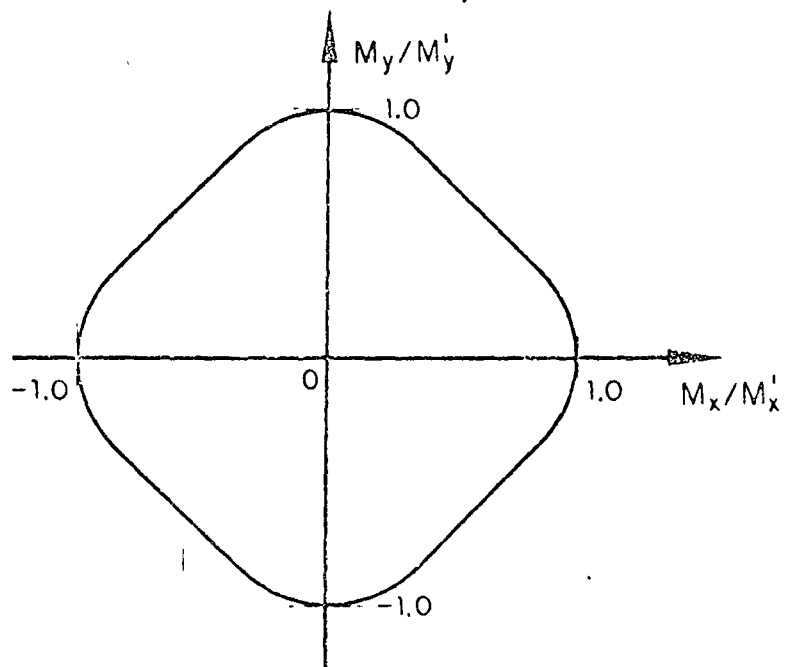


Fig 2. Failure "surface" for moment - moment in reinforced concrete column under fixed axial force

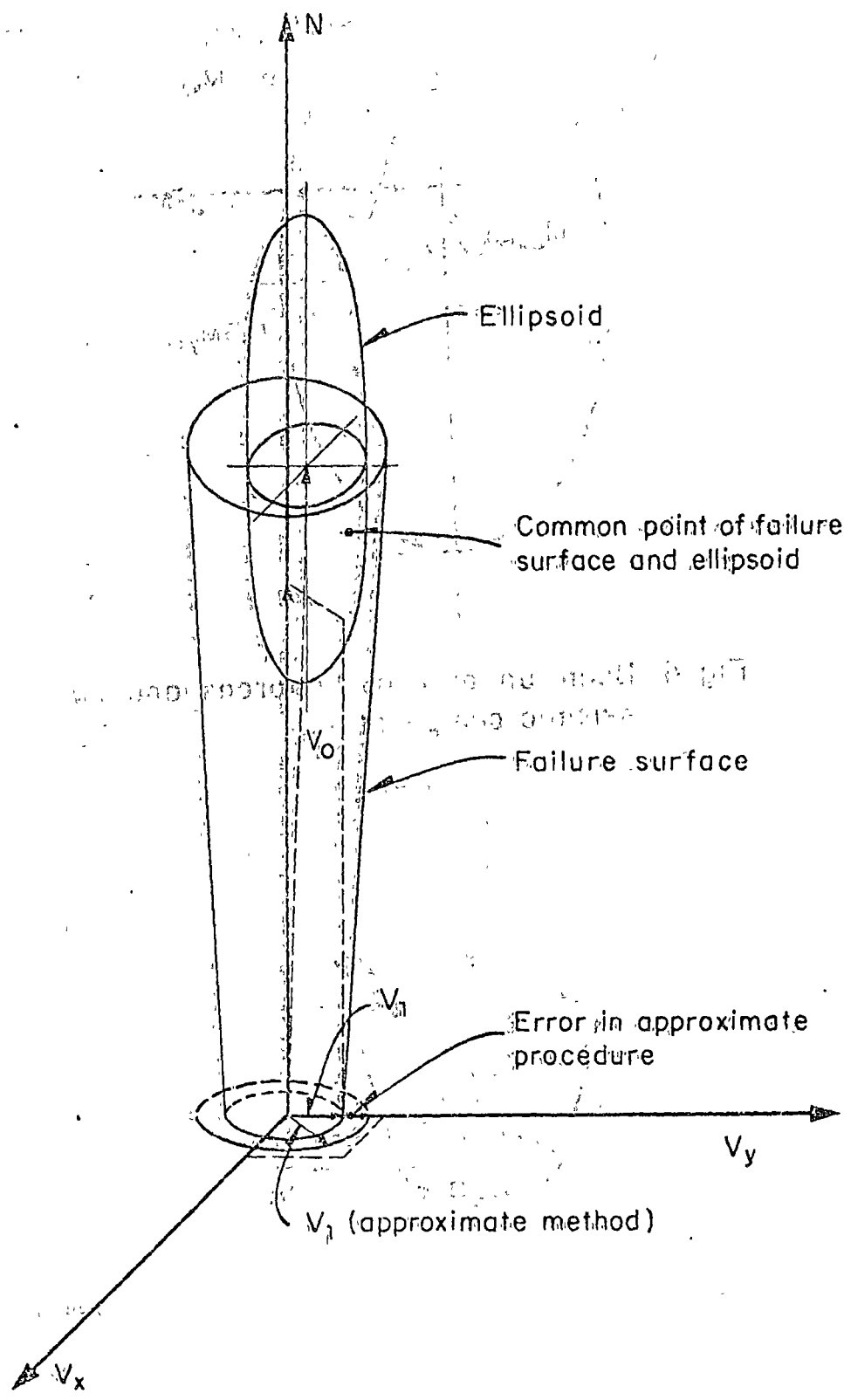


Fig 3. Extreme errors in approximate procedure

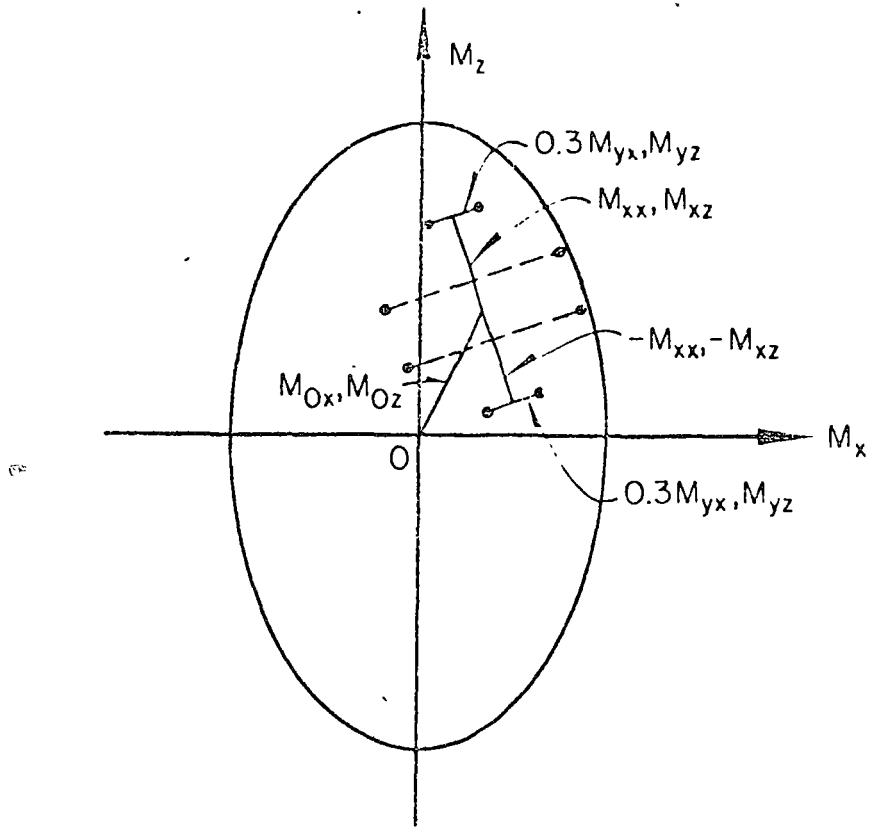


Fig 4. Beam under gravity forces and two seismic components

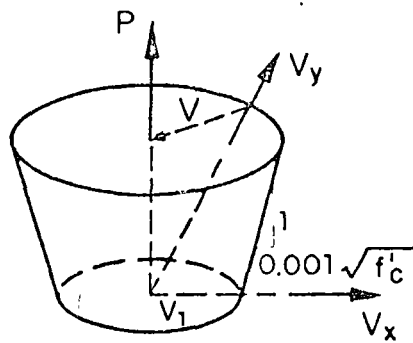


Fig 5. Failure surface for circular section column under shear and axial force

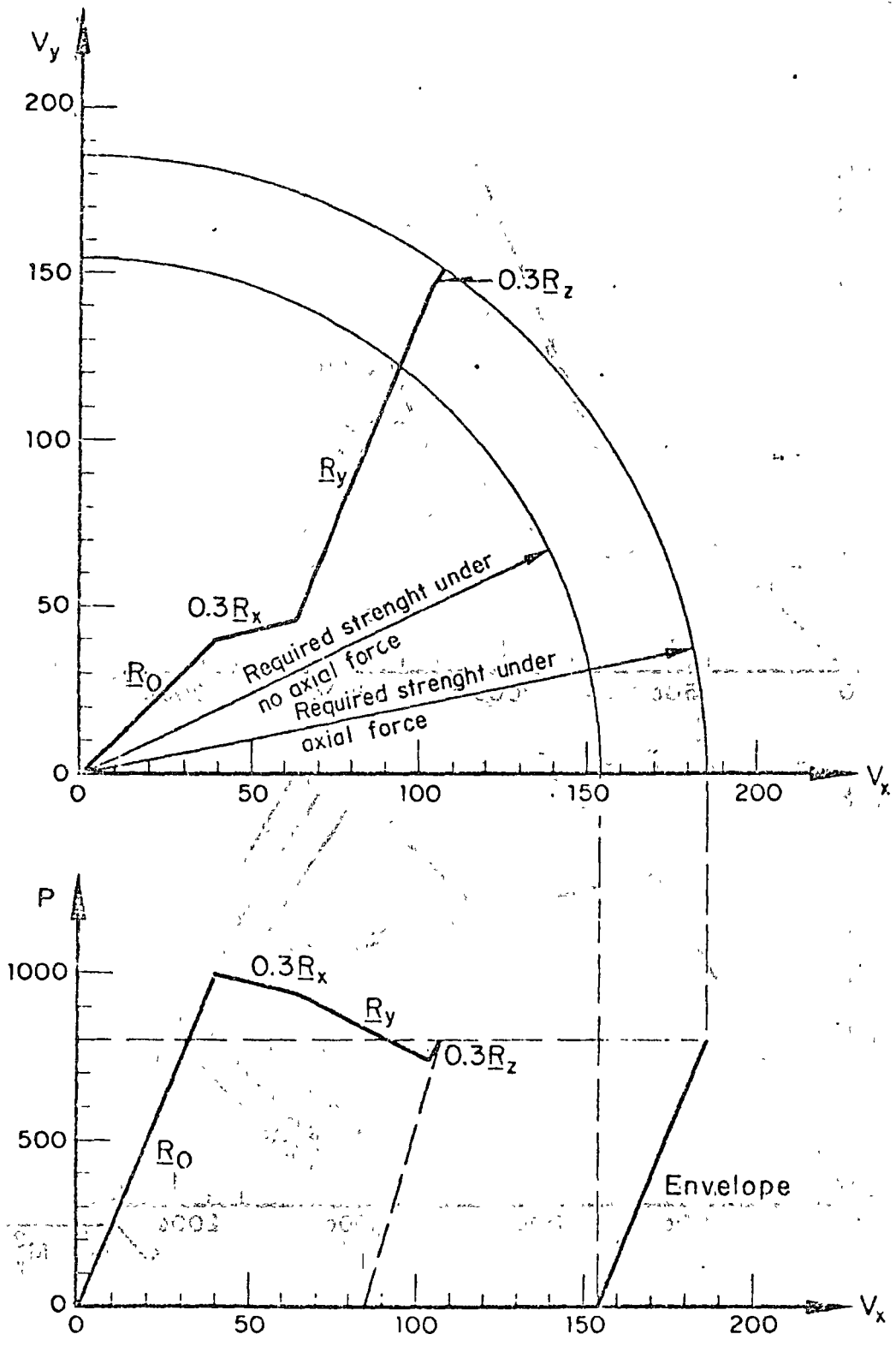


Fig 6. Solution of Example 1 : design under shear

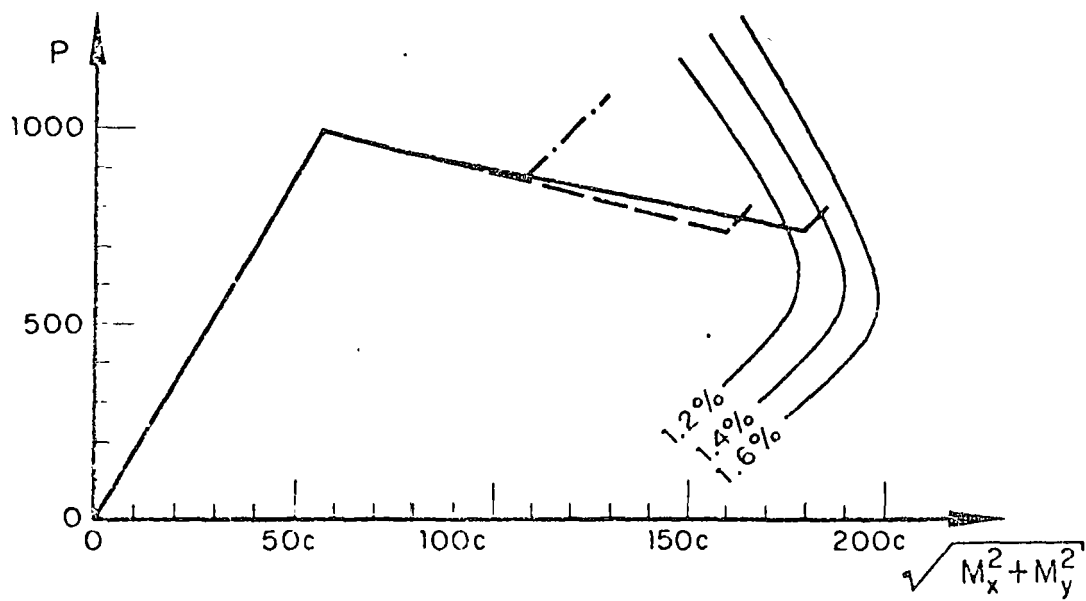
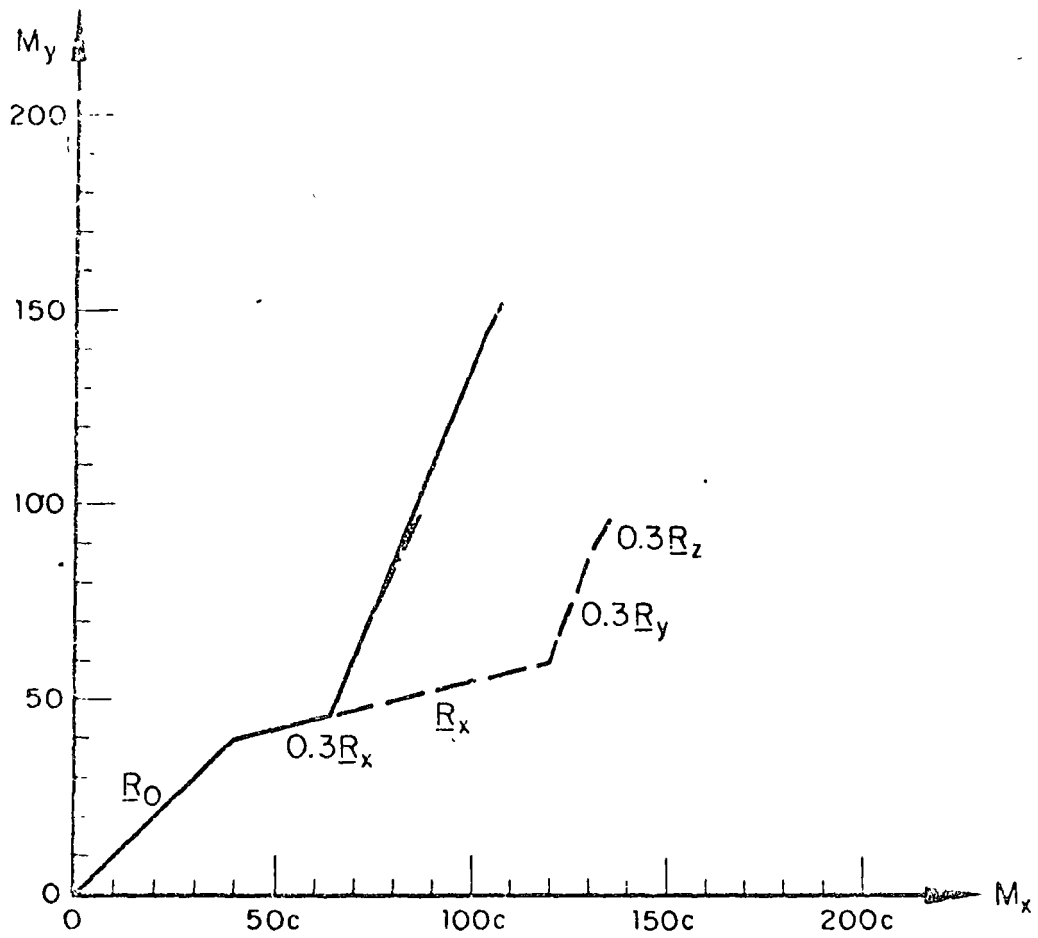


Fig 7. Solution of Example 2. Design under eccentric compression

EFFECTOS DEL COMPONENTE SISMICO VERTICAL

EN EDIFICIOS ALTOS

Emilio Rosenblueth

Introducción

A veces somos demasiado conscientes de que las estructuras llamadas a resistir temblores se diseñan para que resistan la acción de la gravedad. Ello conduce a desprestigiar en diseño sísmico los efectos de la aceleración vertical del terreno, bajo la hipótesis de que el diseño por cargas gravitacionales asegura la resistencia a este componente sísmico. La falta de experiencia con el comportamiento de edificios altos y estructuras de grandes claros en zonas próximas a los epifocos de macrosismos, ha hecho que solo muy recientemente comience a acumularse evidencia de que el componente vertical puede ser importante en condiciones prácticas.

Vale citar las experiencias de Acapulco¹, 1962, así como durante otros sismos de los últimos años; San Salvador², 1965, y San Fernando³, 1971. A raíz de la mayoría de los temblores más intensos de Acapulco se han recogido informes de testigos oculares en cuanto a que algunas vigas habían golpeado contra elementos no estructurales situados arriba de ellas y en un caso el golpeo dejó huellas visibles. Ello indica la aparición de aceleraciones verticales, una vez amplificadas por el comportamiento dinámico de la estructura, mayores que la aceleración de la gravedad. Además se detectaron algunas fallas de compresión y grietas horizontales en columnas que parecen confirmar esta aseveración. Sin embargo, las fallas y grietas pudieron haberse debido a momentos de volteo o asentamientos diferenciales y sería difícil hoy dilucidar la causa principal. En el sismo de San Salvador ocurrieron algunas fallas locales que no es fácil explicar sin admitir aceleraciones verticales del terreno mayores que 0.7g. Durante el temblor de San

¹ Investigador, Instituto de Ingeniería, UNAM, México, D F.

Fernando, Cal algunos instrumentos instalados en edificios de alturas moderadas y grandes (máximo 42 pisos) registraron aceleraciones verticales mayores que 0.2g en la base y que 0.4g en el extremo superior del inmueble (g = aceleración de la gravedad.) Los instrumentos no estaban situados, seguramente, en los puntos que experimentaron las máximas aceleraciones en cada edificio y, por otra parte, ninguna de estas estructuras se halla en la zona que experimentó las sacudidas más violentas. Es de suponerse que este evento habría causado aceleraciones verticales más elevadas que las registradas si hubiera habido instrumentos estratégicamente situados en edificios ubicados más desfavorablemente.

Usando un registro de movimiento vertical del terreno en San Fernando, se han calculado las respuestas de un edificio de diez pisos con estructura constituida por marcos⁴. Se encuentra que la aceleración vertical del terreno trae consigo fuertes aumentos en la demanda de ductilidad en los miembros estructurales de los niveles superiores.

Admitiendo que ciertas estructuras deben analizarse ante el componente vertical del movimiento del terreno, estaría desproporcionado exigir tal análisis en todos los casos. Vale la pena analizar aquí edificios idealizados de manera sencilla para conocer el orden de magnitud de las respuestas y la influencia de algunos parámetros a fin de establecer criterios prácticos, así sean aproximados.

Idealización de la estructura

Por sencillez idealizaremos la estructura de los edificios altos primeramente como una barra de sección uniforme a la que están fijas láminas flexibles infinitamente próximas entre sí y de masa uniforme a lo alto del edificio (fig 1). La barra representa las columnas del edificio, y las láminas los sistemas de piso. Después consideraremos estructuras en que el área transversal de las columnas decrece gradualmente hacia arriba.

Para conocer el orden de magnitud de la rigidez de la barra notemos que en una estructura metálica las columnas de los primeros entrepisos están sujetas a un esfuerzo normal medio (despreciando momentos flexionantes) del orden de 1 ton/cm^2 ante la acción de la gravedad y que su módulo elástico es 2100 ton/cm^2 . Por tanto su unidad de longitud posee una rigidez del orden de $2100ghm$, donde h y m son la altura y masa por unidad de altura del inmueble. Tratándose de columnas de concreto reforzado el esfuerzo normal medio (obtenido como la fuerza longitudinal entre el área transformada suponiendo concreto con resistencia a la compresión de 0.4 ton/cm^2) es del orden de 0.08 ton/cm^2 y el módulo elástico de 320 ton/cm^2 . Por consiguiente la rigidez de un elemento de longitud unitaria es del orden del doble que para las columnas de acero. El periodo fundamental de un edificio con columnas metálicas y pisos infinitamente rígidos valdría $T_1 = 4h(m/K)^{1/2}$, donde $K =$ rigidez de las columnas, es decir $T_1 = 4(h/2100g)^{1/2}$, estando h en centímetros. Con $h = 3 \text{ m/piso}$ los edificios de 10, 20, 50 y 100 pisos tendrían periodo fundamental de aproximadamente 0.15, 0.22, 0.34 y 0.48 seg respectivamente. Si su estructura es de concreto reforzado estos valores se reducen a 0.11, 0.15, 0.24 y 0.34 seg. Si el área transversal de las columnas disminuye hacia arriba, el periodo fundamental excede al calculado con base en las columnas de planta baja. El exceso es cercano a 20 por ciento cuando la variación en área es lineal entre el desplante y el extremo superior y el área mínima vale 20 por ciento de la máxima.

Las flechas de las vigas principales (trabes) ante carga gravitacional suelen limitarse a una fracción de su claro y lo mismo es cierto, directa o indirectamente, de las flechas de las losas o vigas secundarias. Dicha fracción depende del reglamento que se adopte pero difícilmente excede de $1/300$ para cada viga o losa respecto a sus apoyos. Al centro de un tablero podrán presentarse valores del doble de este, es decir $1/150$ del claro. En sistemas de piso de concreto refor-

zado se limitan las flechas a largo plazo, y éstas raras veces son menores que el doble de las flechas instantáneas. Es razonable, en resumen, suponer que en sistemas de piso metálicos o de concreto presforzado la flecha máxima bajo la acción estática de la gravedad puede alcanzar 1/150 del claro y que la correspondiente flecha ante cargas de corta duración en concreto reforzado no pasa de 1/300 del claro. Los claros usuales en las plantas tipo de la mayoría de los edificios altos están comprendidos entre 6 y 12 m. Para sistemas de piso metálicos hallaremos, pues, flechas estáticas menores que $1200/150 = 8$ cm y en los de concreto reforzado, de 4 cm. Estudiaremos también edificios metálicos en que las flechas sean de 4 cm pues en principio cabría la posibilidad de simplificar los requisitos de diseño en edificios con sistemas de piso moderadamente rígidos.

Empleando un método energético puede calcularse de manera aproximada el periodo fundamental de vibración de un sistema de piso, apoyado en columnas que no admiten desplazamiento vertical. Se demuestra en el apéndice A que en condiciones representativas este periodo vale, en segundos, $0.16\sqrt{z_s}$, en que $z_s =$ flecha en centímetros. Dado que el periodo natural de un sistema con un grado de libertad vale $0.20\sqrt{z_s}$, concluimos que los sistemas de piso cuya masa y rigidez por unidad de altura del edificio valen m y k , respectivamente, y cuyo periodo es $2\pi(m/k)^{1/2}$, equivalen a sistemas como el representado en la fig 2 con masa m y rigidez $(0.16/0.20)^2 gm/z_s = 0.64gm/z_s$ por unidad de altura. Notamos que para edificios con sistemas de pisos flexibles con columnas indeformables el periodo natural máximo de cada piso es del orden de 0.45 o 0.32 seg según se trate de sistemas metálicos o de concreto reforzado, y que con flechas no mayores de 4 y 2 cm estos límites superiores se reducen respectivamente a 0.32 y 0.23 seg.

El periodo fundamental teniendo en cuenta deformaciones de los pisos y de las columnas es sensiblemente igual a la raíz de la suma de los cuadrados de los

periodos con columnas indeformables y con pisos infinitamente rígidos. En todos los casos de interés práctico el periodo fundamental cae en un intervalo en que las ordenadas espectrales de aceleración son considerablemente mayores que la máxima aceleración vertical del terreno.

Modos naturales de vibración en edificios uniformes

Idealizaremos aquí un edificio alto como una barra uniforme carente de masa, cuya rigidez en un tramo unitario vale K y a la cual están ligados elementos elásticos de rigidez k y masa m por unidad de altura. Sea $z(x,t)$ el desplazamiento de un punto de la barra situado a la altura y sobre el terreno, en el instante t y sea $y(x,t)$ el desplazamiento relativo de una masa, situada a la misma altura, con respecto a un soporte, en el mismo instante. Al considerar las fuerzas elásticas y de inercia que obran en un elemento de longitud dx (fig 3), el principio de D'Alembert⁵ permite escribir

$$K \frac{\partial^2 z}{\partial x^2} + ky = 0 \quad (1)$$

$$m \frac{\partial^2 (y + z)}{\partial t^2} + ky = 0 \quad (2)$$

Las ecuaciones diferenciales han de resolverse suponiendo que y y z son funciones de x por una función armónica de t y que deben satisfacerse las condiciones de fronteras

$$z(0,t) = 0 \quad (3)$$

$$\left. \frac{\partial z}{\partial x} \right|_h = 0 \quad (4)$$

(La ec 4 proviene de la condición de que no se aplica ninguna fuerza al extremo superior del edificio.) El sistema de ecuaciones se resuelve en el apéndice B, donde se encuentra que la n -ésima frecuencia natural vale

$$\omega_n = \left(\frac{k/m}{1 + k/h\beta_n^2} \right)^{1/2} \quad (5)$$

donde

$$\beta_n = \frac{(2n-1)\pi}{2h} \quad (6)$$

el enésimo modo natural es

$$z_n = \text{sen } \beta_n x \quad (7)$$

$$y_n = (k\beta_n^2/k) z_n \quad (8)$$

y el enésimo coeficiente de participación vale

$$\alpha_n = \frac{4/(2n-1)\pi}{1 + k\beta_n^2/k} \quad (9)$$

De acuerdo con las estimaciones anteriores tomaremos como propios de estructuras metálicas con flechas hasta de 8 cm los valores mínimos $(k/m)^{1/2} = 14 \text{ seg}^{-1}$, $(k/m)^{1/2} = 1435 \text{ h}^{1/2} \approx 1400 \text{ h}^{1/2}$. Con flechas hasta de 4 cm, $(k/m)^{1/2} = 20 \text{ seg}^{-1}$. En estructuras de concreto supondremos rigideces del doble de las de acero.

En la tabla 1 se consignan los primeros seis periodos naturales T_1 de edificios de acero con diversos números de pisos N , flechas de 8 cm, sistemas flexibles de piso y $h = 3 \text{ m/piso}$ de conformidad con los criterios anotados. Llama la atención la extrema proximidad entre estos periodos en cada edificio con pisos flexibles; sería aun mayor de haber considerado reducción de K con la altura sobre el terreno.

Modos naturales de vibración con columnas de sección variable

En muchos casos se idealiza satisfactoriamente un edificio alto asignando a K una variación gradual con la altura mientras k y m se toman como constantes. En estas condiciones la ec 1 se convierte en

$$K \frac{\partial^2 z}{\partial x^2} + \frac{\partial K}{\partial x} \frac{\partial z}{\partial x} + ky = 0 \quad (10)$$

Las ecs 2-4 siguen siendo válidas,

$$y_n = \frac{z_n}{k/m\omega_n^2 - 1} \quad (11)$$

y ω_n se obtiene al satisfacer las ecs 3 y 4.

La variación del área transversal de las columnas con la altura en los primeros niveles de un edificio constituido por plantas tipo es bastante más lenta que lo

que daría de ser proporcional a $h - x$. Además el área es finita en el extremo superior. Tomaremos como representativa la variación

$$K = (1 - 0.8x^2/h^2)K_0 \quad (12)$$

donde K_0 = rigidez a nivel de desplante (fig 4). En el extremo superior, $K = 0.2K_0$.

Si bien es posible resolver analíticamente este sistema de ecuaciones se prefirió hacerlo numéricamente. En la fig 5 se compara el modo fundamental de un edificio cuya rigidez de columnas varía según la ec 12 con el de uno con rigidez uniforme. Con pisos infinitamente rígidos el periodo fundamental es 13 por ciento mayor que si la rigidez fuera uniforme e igual a K_0 . Con pisos flexibles las diferencias en periodos naturales de ambos tipos de edificio son bastante menores.

Espectros del componente vertical

Es sabido que la aceleración vertical máxima del terreno como fracción de la horizontal crece conforme nos acercamos al epifoco⁵. En las inmediaciones de este ambas aceleraciones son del mismo orden e incluso quizás la vertical sea superior.

Dada la tendencia a estratificación horizontal de roca y suelos, sobre todo en los valles en que se asientan las grandes ciudades, en el componente vertical predominan las ondas longitudinales mientras que en el horizontal lo hacen las de cortante. Los contenidos de frecuencias difieren por tanto en ambos componentes. Cabe estimar que los espectros para el componente vertical serán parecidos a los de un componente horizontal, con modificación en la escala de ordenadas espectrales y reducción a un 70 por ciento en la escala de periodos.

Atendiendo a estas consideraciones y a que cuanto mayores son la magnitud y la distancia focal de un temblor más largos son sus periodos dominantes⁵ y a la luz de varios espectros disponibles del componente vertical³, se postula para amortiguamiento igual a 5 por ciento del crítico, el espectro que con trazo interrumpido muestra la fig 6. Si bien es pequeña la ductilidad asociada a los efectos

estructurales de la aceleración vertical no parece exagerado suponer que el comportamiento de la estructura equivaldrá al desarrollo de un factor de ductilidad de 3. Con esta hipótesis se ha estimado la línea llena en la fig 6. (Probablemente sea admisible la hipótesis de factores de ductilidad apreciablemente mayores cuando la cedencia plástica de la estructura está obligada a ocurrir en las vigas, sobre todo si estas son de concreto reforzado, pues entonces podrá haber cedencia tanto hacia arriba como hacia abajo. En efecto, el suministro de cuantías adecuadas de refuerzo longitudinal puede dar como resultado curvas fuerza-deformación (descontada la gravedad) prácticamente simétricas. En sistemas de piso metálicos, en cambio, la cedencia es casi necesariamente solo hacia abajo por la acción de la gravedad y pueden acumularse los daños debidos a temblores sucesivos.)

Llevaremos adelante el análisis con base en la línea de trazo lleno a reserva de que se realice un estudio de sismicidad en cuanto al componente vertical por lo menos con el detalle con que para los componentes horizontales contienen la ref 7 y el estudio que actualmente está en marcha en el Instituto de Ingeniería para mejorar esas cartas sísmicas.

Cálculo de respuestas

Cuando las frecuencias de los modos naturales que contribuyen significativamente a una respuesta estructural difieren apreciablemente entre sí, pueden combinarse las correspondientes respuestas modales como la raíz de la suma de sus cuadrados⁵. Cuando no se cumple esta restricción -- y evidentemente en el caso que nos concierne no se satisface ni remotamente -- es necesario acudir a una expresión que contiene los dobles productos de las respuestas modales afectados de ciertos coeficientes⁵, expresión que puede ponerse en la forma

$$Q = \left(\sum_{i,j} \frac{Q_i Q_j}{1 + \varepsilon_{ij}} \right)^{1/2} \quad (13)$$

donde

$$\epsilon_{ij} = \frac{\omega_i' - \omega_j'}{\zeta_i' \omega_i + \zeta_j' \omega_j} \quad (14)$$

$$\omega_i' = \omega_i (1 - \zeta_i^2)^{1/2} \quad (15)$$

ω_i' = iésima frecuencia circular natural amortiguada

$$\zeta_i' = \zeta_i + \frac{2}{\omega_i s} \quad (16)$$

ζ_i = grado de amortiguamiento del iésimo modo natural

s = duración de un segmento de proceso gaussiano estacionario equivalente a la familia de temblores de interés

Las respuestas modales Q_i deben tomarse con el signo de su coeficiente de participación. Adoptaremos $\zeta_1 = 0.05$ y $s = 20$ seg. Nótese que si las frecuencias naturales están bien diferenciadas y ζ_i' es pequeño, $\epsilon_{ij} \ll 1$ cuando $i \neq j$ pero $\epsilon_{ii} = 0$ en todos los casos, así que la ec 13 equivale sensiblemente a la raíz de suma de cuadrados. Si en cambio todas las frecuencias naturales fuesen iguales entre sí tendríamos $\epsilon_{ij} = 0$ y la ec 13 equivaldría a $Q = \sum_i Q_i$.

Empleando la ec 13 y los resultados de los cálculos anotados anteriormente, se han obtenido las distribuciones de aceleraciones máximas en los pisos y las fuerzas axiales por sismo en las columnas que muestran las figs 7-10. Las curvas que representan aceleraciones máximas en los pisos se han ajustado en el tramo inferior de cada edificio, en una longitud del orden de un décimo de la altura del inmueble, para hacer coincidir la aceleración en la base de la estructura con la aceleración máxima del terreno. Las discrepancias que en este concepto arrojó el cálculo realizado son atribuibles a la discretación de la estructura y posiblemente al criterio empleado para la combinación de respuestas modales. Dicho criterio ha sido calibrado, y se lo hallado satisfactorio, en sistemas con dos grados de libertad⁶ pero se desconoce la bondad de la aproximación que suministra en sistemas con número elevado de modos naturales significativos. A alturas mayores de los inmuebles no es de esperarse que introduzca errores importantes en vista de

la preponderancia de los primeros modos naturales de vibraciones especialmente el fundamental.

Para el espectro supuesto, reducido por ductilidad, las aceleraciones verticales de diseño aumentan moderadamente, en términos generales, con la altura sobre el terreno, especialmente cuando las rigideces de los pisos no son pequeñas y cuando las de las columnas disminuyen con esa coordenada. Se alcanzan las aceleraciones máximas en edificios de altura intermedia. Las fuerzas axiales en columnas son muy ligeramente menores que la integral de las fuerzas en los pisos evaluada desde la azotea hacia abajo y, en general, exceden solo en unas decenas por ciento a la masa del edificio por la aceleración máxima del terreno.

La variación de aceleraciones con la altura sobre el terreno es bastante menos pronunciada que la que manifiestan la mayoría de los registros disponibles.³ Ello ha de atribuirse a que los edificios reales en cuestión con seguridad no excursionaron apreciablemente en el dominio plástico. Si hubiésemos llevado a cabo los análisis del presente artículo empleando el espectro de comportamiento lineal en vez del reducido por comportamiento inelástico, habríamos encontrado también una fuerte amplificación con la altura sobre el terreno.

La forma de realizar el análisis implica que vigas y columnas cederán plásticamente por igual, y esta hipótesis es debatible. Si se sobrediseñan las columnas, las vigas tendrán que desarrollar ductilidades bastante mayores que las supuestas, sobre todo en las plantas superiores, y esto probablemente se logre en la práctica con tan sólo tomar precauciones menores en su diseño; pero la situación inversa no es válida ya que la falla de columnas en compresión no suele desarrollar grandes ductilidades, especialmente en columnas de concreto reforzado provistas de estribos y en toda ocasión en que puede ocurrir pandeo inelástico. Se concluye la conveniencia de adoptar criterios más conservadores para el diseño de

columnas ante carga axial que para el diseño de todos los miembros estructurales, incluyendo las columnas, en flexión.

Si bien los resultados que consigna el presente artículo no manifiestan la aparición de aceleraciones verticales sísmicas en la estructura mayores que la gravedad, sí dejan poca duda respecto a que aceleraciones elevadas se podrán presentar cuando la estructura sea incapaz de desarrollar ductilidades importantes. De aquí que en toda viga de concreto reforzado o presforzado deba suministrarse suficiente refuerzo longitudinal, en el lecho opuesto al que indica en cada sección la aceleración de la gravedad, para asegurar capacidad y ductilidad adecuadas. Las cuantías requeridas son pequeñas pues el concreto reforzado desarrolla gran ductilidad cuando cede por tensión en flexión y está subreforzado, pero deben ser suficientemente grandes como para que la capacidad sea mayor que la del concreto simple (que fallaría frágilmente) y para distribuir las grietas por flexión. Con estos fines son adecuadas las cuantías mínimas que suelen fijar los reglamentos de construcción para el acero en la cara de tensión.

Por las mismas razones ha de preverse la aparición de tensiones axiales pequeñas en las columnas. Esto se reflejará en el diseño de conexiones de columnas metálicas, en la elección de dispositivos de traslape para el acero longitudinal de las de concreto y en reducciones de la capacidad de estas para resistir fuerzas cortantes.

El espectro elástico que adoptamos en el presente análisis se basa en una interpretación somera de datos parciales sobre los efectos de un solo tambor. Sin duda en la práctica ocurrirán sismos cuyos contenidos de frecuencias difieran apreciablemente del que supusimos. Aunando a esta consideración la incertidumbre en periodos naturales de vibración y de manera destacada la que proviene de posible interacción suelo-estructura, se vuelve palpable que sería prematuro adoptar

critérios de diseño en los que la aceleración vertical variara sensiblemente como indican los presentes análisis en función de la altura sobre el terreno y de los demás parámetros pertinentes. Es claro, por otra parte, que si se adoptan criterios sencillos y aproximados no cabe hacer distinciones en función del material constitutivo de la estructura, rigideces de los pisos y altura del inmueble.

Una manera sencilla de cubrir los resultados obtenidos y su extrapolación a condiciones probables excluidas del análisis consiste en especificar que, en zonas donde sea alta la probabilidad de que durante un lapso de varios decenios ocurran temblores intensos con epifoco cercano al sitio de la construcción, se incremente el factor de carga que se aplique a las acciones gravitacionales al analizar su efecto combinado con el de temblores. Un incremento de 20 por-ciento en dicho factor, por encima de lo que sería adecuado de no obrar aceleraciones verticales, cubriría una aceleración máxima de 0.44g sin requerir de ductilidades mayores que las supuestas en estos análisis. La aseveración se basa en que el mínimo cociente usual de cargas viva a muerta en vigas es del orden de $1/3$; si la carga viva durante un sismo intenso no excede de $1/3$ del valor de diseño para carga gravitacional, las vigas podrán tomar una aceleración vertical de $1.2 \times 1.33/1.11 - 1 = 0.44$ de la aceleración de la gravedad. En las columnas esta reserva se ve disminuida porque la carga viva que se toma para su diseño ya se halla reducida pero debe tenerse en cuenta que los efectos más desfavorables de las aceleraciones verticales en estos miembros consisten en aumentos de la demanda de ductilidad ante la combinación de dichas acciones y los momentos de volteo. Donde dominan las fuerzas axiales provocadas por estos momentos la combinación de ambos fenómenos puede aproximarse tomando íntegro el efecto de momentos de volteo y 0.3 de los de aceleraciones verticales⁸. Así, si los efectos de fuerzas gravitacionales son del mismo orden que los de temblor, un aumento de 20 ciento en el factor de carga de los primeros permite resistir aceleraciones sísmicas hasta de 0.56g. Como una aceleración máxima de 0.44g en las vigas significa una aceleración media menor que esta cantidad cual-

quiera que sea el tramo vertical que se considere del edificio y las fuerzas verticales inducidas en las columnas son poco menores que la integral de las que obran en las vigas, el criterio es conservador para las columnas, como era deseable.

Dado que las aceleraciones verticales del terreno pueden no solo aumentar sino también disminuir desfavorablemente las cargas gravitacionales (por ejemplo en miembros estructurales verticales en que la combinación de estas y de los efectos de momentos de volteo introduzca tensiones o disminuya la capacidad para resistir fuerza cortante, capacidad que en un amplio intervalo de interés práctico crece con la compresión axial), procederá también revisar la estabilidad ante la combinación de fuerzas gravitacionales y laterales reduciendo el factor de carga de las primeras multiplicándolo, digamos, por 0.8.

Un criterio sencillo, poco más refinado que el que antecede, haría variar el factor de carga con la altura sobre el terreno, pero difícilmente se justificaría en la presente etapa.

Conclusiones

Los análisis realizados señalan la aparición de aceleraciones verticales, en los pisos de edificios altos, que son en términos generales funciones moderadamente crecientes de la altura sobre el terreno. La amplificación dinámica que se encuentra es baja en relación con los registros obtenidos durante sismos en prototipos debido a la ductilidad que se ha supuesto que se desarrolla. Dicha amplificación es más pronunciada cuanto más rígidos son los pisos en comparación con las columnas y cuanto más rápidamente decrece la rigidez de estas con la altura.

Son máximas las aceleraciones en edificios de altura intermedia (20 a 50 pisos), y resultan poco mayores en estructuras de concreto que en las metálicas.

Para asegurar el desarrollo de ductilidades adecuadas, las columnas han de diseñarse más conservadoramente ante carga axial que las columnas y las vigas

que la integral de las que ^{obran} en las vigas, el criterio es conservador para las columnas, como era deseable.

Dado que las aceleraciones verticales del terreno pueden no solo aumentar sino también disminuir desfavorablemente las cargas gravitacionales (por ejemplo en miembros estructurales verticales en que la combinación de estas y de los efectos de momentos de volteo introduzca tensiones o disminuya la capacidad para resistir fuerza cortante, capacidad que en un amplio intervalo de interés práctico crece con la compresión axial), procederá también revisar la estabilidad ante la combinación de fuerzas gravitacionales y laterales reduciendo el factor de carga de las primeras multiplicándolo, digamos, por 0.8.

Un criterio sencillo, poco más refinado que el que antecede, haría variar el factor de carga con la altura sobre el terreno, pero difícilmente se justificaría en la presente etapa.

Conclusiones

Los análisis realizados señalan la aparición de aceleraciones verticales, en los pisos de edificios altos, que son en términos generales funciones moderadamente crecientes de la altura sobre el terreno. La amplificación dinámica que se encuentra es baja en relación con los registros obtenidos durante sismos en prototipos debido a la ductilidad que se ha supuesto que se desarrolla. Dicha amplificación es más pronunciada cuanto más rígidos son los pisos en comparación con las columnas y cuanto más rápidamente decrece la rigidez de estas con la altura.

Son máximas las aceleraciones en edificios de altura intermedia (20 a 50 pisos), y resultan poco mayores en estructuras de concreto que en las metálicas.

Para asegurar el desarrollo de ductilidades adecuadas, las columnas han de diseñarse más conservadoramente ante carga axial que las columnas y las vigas en

en flexión. Además, en zonas donde sea probable que ocurran temblores intensos de epifoco cercano debe preverse la inversión de momentos flexionantes en los sistemas de piso. Para ello bastará, en miembros de concreto reforzado, con suministrar, en la cara que ordinariamente sería de compresión, el refuerzo longitudinal mínimo de tensión que marcan los reglamentos. Esta precaución es especialmente de atenderse en vigas de concreto presforzado. Además deberá preverse la aparición de pequeñas tensiones en las columnas.

Teniendo en cuenta las incertidumbres actuales sobre las formas de los espectros del movimiento vertical del terreno y en lo que atañe a interacción suelo-estructura, no se justifica generalmente un criterio refinado de diseño para cubrir los efectos de este componente sísmico. En zonas como las mencionadas bastará con especificar que los factores de carga usuales para fuerzas gravitacionales, cuando actúan simultáneamente con las fuerzas sísmicas, se incrementen y disminuyan ligeramente. La mayor parte de los efectos en cuestión quedarán cubiertos con factores del orden de 1.2 y 0.8 en las fuerzas gravitacionales.

Como alternativa cabe llevar a cabo análisis dinámicos refinados de los efectos de la aceleración vertical del terreno. En ellos deberán reconocerse las incertidumbres que se han mencionado.

Los análisis hechos mejorarían en precisión y alcance si abarcaran un mayor rango de condiciones y si tuvieran en cuenta las deformaciones locales del terreno cuando estas fuesen importantes.

Los espectros supuestos en este trabajo son representativos de lo que cabe esperar en la vecindad del epifoco de temblores intensos en terreno firme. Para establecer criterios dignos de confianza se requerirá el cálculo de los espectros con base en estudios de sismicidad. Aun en el estado actual cabe decir que para fines reglamentarios pueden eximirse de análisis por componente sísmico vertical los edificios que se hallan en vastas zonas donde la probabilidad de que ocurra

un temblor intenso de epifoco cercano es sumamente pequeña.

merecerá asimismo atención más profunda que la que le hemos dedicado el efecto del comportamiento no lineal de la estructura.

En la ref 9 el lector hallará un tratamiento paralelo e independiente de los temas aquí cubiertos. Las recomendaciones de la ref 9 son más conservadoras que las enunciadas en los párrafos precedentes.

Reconocimiento

El autor agradece a Alejandro Asfura sus interesantes discusiones, la revisión crítica del manuscrito y la realización de los cálculos numéricos.

La producción de este artículo ha sido estimulada por el intercambio de ideas del autor con los grupos que tienen a su cargo la elaboración del Reglamento de Construcciones en el Distrito Federal y las disposiciones generales en Estados Unidos, estas bajo el patrocinio del Applied Technology Council de ese país.

Apéndice A. Periodo fundamental de sistemas de pisos

Consideremos una viga prismática libremente apoyada. Sabemos que su frecuencia circular fundamental⁵ es

$$\omega = \frac{\pi^2}{L^2} \sqrt{\frac{EI}{\rho}} \quad (A1)$$

donde L = claro, E = módulo elástico, I = momento de inercia de la sección transversal y ρ = masa por unidad de longitud. La flecha de la viga ante la acción estática de la gravedad vale

$$z_s = \frac{5g\rho L^4}{384EI} \quad (A2)$$

De aquí que su periodo fundamental $2\pi/\omega$ sea $(2/\omega) (384/5gz_s)^{1/2} = 2\pi(0.788z_s/g)^{1/2}$, que ha de compararse con $2\pi(z_s/g)^{1/2}$ para un sistema con un grado de libertad.

Consideremos ahora un sistema de piso constituido por vigas ortogonales continuas. Supondremos nulas sus rotaciones en los apoyos e iguales las flechas en ambas di-

recciones, con respecto a los correspondientes apoyos. Además supondremos que la deflexión a los cuartos del claro es igual a la mitad de la flecha. La configuración supuesta se exhibe en la fig A1. Por simetría, para estimación del periodo fundamental basta examinar un octavo de tablero, como se muestra en la fig A2 con las flechas y áreas tributarias que corresponden al apoyo, cuartos y centros de las vigas ortogonales.

La frecuencia fundamental puede aproximarse satisfactoriamente mediante el cociente de Schwartz⁵:

$$\omega^2 = \frac{\sum W_i z_i}{g \sum F_i z_i} \quad (A3)$$

donde W_i = peso de la i ésima masa supuesta concentrada, mediante cuyo conjunto se discretiza el sistema, z_i desplazamiento correspondiente y F_i = fuerza de inercia que obra en dicha masa. Aplicando esta expresión encontramos el periodo fundamental igual a $2\pi(0.625z_s/g)^{1/2}$, donde z_s = flecha al centro del tablero.

En un piso típico habrá generalmente un número dominante de tableros cuyas condiciones de apoyo y continuidad se aproximen a las del que acabamos de analizar y algunos tableros o voladizos cuyas condiciones de apoyo y continuidad estén más próximos a las de una viga libremente apoyada. Por tanto es razonable aproximar el periodo fundamental como $2\pi(0.064z_s/g)^{1/2} = 0.2(0.64z_s)^{1/2} = 0.16\sqrt{z_s}$, estando z_s en centímetros y el periodo en segundos.

Apéndice B. Modos naturales de estructuras uniformes

Deseamos resolver las ecs 1-4. Las ecuaciones diferenciales en cuestión son separables. Supongamos $z(x,t) = Z(x)\theta(t)$, $y(x,t) = Y(x)\theta(t)$. La hipótesis es congruente con la condición de vibración libre en un modo natural. Sustituyendo en las ecs 1 y 2 obtenemos

$$kZ''\theta + kY\theta = 0 \quad (B1)$$

$$m(Y + Z)\ddot{\theta} + kY\theta = 0 \quad (B2)$$

donde las primas significan derivadas respecto a x y los puntos respecto a t . Es-

tas expresiones deben satisfacerse para toda x y toda t . Por tanto podemos dividir ambos miembros de la ec B2 entre kY'' :

$$\frac{m}{k}(1 + \frac{Z}{Y}) = - \frac{\ddot{\theta}}{\ddot{\theta}} \quad (B3)$$

El primer miembro no depende de x y el segundo no depende de t . Por tanto ambos son iguales a una constante, digamos ω^{-2} . Nos quedan pues las ecuaciones

$$-\ddot{\theta} = \omega^2 \theta \quad (B4)$$

$$Y = \frac{Z}{k/m\omega^2 - 1} \quad (B5)$$

Salvo por la amplitud (que es arbitraria) y un desfaseamiento (que es irrelevante) la solución de la ec B4 es

$$\theta = \text{sen } \omega t \quad (B6)$$

Por tanto ω es frecuencia natural del sistema.

Sustituyendo la ec B5 en la B1 y dividiendo ambos miembros entre θ queda

$$kZ'' + \frac{kZ}{k/m\omega^2 - 1} = 0 \quad (B7)$$

cuya solución general es

$$Z = a \text{ sen } \left[\left(\frac{k/K}{k/m\omega^2 - 1} \right)^{1/2} x \right] + b \text{ cos } \left[\left(\frac{k/K}{k/m\omega^2 - 1} \right)^{1/2} x \right] \quad (B8)$$

donde a y b son constantes. De la ec 3, $b = 0$. Por la arbitrariedad de la amplitud podemos tomar $a = 1$. De la ec 4,

$$\left(\frac{k/K}{k/m\omega_n^2 - 1} \right)^{1/2} = \frac{(2n - 1)\pi}{2h} \quad (B9)$$

donde hemos introducido $n = 1, 2, \dots$ para identificar la enésima frecuencia natural.

De la ec B9 deducimos las 5 y 6. De las ecs B8 y B9 la 7 y de las ecs 5 y B5 la 8.

El coeficiente de participación⁵ se calcula mediante la expresión

$$\alpha_n = \frac{\int_0^h m(y_n + z_n) dx}{\int_0^h m(y_n + z_n)^2 dx} \quad (B10)$$

Sustituyendo y_n y z_n de las ecs 7 y 8 obtenemos la 9.

Notación

- A** = aceleración espectral
- a** = coeficiente en la expresión para los modos naturales
- b** = coeficiente en la expresión para los modos naturales
- E** = módulo de elasticidad
- F** = fuerza de inercia
- g** = aceleración de la gravedad
- h** = altura de un edificio
- I** = momento de inercia
- K** = rigidez axial de un tramo unitario de columna
- K₀** = valor de K en $x = 0$
- k** = rigidez de los sistemas de piso en un tramo de longitud unitaria de las columnas
- L** = claro de una viga
- m** = masa por unidad de altura de un edificio
- N** = número de pisos
- Q** = respuesta estructural de diseño
- s** = duración de un proceso estacionario equivalente a la familia de tensores de diseño
- T** = periodo natural
- t** = tiempo
- W** = peso de un elemento que integra un sistema estructural
- x** = coordenada axial de un edificio
- Y** = función de x
- y** = desplazamiento relativo máximo entre un piso y las columnas que lo

soportan

z = función de x

z = desplazamiento de las columnas en cualquier punto de un edificio

z_s = flecha al centro de un tablero ante carga gravitacional de corta duración

α = coeficiente de participación

β = parámetro requerido para satisfacer la condición de frontera en el extremo superior de un edificio

ζ = grado de amortiguamiento

ζ^o = grado equivalente de amortiguamiento

θ = función de t

ρ = masa por unidad de longitud de una viga

ω = frecuencia circular

Referencias

1. Esteva, L, "Los temblores de mayo de 1962 en Acapulco"; Rev Soc Mex de Ing Sism. 1, 2, dic 1963, 39-60. Informe 94 del Instituto de Ingeniería, UNAM.
2. Rosenblueth, E y Prince, J, "El temblor de San Salvador, 3 de mayo 1965: ingeniería sísmica", Rev Soc Mex de Ing Sism, 3, 2, dic 1965, 33-60; Ingeniería, 35, 1, ene 1966, 31-58.
3. Trifunac, M D, Brady, A G y Hudson, D E, "Analyses of strong motion earthquake accelerograms", partes A, B, etc, vol 3: Response spectra, Earthquake Engineering Research Laboratory, California Institute of Technology, Pasadena, Cal, 1973 y 1974.
4. Anderson, J C y Bertero, V V, "Effects of gravity loads and vertical ground acceleration on the seismic response of multistory frames", Proc Fifth World Conf on Earthq Engng, Roma, 1973, 2, 2914-23.
5. Newmark, N M y Rosenblueth, E, Fundamentals of earthquake engineering, Prentice Hall, Inc, Englewood Cliffs, N J, 1971.

6. Rascón, O A y Villarreal, A, "Estudio estadístico de los criterios para estimar la respuesta sísmica de sistemas lineales con dos grados de libertad", Memorias del Primer Congr Venezolano de Sismolog e Ing Sism, en prensa, Caracas, Venezuela, oct 1974; Ingeniería, 43, 4 (oct-dic 1974), 375-96; Instituto de Ingeniería, UNAM, Informe 343, oct 1974.
7. Esteva, L, "Consideraciones prácticas en la estimación bayesiana de riesgo sísmico", Instituto de Ingeniería, UNAM, Informe 248, 1970.
8. Rosenblueth, E, "Criterio aproximado de diseño ante sismos de varios componentes", a ser presentado en Cuarto Congr Nac de Ing Sism, Oaxaca, Oax, nov 1975.
9. Krawinkler, H, "Vertical ground motion in earthquakes -- its nature and its effects on the response of buildings", en A study of seismic risk for Nicaragua, parte 1, por H C Shah, C P Mortgat, A Kiremidjian y T C Zsutty, The John A Blume Earthquake Engineering Center, Dept of Civ Engng, Stanford University, 11, ene 1975, A6.1-32.

Tabla 1. Periodos naturales de vibración (T_i , seg)

F	Pisos flexibles				Pisos infinitamente rígidos			
	N = 10	N = 20	N = 50	N = 100	N = 10	N = 20	N = 50	N = 100
1	0.4753	0.5004	0.5691	0.6681	0.1565	0.2213	0.3498	0.4947
2	0.4518	0.4548	0.4637	0.4782	0.0522	0.0738	0.1166	0.1650
3	0.4499	0.4510	0.4542	0.4596	0.0313	0.0443	0.0700	0.0990
4	0.4494	0.4499	0.4516	0.4543	0.0224	0.0316	0.0500	0.0707
5	0.4491	0.4495	0.4505	0.4522	0.0174	0.0246	0.0389	0.0550
6	0.4490	0.4492	0.4499	0.4510	0.0142	0.0201	0.0328	0.0450

$$(k/m)^{1/2} = 14 \text{ seg}^{-1}, \omega$$

$$(k/m)^{1/2} = 1400h^{-1}$$

$$h = 300N \text{ cm}$$

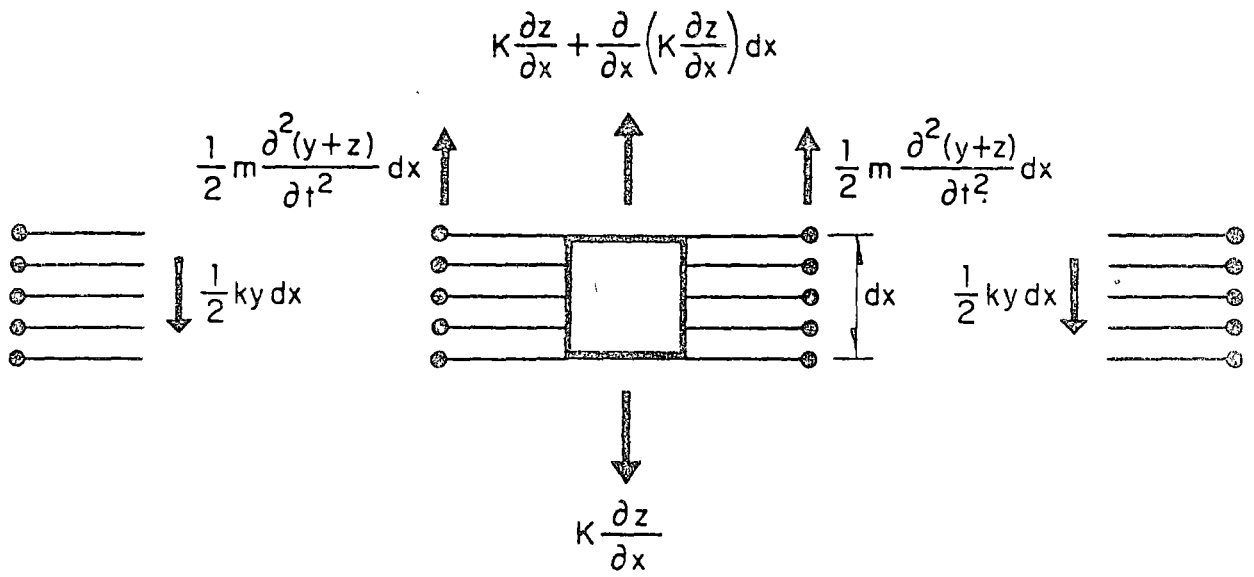


Fig 3. Fuerzas elásticas y de inercia en un elemento diferencial

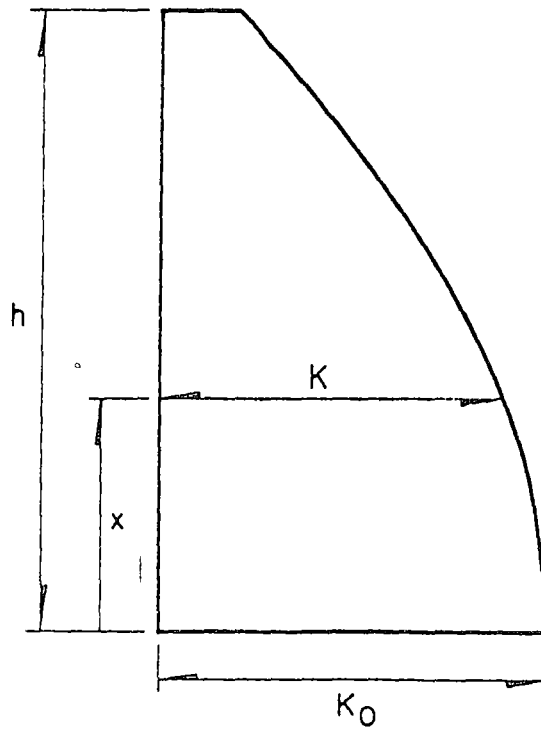


Fig 4. Variación de la rigidez de columnas

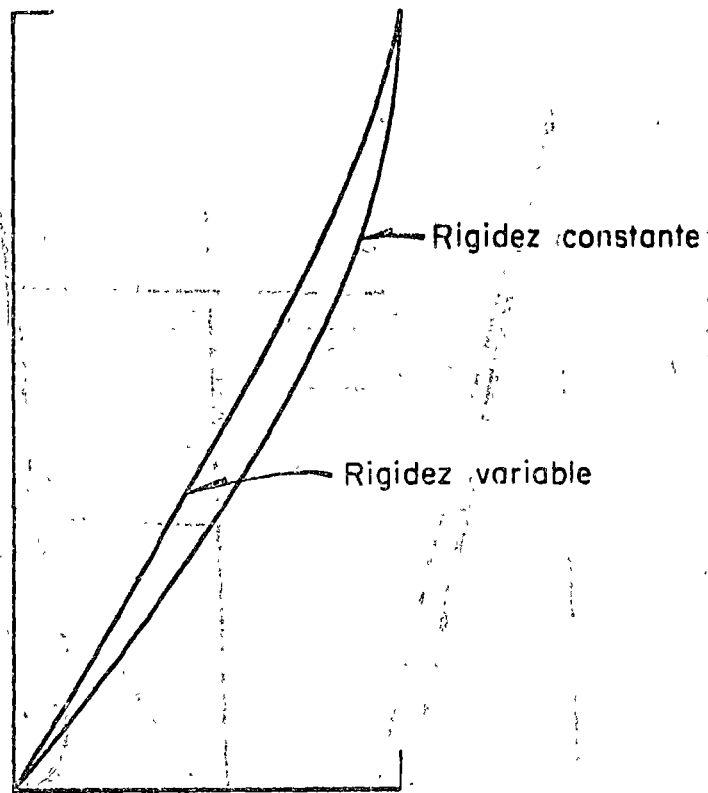


Fig 5. Comparación de modos fundamentales

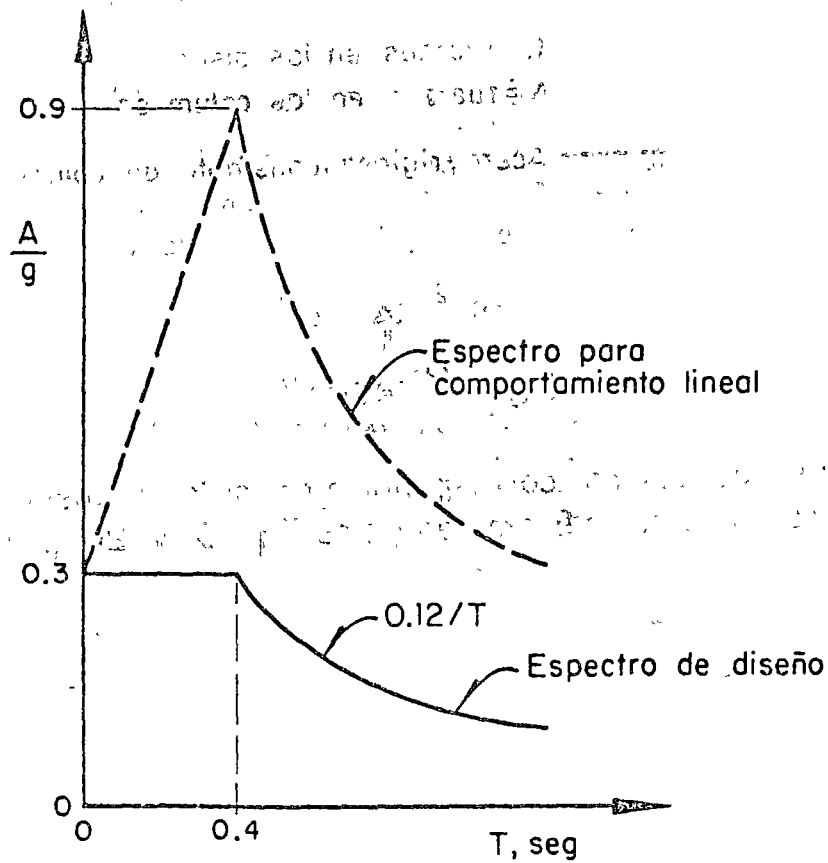
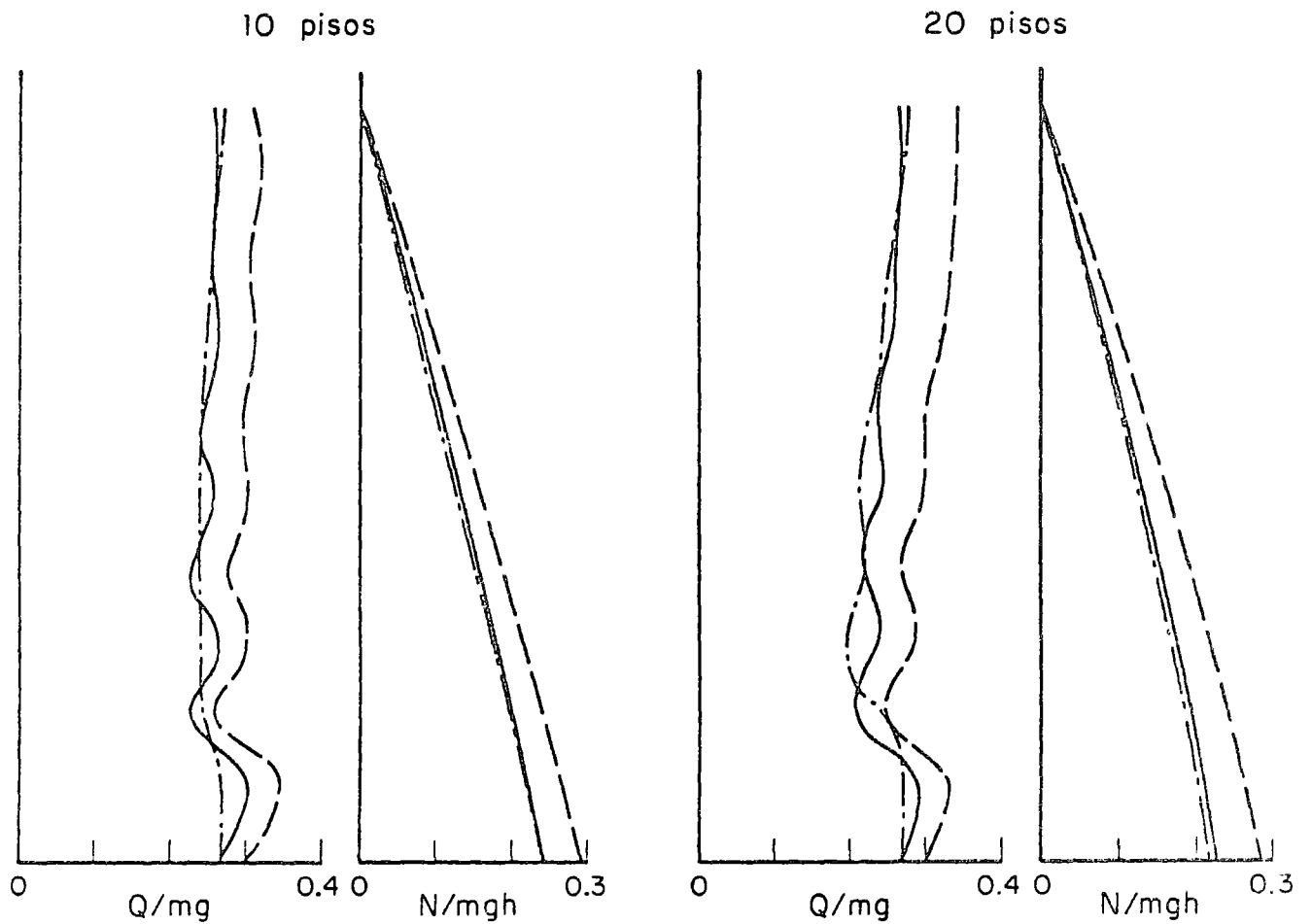


Fig 6. Espectros supuestos para movimiento vertical del terreno



Q = fuerzas en los pisos

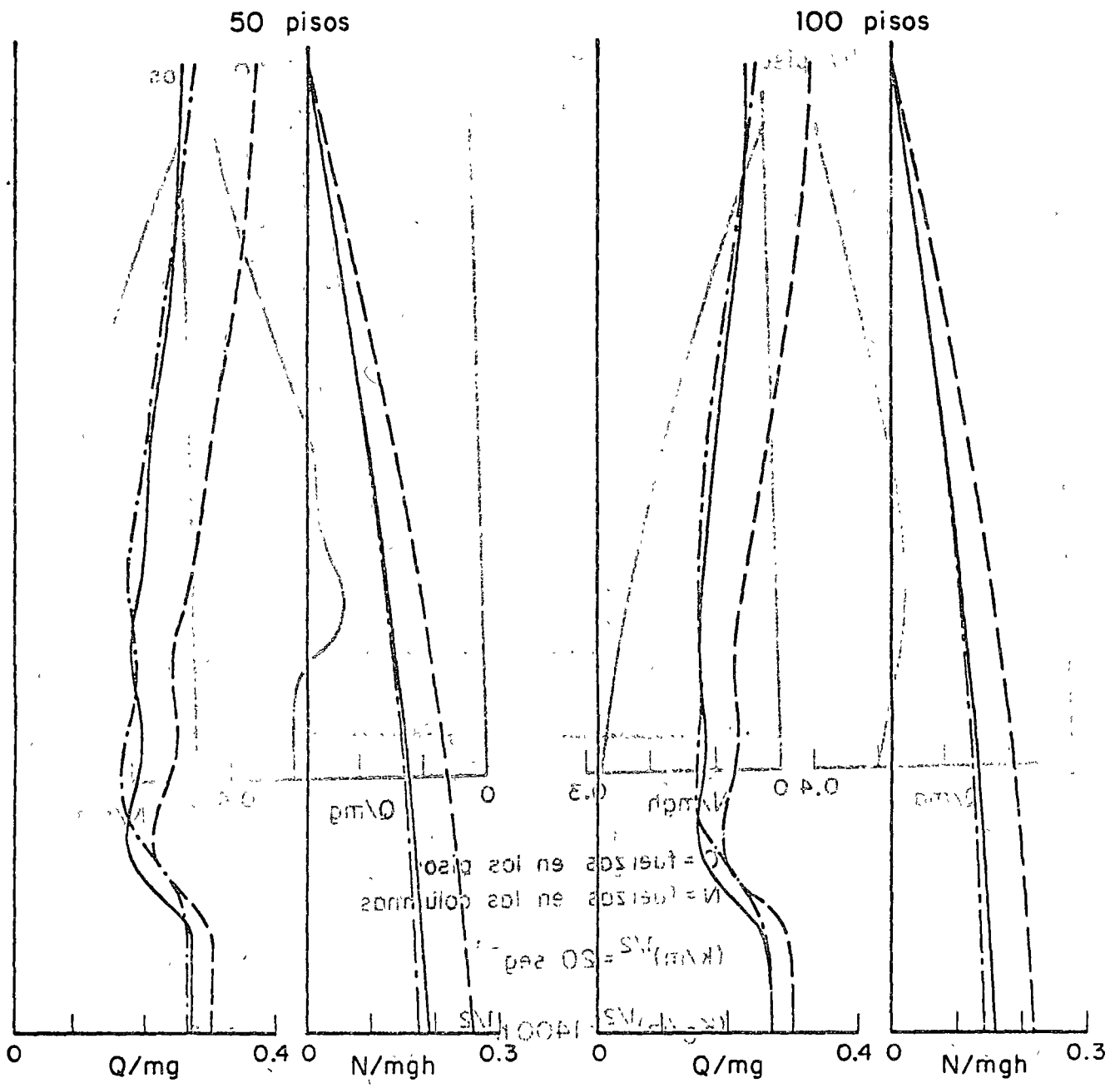
N = fuerzas en las columnas

- Acero, rigidez constante de columnas
- — Concreto, rigidez constante de columnas
- · - Acero, rigidez variable de columnas

$$(k/m)^{1/2} = 14 \text{ seg}^{-1}$$

$$(K_0/m)^{1/2} = 1400 \text{ h}^{1/2}$$

Fig 7. Fuerzas de diseño correspondientes al componente vertical, flecha estática en pisos = 8 cm, edificios de 10 y 20 pisos



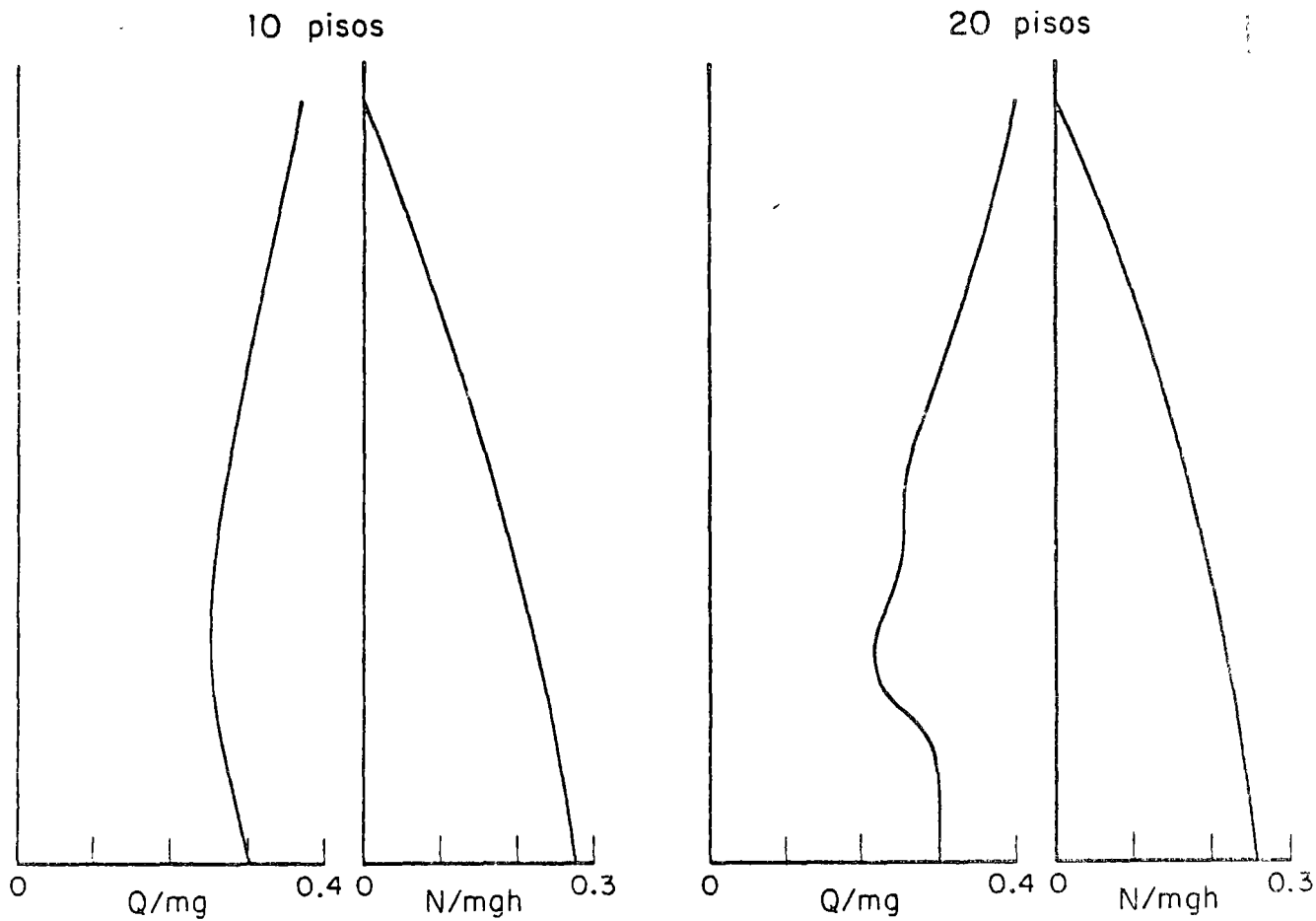
Q = fuerzas en los pisos
 N = fuerzas en las columnas

- Acero, rigidez constante de columnas
- - - Concreto, rigidez constante de columnas
- · - Acero, rigidez variable de columnas

$$(k/m)^{1/2} = 14 \text{ seg}^{-1}$$

$$(K_0/m)^{1/2} = 1400 h^{1/2}$$

Fig 8. Fuerzas de diseño correspondientes al componente vertical, flecha estática en pisos = 8 cm, edificios de 50 y 100 pisos



Q = fuerzas en los pisos
 N = fuerzas en las columnas

$$(k/m)^{1/2} = 20 \text{ seg}^{-1}$$

$$(K_0/m)^{1/2} = 1400 h^{1/2}$$

Fig 9. Fuerzas de diseño correspondientes al componente vertical, flecha estática en pisos = 4 cm, edificios de 10 y 20 pisos

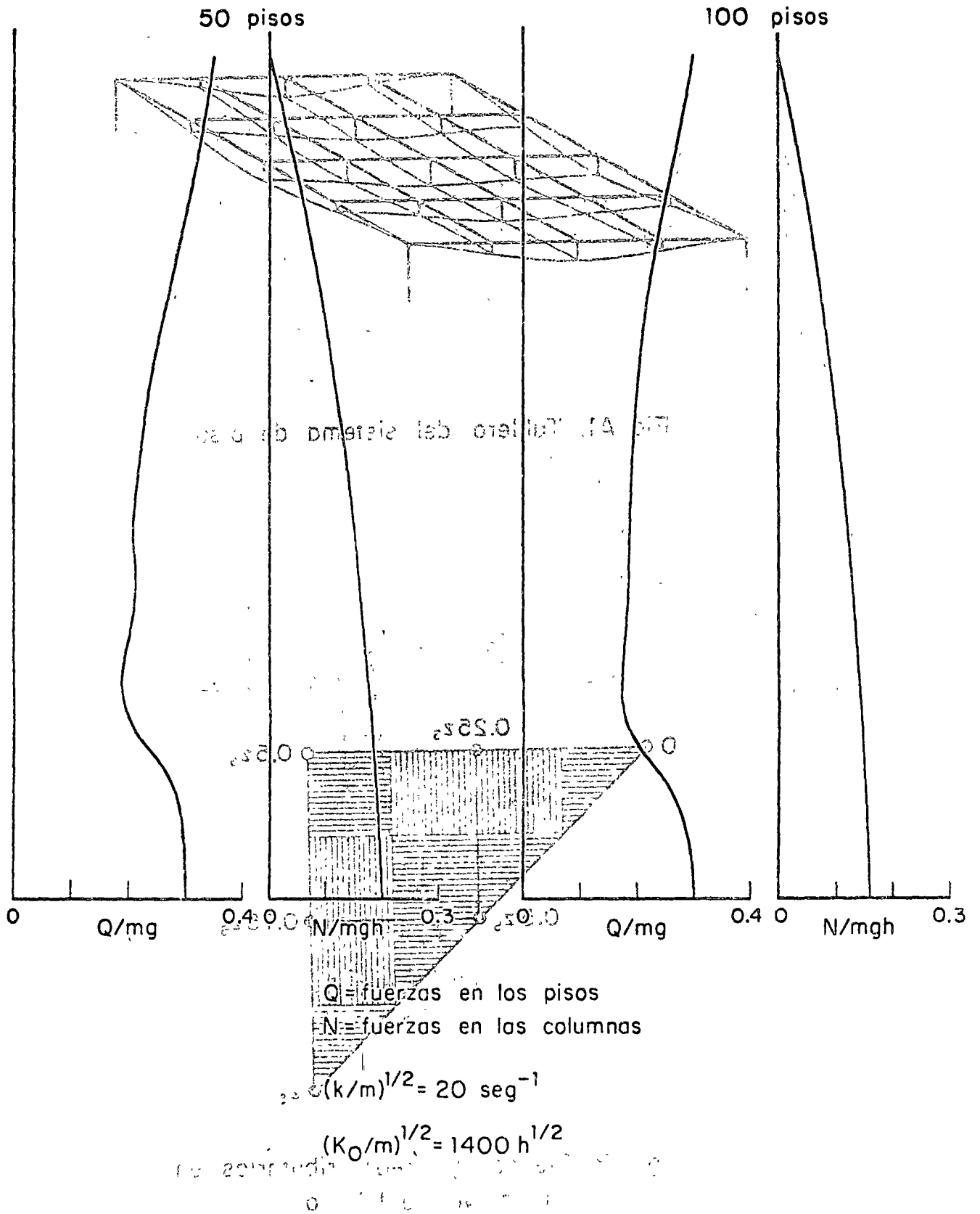


Fig 10. Fuerzas de diseño correspondientes al componente vertical, flecha estática en pisos = 4 cm, edificios de 50 y 100 pisos

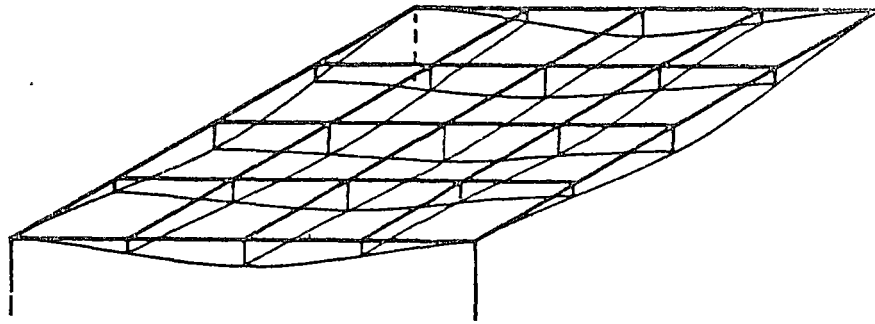


Fig A1. Tablero del sistema de piso

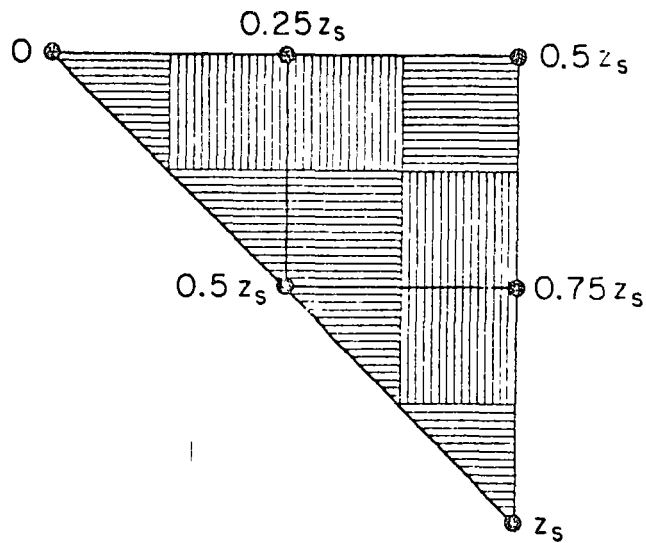


Fig A2. Flechas y áreas tributarias en un octavo de tablero

RESPUESTAS DE EDIFICIOS ALTOS A TEMBLORES CON CINCO COMPONENTES

Emilio Rosenblueth*

Introducción

En diseño suelen idealizarse los temblores como si solo tuvieran un componente y este actuara en una de dos direcciones horizontales ortogonales a la vez. El presente artículo examina la influencia de otros componentes. Se toma el movimiento en campo libre (es decir, el que tendría la superficie libre del terreno si sobre este no existiera estructura alguna) como consistente en dos componentes horizontales de traslación y tres componentes rotacionales, y dicho movimiento se promedia en lo que es la base del edificio. Por lo demás no se tiene en cuenta la interacción suelo-estructura. No se incluye un tratamiento de la traslación vertical porque la idealización que aquí se adopta del comportamiento de los edificios no se presta a ello. Ante la ausencia de registros adecuados el movimiento del terreno se supone coincidente con las soluciones teóricas para formaciones de suelo regulares y homogéneas. El edificio se idealiza como una viga uniforme, de comportamiento lineal, que solo admite deformaciones en corte y torsión.

El trabajo se basa en la ref 5, que a su vez tomó como fuente la ref 4 haciéndole ciertas correcciones. Existe un estudio paralelo que se refiere a edificios con planta de forma arbitraria sujetos a ondas de cortante que inciden a un ángulo cualquiera⁶. En él algunas hipótesis difieren de las que aquí se adoptan.

Análisis modal

Supondremos que la estructura tiene modos naturales clásicos de vibración, es decir, que es capaz de describir, en vibración libre, movimientos dados por el

producto de una función de posición y una función del tiempo². Tal no es rigurosamente cierto aun para la mayoría de las estructuras ideales de comportamiento

* Investigador, Instituto de Ingeniería, UNAM, México, D F.

lineal, pero el error que se introduce al suponer que la estructura está provista de modos clásicos es sumamente pequeño cuando sus grados de amortiguamiento son pequeños, digamos de no más de unos cuantos por ciento, cual sucede en la mayoría de los casos de interés práctico.

En ciertas condiciones, cuando se imparte el movimiento a la estructura a través de un grado de libertad de su base y aquella posee modos clásicos de vibración puede aproximarse la respuesta de diseño que corresponde a una probabilidad fija de excedencia como la raíz de la suma de cuadrados de las respuestas modales asociadas a la misma probabilidad de ser excedidas³. Para ello se requiere que los modos naturales que contribuyen significativamente a las respuestas cumplan las siguientes condiciones: 1 sus frecuencias naturales no son demasiado elevadas, demasiado pequeñas ni demasiado próximas unas a otras, y 2 los grados de amortiguamiento de dichos modos son pequeños. En términos cuantitativos se requiere que cuando mucho una frecuencia de los modos en cuestión exceda apreciablemente al cociente de la aceleración a la velocidad máximas del terreno; que cuando mucho una de ellas sea menor que 2π entre la duración de un segmento de movimiento estacionario equivalente al temblor en cuestión, y que las diferencias entre las frecuencias naturales de interés satisfagan una limitación contenida en la ref 2 en que intervienen los grados de amortiguamiento.

La manera en que han de combinarse los efectos de movimientos según los grados de libertad de la base es función de la correlación que exista entre tales movimientos. Consideraremos dos casos extremos. Cuando no hay ninguna correlación entre los movimientos el efecto de su combinación es sensiblemente igual a la raíz de la suma de cuadrados de las respuestas a cada componente. Cuando la correlación es total debe calcularse la respuesta en cada modo natural sumando los efectos de todos los movimientos de la base y después combinarse las respuestas modales.

Perturbaciones

Consideraremos tres tipos de ondas:

1. Ondas S de trayectoria vertical que llegan síncronamente a la base de la estructura y solo producen excitación horizontal. Las ondas S, como las P, son ondas llamadas de cuerpo pues ambos tipos se presentan en interior de los sólidos. Las ondas S (secundarias), llamadas ondas transversales u ondas de cortante, van acompañadas de deformaciones de corte puro y de oscilaciones perpendiculares a la dirección en que se transmiten, al igual que las ondas de luz. Debido a que en general las ciudades de gran tamaño se construyen en valles cuyo subsuelo esté estratificado en direcciones aproximadamente horizontales, las ondas S sufren una serie de refracciones que dan por resultado su incidencia prácticamente normal a la superficie libre del terreno. Por tal motivo producen oscilaciones prácticamente horizontales y casi simultáneas en toda la base de un edificio de dimensiones moderadas. No consideraremos ondas P (primarias, pues dada su mayor velocidad de transmisión son siempre las primeras en llegar), llamadas ondas longitudinales o de compresión, ya que también estas tienden a llegar viajando casi verticalmente, y acordamos no analizar aquí el efecto de vibraciones verticales de la base del edificio.

2. Ondas de Rayleigh (R) que contienen componentes estrictamente correlacionados de traslación vertical y horizontal así como de rotación con respecto a un eje horizontal. De los diversos tipos de onda superficial que han recibido atención analítica las más conocidas son las ondas de Rayleigh. Estas se presentan en semiespacios homogéneos y en suelos estratificados. Consisten en oscilaciones vertical y horizontal cuyas amplitudes decrecen con la profundidad (decrecen exponencialmente en un semiespacio). Las oscilaciones se verifican en planos verticales que contienen a la dirección de transmisión, la cual es horizontal. Cada partícula del suelo describe una elipse. La velocidad de transmisión de las ondas

de Rayleigh depende del coeficiente de Poisson del terreno. Cuando este coeficiente vale 0.25 la velocidad de las ondas en cuestión en un semiespacio homogéneo es 0.92 de la velocidad de las ondas de cortante². El componente rotacional obedece a que la superficie del terreno se inclina al paso de las ondas.

3. Ondas de Love (L) que constan de un componente horizontal de traslación y uno de rotación con respecto a un eje vertical. Ambos componentes están totalmente correlacionados. Las ondas de Love también son superficiales. Su amplitud es máxima en la superficie libre del terreno. Se presentan en suelos estratificados. Las trayectorias de las partículas son normales a la dirección de propagación de las ondas; de aquí que den origen a rotación con respecto a un eje vertical. La velocidad de propagación de las ondas L depende de la frecuencia de oscilación, es decir, de la longitud de onda. En formaciones que constan de un estrato horizontal que descansa sobre un semiespacio homogéneo la velocidad de las ondas cuya longitud es pequeña en relación con el espesor del manto se aproxima a la de ondas S en dicho manto; la velocidad de aquellas cuya longitud excede apreciablemente al espesor del manto se acerca a la de ondas S en el semiespacio².

Respuestas estructurales

El cálculo de respuestas estructurales no presenta dificultad. Se obtiene el promedio de las traslaciones basales del edificio, cuando estas son senoidales y se deben a ondas R y L, multiplicando su amplitud por $(\sin \lambda)/\lambda$, donde $\lambda = \pi B/L$, B = dimensión de la base en la dirección en que se propagan las ondas y L = longitud de onda. La amplitud media de la rotación basal es $(2/B) \sin \lambda$ por la amplitud de las oscilaciones verticales u horizontales según se trate de ondas R o L respectivamente.

En un edificio de planta simétrica, las ondas S sólo causan cortantes de entrepiso y momentos de volteo; las ondas R producen oscilaciones verticales, cortan-

tes de entrepiso y momentos de volteo, y las ondas L originan cortantes de entrepiso, momentos de volteo y torsiones de entrepiso.

Para las ondas R cada respuesta modal incluye los efectos de rotación y traslación. El momento de volteo (mas no así la fuerza cortante) que resulta de combinar estas respuestas modales se combina a su vez (empleando la raíz de suma de cuadrados) con la respuesta que daría el sistema si fuera una barra rígida:

$$M = \frac{(H - Z)WB^2}{12Hg} \max_t |\ddot{\theta}| \quad (1)$$

Aquí M = momento de volteo, H = altura del inmueble, W = peso del mismo, g = aceleración gravitacional, t = tiempo, θ = rotación basal, la testa indica promedio en el área de la base y los puntos significan derivadas con respecto al tiempo. $|\ddot{\theta}|$ es igual a $1/B$ por la diferencia de aceleraciones verticales \ddot{z} entre los extremos opuestos de la base. Si \ddot{z} es un proceso gaussiano estacionario (es decir, si la distribución de probabilidades de z es normal e independiente del tiempo) en la vecindad de $\max |\ddot{z}|$, el cociente $\max |\ddot{\theta}| / \max |\ddot{z}|$ es igual al cociente de las desviaciones estándar de $\ddot{\theta}$ y \ddot{z} , pues la esperanza de cada una de estas variables es idénticamente nula. Por consiguiente,

$$\max_t |\ddot{\theta}| = \sqrt{2 - 2\rho(t_1)} \max_t |\ddot{z}| / B \quad (2)$$

donde ρ = coeficiente de autocorrelación de \ddot{z} (es decir, $\rho(t_1)$ es igual a la esperanza de $\ddot{z}(t)\ddot{z}(t + t_1)$ entre la variancia de \ddot{z}). Según la ref 2, tratándose de temblores en terreno firme puede aproximarse ρ mediante la expresión

$$\rho(t_1) = e^{-\alpha|t_1|} \cos \beta t_1 \quad (3)$$

donde $\alpha \approx 8 \text{ seg}^{-1}$ y $\beta \approx 14 \text{ seg}^{-1}$. (Son de esperarse valores de α y β considerablemente mayores para las ondas R, en las que predominan periodos mucho más largo que para el temblor en su conjunto.) Esta relación solo será aplicable cuando B no sea excesivamente pequeño, pues ρ está poco definido cuando t_1 tiende a cero. Evidentemente, $\max |\ddot{\theta}| < \max |\ddot{\theta}|$, y esta última cantidad puede estimarse acudiendo a una sugerencia de Newmark¹:

$$\max_t |\ddot{\theta}| = \frac{\delta \max(z^2)}{c_r \max |z|} \quad (4)$$

donde c_r = velocidad de las ondas de Rayleigh. El coeficiente δ se sugiere con base en el registro del temblor de El Centro 1940. Tratándose de otros movimientos del terreno dicho coeficiente puede yacer entre 5 y 15. En el análisis tomaremos $\max |\ddot{\theta}|$ como lo suministra la ec 2 pero con una cota superior igual a la que da la ec 4.

Cada tipo de onda corresponde a dos direcciones. Los componentes del movimiento del terreno según estas direcciones están parcialmente correlacionados entre sí³, y tal correlación debería tenerse en cuenta al combinar sus efectos.

Ejemplo

Consideremos un edificio de planta cuadrada y simétrica, para el que $B = 30$ m, $H = 60$ m y el periodo fundamental de vibraciones en cortante así como en torsión vale 2 seg. Adoptemos para cada tipo de onda un espectro de aceleraciones de diseño (ya corregido por amortiguamiento) que sea independiente del periodo para periodos menores que 0.2 seg e inversamente proporcional al periodo fuera de este intervalo. Para ondas R y L consideremos asimismo un espectro plano de aceleraciones de diseño, es decir, cuyas ordenadas son independientes del periodo en todo al intervalo de interés. En lo que toca al primer espectro asignaremos a α y β la mitad de los valores que se consignan a continuación de la ec 3, y en lo atañe al segundo espectro, la décima parte de estos valores. Tomemos $c_r = 300$ m/seg. Al analizar los efectos de las ondas L supondremos que el edificio se apoya en un estrato horizontal de 30 de espesor subyacente por un semiespacio de roca. Las velocidades respectivas de ondas de cortante valen 300 y 3000 m/seg y el cociente de los módulos de rigidez en ambos materiales es 100. Las velocidades resultantes c_r de ondas L se muestran en la fig 1.

Las figs 2-4 consignan las respuestas de diseño calculadas, normalizadas con respecto a la aceleración espectral asociada al modo fundamental, A_1 . Ameritan ser

comentadas tres particularidades de estas curvas: 1 La fuerza cortante basal para ondas R excede a $A_1 W/g$ siendo que nunca sucede así en respuesta a perturbaciones puramente traslacionales²; tal resultado refleja la contribución del componente rotacional del terreno. 2 La derivada del momento de volteo, dM/dZ , es finita para las ondas R en el punto $Z = H$ mientras que tal derivada es siempre nula en respuesta a perturbaciones de traslación pura; la diferencia proviene de los momentos que suministra la ec 1; la omisión de estos últimos momentos introduce grandes errores en momento de volteo cerca del extremo superior del edificio si se compara con los momentos de respuesta modal, pero estos son tan pequeños que no consta que el error mencionado deba conducir a modificaciones en el diseño de las estructuras usuales; y 3 Las torsiones de entrepiso son grosso modo constantes a lo alto de casi toda la estructura mientras que los requerimientos que generalmente contienen los reglamentos establecen torsiones "accidentales" de entrepiso proporcionales a las fuerzas cortantes de entrepiso; puede explicarse este resultado al observar que cuando los modos naturales de orden 1, 2, 3, ... se normalizan con respecto a la respuesta máxima, su importancia relativa en una viga de corte sujeta a una perturbación horizontal de traslación con espectro hiperbólico de aceleraciones se halla en la proporción 1:1/3:1/5: ...; estos coeficientes han de dividirse entre las correspondientes longitudes de onda (las cuales son inversamente proporcionales a las rotaciones medias del terreno) para obtener la importancia relativa de las torsiones modales, así que en un intervalo de periodos en que la velocidad c_g fuese constante todos los modos naturales serían igualmente importantes; en el ejemplo que hemos resuelto predominan los modos 4, 5 y 6 debido a la variación de c_g con el periodo y al corte en el espectro de diseño que supusimos en un periodo de 0.2 seg.

Conclusiones

Se encontró que los siguientes efectos de componentes del movimiento sísmico, adicionales a los de traslación horizontal ameritan atención: 1 la cortante basal

causada por las ondas de Rayleigh, pues excede al producto de la masa del edificio y la aceleración espectral que corresponde al periodo fundamental de vibración; 2 los momentos de volteo cerca del extremo superior del edificio, originados por rotación de la base con respecto a ejes horizontales, en vista de que estos momentos son superiores a la integral de la envolvente de cortantes de entrepiso, y 3 la torsión que producen las ondas de Love, especialmente en la porción superior de la obra, dado que no son proporcionales a las fuerzas cortantes de entrepiso.

Para lograr un análisis más confiable de los fenómenos descritos se necesitará registrar simultáneamente los seis componentes de los temblores y adoptar idealizaciones más realistas de las estructuras.

Reconocimiento

El autor agradece a L Esteva sus útiles críticas al manuscrito de este trabajo.

Referencias

1. Newmark, N M, "Torsion in symmetrical buildings", Proceedings of the Fourth World Conference on Earthquake Engineering, Santiago, Chile, 1969, 2, 19-32.
2. Newmark, N M y Rosenblueth, E, Fundamentals of earthquake engineering, Prentice-Hall, Inc, Englewood Cliffs, N J, 1971.
3. Penzien, J y Watabe, M, "Simulation of 3-dimensional earthquake ground motions", Bulletin of the International Institute of Seismology and Earthquake Engineering, 12 (1974), 103-15.
4. Rosenblueth, E, "The six components of earthquakes", Proceedings of the Twelfth Regional Conference on Planning and Design of Tall Buildings, Sidney, Australia, 1973, 63-81.
5. Rosenblueth, E, "Tall buildings under five-component earthquakes", enviado para su publicación en Proceedings, American Society of Civil Engineers.
6. Tani, S, Sakurai, J e Iguchi, M, "The effect of plan shape and size of buildings on the input earthquake motions", Proceedings of the Fifth World Conference on Earthquake Engineering, Roma, 1973, 2, 1973, 1927-40.

Nomenclatura

A_1 = aceleración espectral para el periodo fundamental de vibración en cortante

- B** = dimensión de la base del edificio en la dirección de trasmisión de las ondas
- c_l** = velocidad de las ondas de Love
- c_r** = velocidad de las ondas de Rayleigh
- H** = altura del edificio
- L** = longitud de onda
- M** = valor de diseño del momento de volteo
- S** = valor de diseño de la fuerza cortante de entrepiso
- T** = periodo natural
- t** = tiempo
- t_1** = tiempo de recorrido, de la base del edificio, por una onda
- Z** = coordenada vertical
- z** = desplazamiento vertical
- α** = coeficiente que aparece en la función de autocorrelación
- β** = coeficiente que aparece en la función de autocorrelación
- θ** = rotación de la base con respecto a un eje horizontal
- λ** = $\pi B/L$
- ρ** = coeficiente de autocorrelación en los acelerogramas

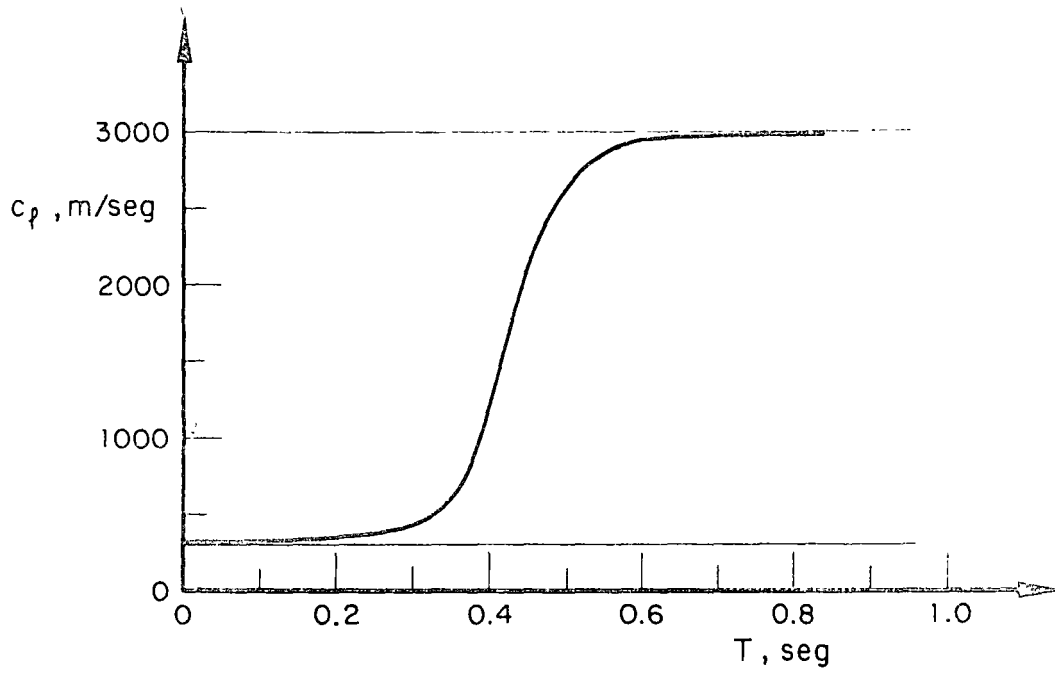


Fig 1. Velocidad de las ondas de Love

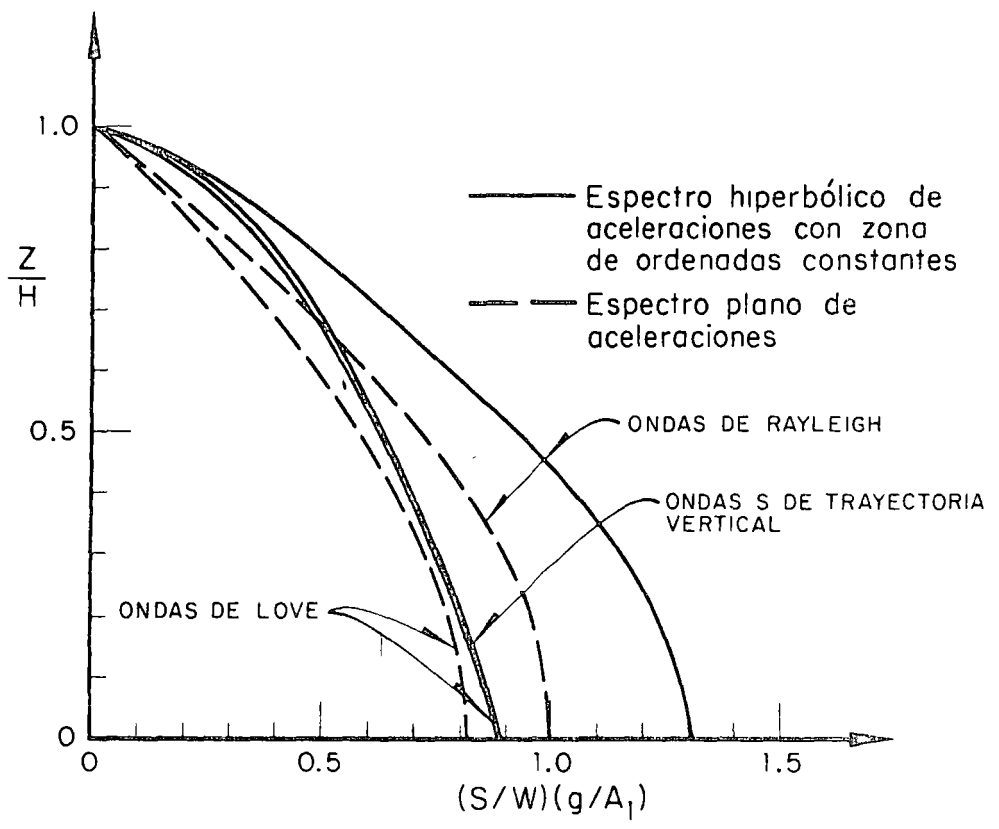


Fig 2. Distribuciones de cortante

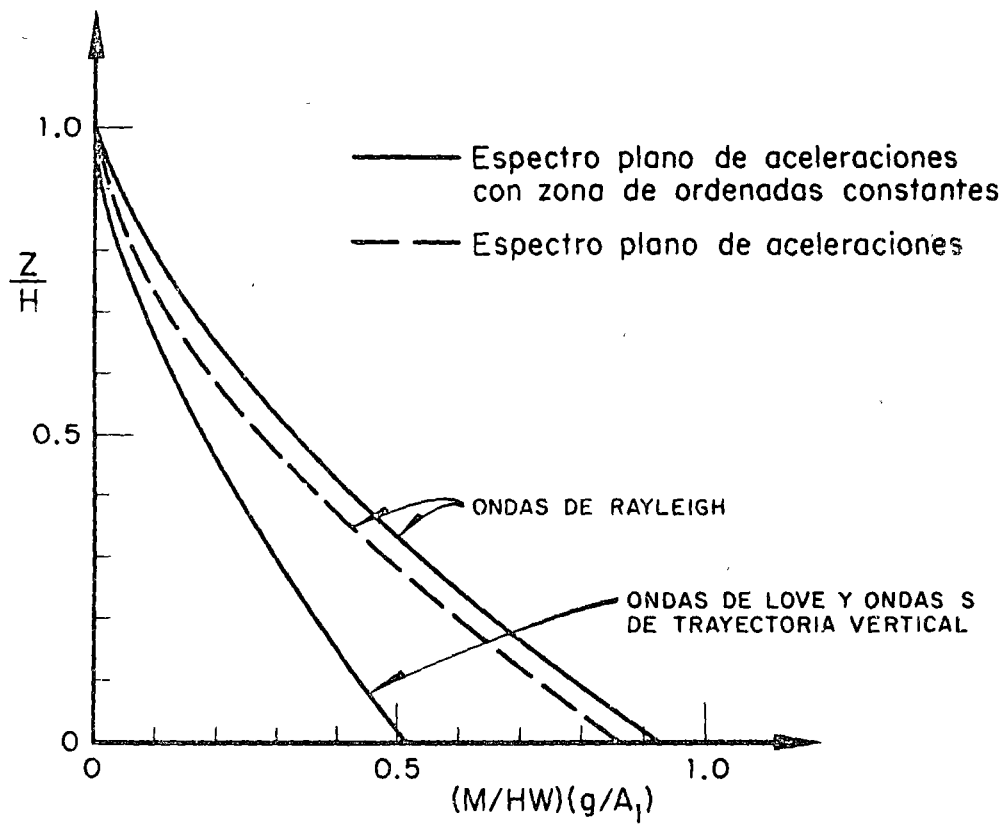


Fig 3. Distribuciones de los momentos de volteo

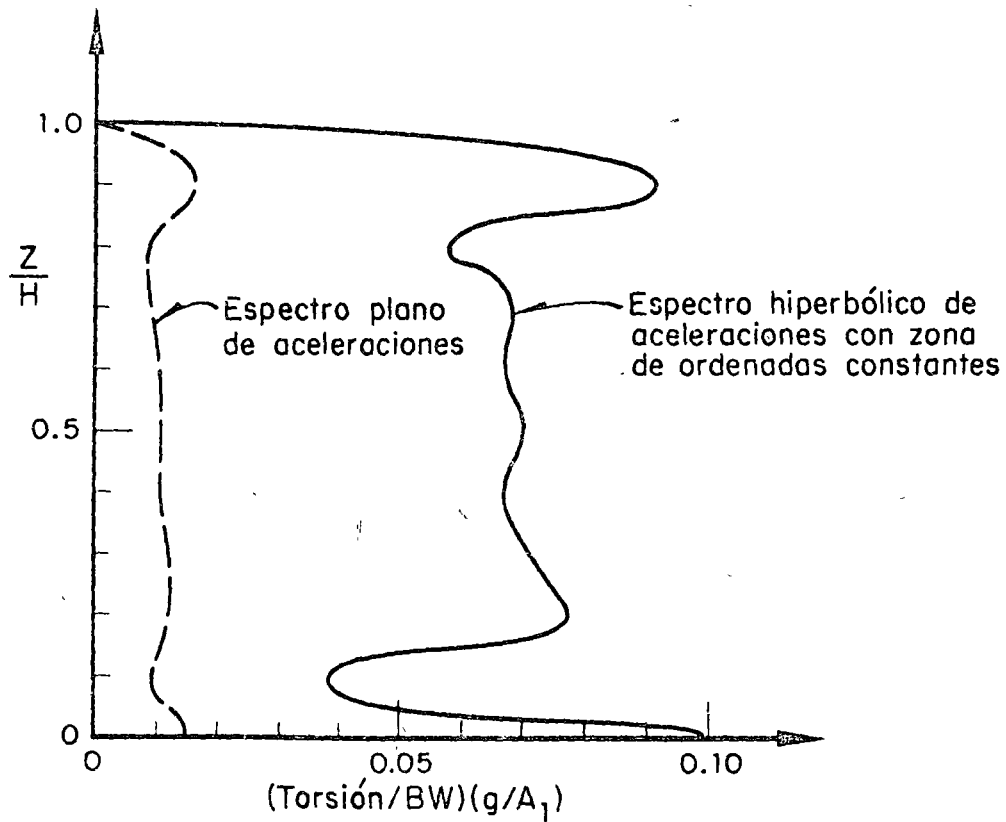
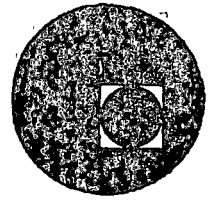


Fig 4. Distribución de torsiones inducidas por las ondas de Love



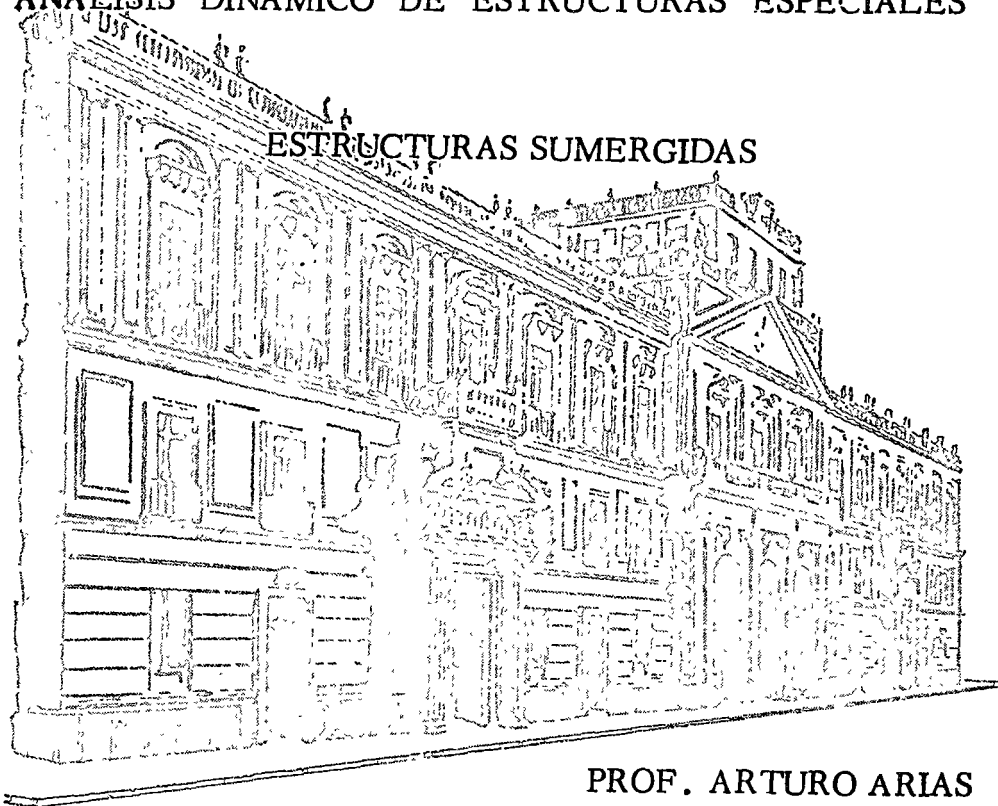


centro de educación continua
división de estudios superiores
facultad de ingeniería, unam



III CURSO INTERNACIONAL DE INGENIERIA SISMICA

ANÁLISIS DINAMICO DE ESTRUCTURAS ESPECIALES



PROF. ARTURO ARIAS

Julio-AGOSTO, 1977.

Handwritten text at the top of the page, possibly a title or header, which is mostly illegible due to fading and bleed-through. Some words like "Number" and "Date" are faintly visible.



EARTHQUAKE-PROOF MEASURES
FOR
A WATER SUPPLY SYSTEM

THE JAPAN WATER WORKS ASSOCIATION
PUBLISHED BY THE ASSOCIATION
TOKYO, JAPAN, 1950

JAPAN WATER WORKS ASSOCIATION

THE 1ST SUBCOMMITTEE ON COUNTERMEASURE
FOR EARTHQUAKE DISASTER
JAPAN WATER WORKS ASSOCIATION

Chairman

Tamon Ishibashi

Vice Chairman

Kōji Kaneda

Members

Kenji Kunikawa

Hideo Suzuki

Jūzaburō Asada

Tomoji Yoshikawa

Masao Yamashita

Hiroji Kawasaki

Asachi Ōishi

Susumu Tanaka

Kimio Shiozawa

Masabumi Tada

Takashi Koide

Tōichi Kawai

Masatoshi Kageura

1. GENERAL PRINCIPLES

1.1. INTRODUCTION

1. Every key installation constituting a water supply system shall have its structure determined through a reasonable computation based on due evaluation of the effects of an earthquake.

2. For such installations which may not be sufficiently protected against an earthquake due to financial limitations, the following precautions shall be exercised:

(1) To adopt means to confine damages caused by an earthquake to a certain extent.

(2) To apply devices to facilitate recovery of the earthquake-damaged units.

(3) To provide measures to prevent secondary effects of the earthquake damages.

3. Such installations which are especially important, which are liable to earthquake damages due to structural characteristics, which may develop damages not easily detectable, or which will present difficulties in or demand a long duration for recovery from the earthquake damages, shall not be built as an integral unit, but either divided into two separate units or equipped with an emergency installation.

4. It is desirable to place the installations on a solid uniform foundation. In order to ascertain the quality of a ground, characteristics of the ground, height of ground water level, bearing capacity etc. shall be examined carefully through an examination of geological structures, and with the above result earthquake-proof measures shall be adopted in construction of each installations.

When placing them on a soft ground due to inevitable circumstances, the ground shall be treated to make a solid uniform foundation by pile driving, soil replacing, tightening, consolidation by drying, solidifying and other suitable measures.

5. The installations shall not be built of such materials as wood or brick, stone etc., as a rule they shall be built of steel or reinforced concrete.

6. For such installations which require water-tightness sufficient care shall be exercised in design and construction about mix of concrete, thickness of wall, water-proof measures, expansion joint so that the water-tightness may not be impaired by an earthquake.

7. When connecting the structures of exceedingly varying rigidities, the earthquake-proof joints shall be placed between them.

8. Whenever so specified, only the standardized items shall be used.

9. The surrounding conditions shall be studied in advance to determine the construction site of adequate safety, for the earthquake damages occurring at the neighborhood (namely, collapse, failure or other types of destruction) are apt either to affect safety of the installation or hinder effective operation of the system. When and where such precautions are impossible, a protection work shall be provided.

10. The design and practice of plain and reinforced concrete structures shall comply with Standard Specifications for Concrete (1956), Japan Society of Civil Engineers.

11. The Earthquake-proof computation and details of construction of buildings

shall comply with Building Codes (Act 201, May 24, 1950), Provisions for Building Codes (Ordinance 338, November 16, 1950) and various criteria of structural computation established by Architectural Institute of Japan.

1.2. CRITERIA OF EARTHQUAKE-PROOF DESIGN

1.2.1. Design Seismic Coefficient

1. The earthquake forces shall be determined by multiplying the dead load (fixed and surcharge loads) by a design seismic coefficient.

2. The standard horizontal coefficient shall be carefully determined for each province by considering the characteristics of regional geographical settings and within the ranges shown in Fig. 1. However, the values thus determined shall on no account be less than 0.1.

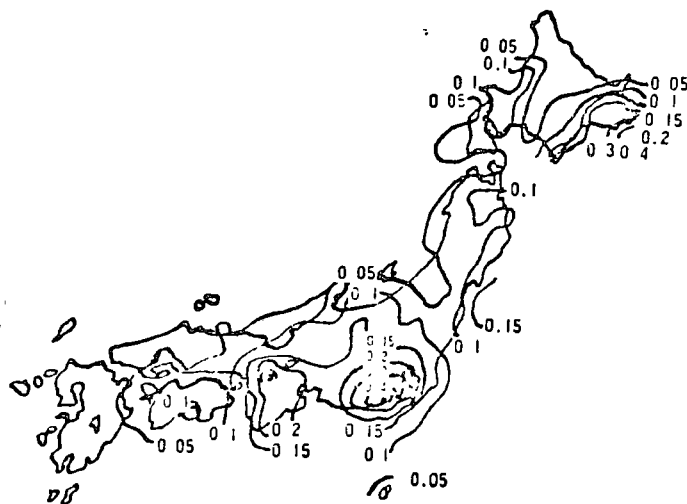


Fig. 1

3. The design seismic coefficient for structures shall be obtained by multiplying the standards coefficient by the ratios classified in Table 1 for each type of foundation and installation. However, when the resultant value is less than 0.1, the design coefficient shall be assumed at just 0.1, and when it exceeds 0.3, it may be modified to be just 0.3. For tower-shaped structures, aqueducts and other special types of structure, however, this value shall be over 0.4.

Table 1. Multipliers for Seismic Coefficient vs. Types of Foundation and Installation

Type of foundation	Water purification installation and open channel	Tower-shaped structure and aqueduct	Subsoil pipeline
Rock foundation and solid sand gravel layer	0.4	0.5	0.3
Diluvial layer	0.7	0.7	0.7
Alluvial layer	1	1	1
Soft foundation	2	2	2

1.2.2 Unit Weights

The unit weights of materials to be used for designing shall refer to the values shown in the following table, with exception of some special items:

Table 2. Unit Weight

Materials	Unit Weight (kg/m ³)	Materials	Unit Weight (kg/m ³)	Materials	Unit Weight (kg/m ³)
Water	1,000	Steel	7,850	Stone	2,600
Reinforced Concrete	2,400	Cast Steel	7,850	Gravel or Rock Fragment	1,900
Plain Concrete	2,300	Cast Iron	7,270	Sand	1,900
Mortar	2,100	Cast Iron Pipe	7,200	Soil	1,600
Brick	2,000	Wrought Iron	7,800	Timber	800
Prestressed Concrete	2,450	Lead	11,100		
		Copper	8,900		

Unit weight of sand, gravel or rock fragment, 1,900 kg/m³, is that in case saturated with water.

1.2.3. Allowable Stress

1. Allowable stresses of concrete and metals shall be determined making reference to Standard Specifications for Concrete, Japan Society of Civil Engineers, Design Specifications for Steel Road Bridge, Japan Road Association, Building Codes, Provisions for Building Codes and various criteria of structural computation, Architectural Institute of Japan.

2. The allowable stress of a foundation shall be determined by Table 3, through an examination of geological structures in site. However for such structures which are especially important, actual loading test shall be exercised.

Allowable stresses under earthquake conditions shall be the same values as those in Table 3 for foundations except rock foundation, and 1.5 times these values for rock foundations

Table 3. Allowable Stresses of Foundations
(cf. Provisions for Building Codes, Ordinance No. 93)

Fondation	Allowable stresses (t/m ²)	Remarks
Hard rock bed	400	
Soft rock bed	250	
	100	
Gravel	30	
Mixture of gravel and sand	20	
Sandy clay, or loam	15	
Sand or clay	10	

For the foundations not specified in the table above, the allowable stresses shall be determined analogously to the specified foundations of a similar nature.

3. The allowable bearing capacity of the foundation piles shall be determined by a loading test. For simpler types the values may be less than those computed from Table 4.

These same values shall also be used when an earthquake shock is taken into consideration.

Table 4. Allowable Bearing Capacity of Foundation Pile
(cf. Provisions for Building Codes, Ordinance No. 93)

Method of Pile Driving	Long Time Allowable Bearing Capacity	Short Time Allowable Bearing Capacity
Drop Hammer or Single Acting Hammer	$R = \frac{WH}{5S+0.1}$	2 times Long time Allowable Bearing Capacity
Double Acting Hammer	$R = \frac{F}{5S+0.1}$	

Denotation: R = allowable bearing capacity of a pile (t)
 W = weight of a hammer (t)
 H = drop height of a hammer (m)
 F = shock energy of a double acting hammer (t-m)
 S = final penetration depth of a pile (m)

1.3. METHODS OF EARTHQUAKE-PROOF COMPUTATION

1.3.1. Principles of computation

The computation of the stresses which develop in the structure during an earthquake is carried out under the assumption that the external force, i.e., the mass of the structure multiplied by the design seismic coefficient, acts statically in a horizontal direction. It is also assumed here that the magnitude of the coefficient is uniform for the entire members of the structure. For the structures which are apt to resonate at the time of earthquake, however, the coefficient shall be somewhat magnified at the upper level.

1.3.2. Earth pressure during earthquake

As to the earth pressure occurring in time of earthquake the computation of positive and resisting earth pressure is exercised on the assumed condition that the combined masses of the foundation and superstructures, with the entire weights magnified by $(1+K/2)$ times, revolve toward the danger side by an angle

$$\theta = \tan^{-1}K \quad (K: \text{seismic coefficient})$$

against the ordinary perpendicular direction. The Zimmerman's diagrammatical method based on the Coulomb's soil wedge theory is recommended as convenient for determining the each pressure in practice.

1.3.3. Water pressure during earthquake

The increment of water pressure against a containing wall occurring due to earthquake is given by the formula.

$$p = \frac{7}{8} Kw \sqrt{Hy}$$

where: p = increment of water pressure due to earthquake, (kg/m²),

K = seismic coefficient,

w = weight of a unit volume of water (kg/m³),

H = water depth (m),

y = depth below surface at the acting position of p (m).

The water pressure may also be obtained hydrostatically on the assumption that in time of earthquake the free surface exists at an imaginary level h above the estimated high-water level, as shown by the following formula:

$$h = 2K^2 H \quad (\text{m})$$

1.3.4. Earthquake-proof computation of a retaining wall

In the earthquake-proof computation of a retaining wall the forces acting on the wall surface shall include the earth pressure in time of earthquake, the weight, earthquake force and buoyancy of the wall, the resisting pressure of the soil in front of the wall, the difference of the water levels before and behind the wall, the weight of and earthquake effects of the surcharge load on the surface of the retained soil.

The combined horizontal component of these forces shall not exceed the frictional resistance of the wall foundation; the maximum pressure occurring at the bed shall not exceed the allowable stress of the foundation during earthquake; and the resultant vector of these forces shall not fall beyond 1/4 of the base length from the center of the base. However, this proportion may be increased up to 1/3 for a strong foundation.

2. DETAILED TREATISE

2.1. WATER SOURCE INSTALLATIONS

2.1.1. River sources

1. Even at ordinary times good care shall be exercised to prevent denudation of the hill slope in the watershed.

2. Careful precaution shall be exercised so that intakes of gate and pipe type may not be clogged by surface soils and rock debris originating from adjoining hills at the time of earthquake.

3. The intake pipe crossing an embankment shall be made of cast iron, ductile cast iron or steel, laid upon a strong solid foundation, well protected with concrete, and refilled with special care.

4. Intake tower:

(1) The most desirable type of an intake tower is a reinforced concrete structure of a cylindrical appearance.

(2) The intake tower shall be given a reasonably deep embedment into a strong foundation. When a sunk-well technique is applied, the embedment depth shall be sufficiently deep and the bottom shall be lined with concrete to a considerable thickness.

(3) The conduits leading away from the intake tower shall be of cast iron pipes, ductile cast iron pipes or steel pipes, and be constructed strongly.

(4) A foot bridge approaching the intake tower shall be as light as possible, so that the tower may remain free from any extra load.

(5) It shall be avoided to locate the intake tower at such places where there is a possibility of burial due to collapse of river embankment or hill slopes, or of scouring due to currents.

(6) In computing the stability of an intake tower, a particular emphasis shall be placed on the buoyancy so that the safety of the structure may be guaranteed against earthquake shocks when the interior is empty.

2.1.2. Reservoir dam and related works

1. The design and construction of a reservoir dam shall comply with the following provisions unless otherwise designated:

Japanese National Committee on Large Dams, Specifications for Dams.

Standard Specifications for Gravity Dam Concrete, Japan Society of Civil Engineers 1956.

2. For the outlets and outflow channels, either of open-channel or of tube type, the same sort of care shall be exercised as for the case of item 2.1.1.

3. For the intake tower, the same sort of care shall be exercised as for the case of the item 2.1.1-4.

2.1.3. Infiltration gallery

1. A perforated reinforced concrete pipe of sufficient strength with socket shall be laid on a homogeneous foundation; the spigot shall be inserted sufficiently deep into the socket and its periphery protected with strong wood frames or other devices.

2. It is desirable that the attached manholes and junction wells shall be placed on an especially strong foundation, and the joints connecting 2 or 3 succeeding pipes immediately adjoining them on both sides shall be dressed in the comparatively long thimbles.

2.1.4. Shallow well

The side walls shall be, as a rule, of a cylindrical form and built of reinforced concrete.

2.1.5. Deep well

1. The well casings shall be equal or superior to the JIS-G3452-type carbon steel pipe for pipeline; the joints and strainers shall also possess sufficient strength.

2. The casings shall project beyond the floor slab of the pump chamber.

3. It is not advisable to shape the upper portion of the deep well casing similar to that of a shallow well in order to use it also as a pump well.

2.2. OPEN CHANNEL INSTALLATION

2.2.1. Open conduit and covered conduit

1. In principle, an open conduit and a covered conduit shall be built of reinforced concrete, and the entire section shall be a monolithic structure.

2. It shall be avoided to place them on or inside the refilled soil. When otherwise impossible, the techniques described in the item 2.3.1-2 shall be applied.

3. The expansion joints shall be installed at approximately 10 to 20 m intervals; they shall also be used at such places where different geological formations meet, and before and behind a bridge, weir, manhole and gate, etc.

4. Since the toe and shoulder of a hill slope are apt to collapse, sufficient care shall be exercised in location and actual construction.

5. At such places where they cross rivers and other concave topographies by a siphon or pipe bridge, the earthquake-proof measures shall comply with the items 2.4.6 and 2.4.7.

2.2.2. Tunnel

1. As a rule a tunnel shall be lined with concrete.

2. The route shall avoid such places as a hill slope which exerts a biased load.

3. Since the entrance and exit are apt to collapse, they shall be protected adequately.

4. The cross-sectional shape shall be as circular as possible. When the horseshoe shape is used the bottom shall be an inverted arch of considerably large rise and increased thickness at both ends.

5. At such places where there is a fault line running in the vertical direction or where sharply differing geological formations meet, the lining shall be insulated in the longitudinal direction, and the lining before and behind this position particularly strengthened.

6. In the case of a clear water conveyance tunnel, expansion joints shall be inserted at construction joints and the insulation places described in the item 5.

2.2.3. Aqueduct bridge

1. An aqueduct bridge shall be built of reinforced concrete or steel, and its earthquake-proof design shall comply with the provisions specified for ordinary bridges.

2. Since the structure is top-heavy, the design shall be so arranged as to prevent it from falling off the bearing plate due to a horizontal thrust caused by an earthquake. For such purposes it is advisable to extend arms from bridge piers, and connect the bridge piers to the aqueduct beams with diagonal members so that both tensile and compressive stresses may be transmitted directly to the piers.

3. The bridge piers shall be equipped with appropriate transversal straddling post to prevent overturning due to earthquake.

4. The post of the pier and the foundation shall be connected adequately.

5. The abutment, which is generally vulnerable to earthquake shocks, shall rest on a firm solid foundation with a large embedment depth.

6. Special care shall be exercised in designing and constructing the wing walls of the abutment to make them substantially earthquake-proof, so that the back-filling may not be washed due to collapsing of the wing walls to invite destruction of the conduit.

7. Since the connection of the conduit and aqueduct bridge constitutes one of the most vulnerable points, an effective expansion joint shall be installed at this position. In cases where an intensive earthquake shock is expected, a further safety shall be

guaranteed by installing two joints at a relatively close interval.

2.3. INSTALLATIONS FOR WATER PURIFICATION AND DISTRIBUTION

2.3.1. Basin-well type structure

1. It is defined that the term "basin-well type" represents various types of impounding structures shaped like a basin or well, such as a grit chamber, a mixing basin, a sedimentation basin, a filtration basin, a clean water basin, a distribution basin, a conveying pump well, etc.

2. A structure of this category shall not be placed upon a refilled earth, or near a slope shoulder or toe which is apt to collapse. If otherwise impossible, it shall rest on a pile foundation or reinforced concrete columns supported on the existing ground, and in both case the bearing capacity of the refilled earth shall be disregarded in the process of computation.

3. The tops of the foundation piles shall penetrate into the structure as deeply as possible.

4. The material of the foundation piles which stand over the ground water table shall not be wood but reinforced concrete.

5. If it is necessary to construct a unit structure astride foundations with different bearing capacity, a soft part of the foundation shall be strengthened by pile driving or other devices so that the bearing capacity of the foundations may become almost uniform, then the structure shall be constructed on the foundations. Besides an expansion joints shall be installed at the position between the foundations.

6. Any type of structure having simpler appearance both in plan and profile and devoid of abrupt changes in configuration is advantageous in resisting earthquake shocks. Accordingly a circular plan shape is generally preferable to angular one for better resistance against earthquake shocks.

7. A large haunch shall be placed at the corners of a structure.

8. Particular care shall be exercised in designing the connecting points of different structures by means of installing expansion joints or increasing strength since they are vulnerable to earthquake shocks.

9. The floor and side wall of the basin-well shall be built of reinforced concrete in accordance with the earthquake-proof design and rest on a solid foundation so that their combination may act as a monolithic unit.

10. The side wall and floor of the basin-well shall be made watertight by elaborately applying high-quality concrete. In case a waterproof mortar coating is applied to a purified water storage basin or a basin of a large depth, it shall be reinforced with metal laths. The same precaution will also improve the safety of the protection concrete or mortar coating for a water proof layer of asphalt or other materials.

11. On the side walls the expansion joints shall be placed near the corners. At other portions the expansion joints shall be inserted at intervals of 10~15 m for a thin wall and 20~30 m for a thick wall. The gap of the joint shall be ordinarily 1 to 3 cm.

12. A rigid frame structure of reinforced concrete shall be provided with bar arrangements not in the manner shown in (a) but in (b), Fig. 2.

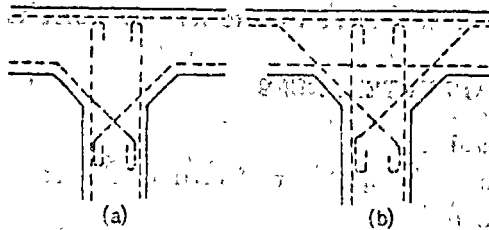


Fig. 2

13. Flexible joints, such as mechanical joints or Gibault joints shall be inserted in both the inlet pipe and the outlet one at the connecting portions to the basin.

14. The axial bars in a column shall be well buried in the concrete up and below. The effects of hooks shall not be counted in computing the bond stress. The end portions of the column shall have particularly dense arrangements of either tied or spiral bars.

15. A canopied basin shall be designed in such a manner as to allow safe entrance and exist even in time of earthquake.

16. Since the doorway and inspection windows are vulnerable to local damages due to earthquake, they shall be reinforced with special care.

2.3.2. Water tower

1. The foundation of a water tower shall rest on a ground of particular reliability. It is desirable even on a favorable ground to secure as great an embedment as possible.

2. A cylindrical structure of water tower is advantageous to safety against earthquake.

3. The riser portion of an inlet pipe which is housed inside the tower shall be supported along the wall surface. It shall be born, if available, by the columns in the center which support a canopy for a large tower. It is advisable to connect the columns with horizontal diagonals.

4. If further the inside face of the tower wall is made water-tight by lining with steel plates more than 3 mm thick, a fear of leakage will be much relieved assuring extreme safety against earthquake shocks.

2.3.3. Elevated tank

1. The material for an elevated tank shall be steel in preference to reinforced concrete in view of safety against earthquake shocks.

2. The riser portion of various attached pipes shall be equipped with earthquake proof joints near the ground surface.

3. The design value of seismic coefficient for an elevated tank shall assume that specified in item 1.2.1 up to the height of 16 m; for a portion beyond this height the coefficient shall be increased by 1/20 times this value per each height increment of 4 m.

4. The elevated tank shall be provided with as many supporting columns as possible, with horizontal and diagonal members adequately arranged to prevent buckling.
5. The tank shall be tied fast to the supporting frame.

2.3.4. Pressure tank

A reclining type is recommendable as safe for a pressure tank.

2.4. PIPELINE AND APPURTENANCES

2.4.1. Pipeline in general

1. The most preferable earthquake-proof method is to select a reliable ground for the site of a pipeline route.

2. The route shall avoid an abrupt bend either horizontal or vertical. When an abrupt bend is included due to unavoidable circumstances, it is necessary for safety to place an anchor block equipped with earthquake-proof joints before and behind it.

3. If a pipeline is laid on a refilled earth, the site where collapsing of ground is likely to occur, such as shoulder of road, shall be avoided.

4. The embedment depth of a pipeline shall be arranged in such a manner as to allow convenient maintenance as well as easy repair.

5. A solid uniform ground is desirable along the entire route.

When a pipeline is laid on a soft ground due to unavoidable circumstances, steel pipes or ductile cast iron pipes with flexible joints shall be used, and, if necessary, the ground shall be reinforced by ladder struts, pile driving etc..

6. At such places where soft and firm grounds join, an earthquake-proof joints shall be installed near the latter.

7. It shall be avoided as a rule to lay the main pipe on the reclaimed area, vicinity of ditches, river shores, beaches, cliffs or bulkheads.

8. When a pipeline is laid across or near other installations under ground, a space more than 30 cm at least shall be maintained between them.

9. The distribution pipeline system is desired to be installed as block systems such as Fig. 3, so that in event of damages inflicted on any part of the system the suspension of water supply operation could be confined to as small a region as pos-

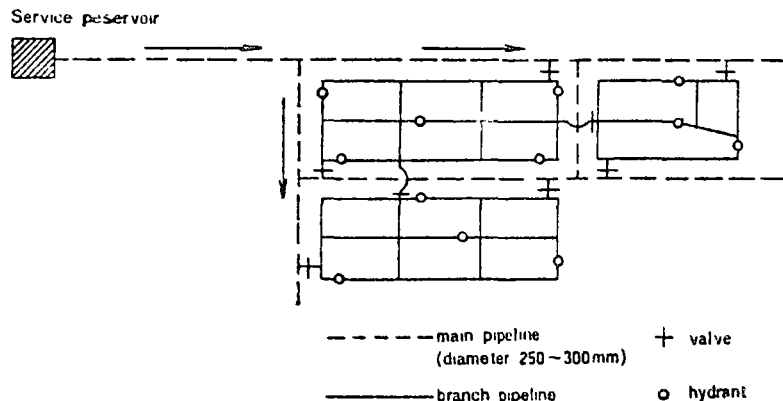


Fig. 3. An example of block system

sible, and supplying of water could be begun again as soon as possible after repair of earthquake damages.

10. Even such types of pipe as a water conveyance pipe and a distribution main pipe which do not possess branch pipes shall be equipped with valves at an interval of about 500 m to 1000 m.

11. It shall be avoided to lay the special fittings continuously. A straight pipe or a cut one shall be inserted between two adjoining special fittings.

12. Near the position of a tee or cross pipe of a key pipeline it is desirable to install flexible joints at the two pipelines meeting at right angle.

13. When a bend pipe or a tee pipe is protected with a concrete block, it is desirable to avoid to install the pipe deeply inside the concrete block.

14. When inserting along the pipeline such appurtenances as a fire-hydrant or a gate valve, etc., which present different characteristics of vibration due to earthquake from that of the pipe, it is desirable to install flexible joints before and behind it.

15. Various types of pipe which penetrate through the surrounding wall or bottom slab shall not touch the wall body directly. When it is necessary to install them in direct contact to the wall in order to ensure water-tightness, flexible joints shall be installed apart from but near the wall. The same procedure is recommendable between a pump and a suction or delivery pipe.

16. A suction pipe which is suspended down a pump well shall be fixed to the wall with strong metal fittings to prevent it from vibrating in a mode different from that of vibration of the wall.

17. When a pipe is laid on a steep slope near a distribution reservoir, the pipe shall be fixed in the ground by anchor blocks, for instance in such a manner that it is fixed by steel bars to the dented anchor blocks, and expansion joints shall be installed between them.

2.4.2. Ductile cast-iron pipe for water works and cast-iron pipe for water works

1. In case a ductile cast-iron pipe for water works or a cast-iron pipe for water works is used, as a rule that of mechanical joint shall be used.

2. A flange joint shall not be used except before and behind a valve or at the position of the pipe appurtenances to a pump which is subject to occasional removal and liable to vibration.

3. A favorable ground shall bear the pipe directly on the natural surface, avoiding, if possible, the use of the foundation block.

4. When the foundation block is used, the bearing area shall be adequately large lest it present a concentrated load on the pipe.

2.4.3. Galvanized steel pipe for water service and coated steel pipe for water service

When galvanized steel pipe for water service or coated steel pipe for water service is used, screw joint or arc-welded joint shall be used as a rule and, when necessary, expansion joint shall be inserted.

2.4.4. Centrifugal reinforced concrete pipe and prestressed concrete pipe

1. The allowable head of a pressure pipe shall be based on an adequate factor of

safety regarding the pressure bearing capacity of the pipe.

2. An flexible joint such as Gibault joint shall be inserted at an interval of 20 to 30 m along the pipeline, and the position of the joint shall be located along the straight portion of the pipeline both in the plan and elevation.

But in case of prestressed concrete pipe it is not necessary to comply with this item.

3. The foundation shall be particularly strong.

2.4.5. Asbestos cement pipe for water service

1. The foundation shall be finished uniformly so that the pipe may never be subjected to bending action.

2. The connecting portion of the pipes shall maintain an gap of at least 5 to 10 mm at the center of the sleeve.

3. It is desirable to insert a cut pipe 1 m long in addition to a short pipe before and behind a valve or a fire-hydrant.

4. The drilled portion of a ferrule shall be treated with special care, since it is extremely vulnerable to earthquake shocks. A branching saddle shall be used in placing a ferrule and a ferrule shall not be entered into the pipe body.

2.4.6. Siphon crossing

1. A siphon crossing shall not be built under unfavorable ground conditions.

2. A siphon crossing shall be built of coated steel pipes for water service or ductile cast-iron pipe for water works, and the foundation shall be prepared with care.

3. The pipes used for a siphon crossing shall be those of flexible joints. However, when steel pipes are used, those of flexible joints shall be installed only at the portion of bending at both ends.

4. The approach pipes before and behind a siphon crossing shall have as gentle a bending as possible, and any bending shall be fixed sufficiently to a concrete anchor block.

5. Valves shall be placed at both ends of a siphon crossing.

6. A siphon crossing of a large-calibered pipe or of a key trunk line is desired to be divided into two or more branches for safety.

2.4.7. Pipebridge and bridge-born pipeline

1. Unless otherwise unavoidable, a pipeline shall not be laid on a wooden bridge.

2. Pipebridge shall be located away from an existing wooden bridge by at least more than 2 m.

3. Pipebridge shall be built of fire-proof material, and on a soft foundation it shall be simple beam type structure.

4. It is advantageous against earthquake shocks to build the superstructure as a continuous system on a relatively favorable ground.

5. The top of a bridge pier shall be wide in axial direction, and the superstructure shall be adequately anchored to the substructure with anchor-bolts in order to prevent it from falling off the position in time of earthquake.

6. The provisions for a bridge pier, abutment and wing wall shall comply with those specified in the item 2.2.3.

7. It is safe to use a steel pipe for a bend pipe or an offset pipe which connects a bridge-born pipe to an underground straight pipe behind the abutment.

It is advisable to treat the joints of the steel pipe by electric welding.

8. A bridge-born pipe shall be fixed to the superstructure at each span, and equipped with an expansion joints also at each span.

9. For a bridge-born pipe made of cast-iron a flange joint shall be avoided.

10. At the position where connection is made to the bend on either end of a bridge-born pipe an expansion joint shall be placed without exception, and the bend pipe shall be anchored to the abutment by an anchor band.

11. A pipe mounting to the abutment shall be sloped by less than 45° and flexible joints shall be installed at the connecting portions to the straight pipes before and behind the bridge. (See Fig. 4)

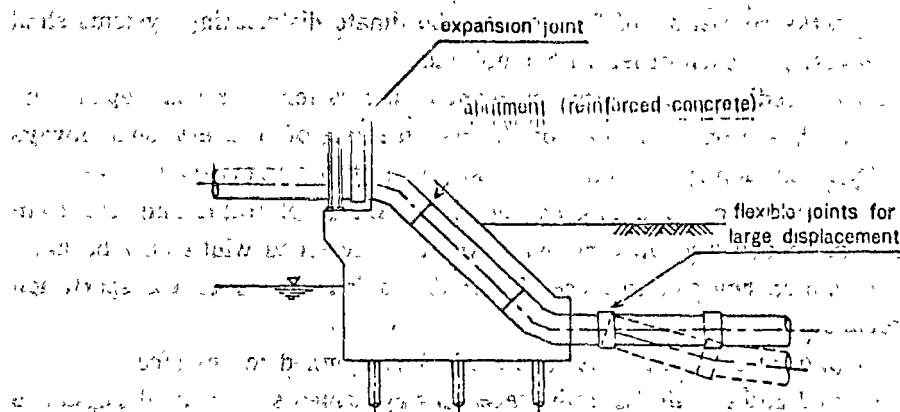


Fig. 4. Pipe connection at the abutment

12. The both ends of a bridge-born pipe shall not be fixed to the abutments, but allow for a considerable clearance around the pipe.

13. Special care shall be exercised to refilling the banking behind the abutment, and a foundation supporting a bend pipe shall be particularly reinforced by pile driving.

14. Pipebridge having the steel pipe itself as the main girder shall be equipped with flexible joints on the abutment and piers, considering the ground sinking especially on a soft ground.

15. A steel pipe bridge such as mentioned above shall be equipped with ring-type stiffeners at the supports.

16. Pipebridge of a considerable length shall be equipped with an alley on either one of the sides or, if possible, both sides of the pipe to facilitate checking and maintenance.

17. Valves shall be installed on the pipeline before and behind the bridge.

2.4.8. Valve

The location of a valve shall be determined to be such a place that it can be easily and rapidly renewed, repaired and maintained.

2.4.9. Water service installations

When a galvanized steel pipe for water service, a rigid polyvinyl chloride pipe for water service, or copper pipe for water service is used as a service pipe, a lead pipe approximately 500 mm long shall be inserted before and behind the connection to a ferrule, curb stop or water meter, and it is desirable that an adequate sag is given to the lead pipe.

2.5. POWER AND PUMP

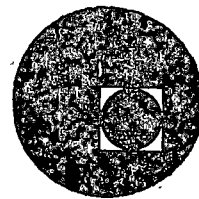
1. As to the power reserve equipments such as diesel engines which have at least more than a half of the full capacity of the station shall be equipped.
2. When only the electric power is available, an extra unit with different source of power and supply route shall be provided for emergency use.
3. The delivery pipe of the pump shall be directed horizontally or obliquely downward.

APPENDIX

1. A water works consisting of 2 or more subordinate distributing systems shall have them connected to each other with trunklines.
2. In order to expedite repair works in event of a disaster as much repair materials as possible, based on estimation of the possible rate of recovery, shall always be stored at adequately deployed dumps. The locations of the dumps shall be selected from among such places commanding exceeding advantage of traffic and free from fire hazards, since in event of an earthquake the effective road width may be hampered by the collapsed houses and since the traffic is jamed due to transportation of relief materials.
3. A rapid supply of labor shall be well studied or planned in advance.
4. The interested cities shall maintain necessary agreements for mutual assistance prearranged at ordinary times concerning reconstruction of establishments and emergency water supply. If possible, it is desirable to connect the ends of distribution pipelines of the adjoining cities with each other, so that mutual assistance of water supply can be exercised in event of disaster.



centro de educación continua
división de estudios superiores
facultad de ingeniería, unam



III CURSO INTERNACIONAL DE INGENIERIA SISMICA



JULIO-AGOSTO, 1977.

Chapter 16

EARTHQUAKE RESISTANCE OF WATER WORKS

16.1. INTRODUCTION

In great earthquakes in the past, severe damage to water works has occurred repeatedly. Actually, however, it is impossible for structures of water works facilities, which function as a unit while being spread over a wide area to escape earthquake damage entirely. Therefore, the fundamental thinking in planning such facilities is based on the following three points:

1. Methods of localizing earthquake damage as much as possible are to be adopted.
2. Considerations should be taken to make repairs of earthquake-damaged portions as easy as possible, and
3. Secondary damage due to earthquake damage should be prevented.

In the past, since destruction to water works was so severe, there was a concept that earthquake damage to water works facilities, especially buried pipelines, was inevitable. Now that water works facilities have become so important, positive measures must be taken for earthquake resistance even if difficulties exist.

Damage to water works consists of damage to water quality and damage to the structure. Since water quality is impaired due to devastation of the water source area, it is necessary for locations with little risk of devastation to be selected as water sources and for erosion control to be exercised in these areas. As for structural damage, those types peculiar to water works are destruction of underground pipelines, reservoirs, water pipe bridges, inverted siphons and water tanks.

16.2. UNDERGROUND PIPELINES

(1) Relationship of Depth and Direction of Underground Pipelines to Earthquake Damage

Earthquake damage to underground pipelines consists of pull-outs and cracking. The degree of hardness of the ground is intimately related to such damage. Figure 16.1b indicates the damage to pipe lines in Tokyo at the time of the Kantō earthquake. On looking at the distribution of damaged water pipes destruction was greatest in the area between the Imperial Palace and Furu River and the area to the east between Furu River and the Sumida River. These areas were followed by the alluvial area on the left side of the Sumida River, while

there was little damage in the western higher areas of Tokyo. The same trend was seen in the distribution of damage to sewer lines. Figure 16.1 (a) indicates the damage to buildings in Tokyo at the time of the same earthquake. It is interesting to note that the areas of pipeline damage were somewhat different from the distribution of damage to wooden buildings. Although there is general agreement that damage was greater in the lower areas than in the higher areas, the damage to wooden buildings was the greatest on the east side of the Sumida River while the damage to pipelines was the greatest in the area between the Sumida River and the western higher areas.

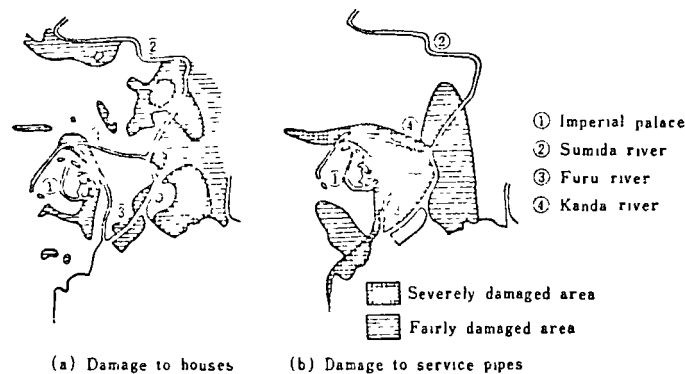


Fig. 16.1 Damage to buildings and water supply pipes (Kantō earthquake of Sept. 1, 1923).

The geology of these districts is diluvial loam layers in the higher district and alluvial silt on sand-gravel in the lower district. On the east side of the Sumida River, alluvial deposits develop in a uniform manner while in the area between the Sumida River and the western higher district, there were sand-gravel layers with outcrops here and there of diluvial layers so that the distribution of soil strata was exceedingly intricate. This naturally leads to the supposition that ground motion was uneven for the various locations in the latter case. This is thought to have been the reason for the great damage to buried pipelines.

Taking this into consideration, hard ground is best for embedding pipes and soft ground is worst. Moreover, if it is uniform soft ground is comparatively suitable whereas ground with hard and soft areas intermingled is thought to be unsuitable.

Besides the hardness of the ground, the depth of embedment also influences earthquake damage: in general, when the depth of embedment is great the earthquake damage appears to be small. The distributing pipes of Hatano town, located near from the epicenter of the Kantō earthquake, were ceramic pipes with an inner diameter of 9 cm and were not of high strength, but whereas parts buried 1.2 m underground were destroyed at a ratio of 1 in 3 lengths, those which were 2.4 m underground were not damaged at all. There were no differences between these two cases in regard to topography, geology and the directions of

embedment; such a difference in earthquake resistance was entirely due to the effect of depth of embedment.

However, it cannot immediately be said from this that seismic intensity is small at a depth of several meters underground. Rather, it is thought that there is less earthquake damage in the case of greater depth of embedment because of greater confining earth pressure. In which case the depth required for earthquake resistance is related to the diameter of the pipe and there would be little effect unless depths are increased with increasing pipe diameters. Judging from examples of damage to sewer pipes in the Kantō earthquake, it appears the damage is greatly alleviated when the depth is greater than 3 m even with fairly large pipes. However, from the standpoint of maintenance, control and ease of discovery and repair of damaged portions, making the depths too great should be considered carefully. Actually, in urban areas the depth of pipes is usually determined by their relationship to other underground facilities.

It is readily conceivable that the direction in which a pipeline is laid and the major direction of vibration of earthquake motion are related to earthquake damage of the pipeline. A pipeline is deflected when subjected to vibrations in the direction orthogonal to the pipes. When the deflection is great there will be strains at joints and the pipes will break at these portions. When pipes are subjected to vibrations in the direction of the pipeline, they will be pulled out, torn apart or will collide with each other to form longitudinal cracks and ruptures. Therefore, although it can be expected that failure of a pipeline will be related to direction, it is difficult to say in general terms which is more likely to cause failure.

In an actual case, water mains laid in a north-south direction in Fukui were severely damaged in the Fukui earthquake. In Fukui the direction of crustal movement in this earthquake was in a north-south direction; and although the direction of the main vibrations is not clearly known judging by the direction of the movement of bridge girders in the city, it is thought that the main vibrations were roughly in a north-south direction.

The direction of the main vibrations in Tokyo in the Kantō earthquake was generally north-northwest to south-southeast. The water main from Yodobashi to Hongō 1,100 mm in diameter, was roughly orthogonal to the direction of the vibrations, while the main of identical diameter from Yodobashi to Shiba was generally diagonal to the vibrations. The ground was mainly loam strata in both cases and is not thought to have been too complex. The former pipe was ruptured at eight places, whereas the latter showed no rupture. In short in this case, the direction orthogonal to the main vibration suffered more earthquake damage. In this earthquake the extent of damage to sewer pipes in connection with the direction of laying was investigated but no correlation was recognized.

(2) Relationship of Types of Pipes and Joints to Earthquake Damage

Pipes used for water works are steel, ductile cast iron, cast iron and asbestos-cement. Steel pipes are jointed by field welding while ductile cast iron pipe, cast

iron pipe and asbestos-cement pipe are jointed with couplings. The damage to cast iron and asbestos pipes in earthquakes in the past consisted of breaking, cracking, rupturing, pull-out and injury to couplings. Steel and ductile cast iron are high in ductility so it is thought cracking and rupturing will not occur with these pipes. The natural gas pipeline from Niigata to Tokyo, made of high pressure steel pipe with welded joints, was not damaged in the Niigata earthquake. This proves that steel pipe line is earthquake resistant. But as steel pipes are jointed generally at field, welding work must be performed very carefully.

Regarding cast iron pipe and asbestos pipe, the former was less worse in earthquake resistance in the Off Tokachi Earthquake of 1952. In the Niigata earthquake, with a diameter of 100 mm as the border line, asbestos pipes of smaller diameter were broken while pipes of larger diameter, both of asbestos or cast iron, were pulled out.

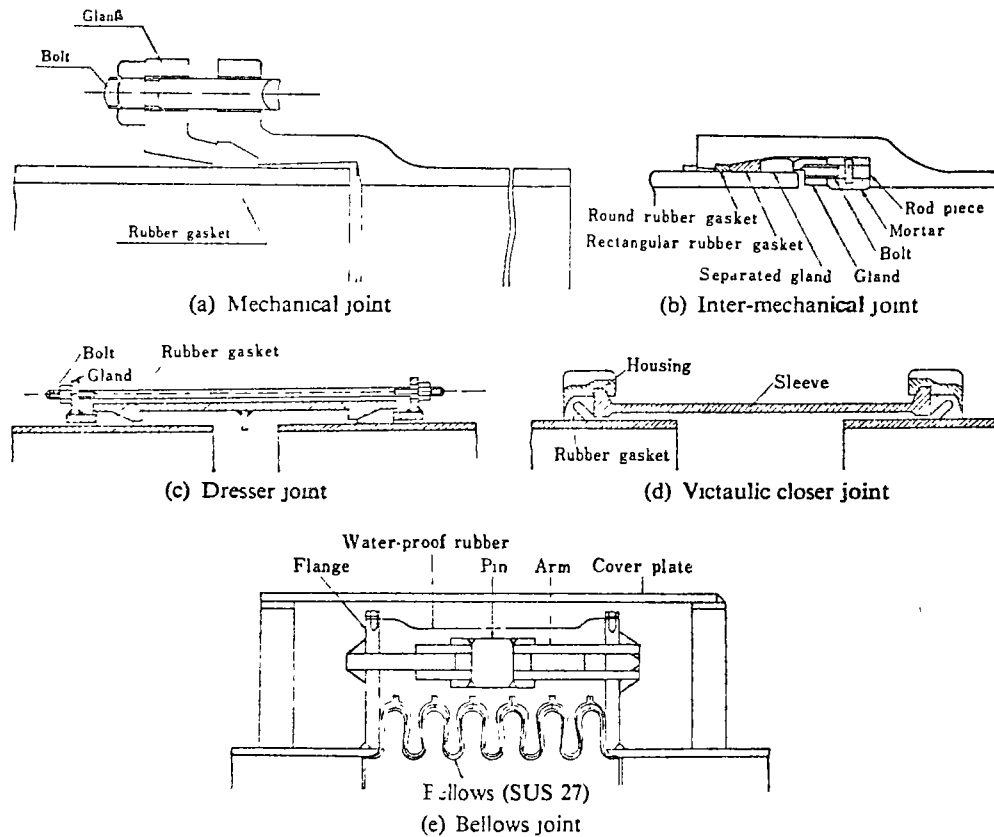


Fig. 16.2 Flexible joint of service.

In order to cope with large ground movements it is necessary to give a pipeline suitable flexibility. Thus, it is desirable for joints to be able to expand and contract at suitable intervals, and it is considered advisable to provide expansion joints at the rate of one to every three couplings. In addition, it is desirable to install so-

called earthquake-resistant couplings with both expansion and contraction characteristics and flexibility at places where uniformity of vibration characteristics might be disturbed, such as points of change in ground conditions, sudden bends, and tees and crosses in major pipelines. Both the bellows and victaulic closer joints are ductile, earthquake-resistant joints. The bellows joint can be bent about 15° and the victaulic closer joint about 5° . Therefore, if a steel pipe is installed between two bellows joints, even if there is a prominent displacement in a length of several meters, this displacement can be resisted. Thus, where large relative displacements are anticipated such as the connection point of a water pipe and a distributing-reservoir or an aqueducts, this type of joint is used.

Mechanical couplings are at times pulled out, but have a fair degree of earthquake-resistant and can be bent up to 2° . Socket joints are liable to be pulled out while flanged joints are easily broken and both are not earthquake resistant.

Pipes which extend above the surface from buried pipe are most liable to be damaged in earthquakes. This is naturally expected from the difference in the movement between the ground surface and the ground at the point of embedment. When the standing pipes are firmly connected to large masses such as buildings and machines, this trend is intensified further. Therefore, in such cases, earthquake resistant joints should be used and connections with buildings should be somewhat flexible.

(3) Forces Acting on Buried Pipes during Earthquakes

1) Introduction

The destruction of underground pipelines is thought to be due to the following causes.

1. The bearing capacity of the ground is reduced due to vibration.
 2. Because of local ground sliding, pipes in a certain area are moved together with the ground and a large shearing force is produced at the boundaries of adjacent portions.
 3. The pipe is pushed to one side due to eccentric earth pressure. Even if this pushing is resisted, the pipe is crushed by the stresses produced when the pipe is weak.
 4. Pipes are distorted by deformation of the ground. When the pipe cannot withstand deformation in its axial direction, it is pulled out or crushed; when it cannot resist deformation in the direction orthogonal to its axis it will break.
 5. When the rigidity of the ground or of the pipeline changes suddenly, a large bending or axial force will act locally.
 6. Pipes are subjected to great bending action at bends.
 7. Hydrodynamic pressures act on dead ends, bends, tees, and tapered pipes.
- There is little work being done to evaluate these phenomena qualitatively, which makes aseismic design of pipelines difficult.

2) Reduction in Bearing Capacity of Ground due to Vibration

Ground of fine sand which is loose or has a high water table loses shearing strength due to vibration, thus reducing bearing capacity. Because of this, water pipes with large dead weights settle while sewer pipes, which have a small dead weight, float up. In order to prevent such occurrences, concrete foundations, furring and pile foundations are provided, which not only increase bearing capacity, but are helpful in preventing the individual pipe from moving separately and pulling apart. When there is danger of liquefaction of the soil, the ends of foundation piles must be driven into ground which will not liquefy. Further, steel pipe is thought suitable for pipelines to be laid in this type of ground.

3) Local Sliding of Ground

It would be impossible to resist and prevent local sliding of ground by making the pipe resist the movement. Since local sliding is limited to soft ground, it would be wise to avoid soft ground in laying important trunk lines. When it is unavoidable to pass through such pockets steel pipe with bellows joints at suitable intervals should be used to provide expansion and contraction.

4) Pipe Stress due to Eccentric Pressure

At the time of an earthquake, active earth pressure works from one side of a pipe while earth pressure resisting this works from the other side. When the equilibrium is broken, pipes are pushed to one side. The relations in this case are summarized in the manner described below (see Fig. 16.3).

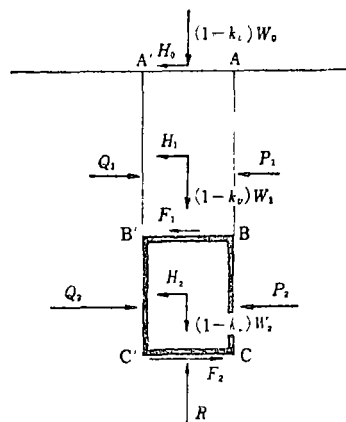


Fig. 16.3

The following are considered as vertical forces acting on the pipe:

$W_0 = (1 - k_v)W_0'$: force due to loads at ground surface;

$W_1 = (1 - k_v)W_1'$: force due to weight of soil on pipe;

$W_2 = (1 - k_v)W_2'$: force due to weight of pipe and substances in pipe; and

R : reaction force from ground under pipe,

where W_0' , W_1' , and W_2' are the load at the ground surface, the weight of the soil on the pipe and the weight of the pipe and the substances in the pipe, respectively. k_v denotes the vertical seismic coefficient.

The following are considered as horizontal forces acting on the pipe:

- P_2 : earth pressure acting on plane BC;
- Q_2 : resistant earth pressure acting on B'C' plane;
- F_1 : tangential force acting on plane BB';
- F_2 : tangential force acting on plane CC'; and
- $H = k_h W_2'$: seismic force acting on pipe and substance in pipe,

where k_h denotes the horizontal seismic coefficient. P_2 is equal to active earth pressure while Q_2 cannot exceed passive earth pressure. When the sum of the active earth pressure P_1 working on the plane AB, seismic load H_0 acting on the ground surface and seismic force H_1 acting on soil on top of the pipe does not exceed the passive earth pressure on the plane A'B' all of this horizontal force is resisted by earth pressure working on A'B'. When the sum exceeds the passive earth pressure of the plane A'B', the shortage is carried by the tangential force F_1 acting on the top surface of the pipe. However, the value of F_1 cannot exceed the shearing strength at the top surface of the pipe.

When the pipe maintains an equilibrium the following equation will be valid.

$$Q_2 + F_2 = F_1 + k_h W_2' + P_2 \quad (16.1)$$

where Q_2 cannot exceed passive earth pressure and F_2 cannot exceed shearing strength at the bottom surface of the pipe. The limits necessary for maintaining equilibrium of the pipe can be obtained from the above.

Also, since F_1 cannot be greater than the shearing strength at plane BC even when the equilibrium of the soil at the top surface of the pile is broken, Eq. (16.1) will be valid and there can be cases when the equilibrium of the pipe will not be broken. However, there will be ground sliding at the top surface of the pipe and the safety of the pipe will be greatly endangered. As such an occurrence is undesirable, considerations should be made to prevent breaking of the equilibrium of soil at the top surface of the pipe.

5) Pipe Deformation

When ground deformation due to earthquake is not so large as to cause ground failure, pipelines may be considered to show roughly the same deformation as the ground. In regard to strain in the direction of the pipe axis, if the velocity amplitude of surface waves advancing in this direction is v , the strain amplitude is ϵ and propagation velocity is c , there is a relation of

$$v = \epsilon c.$$

$$\therefore \epsilon = \frac{v}{c}.$$

Should there be no sliding between the pipeline and the soil, this strain will be equal to the strain in the direction of the axis of the pipeline. Thus if E is its longitudinal coefficient of elasticity, the stress will be as follows:

$$\sigma = \frac{vE}{c}. \quad (16.2)$$

In actual cases since the earthquake motion at the site decreases due to the existence of the buried pipeline, the stress of the pipe is considered to be somewhat smaller than the value given above.

Regarding the direction orthogonal to the pipe axis, the displacement of the pipe will be roughly equal to the displacement of the ground. Therefore, in the range where ground failure does not occur, there is little deformation of the pipe and it is thought that stress is not great. Further, since there is soil on both sides, there can be no case of resonance of the pipe with earthquake motion.

6) *Influence of Non-uniformity of Ground*

When the ground is not uniform, there will be a difference in movement during an earthquake of various places at the surface of the ground even within a fairly small area. This nonuniformity will be marked by the surface of the ground becoming reduced with increased depth, and also marked in acceleration and less obvious with velocity and displacement.

Therefore, where the ground is not uniform the stresses in the pipeline due to nonuniformity of earthquake motion will be fairly great and can be estimated approximately for given earthquake motion using a finite element method. Actually, it is necessary to prevent breaking and crushing of pipe due to concentrated stresses by providing expansion joints at suitable intervals. The case of the Niigata earthquake in which sewer pipes buried about 3 m underground were broken into single pieces of approximately 4 m in length is of reference in determining the spacing of the expansion joints.

Where pipelines are connected to manholes, it is clear that the vibration conditions of the two will be greatly different and there is danger of bending being concentrated at the connections. Therefore, expansion joints are ordinarily provided at these sections. As a result, when the diameter of the pipe is not especially large it is possible to avoid concentrations of bending at these portions, but with concrete pipes with large diameter there is a tendency for bending moments to be concentrated at these places. In order to cope with these bending moments it is necessary to make the connections with the manholes expand and contract as much as possible and rotate readily and to strengthen adequately the pipe in the sections close to the manholes with reinforcing steel.

7) *Stresses at Bends*

Pipes can be thought of as being displaced roughly similarly to the surrounding ground. Therefore, in the curved pipeline axial forces and bending moments are produced during earthquakes. As an experimental study of this problem, a model test was carried out. A model of the ground and pipeline was made with gelatin and a teflon rod, and the displacement and strain of the curved pipe was measured applying shear waves from one end of the gelatin.

The results are shown in Fig. 16.4a in which axial force is produced in the pipeline in the direction coinciding with the direction of application of vibration, while bending moment is produced at the portion of bend. In the pipeline in a direction perpendicular to application of vibration, almost no bending moment

or axial force is produced. When a coupling permitting rotation to the joint between a bend and a straight pipe, or what may be called an aseismic joint, is provided (see Fig. 16.4b), the axial force produced in the direction coinciding with that of application of vibration is reduced. However, it should be noted that bending moment at the portion of bend and straight pipe in the direction orthogonal to the direction of application of vibration is increased, in contrast.

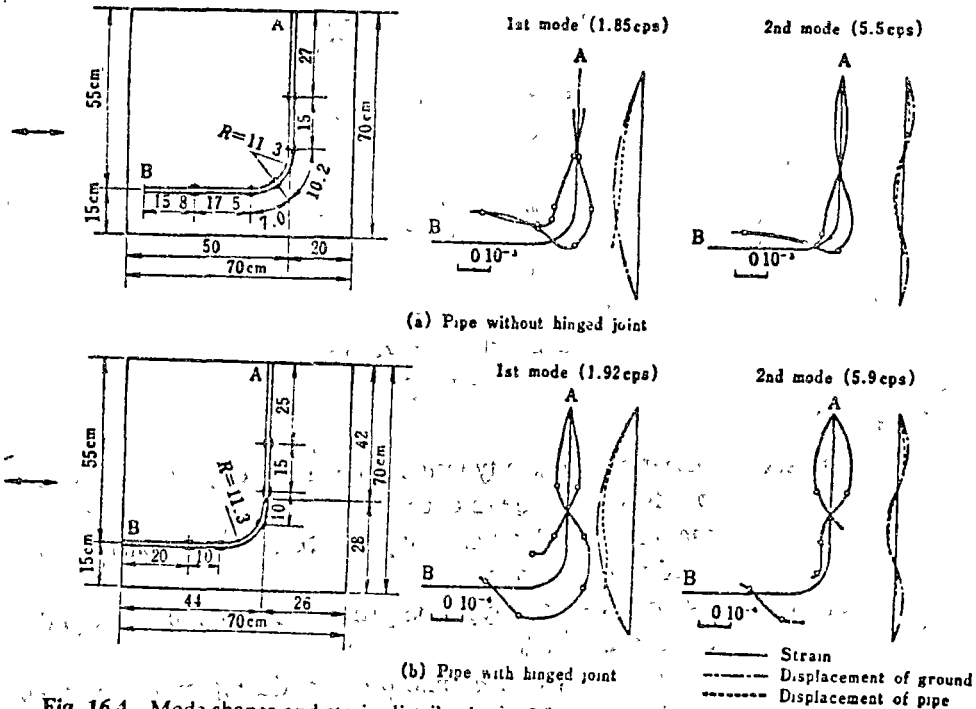


Fig. 16.4 Mode shapes and strain distributions of first two natural vibrations of bent pipe.

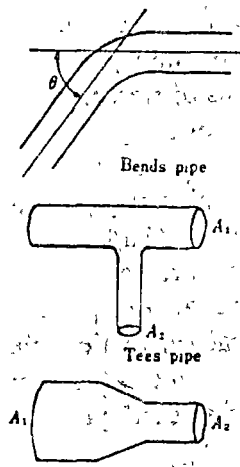


Fig. 16.5

8) *Hydrodynamic Pressure Acting on Pipe*

As water supply pipes are filled with pressurized water, dead ends, bends, tees and tapered pipes are subjected to hydrodynamic pressures at pipe walls during earthquake (see Fig. 16.5). Y. Nakagawa (16.2-2) carried out theoretical studies of this problem and deduced the following formulae:

$$\sigma_{D \max} = \frac{kT}{2\pi} \sqrt{\frac{g\kappa w}{1 + \frac{2\kappa r}{eE}}} \quad (16.3)$$

$$\sigma_{B \max} = \sigma_{D \max} \sin \frac{\theta}{2} \quad (16.4)$$

$$\sigma_{T \max} = \frac{\frac{A_2}{A_1}}{2 + \frac{A_2}{A_1}} \sigma_{D \max} \quad (16.5)$$

$$\sigma_{R \max} = \frac{1 - \frac{A_2}{A_1}}{1 + \frac{A_2}{A_1}} \sigma_{D \max} \quad (16.6)$$

where

- $\sigma_{D \max}$: maximum hydrodynamic pressure during an earthquake produced at a dead end;
- $\sigma_{B \max}$: maximum hydrodynamic pressure during an earthquake produced at a bend;
- $\sigma_{T \max}$: maximum hydrodynamic pressure during an earthquake produced at a tee;
- $\sigma_{R \max}$: maximum hydrodynamic pressure during an earthquake produced at a reduction:
- k : ratio of earthquake acceleration to g ;
- T : period of earthquake motion;
- w : unit weight of water;
- κ : bulk modulus of water;
- r : inside radius of pipe;
- e : thickness of pipe shell;
- E : Young's modulus of pipe material;
- θ : bending angle of bend;
- A_1 : cross-sectional area of pipe; and
- A_2 : cross-sectional area of pipe.

As an example of numerical calculation, the maximum value of hydrodynamic pressure produced in steel pipe with an inside diameter of 2 m and wall thickness of 18 mm in the case of an earthquake of $k = 0.2$ and $T = 1$ sec is given below.

$$\sigma_{D \max} = 3.12 \text{ kg/cm}^2$$

$$\sigma_{D. \max} = 2.21 \text{ kg/cm}^2 \quad (\theta = 90^\circ)$$

$$\sigma_{T. \max} = 1.04 \quad (A_2 = A_1)$$

$$\sigma_{R. \max} = 1.87 \quad (A_2 = 0.25 A_1)$$

The above are hydrodynamic pressures when dead ends, bends tees, and tapered pipes exist singularly, but actually, there are numerous dead ends, bends, and other connections, and since the water hammer pressures produced by these interfere with each other, the hydrodynamic pressures will be somewhat larger than the above values. When the increase is considered to be 1.5 times, the maximum value of hydrodynamic pressure is estimated to be approximately 4.5 kg/cm² in an earthquake of 0.2 g.

In general, 5.0~5.5 kg/cm² water hammer pressure is considered in addition to hydrostatic pressure in designing pipelines for water supply. As it is rare for water hammer and hydrodynamic pressure due to earthquake to work simultaneously, it will not be necessary to consider hydrodynamic pressure during earthquake in particular as a design load of the pipe. However, when the ground is soft and the period long, and moreover, strong earthquakes are anticipated, hydrodynamic pressure will be a problem. Also, when sluice valves are suddenly closed during an earthquake, since forces of $\sigma_{D. \max}$ will act in opposite directions on either side of the valve, hydrodynamic pressure of $2\sigma_{D. \max}$ will be applied to the valve. Again, in a pipeline with pressurized water there are cases when the pump is suddenly stopped due to power failure during an earthquake, and on such occasions there is a possibility of hydrodynamic pressure and water hammer pressure overlapping. In such cases the hydrodynamic pressures on pipelines must be considered in design.

16.3. RESERVOIRS

Damage to reservoirs consists mostly of destruction at the bottom, side walls and diaphragm walls of the reservoir. Bottom destruction occurs when the

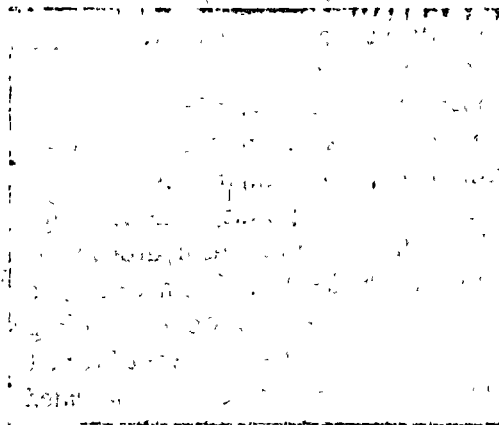


Fig. 16.6 Damage to discharge reservoir at Furu-Shimano river (Niigata earthquake of June 16, 1964).

ground is weak or is not uniform (see Fig. 16.6); examples of such damage are very great in number. When the structure is heavy there will be settlement, and when it is light there will be flotation; in either case the reservoir will be broken into a number of pieces. Therefore, as a foundation for a reservoir a sound and moreover uniform ground or a ground made sufficiently sound using piles and other devices should be selected.

It is also necessary to provide a suitable drainage facility to alleviate rising underground water pressure at the bottom of the reservoir due to an earthquake. Also, when the depth of the reservoir is great or when purified water is to be stored, it is advisable to use metal lathing in the mortar waterproofing layer. It is also safer to use the same method for protective concrete or mortar layers for asphalt and other waterproofing membranes.

The plane configuration of a sidewall is best kept as simple as possible. A circular form is better than a square form, since corners comprise weak points. When there are corners, expansion joints should be provided nearby. Even in sections which are not at corners, it is customary to provide expansion joints at intervals of 10~15 m for thin walls and 20~30 m for thick walls. Copper plates have been used as material for expansion joints in the past, but since this does not permit free expansion and contraction at tees and ells, either rubber or vinyl have been used almost exclusively in recent years.

The earthquake resistance of sidewalls and diaphragms is usually calculated by the seismic coefficient method, but since brick was used extensively in old structures, there were many cases of cracks being formed in walls or of walls falling. If reinforced concrete is used to build integral structures, stresses will be suitably distributed and the spacing of expansion joints can be made wider. It is thought the heavy damage as seen in the past can thus be greatly reduced.

The reinforced concrete reservoirs of the Nagasawa Purification Plant was designed to be consisted of a 40 m \times 40 m pond as one block and a 40 m \times 60 m pond as two blocks. According to the results of construction there was no leakage of water seen when 0.3% thermal reinforcement was used. Also, for the large reservoir divided into two blocks, either half would be a boxlike structure with one end open, but if the foundation is sound it is possible to build a structure which is sufficiently durable against earthquakes of about seismic coefficient of 0.2~0.3 in an economical manner. However, a shear wall with openings was provided at the open ends as a precaution.

Hydrodynamic pressures act on the walls of a reservoir during an earthquake. The pressure is usually calculated using Westergaad's formula. However, in the case of multilevel settling ponds, water is completely enclosed in the lower parts. Under such conditions enormous hydrodynamic pressures will act on the sidewalls during an earthquake. It is thus necessary to provide a suitable escape route for the water in this case. At the two-level settling pond of Nagasawa Purification Plant, cylinders of 1.4-m diameter were erected at a rate of one for every 13-m interval, where free water surfaces were provided to allow water to escape.

16.4. AQUEDUCTS AND INVERTED SIPHONS

When waterways cross rivers, either aqueducts or inverted siphons are used, but since amplitudes of earthquake motions are generally large near rivers, both are liable to suffer damage. In aqueducts or bridges to which water mains are attached, in addition to the necessity for the bridges to be fire- and earthquake-proof, the pipeline must also be earthquake resistant. For this reason steel pipes are used and expansion joints are provided at each span of a bridge. The trouble of providing many expansion joints may be avoided by making the bridge continuous.



Fig. 16.7 Miyagawa water main bridge, Yokohama (Kantō earthquake of Sept. 1, 1923).

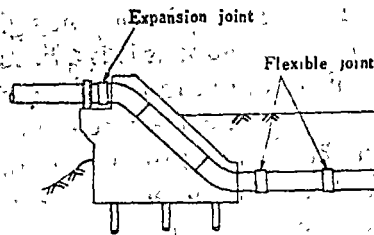


Fig. 16.3

Especially, as seen in the cases of past earthquake damage (see Fig. 16.7), there is a large proportion of pipes being pulled out at sections where pipe rises from behind bridge abutments to extend over to the bridge. Such damage is caused by the large settlement of the embankment at the back of the bridge abutment due to differences in earthquake vibration of the abutment and the embankment. It is important for the embankment to be constructed carefully to reduce settlement as much as possible. Where pipes stand up, the connections with straight pipes at the ends of a bridge must be made flexible and elastic, while

the foundations must be secured by piles of adequate depth so that pipes themselves will not settle. Even then, an aqueduct is a weak point in a waterway and it is customary for sluice valves to be provided in waterways before and behind a bridge abutment as a precaution against accident. Figure 16.8 shows aseismic design of a riser portion of an aqueduct recommended by the Japan Water Works Association.

Regarding inverted siphons, the foundation is of extreme importance and a sufficiently sound and uniform foundation must be built. The connecting pipe at either end should have as gentle bends as possible while any bend must be adequately fixed. It so happens that the damage to inverted siphons in the Yokosuka water supply system during the Kantō earthquake was light, but for damage to be avoided it is necessary for the depth of embedment to be fairly great. Further, inverted siphons at river bottoms consisting of alluvial deposit liable to show liquefaction during earthquake should be avoided.

16.5. WATER TANKS

Elevated water tanks of reinforced concrete do not appear to be very aseismic as seen in past earthquakes. For example, in the Kantō earthquake, the 22-m high reinforced concrete elevated water tank of Mikawashima Sewage Treatment Plant buckled and collapsed in spite of the fact that small structures in the vicinity escaped damage completely. Also, a number of concrete small-scale water supply towers at railroad stations toppled. However, the water tank at Mikawashima was built in the early days of reinforced concrete and the technique was not sufficiently refined, so it cannot necessarily be said that reinforced concrete elevated water tanks are not earthquake resistant. However, it is true that diagonal members are seldom introduced in reinforced concrete because of construction practices. It is undeniable that the rigidity will be reduced because the elevated tank is top heavy, and that it is a liability for members to be subjected to a substantial seismic force due to resonance with the earthquake. It is thought that steel elevated water towers are resistant to earthquakes since diagonal members can readily be provided to increase rigidity and toughness. The 28-m elevated water tank of this type in the Kawasaki water works suffered no damage in the Kantō earthquake.

When a water tank is built using reinforced concrete, the standpipe is more earthquake resistant. The standpipe of the Shibuya water works was a reinforced concrete cylinder 22 m high with an inside diameter of 13 m. In the Kantō earthquake nothing happened to the cylinder with only slight cracking of accessory parts. In general, shell structures such as cylinders and spheres are stronger than beam structures and are expected to withstand earthquakes well. In any case, the problem lies in the bearing capacity of the ground. As the pressures carried by the foundation of a standpipe are extremely large, it is necessary to select hard, uniform ground, and embedment should be as deep as possible.

Further, it is possible to prevent leakage by lining the inside of the standpipe with steel plate of not less than 3-mm thickness.

The seismic force required for calculation of stability and stress of a standpipe is usually determined by the modified seismic coefficient method, while calculation of stresses due to the seismic load distribution is carried out by static methods using cylindrical shell theories.

Chapter 17

EARTHQUAKE RESISTANCE OF UNDERGROUND STRUCTURES

17.1. INTRODUCTION

The recent development of underground facilities has provided eye-opening experiences. Since temperatures are stable and earthquake motion is weak under the ground, underground development will be further expedited with advances in construction techniques. Even with such advances, earthquakes will be a problem for underground structures. The major underground structures consist of water supply and sewage lines, tunnels, underground passageways, underground cavities and subaqueous tunnels. Water works and tunnels have already been discussed. Here the remaining problems will be considered.

When the ground is considered elastic, there are two types of waves propagated in it: shear waves and dilatational waves. At the portion near the ground surface, since the configuration and the structure of the ground are usually complex the earthquake motion at this portion is thought to be the result of the superposition of many bodily waves of different sizes and directions. Therefore it is difficult to ascertain this earthquake motion. For design purposes, assumptions must be made which take this complexity of earthquake motion into account.

In order to estimate the strain produced in the ground during an earthquake, a shear wave advancing in one direction is considered as follows:

$$u = u_0 \sin \frac{2\pi}{T} \left(t - \frac{x}{c_s} \right) \quad (17.1)$$

where

- x : direction of advance of wave motion;
- u : vibration displacement perpendicular to direction x ;
- u_0 : amplitude;
- T : vibration period; and
- c_s : propagation velocity of shear wave.

The strain due to this shear wave is

$$\gamma = \frac{\partial u}{\partial x} = -\frac{2\pi u_0}{T c_s} \cos \frac{2\pi}{T} \left(t - \frac{x}{c_s} \right) \quad (17.2)$$

where γ is strain due to the shear wave. Therefore, if

w : weight per unit volume of soil;
 τ : shear stress inside ground; and
 v_0 : velocity amplitude of earthquake.

then

$$\gamma = -\frac{w}{c_s} \cos \frac{2\pi}{T} \left(t - \frac{x}{c_s} \right) \quad (17.3)$$

$$\tau = -\frac{w}{g} c_s v_0 \cos \frac{2\pi}{T} \left(t - \frac{x}{c_s} \right) \quad (17.4)$$

It can be seen that stress is greater the higher the velocity of earthquake motion and the higher the propagation velocity of seismic wave. In the ground, there exist initial stresses due to dead weight and other factors. Thus, the seismic stress is added to initial stresses. In earthquakes of medium scale the resultant stress is not so large as to cause ground failure with the exception of places near the ground surface where the underground water table is high, or at the edges of cliffs. However, with severe earthquakes the stresses in the soil will become fairly large, and it is anticipated that failure will occur in weak ground.

With respect to ground failure, in addition to failure due to stresses caused by wave motion, there is failure caused by the lowering of the soil strength by vibration, such as landslides and subsidences. Special types of ground which liquefy due to vibration or ground which is intercalated with even a very thin soft layer would be vulnerable to such failure. In this case it is generally thought that the decisive factor in failure is not the velocity of earthquake motion but the earthquake acceleration.

In buried structures, in addition to the elastic strain of the ground, the strain due to nonuniform movements in various parts of the ground, is a problem. At the occasion of the Matsushiro swarm earthquakes in 1965~67, in an area near

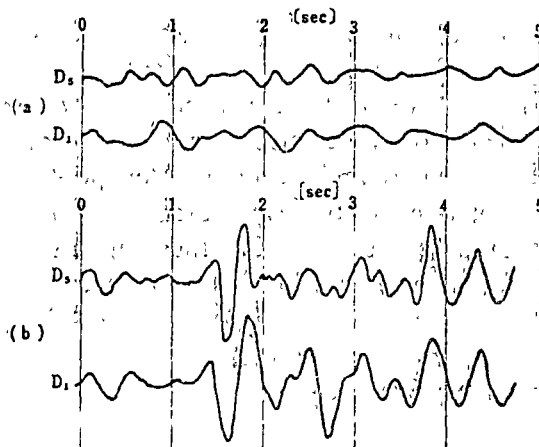


Fig. 17.1 Displacement at a ground surface (Matsushiro earthquake swarm 1965-67).

the epicenter, a base line 120 m long were taken and earthquakes were observed at five points along the base line. The measurement points were provided at 30 m intervals and were designated D_5 through D_1 from north to south. The thickness of the surface layer at the site increased from north to south and the predominant periods of microtremors were 0.36 sec at the northern side and 0.55 sec at the southern side. An example of the records taken is indicated in Fig. 17.1. In Figure 17.1a the waveform of D_1 is 0.4 sec slower than the waveform of D_5 . This indicates there was a wave moving at an apparent velocity of 300 m/sec at the surface of the ground from north to south. In the case of Fig. 17.1b there is no phase difference between D_1 and D_5 , but the time at which the amplitude is suddenly increased is 0.5 sec later in D_1 than in D_5 . This difference is thought to exist because the thickness of the surface layer is greater at D_1 than at D_5 . From such observations, it can be seen that one reason displacements during an earthquake of various points on the ground surface differ is because of surface waves. Another is because of nonuniformity of ground structure.

Measurement of actual earthquake motion underground has progressed in the past several years. In instrument installations, vertical shafts and underground structures are sometimes utilized, but in general, special seismometers designed for underground observation are buried in boring holes. The results of observation, as described in section 5.2, show that within the range of several tens of meters, the depth at which ordinary structures are buried, the underground acceleration is $1/2$ to $1/3$ of the surface of the earth, while at a similar depth there is little difference in displacement between ground surface and underground.

However, it is horizontal motion which is measured here and vertical movements are not observed. The impressions of people who experienced earthquakes inside powerhouses are summarized in Table 17.1, and according to this, it is thought that underground acceleration in the vertical direction is relatively stronger than acceleration in the horizontal direction.

Such vibrations produced underground result variations in stress and pore water pressure in the ground. It should be noted that when the ground is sand or mud, the strength of the ground is reduced by the rise in pore water pressures, and when the ground is rock, variations are produced in the extraneous forces working on the underground structure due to stress concentration and the rise in pore water pressure. It is not clear how much the ground contracts due to earthquake, but it is conceivable that a rise in water pressure of 1~2 m can easily occur. Such a rise in pore water pressure when occurring in sandy ground causes the ground to lose strength and produces water spouting and sand boiling. When these occur in embankments, they cause breaking, and when they occur in ground serving as an abutment for an arch dam, they impair the stability of the abutment.

Furthermore, underground structures suffer severe damage from discontinuous movement of the ground caused by geological discontinuities. This is most terrible, but there are very few studies regarding the quantitative degrees of the discontinuous movement in actual ground

Table 17.1

Earthquake	Date	Magnitude	Power station	Geology	Depth (m)	Epicentral distance	Earthquake motion felt
Kita-Mino	19/8/1961	7.0	Miboro	Quartz porphyry	260	approx. 20 km	Strong vertical motion felt
Western Gifu Prefecture	11/12/1967	7.0	Koyna	Basalt	150	several km	Strong vertical motion felt
			Miboro	Quartz porphyry	260	approx. 30 km	Horizontal motion felt
			Kuzuryu	Slate	140	approx. 30 km	Vertical motion not felt
			Kisenyama	Sandstone	300	140 km	Fairly strong earthquake felt. No earthquake felt
Higashi-Matsuyama	1/7/1968	6.1	Kinugawa	Liparite	60	100 km	Vertical motion assumed to have occurred from action of electrical fixtures

17.2. STRESSES DURING EARTHQUAKES ON AREAS AROUND UNDERGROUND CAVITIES

Although the problem of stress concentration around underground structures due to seismic wave has not been studied extensively, as long as there is stress concentration due to static external forces, there must be a similar phenomena due to dynamic external forces. The dynamic stress concentration can be solved by analytical methods or by photoelastic methods when it is a two-dimensional problem.

1) Analytical Methods

In this problem there is a circular opening in a two-dimensional elastic body of infinite expanse with sinusoidal shear waves coming from one direction. Under such circumstances, shear waves and dilatational waves are reflected from the circumference of the hole and are superposed on the input shear waves to produce stress concentration. According to calculations based on elastic theory, when there is no lining around the hole and the wave length is fairly long compared to the diameter of the hole, the peripheral stresses are given approximately by the following formula (see Fig. 10.6):

$$\widehat{\theta\theta} = \frac{2Gv_0}{c_s} \left(1 - \frac{c_s^2}{c_p^2}\right) \sin 2\theta \sin pt \quad (17.5)$$

where

- G : shear modulus of elasticity of ground;
- v_0 : velocity amplitude of incident shear wave;
- c_s : propagation velocity of shear wave in ground;
- c_p : propagation velocity of dilatational wave in ground; and
- p : circular frequency of incident sinusoidal wave.

From this, the following may be understood:

1. The section at which $\widehat{\theta\theta}$ will be maximum is the side of the opening at which the direction of the incident wave is inclined 45° .
2. The value of $\widehat{\theta\theta}$ is proportional to the product of the velocity of incident wave and impedance of the ground.
3. Gv_0/c_s is the shear stress produced by the incident waves when there is no opening. Therefore, if c_s^2/c_p^2 is neglected, the amplitude of $\widehat{\theta\theta}$ calculated using Eq. (17.5) is equal to the peripheral stress in the case of a semi-infinite plate with a circular opening subjected to uniform shear stress Gv_0/c_s . This suggests that when the wavelength of the incident shear wave is fairly long compared to the diameter of the hole the problem may be handled statically.

When the hole is lined, the stresses in the ground will be alleviated compared to the case where there is no lining. On the other hand, however, the lining will be subjected to seismic stresses and must be able to withstand them. For the sake

of simplicity, it is assumed that the lining is rigid and will not be deformed, that there is no resistance to the relative displacement in the peripheral direction between lining and surrounding rock, and that the lining and the surrounding rock will not be separated radially. The seismic load on the lining will be approximately the following when incident waves are fairly long compared to the diameter of the hole.

$$\hat{r}r = -\frac{6G_s v_0}{c_t} \sin 2\theta \sin pt \quad (17.6)$$

However, since the lining actually used is flexible it is thought the seismic load acting on the lining will be smaller than the value obtained by the above formula. It is difficult to carry out exact calculations for this case, but if the problem is handled statically, the calculations are comparatively simple. According to this, if the rigidity of the lining is lowered the seismic load on the lining will be reduced considerably. From this, it is concluded that for a lining to withstand earthquakes is more effective if the lining is resilient rather than highly rigid but brittle.

2) Photoelastic Method

When the shape of the hole is not circular, mathematical analysis is difficult. In such a case, the photoelastic method can be used to solve the problem experimentally. If the problem is transformed approximately into one of statics, it will become a stress concentration problem produced when a hole is made in a place where uniform shear stress exists. Many experiments have already been made considering this as a case which could be solved using such hard materials as phenolite. Although this has not been taken up as a problem of aseismic considerations, it is a method which should be utilized more in new fields.

In order to handle the problem dynamically, it is necessary to use the dynamic photoelastic method. In this case, it is appropriate to use materials of gel form because structure models made of gel materials are suitable for expressing the effect of dead weight while the moduli of elasticity are low and vibrations are

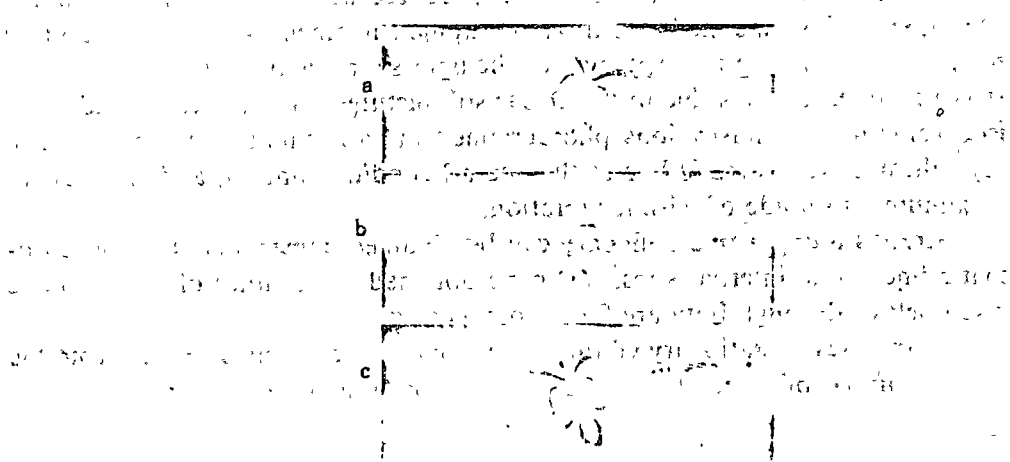


Fig. 17.2 Dynamic photo-elastic experiments using gelatin (stress around a circular hole).

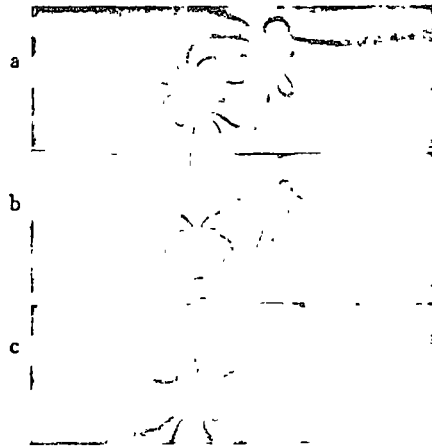


Fig. 17.3 Dynamic photo-elastic experiments using gelatin (stress around two square holes).

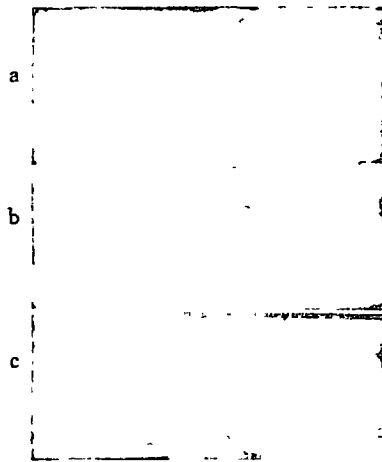


Fig. 17.4 Dynamic photo-elastic experiments using gelatin (stress around a angle-shaped hole).

relatively slow with large amplitudes. In carrying out a dynamic photo-elastic experiment a structure model is placed on a shaking table, vibrated, and the isochromatic line is photographed under polarized light. As the phenomenon is not rapid at this time, high-speed photographic equipment is not needed and by merely synchronizing the switching of the light source and the vibrations of the shaking table, it is possible to take clear still pictures. Figures 17.2, 3 and 4 are isochromatic line illustrations photographed in this manner. In these figures, (b) indicates isochromatic line at the neutral condition and (a) and (c) those at maximum amplitude of seismic vibration.

Stresses along a free boundary can be obtained immediately from isochromatic lines. The internal stresses can be obtained from either of the methods given below although both are fairly complicated.

1. In cases of stationary vibration, the following relation is derived from the compatibility condition and the equation of motion:

$$\left(\frac{\partial^2}{\partial x^2} - \frac{\partial^2}{\partial y^2}\right)(\sigma_x - \sigma_y) + 4 \frac{\partial^2 \tau_{xy}}{\partial x \partial y} = -\frac{\rho \omega^2 (1 - \nu)^2}{E} (\sigma_x + \sigma_y) \quad (17.7)$$

where

- σ_x, σ_y : normal stress;
- τ_{xy} : shearing stress;
- ρ : density of material;
- E : Young's modulus of material; and
- ω : circular frequency of sinusoidal vibration.

As τ_{xy} and $\sigma_x - \sigma_y$ can be obtained directly from the isochromatic lines and isoclinic lines, $\sigma_x + \sigma_y$ can be determined from Eq. (17.7). Therefore, all of the stress components can be obtained. But it is not easy to obtain isoclinic lines.

2. When u and v are displacements in the directions of x and y , respectively, the equation of motion is

$$\frac{\partial \sigma_x}{\partial x} + \frac{\partial \tau_{xy}}{\partial y} = \rho \frac{\partial^2 u}{\partial t^2} \quad \frac{\partial \sigma_y}{\partial y} + \frac{\partial \tau_{xy}}{\partial x} = \rho \left(\frac{\partial^2 v}{\partial t^2} - g \right) \quad (17.8)$$

Integrating this

$$\sigma_x = \sigma_{x0} + \int \frac{\partial \tau_{xy}}{\partial y} dy + \rho \int \frac{\partial^2 u}{\partial t^2} dx \quad (17.9)$$

$$\sigma_y = \sigma_{y0} + \int \frac{\partial \tau_{xy}}{\partial x} dx + \rho \int \left(\frac{\partial^2 v}{\partial t^2} - g \right) dy \quad (17.10)$$

where σ_{x0} and σ_{y0} are, respectively, the values of σ_x and σ_y at $x = x_0$ and $y = y_0$ which are obtained directly from experiments at free boundaries. In this method it is necessary to know the accelerations of the specimen at various points. These can be determined from the mode of the specimen in the case of sinusoidal vibration. The mode can be obtained fairly accurately by employing the Moire method. This is more precise than the previous method if the acceleration can be determined accurately.

17.3. MEASUREMENT OF VIBRATIONS OF UNDERGROUND STRUCTURES DUE TO EARTHQUAKES

During the Matsushiro swarm earthquakes in 1965~67, studies which consisted of measuring strains and displacements of pipelines during earthquake were conducted by actually burying pipelines in the ground.

One experiment was on steel pipe in which a pipe with an outer diameter of 27 cm, thickness of 6.6 mm and length of 90 m was buried at a depth of 1.5 m below the surface. The area around the pipe was packed with sand. A manhole was provided and insulated from the pipe. The main objective of the experiment was to ascertain whether or not the pipe would move integrally with the ground.

Earthquakes of various types up to a maximum 120 gal were occurring at that time and the conclusions obtained were:

1. Resonance vibration of the pipe did not occur.
2. The deformation of the pipe was more or less identical to the deformation of the ground.
3. The strain due to deformation in the axial direction exceeds the strain due to bending. The relation between strain and earthquake motion is given by

$$\epsilon = \frac{\mu}{2\pi} \cdot \frac{T\alpha}{c} \quad (17.11)$$

where

- ϵ : strain;
- μ : constant;
- α : earthquake acceleration;
- T : period of seismic wave (sec); and
- c : propagation velocity of seismic wave (cm/sec).

μ is usually presumed to be unity although it is slightly lower than unity in a model test.

4. Bending strain is seen in curved pipe, but there is no tendency for it to be especially higher than the strain in straight pipe. Also, the strain in the pipe at the connection with a manhole is not particularly high.

Equation (17.11) indicates that strain on the pipe is proportional to the velocity of the earthquake motion and inversely proportional to propagation velocity of seismic waves. Therefore, in a comparison between hard and soft ground, the earthquake will produce much greater strain on pipes buried in soft ground. According to theoretical calculations, it has been deduced that strain will be especially great when seismic wave propagation velocity is less than 300 m/sec.

Another experiment was made on concrete pipe. The pipe consisted of four asbestos-cement pipes 12.5 cm each in inner diameter faced with concrete to which a manhole 3 m high, 4.1 m long and 1.7 m long was attached. The connection between manhole and pipe was made to withstand a considerable amount of bending. The results obtained are given below.

1. The manhole and the ground within at least 5 m from the manhole showed roughly identical movements.
2. A phase difference is recognized between the vibrations of the manhole and the vibrations of the pipeline at sections fairly distant from the manhole.
3. During an earthquake, simultaneous to the arrival of a seismic wave with large acceleration as well as large displacement, a large strain is produced in the pipeline, the strain being larger the higher the earthquake acceleration.
4. On examination of the distribution of strain over the entire length of the

pipeline, the strain becomes large near a joint and is rapidly reduced with increased distance from the joint.

5. At joints, bending stress is a large factor as opposed to axial stress. At a section distant from a joint, the reverse is true.
6. According to the result of investigations of the relation between acceleration of an earthquake and strain in the vicinity of a joint, the strain is increased along with acceleration, but is thought not to exceed a certain limit.
7. In a comparison of stress produced during strong earthquakes in concrete pipe and steel pipe buried underground, for an earthquake in which acceleration was 120 gal, the maximum values of stress in the concrete pipe were approximately 15 kg/cm² at a joint and 5 kg/cm² midway in the pipe where the influence from the joint was small. At this time, stress produced in the steel pipe was 160 kg/cm² and was approximately 10 times the stress in the concrete pipe.

As a result of these two studies, it was learned that except for cases of great earthquakes in which the ground is destroyed, the movement of the ground and the movement of pipe are roughly in agreement. Even in cases when large manholes are connected to the pipe, the ground, the manhole and the pipeline generally move together, but it is felt that at this time the manhole restricts the movement of the soil in its vicinity. It was shown that the major stress was axial for both steel and concrete pipes, as had been expected beforehand from laboratory tests. The influence of a manhole on a pipeline is considerably different for steel pipe and concrete pipe. The existence of a manhole does not make much difference in the case of steel pipe, but for a concrete pipe it has a governing influence on the stresses of the pipe close to the manhole. This probably is due to the difference between connections in steel and in concrete pipes. Also, the tests of the steel pipe show that the influence of a manhole can be greatly reduced when insulation is adequate.

Similar measurements are being made at ductways for high-voltage lines in the downtown districts of Tokyo (see Fig. 17.5). The pipeline is a circular steel shield with an outer diameter of 3 m covered by soil from 11 to 12 m deep. The nature of the soil is silt and silty soil with a high free water table 1 m from the surface of the ground. There are two manholes 78 m apart and seismometers have been installed inside the pipeline between the manholes. Measurements are currently being made, but according to the results obtained so far, the records show acceleration in the duct parallel and perpendicular to the duct axis to be

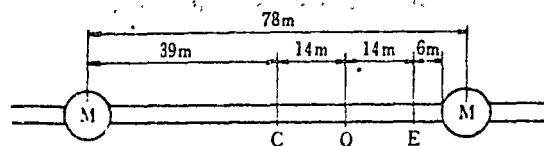


Fig. 17.5

lower than at the ground surface. The ratio is 70~80% in the axial direction and 60~70% in the direction perpendicular to the axis, and in this case the ductway has about the same tendency to move parallel as it has to move perpendicular.

According to displacement records, displacement with a period of approximately 0.9 sec is prominent, and this is thought to be the predominant period of the ground. Displacements in the direction of the axis are being measured at cross section C, which is midway between the two manholes, at cross section Q 14 m distant from C and at cross section E 14 m distant from Q and 6 m from a manhole. In records obtained so far, the movements of points Q and E are in complete agreement while the movement of point C, although no different in phase with the two former points, is approximately 30% smaller. This is thought to reflect the influence of the manhole. According to these observations, there is a difference of 1 mm produced every 14 m which, when converted to strain, is an average of 7×10^{-4} . These measurements have been made up to a maximum 70 gal in acceleration and a maximum 3 mm in displacement, and it is thought that at this degree of seismic intensity the influence of nonuniformity in ground displacement and manholes will not yet be so prominent.

The measurements described above have all been made of comparatively straight structures buried in surface layers of more or less uniform thickness. However, in a model test where a ground with variable thickness of surface layer was made with gelatin and vibrated on a shaking table, the various parts of the ground vibrated prominently with periods according to the respective thicknesses; at a certain period, only a certain part will vibrate prominently, while at other periods, only other parts will vibrate prominently. Therefore, when there is a long pipeline buried in the surface layer the pipeline will not vibrate very much relative to the ground, but depending on the ground conditions, part of it may be forced to vibrate greatly, and as a result there will be large local bending moments and large axial forces produced. In this case, the cross sections at which large axial forces and bending moments are produced will be located where the thicknesses of the surface layer change suddenly.

Also, in the case of a long pipeline model which penetrates ground consisting of two layers with differing rigidities, the same type of phenomenon is seen between the two layers. For instance, in ground consisting of two layers at which the surface layer is harder than the underlying part, there are cases when the surface part does not vibrate while the lower layer vibrates very much. At such times extreme deformation may occur where the pipes crosses from one ground layer into another.

Also, when a bent pipe is buried in the ground and vibration is applied, besides bending moment produced at the bent portion, there will be axial stresses produced near the bend of the pipeline in the direction perpendicular to the advance of the wave motion, as stated in Section 16 2. This characteristic seen at the bend of a pipeline does not agree with the results obtained for curved portions in the

former room in the direction transverse to the passageway. These cracks were parallel to the direction of main reinforcement and were in agreement with construction joints in the concrete. It is thought cracks were prominent in the sector constructed in the first stage because it was not tough due to the lack of auxiliary reinforcement.

4. Cracks 1 to 2 mm wide were formed in the sidewalls of the corridor connecting the turbine and generator room and the transformer room. The cracks formed in the wall concrete only and did not extend to the rock at the back. No separation was seen between wall concrete and rock.
5. Cracks formed in the direction of the tunnel at the top of the ceiling arch of the transformer room.
6. The tailrace tunnel had a rectangular cross section with a semicircular ceiling 8 m wide. The lining was 30 cm thick at the ceiling arch and 15 cm at the invert. A fractured zone 6 m wide consisting of clay containing rock fragments of basalt cuts across this tunnel, but there is no evidence that this cross section moved during the earthquake.

Although actual cases of such earthquake damage have not been seen here, from the experience with structures on the surface, it is thought there is a possibility of the following types of damage occurring in the future. Thorough consideration is necessary before designing such structures.

1. It is possible that abnormalities may progress undiscovered under normal conditions in the area surrounding an underground structure and be the basis for a catastrophe in a great earthquake. For example, in a district where ground settlement is severe, it is conceivable that the foundation ground on which an underground railroad is built will settle. The structure will then be supported by the soil around the sidewalls, and it will appear at a glance that there is no abnormality. If subjected to a great earthquake in this condition, it is inescapable that the structure will settle. Also, there are many cases of large underground cavities which are excavated with the aid of rock bolts during construction and are kept stable by walls. In such cases, through the progress of ground creep and the variation in underground water level, it may be that the stresses in the ground have changed and there is a risk of cave-in and collapse in a large-scale earthquake. In order to prevent such accidents, it is necessary for instruments for measuring deformation of the structure, underground water pressure, and so on be installed so that checks can be made continuously.
2. When two underground structures having foundations with different rigidities are connected, discontinuity may be produced between the displacements of the two at the joint and failure may occur in the vicinity. For example, when there are two structures in soft ground, one having sound foundation piles and the other merely buried in the ground, the former will not settle during an earthquake whereas the latter will settle or float up. As a result, the joint between the two will be destroyed. In

- the event the connecting portion is a passageway from one to the other this may cause great confusion. In order to prevent the damage due to the difference of the rigidities of the connected structures it will be necessary to provide the connecting structure with a high degree of toughness. If there is great resilience the structure will escape collapse even if it cracks.
3. In the case of a vertical shaft running through ground where the hardness changes suddenly, failure will occur around the area where the sudden change occur. In such a case, it is necessary for the structure to be joined at this portion with a flexible joint or conversely for the structure to be made rigid with adequate toughness.
 4. It is necessary for considerations to be made so that evacuees can escape above ground avoiding underground water or water flowing in from the surface due to such accidents as failure of levees. Even in emergencies, water drainage and electricity sources for illumination of the underground structure must be maintained.

17.5. EARTHQUAKE RESISTANCE OF SUB-AQUEOUS TUNNELS

Figure 17.7 indicates a sub-aqueous tunnel provided for crossing the Tama River by a railroad circling the outer side of Tokyo. Recently, because of the demands of urban transportation, similar sub-aqueous tunnels have begun to be laid at various places. At that case, when the ground is soft, the first thing that must be considered is whether the ground will be liquefied during an earthquake. When there is a risk of liquefaction the sub-aqueous tunnel should be abandoned.

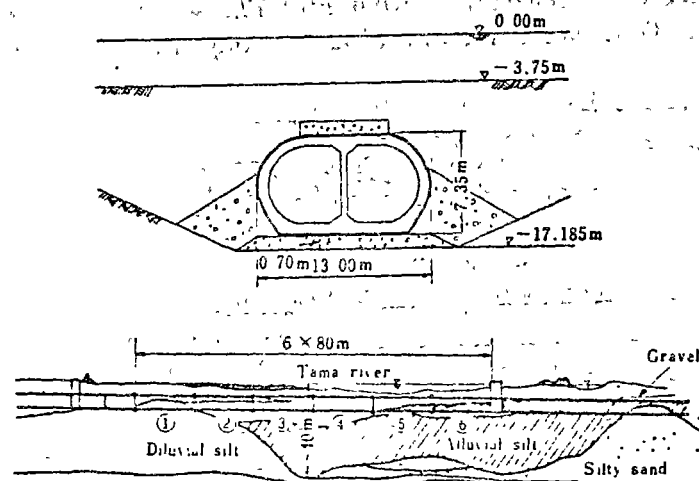


Fig. 17.7. Tamagawa sub-aqueous railway tube.

The second problem is bearing capacity. Since the sub-aqueous tunnel is a hollow structure, the load on the foundation ground will not be very much

different from the load applied by the weight of the soil before the tube is laid. Therefore, there is little fear of the insufficient capacity of the bearing of the ground; rather, flotation should be watched for.

The third problem is member stress produced in the tube due to vibrations. The major wave motion producing vibrations at the ground surface during an earthquake are shear waves traveling vertically in the ground and surface waves propagated over the ground surface. As shear waves are considered to rise vertically, vibrations are more or less of the same phase over the entire length of the tube and thus the bending produced in the tube will be small. However, at the two end sections of the tube, huge structures of ventilation shafts will be built and the movements at these portions will be different from the movement of the middle portion. For this reason, it is thought comparatively great bending moment or axial force will be produced at portions close to the two ends of the tube. When the character of the ground is not uniform, for example when the ground has a surface layer not of uniform thickness, the earthquake motion of each point along the tube will differ considerably both in size and phase, causing complexly distributed seismic force to be exerted on the sub-aqueous tube. When the surface waves are incident parallel to the tube axis, since there are phase differences between the seismic forces acting on the various parts of the tube, strains are produced in the tube in the longitudinal direction.

There are few cases of earthquake motion having been observed in actual submerged tubes. The Tamagawa Tunnel of the Keiyō Line has 6 submerged tubes each 13 m wide, 7.35 m high and 80 m long. Tube No. 1 is on diluvial silt while Tubes No. 4 to 6 are on alluvial silt of thickness of approximately 40 m and Tubes No. 2 and No. 3 are on the transient zone between the two. Tubes No. 2 and No. 4 are each provided with accelerograms and strain gauges. The strain gauges are installed at either sidewall of the cross sections 30 m apart and are set to measure strain in the axial direction (see Fig. 17.8).

Earthquake records obtained are shown in Figs. 17.9~12. Figure 17.9 shows records obtained at Tube No. 2 due to a distant earthquake. Strains at either

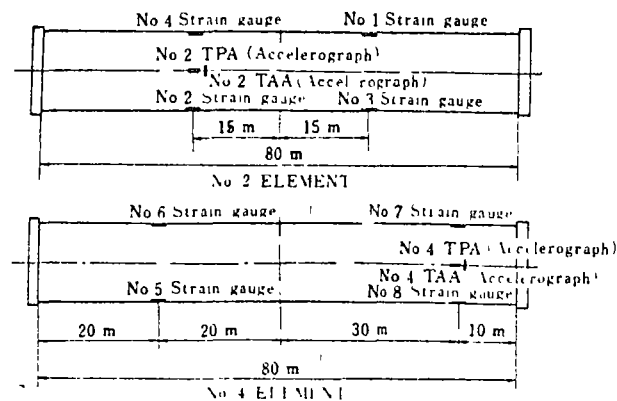


Fig. 17.8 Plan of No. 2 and No. 4 elements of the tunnel.

sidewall of the cross section are of opposite signs indicating the occurrence of bending in the tube. Figure 17.10 shows records due to a distant earthquake of $M=6.2$ and Fig. 17.11 due to a near earthquake of $M=4.8$, both obtained at Tube No. 2. In the former, the maximum acceleration is 2.6 gal, the maximum strain is 1.7μ and the period is long, while in the latter the maximum acceleration is 12 gal, the maximum strain is 1.2μ and the period is very short. Thus the maximum strain of the tunnel per unit gal of the maximum acceleration of the ground ranges from 0.10μ to 0.65μ . In both cases the strains at either sidewall of the cross

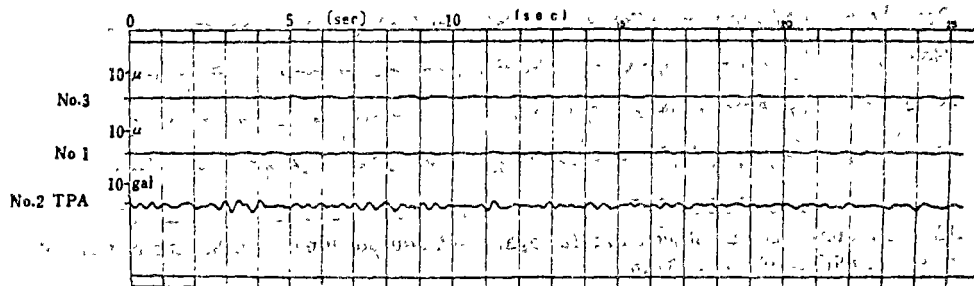


Fig. 17.9 Earthquake records observed at Tamagawa sub-aqueous tunnel (earthquake of May 27, 1970, $M=4.8$, $140.0E$, $27.5N$, $H=deep$).

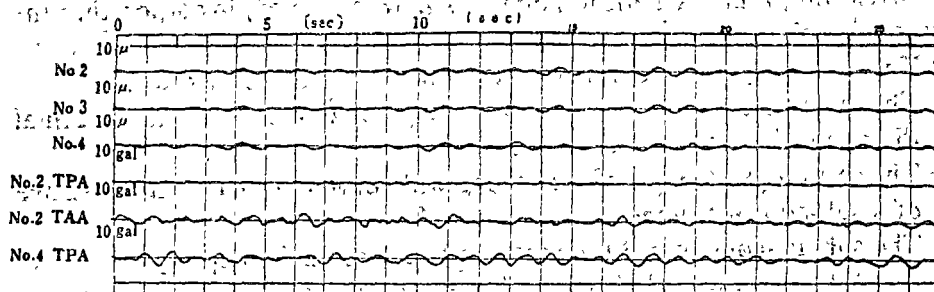


Fig. 17.10 Earthquake records observed at Tamagawa sub-aqueous tunnel (earthquake of Sept. 14, 1970, $M=6.2$, $142.0E$, $38.9N$, $H=40$ km).

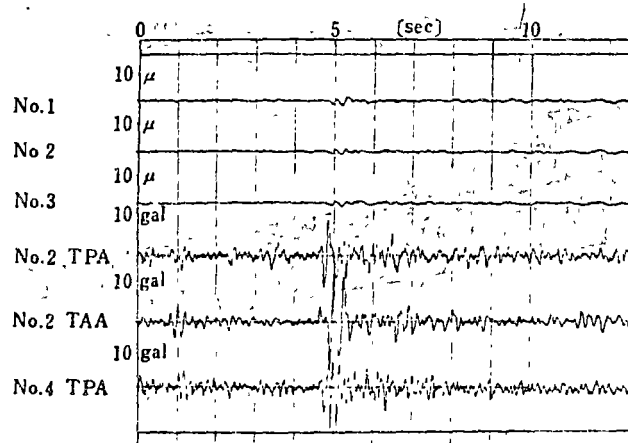


Fig. 17.11 Earthquake records observed at Tamagawa sub-aqueous tunnel (earthquake of Sept. 30, 1970, $M=4.8$, $139.7E$, $35.6N$, $H=50$ km).

section have the same sign, and this shows that the tube is stressed in the direction of its axis.

In Fig. 17.12 accelerations observed at Tubes No. 2 and No. 4 are shown. Many slow vibrations can be seen in the records of Tube No. 4 and this may be caused by the fact that this tube is located on a thick alluvial layer.

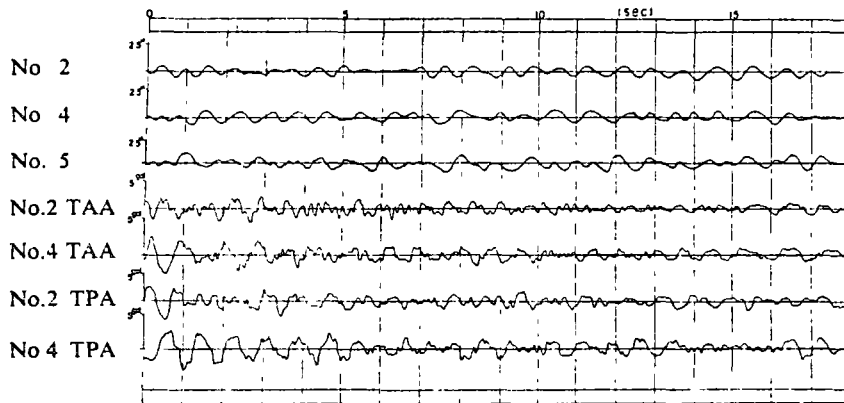


Fig. 17.12 Earthquake records observed at Tamagawa sub-aqueous tunnel (earthquake of Oct 30, 1970, $M=4.9$, $139.9^{\circ}E$, $36.0^{\circ}N$, $H=60$ km)

Based on the model tests and earthquake observations of subaqueous elements carried out, a mathematical model has been proposed, in incorporating the consideration below:

1. The ground is to be represented as a concentrated mass system.
2. The ground masses are mutually spring-connected in the longitudinal direction of the sub-aqueous tunnel.
3. The earthquake motion of the ground will not be affected by the existence of a sub-aqueous tunnel.
4. The sub-aqueous tunnel is connected to the ground by springs.
5. A sub-aqueous tunnel element will deform in bending as well as axially.

Figure 17.13 is an illustration of the mathematical model.

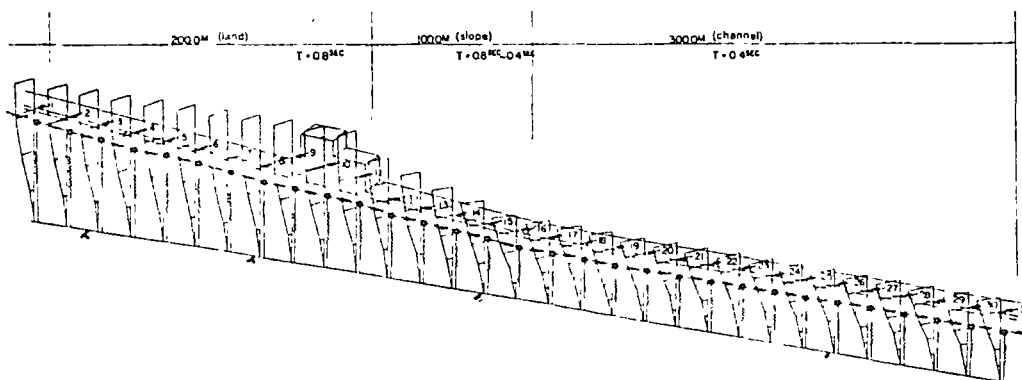
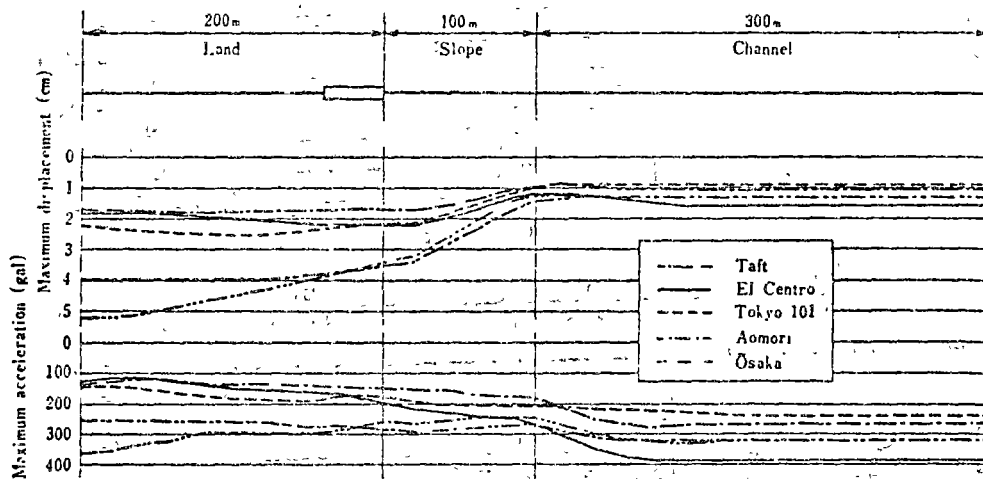
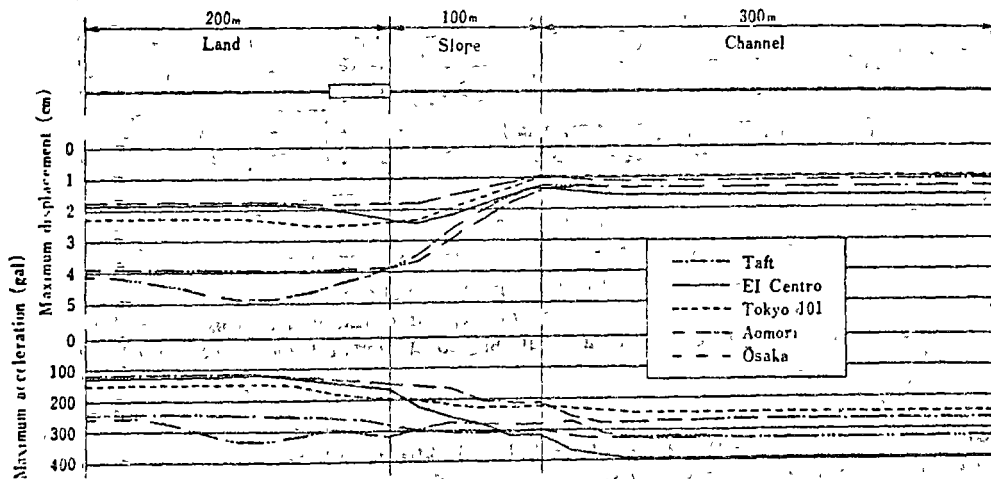


Fig. 17.13 Simulation model of a sub-aqueous tunnel

The earthquake motion of the ground is computed by the finite element method, taking the depth and the mechanical properties of the surface layer of the ground into account. The spring in the direction perpendicular to the axis connecting the sub-aqueous tunnel to the ground is computed by the finite element method assuming plane deformation as a two dimensional elastic body, while the spring in the axial direction is computed considering that there will be shear deformation of the ground in the direction of the tube axis.



(a) In the direction of tube axis.

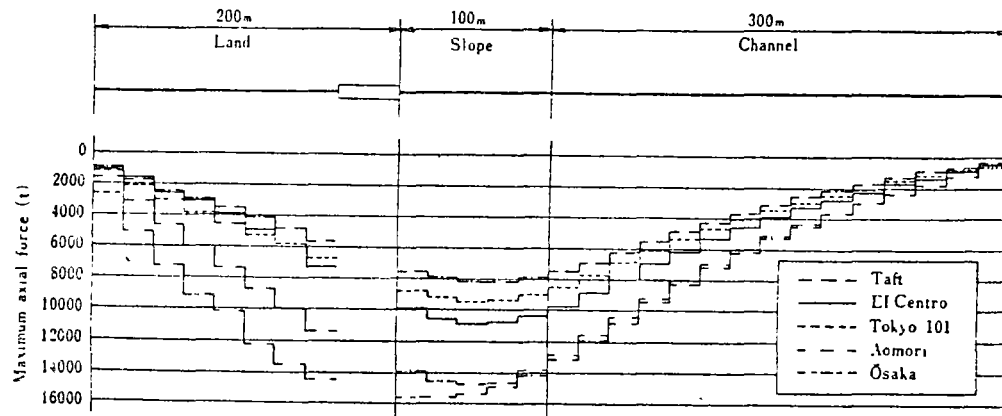


(b) In the direction orthogonal to the tube axis.

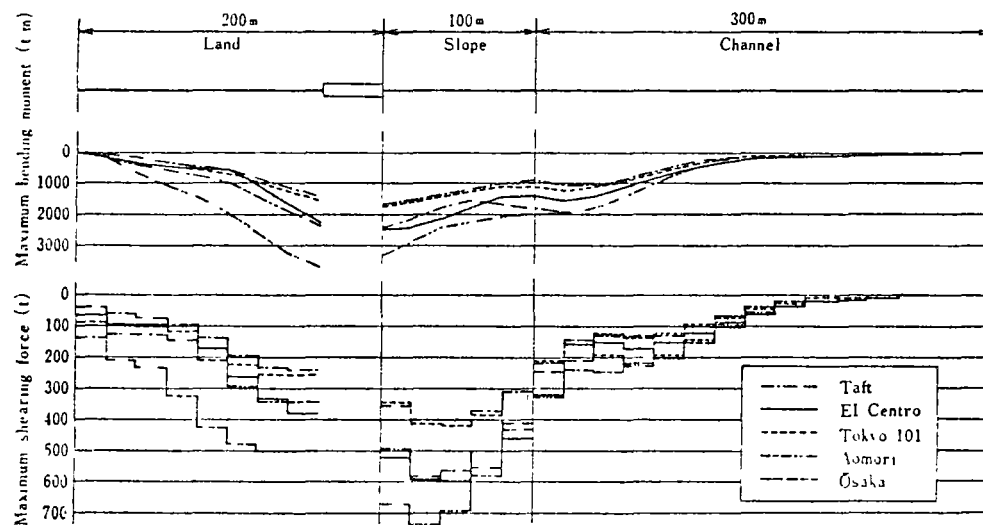
Fig. 17.14 Maximum displacement and maximum acceleration on the ground surface (Input maximum acceleration and damping constant are assumed to be 100 gal and 10% respectively).

C. Tamura used this model to calculate the movement of ground and stresses of a sub-aqueous tunnel to be provided at the channel as shown in Fig. 17.13. Figures 17.14 (a) and (b) are the maximum displacements and maximum accelerations in the direction of the tube axis and in that orthogonal to the tube axis at the

ground surface under the conditions of Tokyo No. 101 earthquake and four other earthquakes with maximum accelerations adjusted to 100 gal, while Fig. 17.15 shows the maximum axial forces, maximum bending moments and maximum shearing forces of the tube caused by these earthquake motions.



(a) Maximum axial force.



(b) Maximum bending moment and maximum shearing force.

Fig. 17.15 Maximum axial force, maximum bending moment and maximum shearing force of the subaqueous tunnel (Input maximum acceleration and damping constant are assumed to be 100 gal and 10% respectively)

From these figures, the following properties become known:

1. The earthquake motion at the ground surface is considerably different according to the place.
2. The earthquake motion at the ground surface is considerably different according to the seismic waveform.

3. Bending moments and shearing forces are large at joints between ventilation towers and submerged tube.
4. Bending moment is relatively large at the connection between the sloped section and the channel section.
5. Bending moment and shearing force are extremely small at the middle of the channel section.
6. Axial forces are large at joints between sub-aqueous tube and ventilation towers.
7. The size of stress of a sub-aqueous tube differs fairly greatly depending on the seismic waveform.
8. The distributions of the maximum deflection, maximum shear and maximum bending moment along the tunnel axis are similar for all earthquake waves mentioned above though they are different in size with one another.

It has been confirmed that these results are in good agreement with the results of model experiments.

The first part of the document discusses the importance of maintaining accurate records of all transactions. It emphasizes that every entry should be supported by a valid receipt or invoice. This ensures transparency and allows for easy auditing of the accounts.

In the second section, the author details the various methods used to collect and analyze data. This includes both primary and secondary research techniques. The primary research involves direct observation and interviews, while secondary research involves reviewing existing literature and reports.

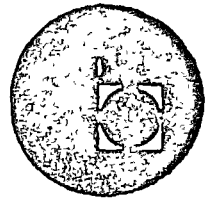
The third part of the document focuses on the statistical analysis of the collected data. It describes the use of various statistical tests to determine the significance of the findings. The results indicate a strong correlation between the variables being studied, which supports the initial hypothesis.

Finally, the document concludes with a summary of the key findings and their implications. It suggests that the results have important implications for the field of study and provides recommendations for further research. The author also acknowledges the limitations of the study and offers suggestions for how these can be addressed in future work.





centro de educación continua
división de estudios superiores
facultad de ingeniería, unam



III CURSO INTERNACIONAL DE INGENIERÍA SISMICA

ANALISIS DINAMICO DE ESTRUCTURAS
ESPECIALES

TUBERIAS Y TUNELES

PROF. ARTURO ARIAS

JULIO-AGOSTO 1977



СЕРТИФИКАТ
автомобильного транспорта
№ 123456789

И. П. Иванов

Адрес: г. Москва, ул. Ленина, д. 10
Индекс: 123456

№ 123456789

СЕРТИФИКАТ

№ 123456789

И. П. Иванов

Dynamic Stresses of Underground Pipe Lines During Earthquakes

by

Akio Sakurai and Tadashi Takahashi

Synopsis

The results on dynamic behaviours of underground pipe lines are presented, which were observed on three kinds of pipe lines during the Matsu-shiro Earthquakes. The observed stresses of pipes are discussed in connection with the observed deformations of ground, the wave character of ground and the phase of seismic waves.

The principal strain of ground are also calculated from the strain records which were observed by the new-designed earth-strain meters. The observed results are compared with the results of vibration tests and many kind of soundings, and an estimative process to the pipe stress are presented.

List of Symbols

- A_0 amplitude of ground movement
- A acceleration of earthquake
- A_0 sectional area of pipe
- C_0 friction per unit pipe length
- C constant relating to pipe strain
- D diameter of pipe or tunnel
- E Young's modulus of pipe material
- f constraint of ground against pipe line
- k spring constant of surrounding ground
- l a half length of seismic wave
- L length of seismic wave
- ω circular frequency of ground movement; $= \frac{2\pi}{T}$
- r_0 radius of pipe or tunnel
- t co-ordinate of time
- T, T' period of ground movement
- u relative displacement between pipe and ground

Senior Research Engineer, Earthquake Engineering Section,
Structure Dept., Technical Laboratory, Central Research Institute of
Electric Power Industry, 1,229 Iwato, Komae-cho, Kitatama-gun, Tokyo.

Fellow Research Engineer, Supervisor, Earthquake Engineering
Section, ditto.

u_0	yield point of ground's constraint
v	apparent velocity of seismic wave incident to pipe line
v_0	velocity of longitudinal wave propagating in pipe line; $= \sqrt{\frac{E}{\rho}}$
v_s	velocity of pure shear wave propagating along the surface if exist.
V	velocity of seismic wave
x	co-ordinate of distance
y	movement of pipe line
Y	movement of ground
$\epsilon, \epsilon_m, \epsilon_m$	strain of pipe line or ground
λ	a distance between anchors
ρ	density of pipe material
ω_0	natural circular frequency of rigid pipe line; $= \sqrt{\frac{k}{\rho A}}$

1. Introduction

Dynamic behaviours of Underground pipe lines during earthquakes remain unknown, while the structures in weak ground have suffered damages from large earthquakes. From the aseismic point of view, the problems lie in the fact that the dynamic behaviours of the structures have little relations to ground acceleration, but to ground deformation, and in the fact that such structures have two dimensional extension along the surface of ground. As many investigations of the earthquake engineering treated ground acceleration such as the one at a point, they give little informations for ground deformation or distribution of ground displacement along the surface.

The Matsushiro Successive Earthquakes offered a lot of earthquakes and many chances to earthquake engineers in a brief period of time. The Earthquakes enabled us to research two or three dimensional properties of seismic wave propagation in ground, and to test dynamic responses of full sized models due to real earthquakes regarding a ground as a large shaking table.

In this paper a consideration on aseismic design of underground pipe lines is presented, based on the observed records of the wave propagative properties, ground strain, and pipe strain for three kinds of pipe lines during the Matsushiro Earthquakes.

2. On the Matsushiro Earthquakes

The Matsushiro Earthquakes occurred at Aug. 3, 1965 and counted the number of earthquake frequencies up 653,908 until March 31, 1967. The earthquakes are inactive, but do not end in present. The maximum magnitude was 5.3 in the past. The activity of earthquakes is shown in Fig. 2. 1 and Table 2. 1.

The focuses of earthquakes were beneath Mt. Minakami in the Matsushi-

ro town, the Nagano province at first, and the region enlarged to the north-east and to the south-west. In Jan. 1967, the new focuses appeared beneath Mt. Kamuriki and Mt. Azumaya. The term of this researches contained the third period of strong activities in Aug. and Sep. 1966 and the forth in Jan. and Feb. 1967 (Fig. 2.2).

3. The Experiments

The test field was sited at the yard of Hokushin transformer station, the Chubu Electric Power Co. and is about 10 kilometres distant from Mt. Minakami in the west and about 11 kilometres from Mt. Kamuriki in the north.

The next items of observations during earthquakes were conducted in order to research the dynamic behaviours of pipe lines;

- (1) The amplitude distribution of acceleration and properties of seismic wave propagation in the direction of depth.
- (2) The amplitude distribution of displacement and properties of wave propagation along the surface of ground.
- (3) The ground strain and properties of the principal strain and the principal angle near the surface.
- (4) The dynamic behaviours and pipe strain for three kinds of pipe lines.

The followings were researched relating to the above observations;

- (1) Boring Soundings to -50.0 metres.
- (2) Standard penetration test and Sweden penetration test.
- (3) Elastic wave soundings and vibrator tests on properties of ground for surface waves.
- (4) Micro-tremour measurements
- (5) Vibrator tests for pipe lines
- (6) Measurements on dynamic spring constant at the test ground.

The three proto-type models of pipe typed electric transmission lines for ultrahigh voltage (60 kV-275 kV) were tested, and their dimensions were presented in Table 3.1. The moving coil type seismographs were used without amplifier considering its stability in long test term. For the research on propagative properties of seismic wave in the direction of depth, a part of the seismographs placed in the ground, one set sitting in -3.0 metres, -10.0 metres and -30.0 metres from the surface and other set in -5.0 metres and -10.7 metres at 50 metres distance from each other. Other seismographs distributed on the pipe lines and in the ground parallel with pipe lines in order to compare the difference of dynamic behaviours between pipe lines and ground.

The ground strain during earthquakes was observed by earth strainmeters which were newly designed by the authors used to the same principle of the seismograph. The 45 and 90 degrees rosette composed by three earth strainmeters was placed 0.4 metres under the ground for calculating the principal strain of ground.

On the Matsushiro Earthquakes, comparably large earthquakes appeared in a brief period of time. That was able to measure pipe line stress by usual method. The electric wire strainmeters and Carlson's strainmeters were used in the experiments. Usual number of measurements was counted up more than 120 points.

4. The Results

The number of earthquake records reached to several hundreds and pipe strain records were counted up to about one hundred. The earthquake 03:04, Oct. 26, 1966 was the maximum one experienced in the term of pipe strain measurements. The Magnitude was 5.3 and its maximum acceleration observed at the test field was 83 gal. Through the observed period of the project which contained this pipe line experiments, the maximum acceleration observed in the test field reached 196 gal in the earthquake 13:09, Aug. 28, 1966 of which magnitude was 5.3.

The observed records concerning the stresses of underground pipe lines showed that

(A) On the dynamic behaviours

- (1) No difference of pipe lines and ground deformation was observed.
- (2) On the ground deformation, the axial deformation was nearly equal to the transverse deformation.

(B) On the pipe strain

- (1) At the straight part of pipe line, the axial strain was predominant.
- (2) At the part of bend, the strain due to bending moment was observed. The strain of the bend did not large compared with the straight part.
- (3) The maximum strain of pipe lines did not appear at the time when the acceleration of ground reached maximum. The maximum strain appeared at the after phase of seismic waves.
- (4) The strain at the connecting part of pipes and man hole did not large compared with another part for 250A pipe, but large stress concentration was observed in the concrete pipe. The bending strain at the connection was predominant, but at brief distance from the part the axial strain became predominant. At the after phase of seismic waves the axial strain at the connection became predominant.

5. Considerations

In order to investigate pipe line stresses during earthquakes, the next problems should be decided: (1) Are there something to differ between pipe line and ground deformation? (2) Which of pipe stress predominate, bending stress or axial stress? (3) Which phase of seismic waves cause the maximum pipe stress?

On the problem (1), the observed records showed that the pipe line

deformation was equal to the ground deformation, and the natural frequencies or the increase of amplitude of pipe deformation did not recognized. Let this problems inspect to further details. Suppose the ground movement as

$$Y(x, t) = a_0 \cdot \sin p(t - x/v) \quad (5.1)$$

and f as constraint of ground

$$f = k' \cdot \frac{u}{u_0} \equiv k \cdot u \quad (0 \leq u \leq u_0) \quad (5.2)$$

$$= C_0 \quad (u_0 < u) \quad (5.2')$$

where

$$u = Y - y$$

In the range of $u < u_0$, the vibrational equation of pipe lines in the axial direction (cf. Fig. 5.1),

$$\rho A_0 \frac{\partial^2 y}{\partial t^2} - EA_0 \frac{\partial^2 y}{\partial x^2} + ky = k \cdot a_0 \sin p(t - x/v) \quad (5.3)$$

The solution of the eq. (5.3) is

$$y(x; t) = \frac{1}{1 + \left(\frac{p}{\omega_0}\right)^2 \left(\frac{v}{v_0}\right)^2 - \left(\frac{p}{\omega_0}\right)^2} Y(x, t) \quad (5.4)$$

The impact test showed that ω_0 was about 100 C/S for 250A pipe without cable. If in the case of pipe with cables, $(p/\omega_0)^2$ may be negligible compared with unit. Then neglecting the inertia effect, the decrease of pipe line deformation compared with ground is shown in Fig. (5.2). The same situation was presented in the transverse vibration. The transverse vibration tests on 250A pipe showed that the dynamic spring constant surrounding pipe was larger than 30Kg/cm/cm, even though sand surrounding pipe became the state of lequifaction. The natural frequency of 250A pipe with cables was larger than 20 C/S. Considering the cycle range of seismic waves in weak ground and the damping due to surrounding ground, dynamic effects of transverse vibration for many pipe lines are negligible. Fig: 5.3 shows the decrease of pipe line deformation for transverse deformation.

The conclusion on the problem (1) is that the deformations of pipe lines used in the experiment can be regarded as the same of ground. In the comparably large earthquakes, axial deformation is not equal to ground. This will be discussed latter.

Though the axial deformation of pipes was nearly equal to the transverse deformation, the axial strain of all pipe lines in all eathquakes was predominant. The fact was explained by the difference of stress sensitivity between axial and transverse deformation. Supposing ground deformation as eq. (5.1) and letting the same amplitude and the same wave length, the calculated ratio axial strain to bending strain of pipe lines is shown in Fig. (5.4). For example, the ratio for 250A pipe is about 30, supposing the seismic wave velocity $v=100$ m/sec period $T=0.5$ sec - or if ground strain is 30×10^{-6} strain, axial strain of pipe lines is 30×10^{-6} strain while bending strain is 1×10^{-6} strain. As the diameters of pipe lines become larger the ratio become smaller, then the bending strain should be supperposed for pipe lines such as subway tunnels (See Appendix).

The conclusive notes of the problem (1) and (2) above mentioned induce the relation for pipe line stresses during earthquakes as follows. As records of earthquakes abound with acceleration records, let obtain

the relation between strain and acceleration. Supposing pipe line strain equal to ground strain and assuming ground deformation as eq. (5.1), axial strain of pipe line is given as

$$\epsilon = -a_0 \cdot \frac{p}{v} \cos p(t-x/v) \quad (5.5)$$

and acceleration of ground as

$$A = -a_0 \cdot p^2 \sin p(t-x/v) \quad (5.6)$$

The maximum strain is

$$\epsilon = \frac{a_0 \cdot p/v}{a_0 p^2} \cdot A = \frac{1}{2\pi} \cdot \frac{T \cdot A}{v} \quad (5.7)$$

The relation (5.7) is supported by the observed records of pipe strain as shown in Fig. (5.5).

Following this relation (5.7), the strain concerns with not only acceleration and period or deformation velocity of ground (T·A), but also the apparent velocity v of seismic waves incident to pipe lines. Also the apparent velocity concerns with the kind of seismic waves and softness of ground. For example, if the seismic waves incident to pipe lines propagate with the normal to them, the apparent velocity v become infinity and no strain of pipe lines induce. The observed records of seismic waves in a direction of depth and along the surface showed that the phase of S wave - especially the first part of S waves - produce no strain of pipe lines layed parallel to the surface. This demonstrated by the fact that the strain of the pipe lines appeared at the time when the maximum acceleration had appeared already.

Do shearing waves propagate along the surface during earthquakes? If shearing waves appear, such a strain as follows will induce. Assuming such seismic wave as pure shear wave, the expansional wave is induced in a direction of 45 degrees to that direction of propagation and the amplitude of induced wave is one half to the original wave. Even in this case, the axial strain will observe in pipe lines, because the strain sensitivity above considered is much larger than 2. The strain induced by pure shear wave is given as

$$\epsilon = \frac{1}{4\sqrt{2}\pi} \cdot \frac{T \cdot A}{v_s}$$

for the incidence of 45 degrees direction to pipe lines.

For the evaluation of pipe line stresses during earthquakes, it is most important which phase of seismic waves cause the maximum pipe stress. It was thought that the principal strain of ground would give good informations for the problem, so the observations of ground strain were conducted in this experiments.

An example of the principal strain calculated by the strain records in three directions is shown in Fig. 5.6. The some of the results was as follows:

- (1) The principal strain of ground surface as same as pipe strain did not reach the maximum when acceleration or displacement of ground became maximum.
- (2) The pure shear wave along the surface was not apparent, because the calculated waves of both principal strain were the same in phase.
- (3) The variation of the principal angle with time duration have some

character at the boundary of P-wave, S-wave and after phase's wave in seismic waves. An example in Fig. 5.5 shows the sudden variation at the boundary of P-wave and S-wave. After the next variation which is not so sudden as at the P-S boundary, the surface wave become to appear which can be distinguished by the observed records of seismic waves under the ground.

Considering the results of ground strain in connection with results of experimental studies for elastic waves and on propagative character obtained by the observed seismic waves, the effective wave for aseismic design of underground pipe lines may not be S-wave but surface wave especially in homogeneous ground.

As the strain of pipe lines concerns with the period of acceleration, the microtremour measurements were conducted and were compared with the periods of strain waves and seismic waves. The results of the measurements at the surface and in the ground gave good agreement with the one of earthquakes. The periods which were 0.10 sec, 0.25 sec and 0.36 sec at the surface correspond to the predominant periods of earthquakes which were 0.15 sec, 0.25 sec and 0.40 sec, while both periods differed slightly from point to point in the test yard. The period when the maximum acceleration appeared is uncertain, relating to the magnitude of earthquakes, the period of seismic activity and etc.. The periods, 0.15 sec and 0.25 sec, appeared mostly at the time when acceleration became maximum, while the predominant period of pipe line strain was 0.40 sec which coincided with the period obtained by the after phase of seismic records. Even though there was a certain case of which the predominant period in after phase was greater than 0.4 sec, it may be said that the predominant period obtained by microtremour offers good informations to the predominant period of pipe line stress.

6. Additional Consideration

The relation (5.7) is in the case of which relative displacement between pipe lines and surrounding ground is negligible. When earthquake becomes a certain extent, the relative displacement occurs in axial direction. The extent is given as follows:

$$u = Y - y \geq u_0 \quad (6.1)$$

or

$$\frac{AT^2}{4\pi^2} = u_0 \left\{ 1 + \frac{1}{\left(\frac{p}{\omega_0}\right)^2 \left(\frac{v_a}{v}\right)^2} \right\} \quad (6.2)$$

$$= u_0 \quad (6.2')$$

Of course, we assume the wave length of earthquake is contained in extent of pipe lines. By quasi-dynamic test on 250 A pipe placed 1.5 metre beneath the surface, and surrounded by sand, u_0 was less than one millimetre. Assuming the relative displacement attain to the extent at large earthquake and uniform frictional force occurs all over pipe line, the upper bound of strain for straight pipe line is

$$\epsilon_u = \frac{C_0 \cdot L}{4EA_0} = \frac{C_0 \cdot vT}{4EA_0} \quad (6.3)$$

During large earthquakes, the movement of man hole, bend and branch contained in pipe line can be regarded as the same as ground movement.

We denote λ as a distance between man hole and branch or so on. When the relative displacement occurs all over pipe line, the mean strain of pipe line in the distance λ is

$$\epsilon_m = \frac{a_0}{\lambda} \left[\sin p\left(t - \frac{T}{4}\right) - \sin p\left\{t - \frac{T}{4}\left(1 + \frac{4\lambda}{L}\right)\right\} \right] \quad (64)$$

The maximum ϵ_m with time duration is

$$\epsilon_m = \frac{1}{2\pi} \cdot \frac{L}{2\lambda} \cdot \frac{AT}{v} \left[1 - \sin \frac{2\pi}{4} \left(1 + \frac{4\lambda}{L}\right) \right] \quad (65)$$

When $2\lambda = v \cdot T'$ or $2\lambda = L$,

$$\epsilon'_m = \frac{1}{\pi^2} \cdot \frac{AT'}{v} \quad (66)$$

Fig. 4.1 and Fig. 4.2 show comparably large strain of pipe lines at the phase of S-waves. This strain was induced by the non-homogeneity of the test field. Fig. 6.1 is a record of ground displacement which was observed by the seismographs distributed on the surface and placed each other apart 30 metres in axial direction. Fig. 6.2 shows the seismic displacement in 30 metres underground which was calculated from the record shown in Fig. 6.1 by the elastic wave theory (1). The calculated waves at S phase resemble each other although the observed record at the surface comparably differ each other. The mean strain of ground calculated from the observed displacement shown in Fig. 6.1 is presented in Fig. 6.3. It is comparably large compared with at after phase.

7. Conclusion

The above considerations enable us to evaluate dynamic stresses of underground pipe lines during earthquakes.

- (1) The axial strain of pipe line become predominant and is presented by the next relation,

$$\epsilon = C \cdot \frac{TA}{V} \quad (71)$$

Following this, the strain concerns with

- (a) the phase of seismic waves (C,V)
 - (b) the softness of ground (V)
 - (c) the deformation velocity of ground (T·A).
- (2) The process to evaluate the stress are as follows:
- (a) To measure the velocity of elastic waves in the ground of which construction of pipe lines is planed.
 - (b) To decide the deformation velocity of the ground. For the aseismic design, acceleration for pipe line need not to adopt the same value for structures constructed on the surface of ground.

(1) E. Shima "Modifications of Seismic Waves in Superficial Soil Layers as Verified by Comparative Observations on and beneath the Surface" Bull. of Earth. Res. Inst. Vol 40, 1962

- (3) The after phase of seismic waves or surface waves may induce large stresses for pipe lines in homogeneous ground, but it is noted that the comparably large stresses will appear in non-homogeneous ground at the S-phase.

Fig. 7.1 shows the relation (7.1) assuming $C=1/2\pi$. By Fig. 7.1, the strain become large when V is less than 300 m/sec. In generally, the velocity of effective seismic waves is less than 150 m/sec in weak ground, then large strain in weak ground will occur during large earthquakes. For example, assuming that $V = 140$ m/sec, $T = 1.35$ sec and $A = 100$ gal, the strain become about $1,500 \times 10^{-6}$ strain. This, ground strain, may explain some of cracks which occur in weak ground during large earthquakes.

8. Acknowledgement

This paper is a part of the research project "Aseismic Researches for electric equipments and facilities, availing the Matsushiro Earthquakes". This researches were accomplished, co-operating with Tokyo Electric Power Co. and Chubu Electric Power Co.. The authors wish to express their sincere thanks to personnels of both companies and groupe members of the research project who supported and carried out the experiments (3).

Bibliography

- (1) Y. Ōtsuki and K. Kanai: [Earthquake Resistant Design] corona-sha, 1961
- (2) S. Okamoto: [Structural design method, considered earthquakes] Ōmu-sha, 1954
- (3) T. Takahashi and others: [Aseismic Researches on Electric Equipments and facilities, availing the Matsushiro Earthquakes] Technical Report No. 66078, March 1967, Central Research Inst. of Electric Power Industry.
- (4) A. Sakurai, T. Takahashi and others: [Aseismic Research on Underground Pipe type cables for ultra-high voltage, availing the Matsushiro Earthquakes] Thechnical Report No. 67058, Oct. 1967, ditto.

Appendix

For pipe lines with large diameter, the bending stress must be superposed to the axial stress. Assuming the ground movement as $Y = a_0 \cdot \sin \rho(t - x/v)$, the bending strain of pipe is given as the next relation.

$$\epsilon = \frac{r_0}{v^2}$$

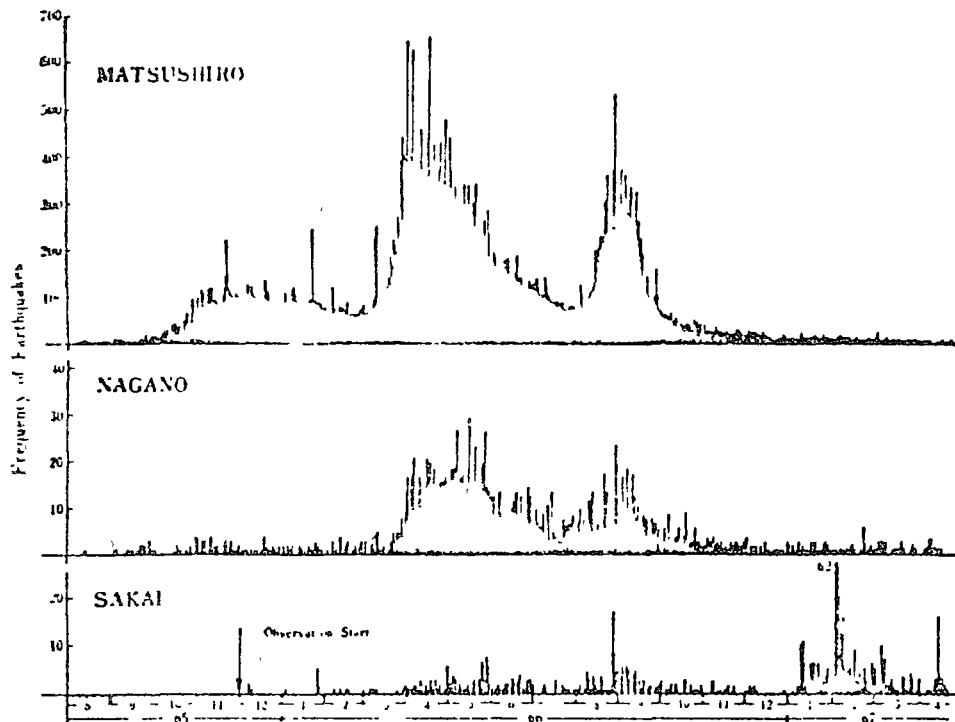


Fig. 2.1 Histogram of MATSUSHIRO Earthquakes

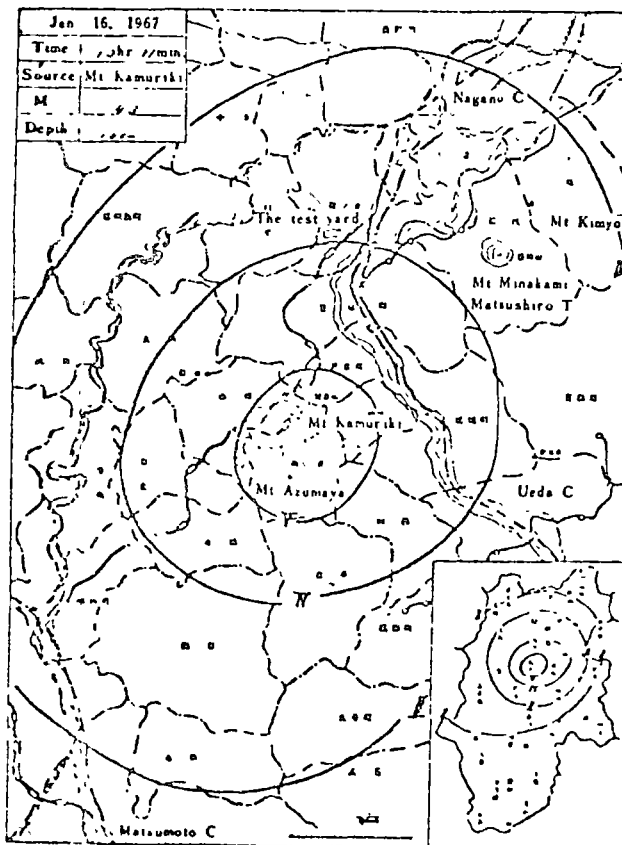


Fig. 2.2 A epicentre of earthquake

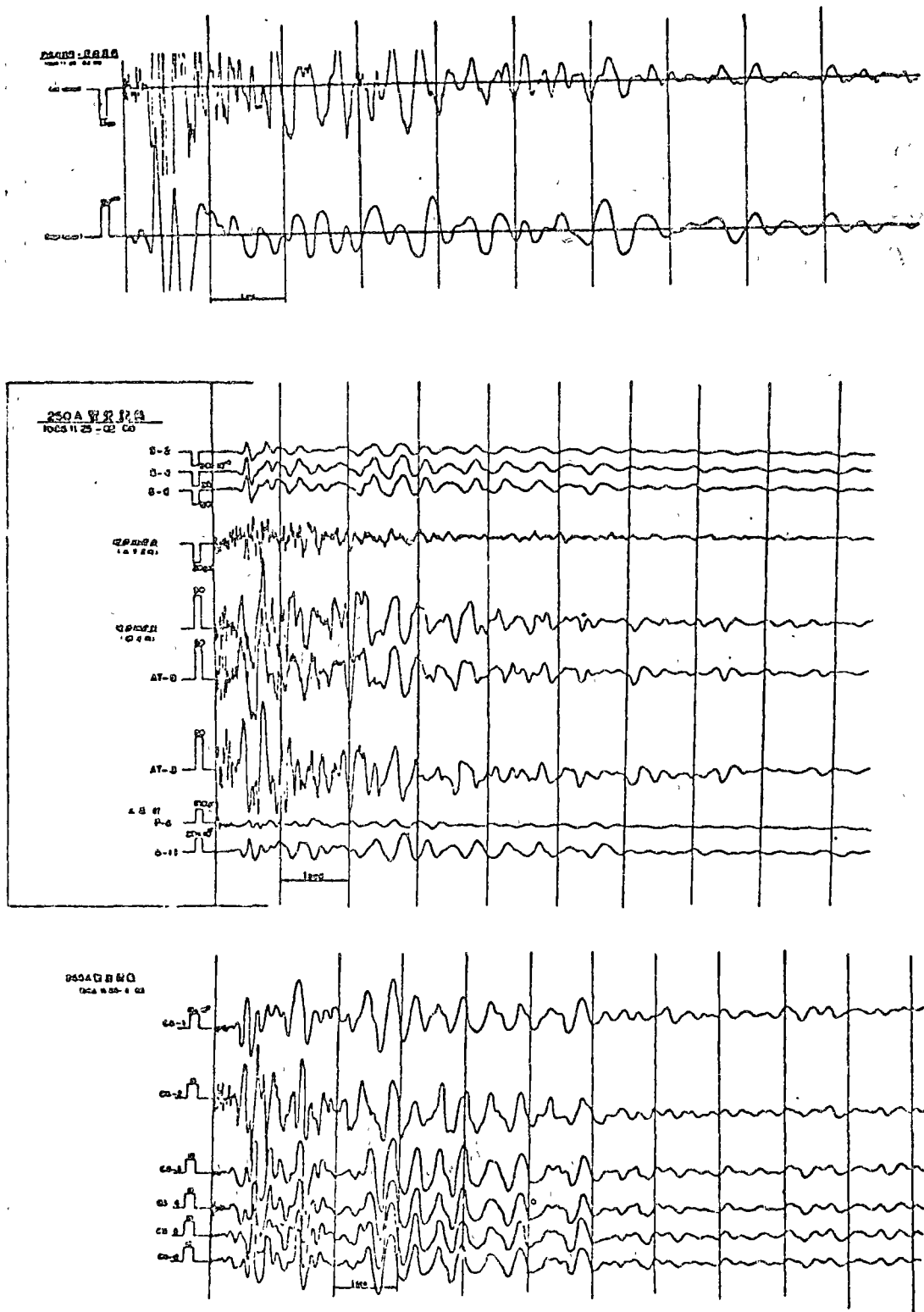


Fig. 4.1 The records of acceleration, displacement and strain of 250A pipe

THE
FIRST
PART
OF
THE
HISTORY
OF
THE
CITY
OF
NEW
YORK
FROM
1609
TO
1624
BY
JOHN
BURNETT
1898

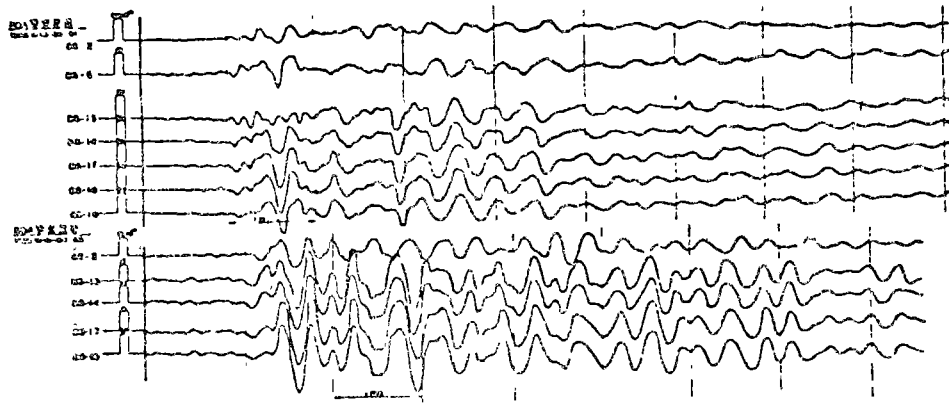


Fig. 4.2 The strain records of 80A pipe

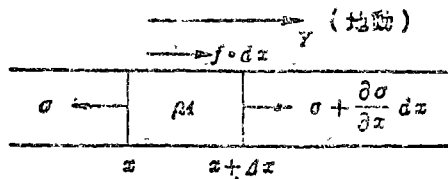


Fig. 5.1

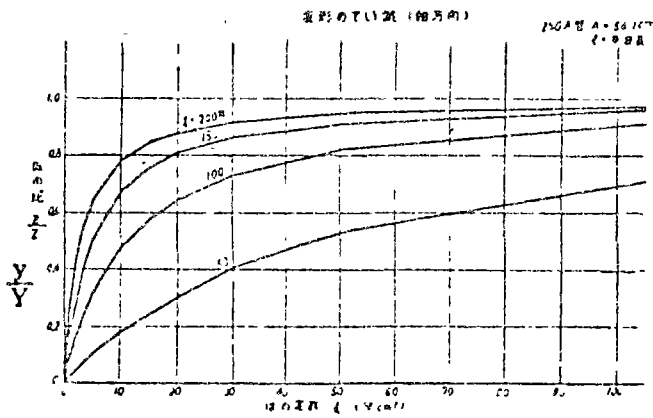


Fig. 5.2
The decrease of pipe's axial deformation due to ground elasticity

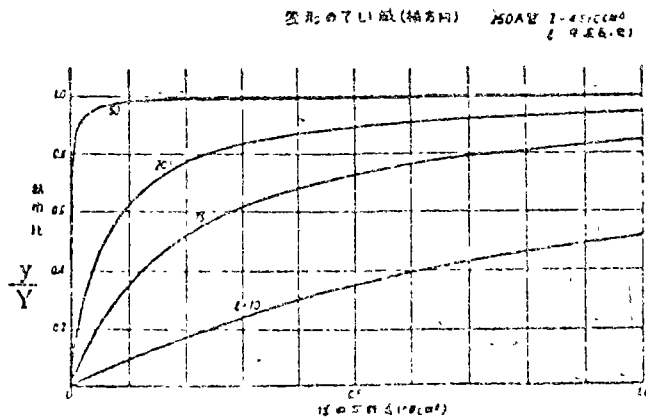
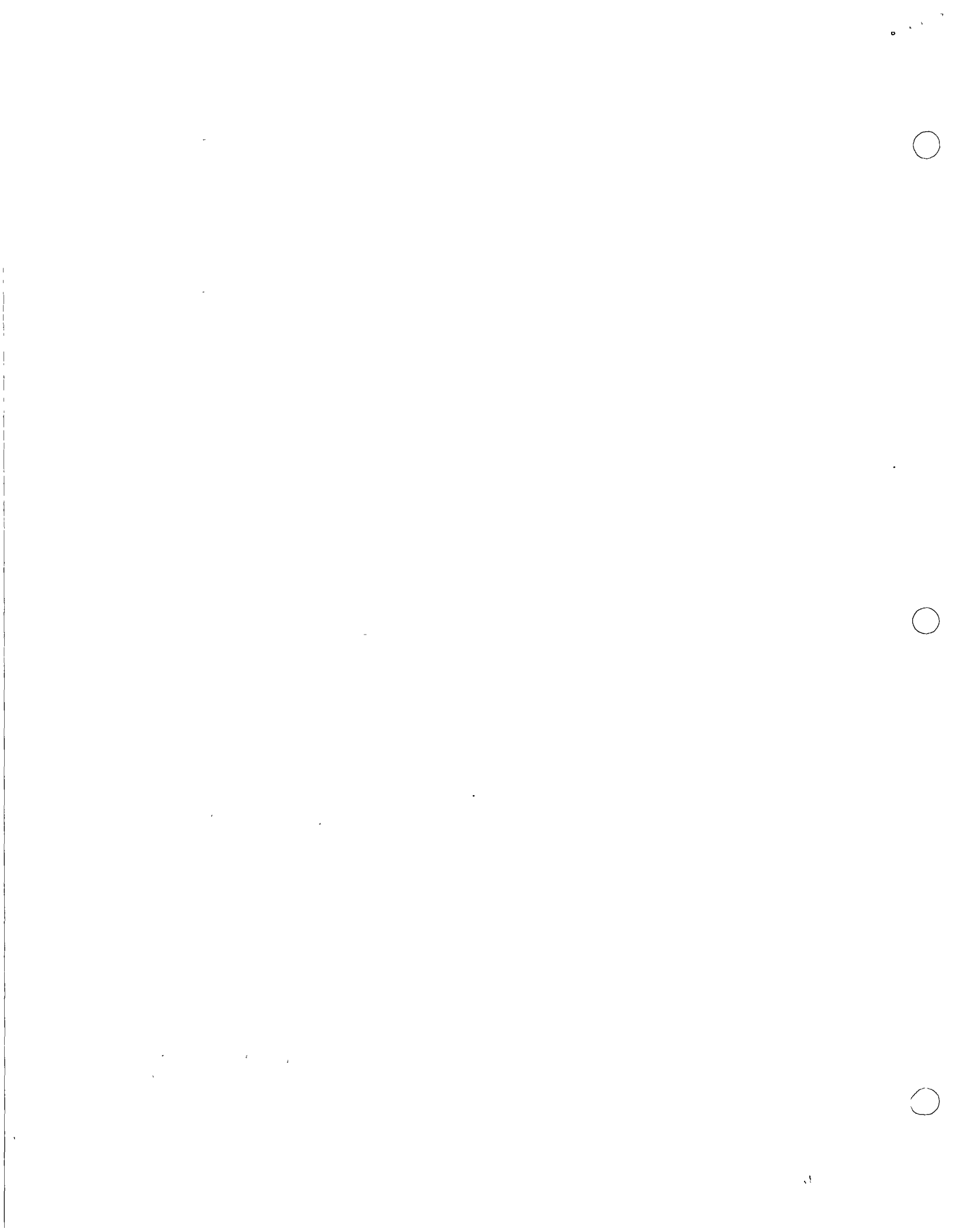


Fig. 5.3
The decrease of pipe's transverse deformation due to ground elasticity



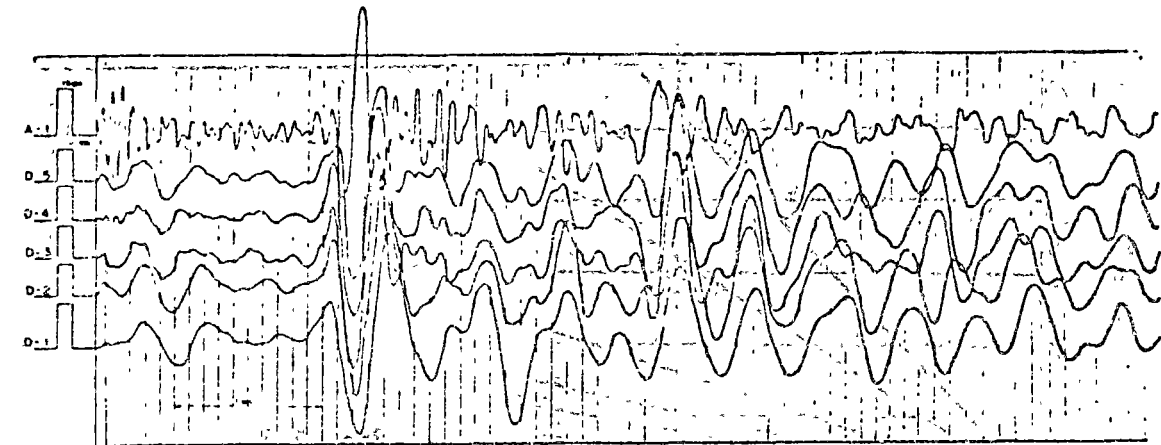


Fig. 6.1 A record of ground displacements at the surface (axial direction)

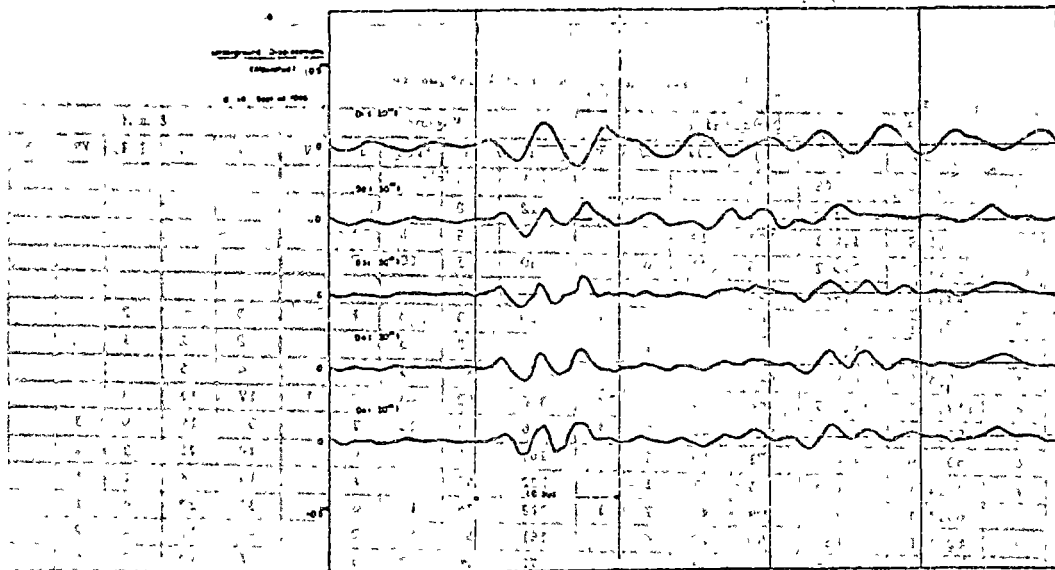


Fig. 6.2 Underground displacements calculated from the surface displacements

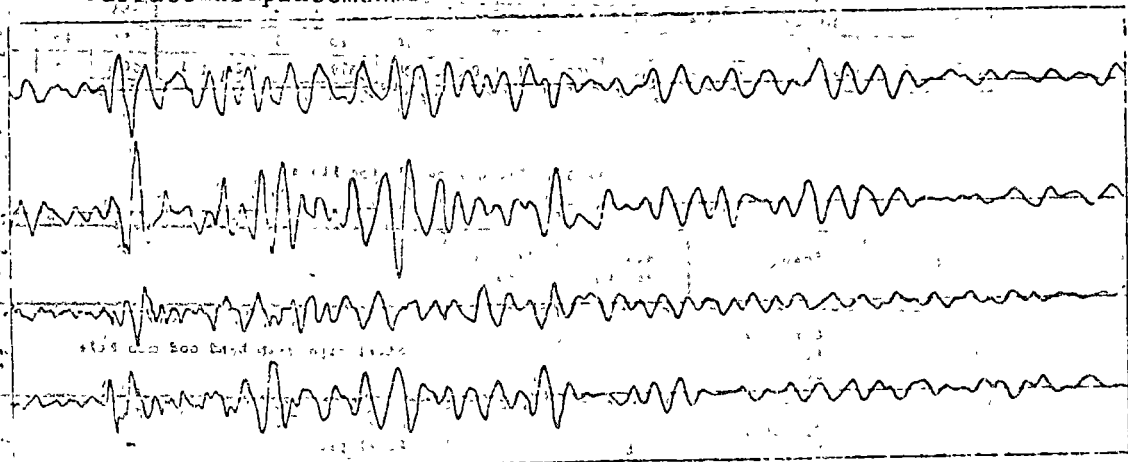


Fig. 6.3 Ground strain calculated from the surface displacements

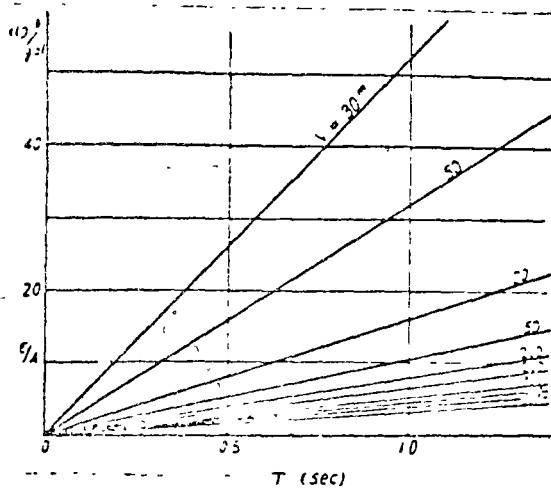


Fig. 7.1
Strain of underground
pipe lines

Table 2-1 Number of Earthquakes

	No.	Matsushiro					Nagano					Sakai					
		I	II	III	IV	V	I	II	III	IV	V	I	II	III	IV	V	
'65	8	3,739	69	1			1										
	9	8,744	176	18			12	2									
	10	15,839	1,021	111	11		7	2	1								
	11	25,186	2,327	343	51	8	30	7	10	2							
	12	22,563	2,471	356	35	2	18	6	2								
'66	1	22,917	2,451	293	27	2	1	20	3	3	1		3		2		
	2	18,727	1,710	162	13	1	1	21	8	3			2	2	1		
	3	43,576	4,903	428	33	3		65	17	5			4	5			
	4	119,035	10,687	968	84	10	4	310	92	48	2	1	17	13	3		
	5	82,544	7,470	517	42	8	1	346	103	26	7		32	19	9	3	
	6	53,629	4,091	271	19	1		167	65	23	4		14	21	3	1	
	7	34,454	2,613	135	7	1		122	52	8	1		14	4	1	1	
	8	63,313	5,750	409	43	7	1	172	76	11	6		39	22	4	1	
	9	62,171	5,856	360	19	4		181	65	10	2		47	17	4	2	
	10	19,666	1,190	68	4			72	26	2	3		8	12	3	6	
	11	11,913	622	32				35	18				14	2	2		
	12	7,371	446	24	1			15	13	2			2	5	1		
'67	1	7,141	385	10	1		14	7	2			57	18	4	1	3	
	2	10,707	564	14	2		12	7	4			155	62	11	2	1	
	3	5,640	284	11	1		18	10	1			55	16	1			
Total		653,505	55,766	4,542	407	47	8	1,639	579	161	28	1	463	218	44	19	4

Table 3.1 Dimensions of pipe lines.

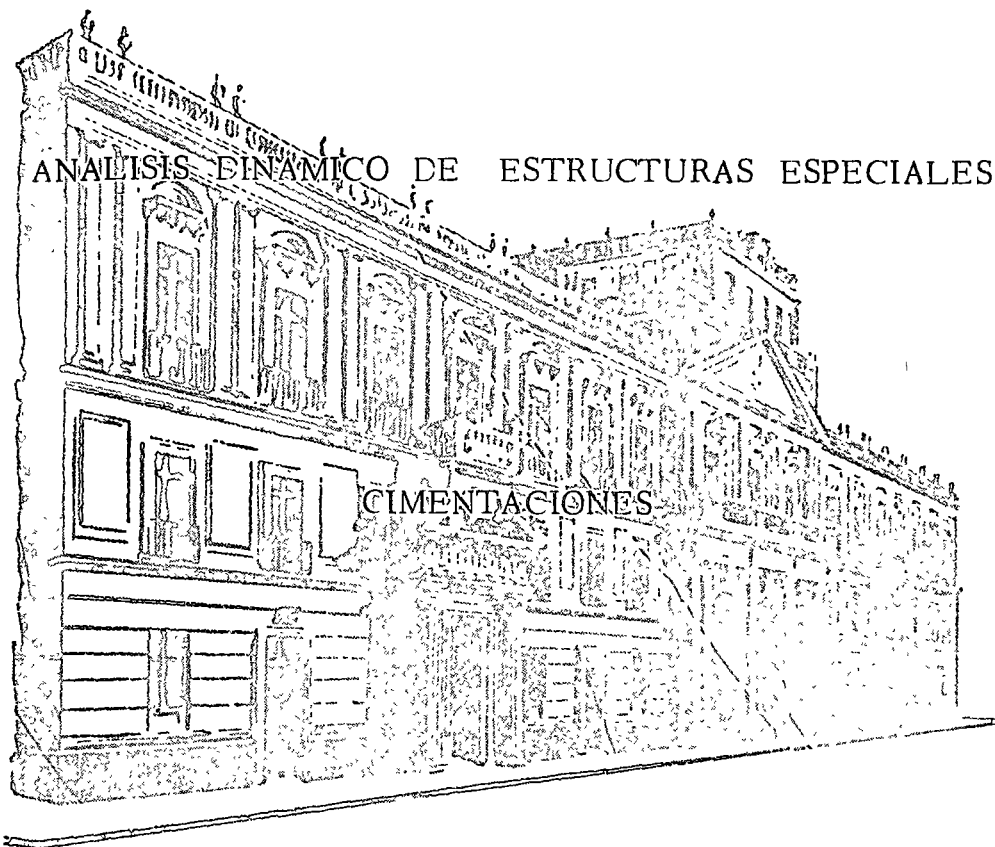
Pipe	Shape	Weight (kg/m)	Length (m)	
250A	Circular Dia. ϕ 267.4	42.4	91	Steel pipe with bend and man hole
80A	Circular Dia. ϕ 89.1	8.7	70	Steel pipe
Asbestos	Rectangular 500 x 630	612	44.1	Asbestos pipe (ϕ 125 x 4) surrounded with concrete, with man hole



centro de educación continua
división de estudios superiores
facultad de ingeniería, unam



III CURSO INTERNACIONAL DE INGENIERIA SISMICA



DR. RAUL FLORES BERRONES

JULIO-AGOSTO, 1977.

Centro de Estudios Políticos y Sociales
Calle de la Princesa, 107
28002 Madrid



APUNTES DE DINAMICA DE SUELOS

Por el Profesor Raúl Flores Berrones

CAPITULO IV

COMPORTAMIENTO DINAMICO DE LOS SUELOS

I) Introducción

En esta parte se estudia el comportamiento de los suelos cuando se les sujeta a cargas o movimientos dinámicos, tales como los originados por sismos o los provocados por algunas máquinas. Primeramente se explica la naturaleza general del comportamiento dinámico de los suelos y los modelos matemáticos que más se utilizan para representar al suelo, así como la determinación de los parámetros que intervienen en el gobierno del modelo viscoelástico. Se proporcionan también algunas fórmulas empíricas que permiten estimar a estos parámetros y se indican los procedimientos de campo y laboratorio que más se utilizan para determinar las propiedades dinámicas de los suelos. Finalmente se dan las conclusiones y recomendaciones referentes a la determinación de esas propiedades.

II) Naturaleza general del comportamiento dinámico de los suelos

En términos generales, se ha observado experimentalmente que un suelo presenta efectos de endurecimiento cuando los esfuerzos aplicados en pruebas unidimensionales están por arriba de 13 a 14 kg/cm². Por el contrario, a niveles bajos de esfuerzo (<3 kg/cm²), el suelo presenta un efecto de ablandamiento (fig 3.1). Este último tipo de efecto es el que sucede en la mayoría de los problemas relacionados en dinámica de suelos.

Ahora bien, cuando a un suelo se le sujeta a cargas del tipo cortantes cíclicas, tal como las producidas en algunas cimentaciones de maquinaria y desde luego por las ondas de cortante sísmicas, las curvas típicas de esfuerzo deformación son como las mostradas por la fig 3.2. Definiendo como *módulo secante cortante* a la pendiente de la recta que une a cada uno de los lazos de histéresis allí formados, y considerando que el área dentro de dichos lazos representa la *energía disipada* (debido fundamentalmente a los efectos no lineales de fricción entre las partículas de suelo), de esta figura se puede ver que ambas cantidades varían con el nivel de las deformaciones.

Así pues, la figura 3.2 señala que un suelo (sea cohesivo o no), cuando se le sujeta a cargas cortantes cíclicas, tiene un comportamiento claramente no lineal. De manera similar se obtiene este tipo de comportamiento cuando a un suelo se le somete a cargas de compresión cíclicas, como los que se producen, por ejemplo, en una prueba triaxial dinámica.

Puesto que en general los movimientos de un sismo están caracterizados por esfuerzos cortantes reversibles que varían en amplitud y frecuencia (fig 3.3), puede decirse que para cada ciclo de carga y descarga se tendrá una curva de esfuerzo-deformación del tipo señalado por la fig 3.2. Dependiendo del nivel de esfuerzos en cada ciclo se tendrá un cierto valor del módulo cortante y un cierto valor del amortiguamiento o pérdida de energía.

Tomando en cuenta que la velocidad de aplicación de las cargas que se producen durante sismos y en varios problemas de cimentación de maquinaria, es relativamente rápida en comparación con la velocidad con que puede fluir el agua entre las partículas de suelo (de manera que no exista presión de poro), puede considerarse que las condiciones de drenaje durante cargas dinámicas corresponde a situaciones no drenadas. (Obviamente este puede no ser el caso, por ejemplo de gravas o arenas muy gruesas, e incluso pueden haber circunstancias intermedias).

Del análisis en pruebas de laboratorio se ha observado que la resistencia de un suelo puede disminuir con el número de repeticiones. La fig 3.4, obtenida de una serie de pruebas, indica el número de ciclos requeridos para alcanzar una deformación del 20%, contra el esfuerzo axial dinámico máximo normalizado con respecto a la resistencia estática; obsérvese en esta figura que después de 15 ciclos la resistencia del suelo empieza a disminuir considerablemente.

III) Modelos empleados para el estudio del comportamiento

Una vez conocido el *tipo de comportamiento* que el suelo tiene bajo cargas dinámicas, o lo que es igual, las curvas de esfuerzo-deformación correspondientes, es posible seleccionar un modelo matemático que reproduzca a dicho comportamiento y que permita un análisis simple del mismo. Este análisis se realiza empleando las soluciones matemáticas que se obtienen para cada modelo.

Existen en general dos criterios para seleccionar el modelo requerido. El primero de ellos consiste en seleccionar un modelo que reproduzca o involucre todas las modalidades que el suelo representado puede tener, tales como la no linealidad y el efecto viscoso. El otro criterio es el de seleccionar un modelo simple, con características de esfuerzo-deformación lineales, pero que proporcione los aspectos claves de un problema específico y tenga sus parámetros ajustados al nivel de deformaciones esperado. Con este segundo criterio generalmente se requiere un proceso iterativo; es decir, se estiman primeramente los parámetros y se calculan las deformaciones, se revisan después los parámetros y el proceso se repite hasta que exista compatibilidad entre el valor de los parámetros y el nivel de deformaciones.

Modelo de Ramberg-Osgood: Un modelo representativo del primer criterio es el llamado de Ramberg-Osgood ilustrado en la fig 3.5; dicho modelo se caracteriza por el punto de fluencia (τ_y, γ_y) que define el límite del comportamiento lineal, el valor inicial del módulo al cortante (G_{max}) , y los parámetros α y R . Las ecuacioo

que gobiernan este modelo, en términos de las relaciones de esfuerzo-deformación cortantes, son:

Y/Y_1 = tau/tau_1 [1 + alpha (tau/tau_1)^{R-1}]; ecuación para la curva que desarrolla carga inicial

(Y-Y_1)/Y = (tau-tau_1)/tau [1 + alpha (tau-tau_1/2tau)^{R-1}]; ecuación para las curvas de descarga o recarga

tau y Y se refieren, respectivamente, al esfuerzo y la deformación cortante de fluencia, mientras que tau_1 y Y_1 se refieren al último punto de regreso del esfuerzo.

alpha es un factor que se puede variar para ajustar la posición de la curva en el eje de las deformaciones y R es un factor que controla la curvatura. La fig 3.6 muestra como se pueden ajustar las curvas de Ramberg-Osgood a las que se tienen en suelos. La ventaja principal de este modelo es precisamente la buena concordancia con los resultados experimentales, pero tiene el inconveniente de que su empleo es costoso.

Modelo viscoelástico lineal. Entre los modelos correspondientes al segundo criterio, el que más se emplea por sus ventajas que ofrece y su buena representatividad a la respuesta del suelo bajo cargas cíclicas, es el modelo viscoelástico lineal, ilustrado en la fig 3.7. Los parámetros principales que gobiernan a este modelo son el módulo lineal equivalente y el amortiguamiento lineal equivalente. El bajo costo que resulta el emplear este

modelo y la buena aproximación que con él se obtiene en la mayoría de los problemas comunes de dinámica de suelos, ha hecho que sea el que en realidad se use en la práctica.

Por lo anterior, en lo que resta de este capítulo se hará énfasis en la determinación de estos dos parámetros que gobiernan al modelo viscoelástico. Dado que ambos parámetros dependen del nivel de deformaciones, primeramente se indicarán los procedimientos más comunes para su obtención junto con los correspondientes rangos de deformación que en dichos procedimientos se producen; posteriormente se indicará la manera de estimar los valores de estos parámetros a niveles diferentes a los obtenidos directamente.

Antes de continuar conviene hacer la siguiente aclaración. Cuando la deformación se indica por un simple número, como 10^{-3} , 10^{-6} , etc, quiere decir que la deformación está expresada en cm/cm o en pulg/pulg, según sean las unidades con las que se está trabajando; sin embargo, cuando va seguida del signo %, quiere decir que la deformación está expresada en por ciento. Así, $10^{-4}\%$ es igual a 10^{-6} .

IV) Determinación de los parámetros que gobiernan el comportamiento del modelo viscoelástico

a) MODULO EQUIVALENTE

En la mayoría de las teorías empleadas en la dinámica de suelos se utiliza el módulo al cortante G o el llamado módulo de Young E . Ambos módulos están relacionados mediante la expresión

$$G = \frac{E}{2(1+\mu)} \quad (3.1)$$

donde μ es la relación de Poisson

El módulo G está relacionado con la velocidad de las ondas al corte mediante la ecuación

$$v_s = \sqrt{\frac{G}{\rho}} \quad (3.2)$$

donde

v_s es la velocidad de propagación de las ondas cortantes y

ρ es la densidad de masa del suelo ($= \frac{\text{peso volumétrico del suelo}}{\text{aceleración de la gravedad}}$)

E , por otro lado, está relacionado con la velocidad de ondas longitudinales en muestras cilíndricas del suelo, mediante la expresión siguiente

$$v_L = \sqrt{E/\rho} \quad (3.3)$$

donde

v_L es la velocidad de propagación de las ondas longitudinales en barras

• les en barras

Ambos módulos están también relacionados con la velocidad de las ondas compresionales de cuerpo v_o , mediante las siguientes ecuaciones

$$v_o = \sqrt{\frac{E}{\rho}} \sqrt{\frac{1-\mu}{(1-2\mu)(1+\mu)}} = \sqrt{\frac{G}{\rho}} \sqrt{\frac{2(1-\mu)}{1-2\mu}} \quad (3.4)$$

Sin embargo, dado que en suelos saturados las ondas compresionales viajan primordialmente a través del agua y por tanto las velocidades de propagación de esas ondas no están relacionadas con la estructura del suelo, en dinámica de suelos se utiliza relativamente poco esta clase de ondas para determinar el valor de los módulos equivalentes.

En este capítulo se hará énfasis en la determinación del módulo equivalente al corte, ya que dicho módulo es el que más interviene en la formulación matemática de los problemas manejados en la dinámica de suelos.

Existen tres formas básicas de hacer la determinación del módulo G ; a) pruebas de laboratorio, b) pruebas de campo y c) fórmulas empíricas. Los procedimientos más comunes dentro de cada una de estas formas se describen a continuación.

Pruebas de laboratorio

Los procedimientos más conocidos para determinar el valor de G en el laboratorio, son:

- | | |
|----------------------------------|--|
| | Pruebas |
| 1) Aplicación de cargas cíclicas | $\left\{ \begin{array}{l} \text{a) triaxial cíclica} \\ \text{b) cortante simple} \\ \text{c) cortante por torsión} \end{array} \right.$ |

- 2) Vibraciones forzadas } Prueba de la columna resonante
- 3) Vibraciones libres } a) columna resonante
 b) cortante con torsión
 c) cortante simple
 d) mesas vibradoras
- 4) Técnica pulsativa

El rango de deformaciones que se puede lograr a través de estas pruebas, y su comparación con el rango que se tiene durante temblores de mediana y alta intensidad, se indica en la fig 3.8.

La única prueba que en dicha figura no aparece es la de la Técnica pulsativa; por lo general, el rango de deformación en el que se trabaja en esta prueba es $\leq 10^{-6}$.

Prueba triaxial cíclica

La prueba triaxial cíclica consiste en aplicar esfuerzos longitudinales de compresión y extensión a una probeta cilíndrica de suelo, montada dentro de una cámara triaxial del tipo convencional.

La fig 3.9 indica los esfuerzos a los que queda sujeta la muestra durante la aplicación de carga axial cíclica. En este caso el valor de E se determina a través de las mediciones directas de las características de esfuerzo deformación, y para obtener el valor de G es necesario utilizar la relación indicada en la ecuación 3.1. Esta prueba tiene la ventaja de variar el nivel de deformaciones a través de un control adecuado de los esfuerzos

aplicados y la de utilizar un equipo que fácilmente se puede con seguir en el mercado. Sin embargo, presenta los serios inconvenientes de no reproducir las condiciones de consolidación y de carga que suceden en la realidad. (En el campo los estratos de suelo se consolidan anisotrópicamente y el estado de esfuerzos durante las cargas que se tienen, para el caso de sismos, es muy diferente al producido en el laboratorio; además, las restriccio nes impuestas por los aparatos en los extremos de la probeta, in ducen concentraciones de esfuerzos en esos lugares).

Prueba cortante simple cíclica

Esta clase de pruebas se han efectuado tanto en probetas pequeñas cilíndricas y cuadradas, como en probetas de tamaño relativamente grande. En el caso de probetas pequeñas, los esfuerzos cortantes cíclicos se aplican directamente a través de las pare des de los aparatos que las contienen (fig 3.10); el módulo al corte se obtiene directamente al determinar los esfuerzos y las correspondientes deformaciones cortantes. Un inconveniente de esta clase de pruebas es el efecto de las fronteras que inducen concentraciones de esfuerzos cerca de las esquinas o extremos de las probetas, así como condiciones no uniformes de deformación; todo esto conduce a que el valor del módulo determinado sea menor que el que en realidad se tiene en el campo para mismos niveles de deformación.

Sin embargo, son este tipo de pruebas las que mejor reproducen las condiciones del campo cuando a un suelo se le sujeta a movimientos intensos de sismo.

En cuanto a pruebas a mayor escala, se utiliza un mecanismo que permite determinar el valor del módulo al cortante a través de las vibraciones libres o de vibraciones forzadas en la muestra de suelo. Las vibraciones libres se obtienen aplicando primero una fuerza horizontal en la parte superior de la muestra (fig 3.11) y relajándola rápidamente para medir el decremento de los desplazamientos o las aceleraciones en función del tiempo; el valor del módulo en este caso se obtiene a través de la siguiente expresión (Ref 14)

$$G = \frac{24\gamma H^2}{g T^2} \quad (\text{en libras/pie}^2) \quad (3.5)$$

donde

γ = peso volumétrico del suelo, lb/pie³

H = altura de la muestra de suelo, pies

g = constante gravitacional, 32.2 pies/seg²

T = período de las vibraciones libres, seg

Las vibraciones forzadas se obtienen aplicando una carga horizontal cíclica en la parte superior de la muestra; de la medición de la fuerza aplicada y los desplazamientos producidos se puede obtener la curva de esfuerzo-deformación, y a partir de ella se determina directamente el módulo al cortante.

Esta prueba cortante cíclica se utiliza sólo en trabajos de investigación y generalmente está limitada a muestras alteradas o remoldeadas de suelo (por la dificultad de obtener muestras intactas a distintas profundidades con las dimensiones señaladas en la fig 3.11).

Pruebas cortantes torsionales cíclicas

Existen dos tipos de pruebas de torsión cíclica que son conocidas y empleadas para determinar el módulo al cortante. La primera de ellas es la desarrollada por Hardin y Drenevich (Ref 5) y consiste en aplicar cargas torsionales cíclicas a una probeta cilíndrica de suelo que puede ser sólida o hueca (fig 3.12). La ventaja de la probeta hueca es la disminución de la variación de las deformaciones cortantes en la sección transversal que se analiza (En la probeta sólida la deformación en el centro es nula mientras que en la orilla es máxima).

De la determinación de la carga aplicada y las deformaciones resultantes se pueden dibujar las curvas histeréticas; el valor del módulo se obtiene entonces calculando la pendiente de la línea que une los extremos de los lazos histeréticos correspondientes.

La ventaja de esta prueba es la posibilidad de determinar el valor del módulo cortante en un rango muy amplio de deformaciones; sin embargo, cuando se usan probetas huecas, existe el inconveniente de no poder emplear muestras inalteradas de suelo.

La otra prueba de torsión cíclica es la desarrollada por el Prof. Zeevaert (Ref 16) y es quizá la más sencilla y práctica para determinar el módulo cortante en cualquier tipo de suelo. El procedimiento consiste en aplicar un par torsionante en el extremo superior de una muestra cilíndrica (fig 3.13), para posteriormente soltarla y provocar vibraciones libres que son registradas mediante un instrumento eléctrico.

Después de que el aparato es calibrado y determinada su frecuencia natural amortiguada de vibración, de la observación de las vibraciones libres del sistema se obtiene la frecuencia circular natural amortiguada del mismo. El valor de G se obtiene entonces de la siguiente expresión:

$$G = \frac{\omega_{nd}^2}{(1-D_s^2) - (1-D_a^2) \left(\frac{\omega_{nd}}{\omega_{ad}}\right)^2} \frac{k_a h}{\omega_a^2 I_p} \quad (3.6)$$

donde

ω_{nd} es la frecuencia circular natural amortiguada del sistema (aparato-suelo)

D_s es la relación de amortiguamiento del sistema (que se obtiene a partir de la determinación del decremento logarítmico de las vibraciones)

D_a es la relación de amortiguamiento del aparato

ω_{ad} es la frecuencia circular natural amortiguada del aparato

ω_a es la frecuencia circular natural del aparato $[\omega_a^2 = \omega_{ad}^2 / (1-D_a^2)]$

k_a es la rigidez del aparato (tanto D_a , ω_{ad} y k_a se obtienen a partir de la calibración del aparato)

h es la altura de la probeta

$I_p = \pi d^4 / 32$, es el momento polar de inercia de la probeta

Cuando el instrumento se diseña de manera que el término

$(1-D_a^2) \left(\frac{\omega_{nd}}{\omega_{ad}}\right)^2$ sea despreciable, el valor de G se obtiene con la

siguiente expresión

$$G = \frac{\omega_{nd}^2}{1-D_s^2} \frac{k_a h}{\omega_a^2 I_p} \quad (3.7)$$

Para mayores detalles de este procedimiento, véase la Ref 16.

Prueba de columna resonante

Esta prueba consiste en someter a una probeta cilíndrica de suelo (similar a la señalada para pruebas de torsión cíclica) a vibraciones que bien pueden ser longitudinales, si lo que se desea medir es el módulo E, o torsionales (cortantes) si lo que se busca es el módulo G (fig 3.14). La frecuencia de excitación se hace variar hasta alcanzar una de las frecuencias de resonancia y poder así determinar la correspondiente velocidad de propagación de ondas. Por ejemplo, en el caso de que la probeta de suelo este fija en su base y libre en su parte superior, las frecuencias de resonancia están dadas por la siguiente expresión

$$f_n = (2n-1) \frac{v}{4H} \quad (3.8)$$

donde

n es un número entero (igual a 1 para la frecuencia fundamental)

H es la altura de la columna

v es la velocidad de onda

Teniendo la velocidad de propagación de las ondas, sean cortantes o longitudinales, el módulo correspondiente se obtiene a partir de la expresión

$$M = \rho v^2 \quad (3.9)$$

donde

M es el módulo (G o E, según sea el caso) y

ρ es la densidad de masa del suelo

Combinando entonces las dos expresiones anteriores se obtiene

$$M = \frac{16\rho H^2 f^2}{(2n-1)^2} \quad (3.10)$$

En esta prueba, donde el nivel de deformaciones con el que se trabaja es relativamente pequeño (del orden de $10^{-4}\%$), las principales ventajas son la simplicidad de su ejecución y la posibilidad de aplicarla en varios tipos de suelos. Es además una de las pruebas que más comúnmente se usan en los laboratorios de dinámica de suelos.

Mesas vibradoras

El empleo de las mesas vibradoras tiene como fin primordial el de estudiar y determinar las propiedades dinámicas de los suelos a través de especímenes más grandes, y por tanto más representativos de lo que se tiene en la realidad. Su uso se ha extendido considerablemente en los centros de investigación, y hoy en día existen varias que ofrecen una gran variedad de modalidades.

El procedimiento más común para determinar el módulo al cortante en esta clase de pruebas, consiste en excitar la base del espécimen a través de desplazamientos horizontales en la base (fig 3.15) y medir la respuesta de vibración libre cuando se suspende dicha excitación. El valor del módulo al cortante se obtiene entonces a través de las mismas expresiones señaladas en la prueba de la columna resonante, para el primer modo de vibración, o sea $G = 16\rho H^2 f^2$. (En la estimación de G , usando este procedimiento,

se está suponiendo que la frecuencia fundamental es aproximadamente igual a la frecuencia natural de vibración amortiguada).

La ejecución de esta prueba es sumamente laboriosa y resulta sumamente cara. Además se presentan varios problemas del tipo práctico, tales como la dificultad de preparación de la muestra, su saturación y lo difícil que resulta aplicar altas presiones de confinamiento.

Todo ello conduce a que esta prueba sea de uso exclusivo para trabajos de investigación.

Técnica pulsativa

La técnica pulsativa consiste en colocar unos cristales piezoeléctricos en cada extremo de una probeta de suelo, y aplicar un pulso eléctrico en los cristales de uno de los extremos. Cuando lo que se quiere medir es la velocidad de ondas al corte, la disposición de los cristales es en forma radial (fig 3.16).

Los cristales son manufacturados en forma tal que, cuando se aplica un pulso eléctrico, se produce una distorsión cortante; dicha distorsión origina una onda transversal que pasa a través de la probeta y es registrada por los cristales del otro extremo. La fig 3.17 muestra el tipo de registro que se obtiene en un osciloscopio, en el cual se puede determinar el tiempo que tarda la onda en llegar al otro extremo.

La velocidad se determina simplemente de dividir la longitud de la probeta entre el tiempo que tardó la onda en pasar de un

extremo al otro. Con dicha velocidad el módulo buscado se obtiene en la forma señalada por la ec. 3.9.

El nivel de deformaciones al cual corresponde el valor del módulo obtenido a través de esta prueba es, como ya se indicó antes, menor o igual a 10^{-6}

Pruebas de campo

Prácticamente existen tres pruebas de campo empleadas para determinar el módulo del suelo: a) pruebas geofísicas, b) empleo de un vibrador y c) pruebas de placa. Una descripción breve de cada una de ellas se hace a continuación.

Pruebas geofísicas

El procedimiento que se emplea para calcular el módulo del suelo consiste en determinar las velocidades de propagación de las ondas que son generadas en un cierto punto y registradas en otro. Dentro de las técnicas geofísicas las más empleadas para determinar el módulo dinámico son las que hacen uso de hoyos para registrar y/o generar las ondas cuya velocidad de propagación se trata de determinar a distintas profundidades. Dependiendo del tipo de ondas que se analice, se puede determinar el módulo E o G, a través de las siguientes expresiones

$$E = \rho v_c^2 \frac{(1+\mu)(1-2\mu)}{(1-\mu)} \quad (3.11)$$

$$G = \rho v_s^2 \quad (3.12)$$

donde

v_c es la velocidad de propagación de las ondas compresionales o dilatantes

v_s es la de las ondas cortantes

ρ es la densidad de masa del suelo, y

μ es la relación de Poisson

Sin embargo, cabe aquí recordar que las ondas compresionales, cuando se propagan por medios saturados, no resultan de utilidad en la determinación de las propiedades del esqueleto de suelo, ya que ellas viajan fundamentalmente a través del agua.

Las técnicas que más se emplean son las señaladas en la fig 3.18. El principio usado es el mismo en todas ellas, aunque existen desde luego ventajas de unas sobre otras, dependiendo de las características del suelo en sí y del equipo empleado. Dicho principio consiste en determinar las velocidades de las ondas que van de la fuente de energía a la fuente receptiva, mediante el uso de osciloscopios que registran el tiempo de salida y el de llegada de cada onda. El principal problema surge al tratar de distinguir las clases de ondas que corresponden a cada señal; esto se debe a que generalmente existen otras fuentes de energía (vibraciones de vehículos, ruidos, etc) y a que los distintos tipos de ondas que se generan, pueden seguir diferentes trayectorias en suelos muy estratificados. Todo esto hace que las señales de llegada sean muy complejas y difíciles de interpretar. Para eliminar este problema, se han ideado varios procedimientos especia

les, entre los que se encuentra el sugerido por Richart (Ref 7), el cual consiste en aplicar un impacto en el punto de excitación e invertir el sentido del mismo a fin de que las trazas generadas divergan en el momento de que las ondas cortantes llegan (fig 3.19).

La principal ventaja de las técnicas geofísicas, como es de hecho la mayoría de las pruebas de campo, es la de trabajar con un material *in situ*. Además, según ya se indicó, se puede determinar el valor del módulo dinámico a diferentes profundidades. Entre las desventajas se encuentra el hecho de que las técnicas geofísicas generalmente emplean, como fuente de energía, un solo impulso, lo cual hace que el patrón de ondas generado sea difícil de duplicar. Para eliminar esta desventaja se ha desarrollado un vibroempacador que puede usarse con la técnica de hoyos paralelos y con el cual se inducen continuamente ondas polarizadas de compresión o de cortante (Ref 1).

Empleo de un vibrador superficial

Esta técnica estriba en medir la longitud de onda superficial que genera un vibrador, trabajando a una determinada frecuencia, en la superficie del terreno. Como se muestra en la fig 3.20, la longitud de onda se determina moviendo un receptor a lo largo de una línea radial al eje del vibrador y localizando los puntos que están en fase. El valor de la velocidad de ondas cortantes se obtiene mediante la expresión

$$v_s = f\lambda$$

donde

f es la frecuencia de excitación en ciclos/seg
 λ es la longitud de onda

Por tanto, el valor de G se obtiene mediante la expresión $G = \rho v_s^2$, ya señalada anteriormente. Una regla semiempírica es suponer que el módulo calculado mediante este procedimiento, corresponde al valor que dicho módulo tiene a una profundidad igual a un medio de la longitud de onda ($\lambda/2$). Por lo tanto, al cambiar la frecuencia de excitación, se puede variar la longitud de onda, y con ello la profundidad de inspección.

Debe aclararse que mediante este procedimiento se está suponiendo que la velocidad de las ondas Rayleigh, que viajan a través de la superficie, son iguales a las ondas cortantes; dicha suposición es válida en la mayoría de los problemas prácticos (Ref 15). Cuando se tiene un medio estratificado, existen teorías que permiten, a través de las matemáticas, determinar los módulos de cada capa (Ref 3); sin embargo, faltan datos experimentales para conocer la validez de dichas teorías y su aplicación desde el punto de vista práctico.

El más serio inconveniente de esta técnica es el de disponer de un vibrador que puede trabajar a bajas frecuencias de operación, de manera que la profundidad de inspección no se limite a valores pequeños. En general la prueba resulta cara y se requiere experiencia y antecedentes teóricos bien fundamentados para hacer una interpretación correcta de los datos.

Pruebas de placa

Estas pruebas consisten en aplicar cargas repetidas sobre una placa de un pie de diámetro (o de lado si es cuadrada), la cual se encuentra apoyada sobre la superficie del terreno o a una cierta profundidad (fig 3.21). Determinando la pendiente de la curva desplazamiento carga (fig 3.22), se obtiene la rigidez k del suelo que se relaciona con el módulo G , mediante la siguiente expresión

$$k = \frac{4 G R}{1 - \mu}$$

donde

R es el radio de la placa

μ es la relación de Poisson

Para extrapolar las rigideces obtenidas usando las placas de pequeñas áreas, a las reales del prototipo, se pueden utilizar las recomendaciones dadas por Terzaghi (Ref 13) para cargas estáticas; o sea

$$\text{suelo cohesivo; } k_{\text{prototipo}} = k_1 \text{ diam }^C$$

$$\text{suelo no cohesivo; } k_{\text{prototipo}} = k_1 \text{ diam } \left(\frac{C+1}{2} \right)^2$$

donde

C es la relación de la dimensión menor de la cimentación real a la dimensión menor de la placa

Existe también una prueba de placa consistente en colocar un pequeño vibrador sobre una placa de 12 a 30 pulgadas de diámetro, y variar la frecuencia de excitación del vibrador hasta alcanzar

la condición de resonancia (fig 3.23) En este caso el valor de la rigidez k del suelo se obtiene mediante la siguiente expresión

$$k = (f_r \cdot 2\pi)^2 M$$

donde

M es la masa del vibrador junto con la de la placa, y

f_r es la frecuencia de resonancia en ciclos/seg

La desventaja más importante que se presenta en el empleo de pruebas de placa (sea usando cargas repetidas o el pequeño vibrador), es la correcta interpretación de los resultados y la multitud de variantes que en ella entran. Por otro lado el procedimiento se limita a determinar valores superficiales del módulo del suelo.

Estos inconvenientes han hecho que las pruebas de placa sean poco usadas en la solución práctica de problemas de dinámica de suelos.

c) Fórmulas semiempíricas

Existen fórmulas semiempíricas que dan el valor máximo de G , es decir, el valor de G correspondiente a niveles de deformación bajos. (Ya se había mencionado que se considera como nivel de deformación bajo el que es menor o igual a 10^{-5}). La fórmula más conocida y empleada es la de Hardin y Drnevich (Ref 5), que proporciona muy buenos resultados para valores pequeños de la relación de vacíos ($e \leq 2.0$), y es además válida tanto para suelos cohesivos como no cohesivos; dicha fórmula queda representada por la siguiente expresión

$$G = 1200 \frac{(3-e)^2}{1+e} (\text{OCR})^a (\bar{\sigma}_o)^{1/2}$$

donde:

$\bar{\sigma}_0$ y G deben estar en lb/pulg²

$$\bar{\sigma}_0 = \frac{\bar{\sigma}_1 + \bar{\sigma}_2 + \bar{\sigma}_3}{3}$$

(σ_1 , σ_2 y σ_3 son, respectivamente, los esfuerzos efectivos normales mayor, intermedio y menor)

OCR es la relación de preconsolidación, y

"a" depende del índice de plasticidad (fig 3.24)

Para el caso de arenas, Seed y Idriss (Ref 12) emplean la expresión

$$G = 1000 k_2 (\bar{\sigma}_0)^{1/2}$$

donde

k_2 depende de la densidad relativa (o de la relación de vacíos), en la forma señalada por la fig (3.25)

Puesto que G es función de los esfuerzos efectivos que se tienen en el sitio, y la resistencia no drenada de los suelos normalmente consolidados (S_u) también lo es, se puede normalizar G con respecto a S_u y expresar G/S_u versus γ . La fig 3.26, a través de la curva llena, se puede usar para fines estimativos de G . Whitman (Ref 15) recomienda emplear

$$G = 1600 S_u$$

para valores de deformación angular entre 10^{-5} y 10^{-6} .

En estas fórmulas se indica muy claramente que el módulo es principalmente función de la relación de vacíos del suelo y de los esfuerzos efectivos que se tienen *in situ*. Existen algunos otros factores de los cuales depende G , como es desde luego el nivel de deformaciones y algunos otros que Richart (Ref 7) señala.

Por ejemplo, está el efecto de la *duración de la carga (time effect)* que se refiere al aumento de v_s en la probeta de la columna resonante, a medida que tiene una mayor duración la aplicación de los esfuerzos de confinamiento.

Otro efecto es el de la *historia de esfuerzos* que se refiere al cambio de los esfuerzos en el suelo y el cual es diferente en el caso de las arenas en comparación con los suelos arcillosos; dicho efecto es solo importante después de ciertos niveles de deformación (10^{-4} en el caso de arenas y 10^{-5} en el caso de arcillas); si lo que se tiene son arenas, el efecto de la historia de esfuerzos origina un aumento en v_s (por el cambio de e), pero si son arcillas se produce una disminución del módulo G y un aumento en el amortiguamiento. (Cabe señalar que cuando un sismo origina grandes cambios de esfuerzo aparejados con grandes deformaciones, el valor de G disminuye en ese momento, pero si se deja en reposo a ese suelo, el valor de G vuelve a su valor original después de cierto tiempo; este hecho ha sido comprobado experimentalmente). Está también el llamado efecto de la *temperatura* el cual es de relativa poca importancia; experimentalmente se ha observado que la velocidad de onda es ligeramente mayor a menores temperaturas. Todos estos últimos efectos aquí seña-

lados deben observarse cuando se hacen pruebas de laboratorio y estudios de investigación.

Un ejemplo de perfil de suelos correspondiente a un depósito profundo de arena, donde se determinaron los valores de la velocidad de onda a diferentes profundidades, se muestra en la fig 3.27. En ella se pueden ver las velocidades determinadas en el laboratorio mediante pruebas de columna resonante, las determinadas en el campo a través de técnicas geofísicas y las calculadas con la fórmula de Hardin y Drnevich para niveles pequeños de deformación. Los resultados no coinciden totalmente, pero desde el punto de vista práctico, se puede decir que las correlaciones son aceptables. En esta figura se puede observar que la tendencia del módulo es aumentar con la profundidad, lo cual es lógico si se considera que los esfuerzos efectivos *in situ* crecen con la profundidad.

La fig 3.28 muestra dos comparaciones entre el módulo medido *in situ* con pruebas geofísicas y el módulo medido en el laboratorio con la técnica de la columna resonante. La fig (3.28a) se refiere a un limo arcilloso y la (3.28b) a una arena; en ambos casos se observan buenas correlaciones.

b) AMORTIGUAMIENTO

El otro parámetro que gobierna el modelo viscoelástico lineal es el que se refiere a la pérdida de energía causada primordialmente por el efecto de histéresis, es decir, el amortiguamiento.

Una de las formas más comunes de expresar esta pérdida de energía es mediante la llamada capacidad de amortiguamiento, ψ , definida mediante

$$\psi = \frac{\text{Energía perdida en cada ciclo de carga}}{\text{Máxima energía de deformación producida en el ciclo de carga}}$$

Haciendo referencia a la fig 3.29, el valor de ψ sería

$$\psi = \frac{\Delta W}{W}$$

donde

ΔW es el área del triángulo azulado, y

W es el área dentro del lazo histerético

Otra forma de indicar el amortiguamiento es mediante la llamada "relación de amortiguamiento", D , definida como sigue

$$D = \frac{\text{Coeficiente de amortiguamiento viscoso actual}}{\text{Coeficiente crítico}}$$

El coeficiente crítico es el que se requiere para suprimir las vibraciones libres, y de acuerdo con los principios de dinámica (Ref 2), dicho coeficiente crítico vale

$$C_{\text{crit}} = 2 \sqrt{kM}$$

donde

k es la rigidez, y

M la masa del modelo equivalente

Esta relación de amortiguamiento es quizá la manera más común de expresar la pérdida o disipación de energía que ocurre en los sistemas reales.

Existe otra forma más de expresar el amortiguamiento y ella es mediante el decremento logarítmico definido como

$$\Delta = \ln \frac{Z_i}{Z_{i+1}}$$

donde

Z_i es la amplitud i ésima, y

Z_{i+1} es la amplitud $i+1$ de la vibración

En la práctica, la determinación de Δ se hace con ayuda de un osciloscopio donde se registra el decaimiento de las vibraciones libres. La fig 3.30a muestra una fotografía de un registro típico; el dibujo de una línea recta como la mostrada por la fig 3.30b, puede auxiliar a determinar fácilmente el valor de Δ .

En dinámica básica se demuestra que estas tres cantidades están relacionadas entre sí por la siguiente expresión.

$$\Delta = 2\pi D = \frac{\psi}{2}$$

Se verá ahora la forma de determinar físicamente el valor del amortiguamiento.

Pruebas de campo

Teóricamente existen tres maneras de determinar el amortiguamiento a través de pruebas de campo.

- 1) Mediante la observación de la disminución de las amplitudes de vibración que ocurren durante un temblor

- 2) A través de la observación de la disminución de la amplitud de vibraciones producidas por explosiones
- 3) Mediante el uso de generadores u otras fuentes de energía que producen microtemblores en el suelo; en este caso se hace variar la frecuencia de excitación y se mide las amplitudes de vibración, hasta obtener la frecuencia de resonancia; el valor del amortiguamiento se obtiene mediante la siguiente expresión

$$D = \frac{\Delta f}{2f_m}$$

donde

$$\Delta f = f_2 - f_1 \quad (f_1 \text{ y } f_2 \text{ están definidos en la fig 3.31)}$$

f_m es la frecuencia de resonancia

Hasta ahora, la experiencia que se tiene en la determinación del amortiguamiento mediante pruebas de campo es muy poca, y puede afirmarse que solo a través de pruebas de laboratorio es como se ha podido determinar el amortiguamiento para fines prácticos. Las mayores dificultades que se presentan, al querer determinar el amortiguamiento a través de pruebas de campo, son

- a) resultan muy caras
- b) el amortiguamiento interno es por lo general muy pequeño y es muy difícil de medirse *in situ* porque se ve opacado por el amortiguamiento radial; éste último, como se verá en el Cap IV, se debe a la disipación de energía a través de ondas que viajan alejándose de la fuente de excitación.

Pruebas de laboratorio

El amortiguamiento de un suelo se puede obtener a partir de la ejecución de la mayoría de las pruebas de laboratorio señaladas. En efecto, para el caso de pruebas donde se aplican cargas cíclicas (triaxiales, cortante simple o por torsión), el amortiguamiento se puede obtener a partir de la determinación del área dentro del lazo histerético; en el caso de vibraciones libres (columna resonante, cortante simple o por torsión y mesas vibratoras), el amortiguamiento se obtiene observando la disminución de la amplitud en las vibraciones y calculando el llamado decremento logarítmico.

Los resultados del amortiguamiento obtenidos mediante las diversas pruebas, son más o menos consistentes para un mismo nivel de deformaciones (Ref 14).

c) DETERMINACION DE G Y D A NIVELES DE DEFORMACION DIFERENTES A LOS OBTENIDOS EXPERIMENTALMENTE O ESTIMADOS A NIVELES BAJOS DE DEFORMACION

Ya se mencionó en un principio que el suelo, cuando es sujeto a fuerzas dinámicas que originan niveles de deformación muy pequeños (menor de 10^{-5}), se comporta prácticamente como un material elástico lineal; es decir, a esos niveles de deformación, tanto el módulo como el amortiguamiento se pueden considerar constantes. Sin embargo, a medida que se incrementa el nivel de deformación, el amortiguamiento aumenta mientras que el módulo disminuye. En este último caso lo que se hace en la práctica es hablar de un módulo lineal y de un amortiguamiento equivalente;

el módulo equivalente se define, según se mencionó anteriormente, como la pendiente de la línea que conecta los valores extremos del lazo de histéresis, y el amortiguamiento equivalente se relaciona directamente al área dentro de ese lazo histerético.

En estas circunstancias, si se desea referirse a un módulo G a niveles altos de deformación, se podrá hacerlo en términos del módulo determinado a pequeñas deformaciones, simplemente afectando este último por un factor de reducción. Análogamente se puede hacer lo mismo con el amortiguamiento, sólo que al factor por aplicar será de amplificación en vez de reducción.

La fig 3.32 presenta una banda donde caen los factores de reducción de la mayoría de los suelos, basados precisamente en la definición de módulo equivalente y a partir de resultados obtenidos en pruebas de laboratorio (principalmente de columna resonante). Varios resultados experimentales de campo han demostrado la buena validez de esta gráfica, Whitman (Ref 15) recomienda utilizar una curva promedio de esta banda, para aplicarla en trabajos prácticos que involucren cualquier suelo.

Para el caso del amortiguamiento, la fig 3.33 nos muestra una curva análoga a la (3.32); dicha figura fue dibujada a partir de una gran variedad de información. A pesar de tener una gran dispersidad de valores, puede observarse que en general el amortiguamiento crece a medida que el nivel de las deformaciones aumenta. En este caso la curva que se recomienda es la inferior, a fin de estar del lado de la seguridad.

Conviene recordar que para emplear estos conceptos de módulo y amortiguamiento equivalente, es necesario aplicar el proceso iterativo señalado al principio de este capítulo.

En el caso de ingeniería sísmica, donde se tienen cargas transitorias que involucran varios ciclos y cada uno induce un nivel de deformación diferente, resulta complicada la definición de un módulo y un amortiguamiento equivalente. Una manera de manejar este caso consiste en determinar el valor máximo de las deformaciones y tomar el valor correspondiente a 2/3 del máximo como valor promedio o representativo de las deformaciones.

La determinación del amortiguamiento D y el módulo al cortante G a distintos niveles de deformación γ , se pueden obtener a través de la fórmula de Hardin y Drnevich mediante las siguientes expresiones.

$$G = \frac{G_{\max}}{1 + \gamma/\gamma_r}$$

donde
$$\gamma_r = \frac{\tau_{\max}}{G_{\max}}$$

$$\tau_{\max} = \left\{ \frac{1+k_0}{2} \bar{\sigma}_v \sin \bar{\phi} + \bar{C} \cos \bar{\phi} \right\}^2 - \left(\frac{1-k_0}{2} \bar{\sigma}_v \right)^2 \right\}^{1/2}$$

k_0 = coeficiente de los esfuerzos horizontales $\left(\frac{\sigma_h}{\sigma_v}\right)$

$\bar{\sigma}_v$ = esfuerzos efectivos verticales

y \bar{C} y $\bar{\phi}$ son los parámetros de resistencia estáticos en términos de los esfuerzos efectivos

Para el amortiguamiento la expresión resultante es la siguiente

$$D = \frac{D_{\max} \frac{\gamma}{\gamma_r}}{1 + \gamma/\gamma_r}$$

donde D_{\max} es el amortiguamiento máximo correspondiente a deformaciones muy grandes. Para el caso de arenas limpias

$D_{\max} = 30 - 1.5 \log N$ (N = número de ciclos) y para suelos cohesivos saturados $D_{\max} = 31 - (3 + 0.03f) (\bar{\sigma}_o)^{1/2} + 1.5f^{1/2} - 1.5 \log N$; en esta última expresión f es la frecuencia con que se aplica la carga cíclica (dada en revoluciones/segundo).

d) RELACION DE POISSON

La relación de Poisson μ , para la mayoría de los suelos, varía por lo general en un rango relativamente estrecho. En el caso de suelos secos o con bajo grado de saturación el valor de μ alrededor de 0.35; para suelos saturados μ anda cerca de 0.5. Un valor promedio de la relación de Poisson, en la mayoría de los suelos se puede considerar que se encuentra entre 0.4 a 0.5.

Cuando se quiere estimar en forma más precisa esta relación, teóricamente puede hacerse mediante la determinación de dos de las velocidades de propagación de ondas. Sin embargo, los pequeños errores que puede haber en la estimación de μ , no afecta de manera significativa los resultados que se obtienen en problemas prácticos de dinámica de suelos y basta hacer la estimación en forma aproximada.

V) Conclusiones

Las principales conclusiones que se pueden extraer de lo señalado en este capítulo son:

- 1) El comportamiento del suelo cuando se le sujeta a cargas dinámicas es muy complejo, caracterizándose particularmente por la no linealidad a deformaciones grandes como las que ocurren en temblores fuertes.
- 2) La presión que se crea en el agua localizada dentro de los poros de un suelo, como consecuencia de las cargas rápidas que se aplican durante sismos o fuerzas de maquinaria, desempeña un papel importante en el comportamiento dinámico de dicho suelo.
- 3) Para fines prácticos, se puede utilizar el modelo matemático viscoelástico para analizar el comportamiento del suelo en la mayoría de los problemas de dinámica de suelos.
- 4) La determinación del módulo dinámico cortante G , a niveles pequeños de deformación (menos o iguales a 10^{-5}), se puede determinar satisfactoriamente tanto en el campo (por ejemplo, a través de pruebas geofísicas) como en el laboratorio (mediante la prueba de la columna resonante). Sin embargo, se puede estimar el módulo equivalente a niveles grandes de deformación mediante procedimientos confiables.
- 5) El amortiguamiento interno del suelo sólo se puede determinar prácticamente mediante pruebas de laboratorio. Cuando se

desea determinar el amortiguamiento a distintos niveles de de formación a partir de los datos obtenidos en pruebas de laboratorio, ésto se puede realizar satisfactoriamente utilizando curvas empíricas.

- 6) Las pruebas de laboratorio que más se utilizan para la determinación de las propiedades dinámicas de los suelos son la triaxial cíclica y la de la columna resonante. Sin embargo, la prueba torsional cíclica con vibraciones libres es quizá la que presenta más ventajas (simplicidad, niveles de deformación iguales a los que se tienen durante sismos, etc), por lo que es muy factible que en un futuro próximo sea la más empleada.

REFERENCIAS DEL CAPITULO IV

1. Ballard, R.F., Jr, and Leach, R.E. (1969) "Development of Vibropacker System for Inducing Polarized Shear Waves and Compression Waves at Depths", Misc Paper S-69-30, U.S. Army Eng Waterway Experiment Station, Vicksburg, Miss, Julio.
2. Biggs, J.M. (1964) "Introduction to Structural Dynamics", McGraw-Hill Book Company.
3. Blain, J. (1968) "Resultats obtenus au Laboratoire Central en 1965 et 1966", Bulletin des Laboratoires Roatiers.
4. Faccioli, E. and Resendiz D. (1975) "Soil Dynamics Behavior Including Liquefaction", E15, Instituto de Ingenieria, UNAM Mayo.
5. Hardin, B.O., and Drnevich, V.P. (1970b) "Shear Modulus and Damping in Soils; 2, Design Equations and Curves", Tech Report 27-70-CE 3, Soil Mechs Series No. 2, Univ of Ky, College of Eng, July.
6. Kovacs, W.D. (1968) "An Experimental Study of the Response of Clay Embankments to Base Excitation", Ph.D. Thesis, Univ of Calif, Berkeley.
7. Richart, F.E., Jr. (1975) "Some Effects of Dynamic Soil Properties on Soil-Structure Interaction", Journal of the Geotechnical Engineering Division, ASCE, Vol 101, No. GT12, Proc Paper 11764, December, pp 1193-1240.
8. Richart, F.E., Jr, Hall, J.R., Jr, and Woods, R.D. (1970) "Vibrations of Soils and Foundations", Prentice-Hall, Inc, Englewood Cliffs, N.J.
9. Seed, H.B., and Chan, C.K. (1966) "Clay Strength under Earthquake Loading Conditions", Journal of the Soil Mech and Found Div, ASCE, Vol 92, No. SM2, Mar, pp 53-78.
10. Seed, H.B., and Idriss, I.M. (1967) "Analysis of Soil Liquefaction: Niigata Earthquake", Jour of the Soil Mech and Found Div, ASCE, Vol 93, No. SM3, Mayo, pp 83-108.
11. Seed, H.B., and Idriss, I.M. (1969) "Influence of Soil Conditions on Ground Motions During Earthquakes", Jour of the Soil Mech and Found Div, ASCE, Vol 95, No. SM1, Enero, pp 99-137.
12. Seed, H.B., and Idriss, I.M. (1970c) "Soil Moduli and Damping Factors for Dynamic Response Analysis", Report No. EERC 70-10, December, Univ of California, Berkeley.

13. Terzaghi, K. (1955) "Evaluation of Coefficients of Subgrade Reaction", Geotechnique, pp 297-326.
14. U.S. Atomic Energy Commission (1972) "Soil Behavior Under Earthquake Loading Conditions", State of the Art Evaluation of Soil Characteristics for Seismic Response Analysis, Chapter 4, Enero.
15. Whitman, R.V. (1973) "Soil Dynamics Notes", Massachusetts Institute of Technology, Civil Engineering Department.
16. Zeevaert, L. (1973) "Foundation Engineering for Difficult Subsoil Conditions", Van Nostrand Reinhold, pp 531-541.

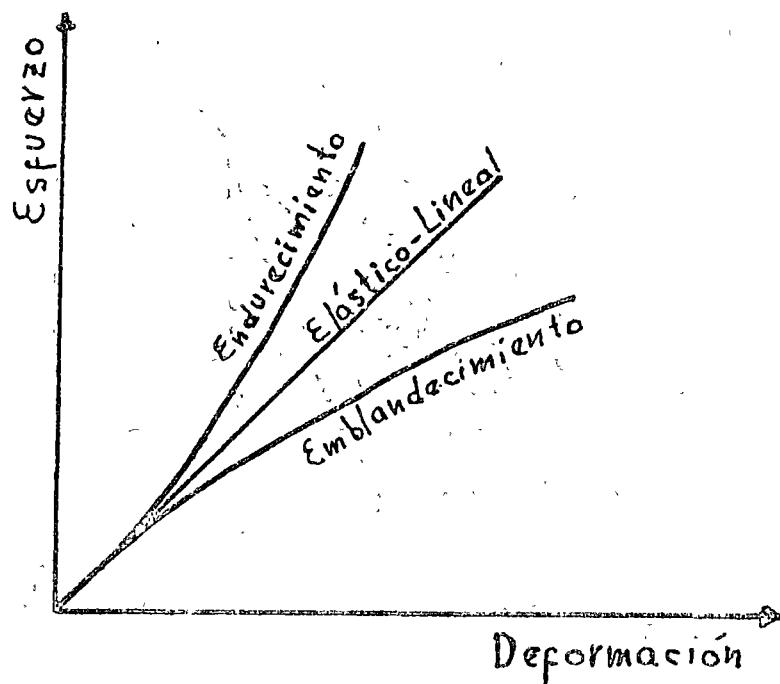


Fig 3.1 Tipos de Curvas Esfuerzo-Deformación
(Ref # 7)

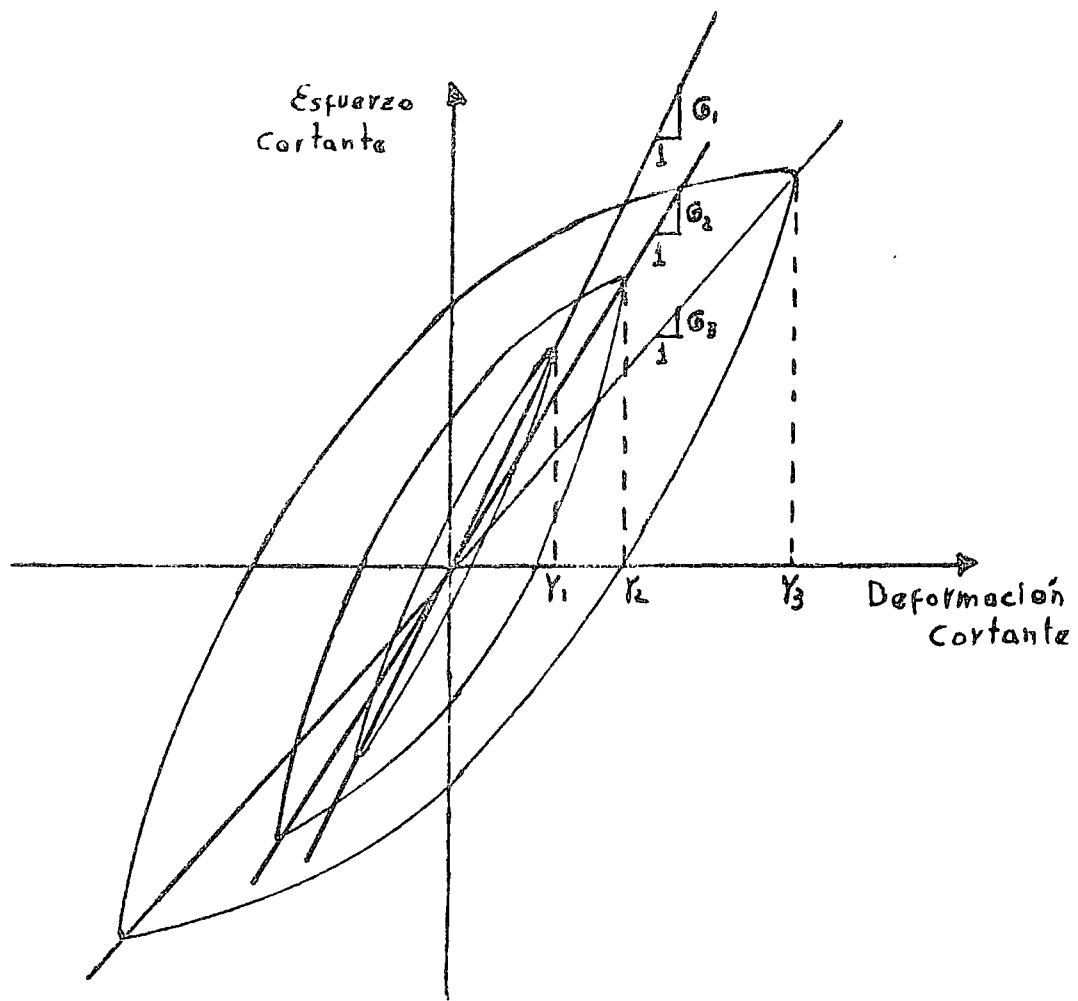


Fig 3.2 Curvas Histeréticas Esfuerzo-Deformación en Pruebas Torsionantes Cíclicas

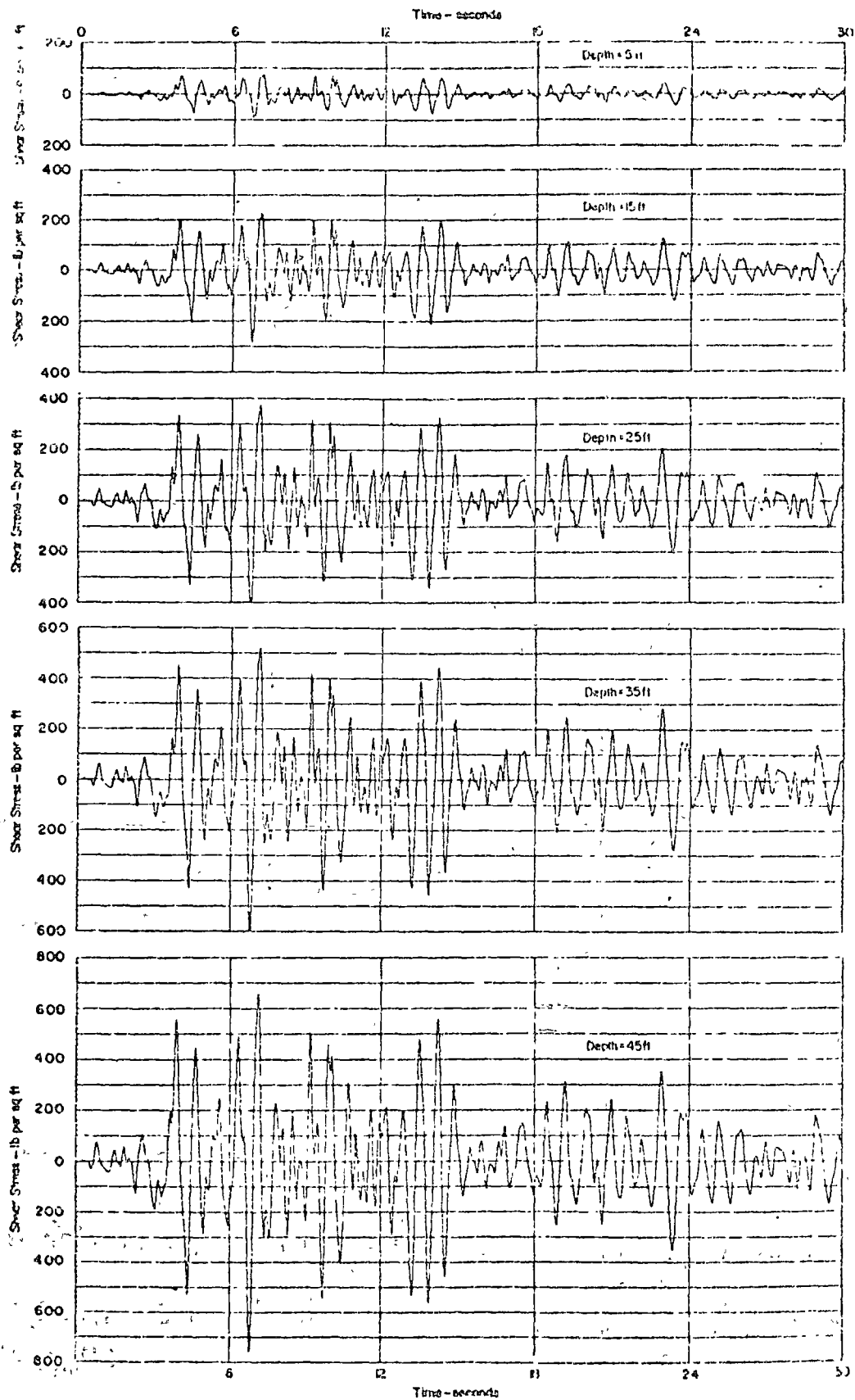
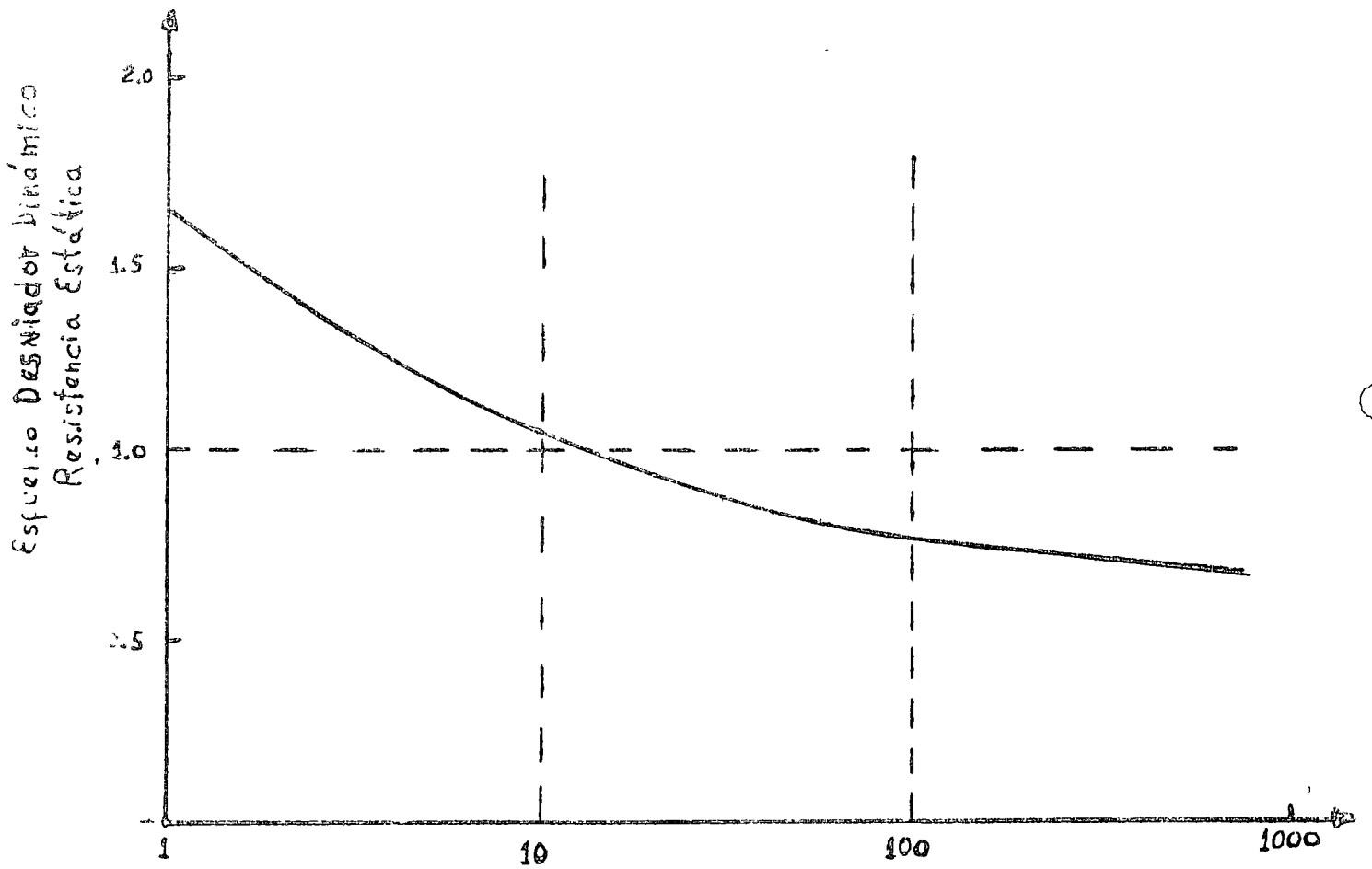


Fig. 3.3 SHEAR STRESS VARIATION DETERMINED BY RESPONSE ANALYSIS FOR THE NIIGATA EARTHQUAKE

(Ref #10)



No. de Ciclos Requeridos para Alcanzar una Deformación del 20%

Fig 3.4 Efecto de Fatiga en una Arcilla Limosa Inalterada
(Ref. # 9)

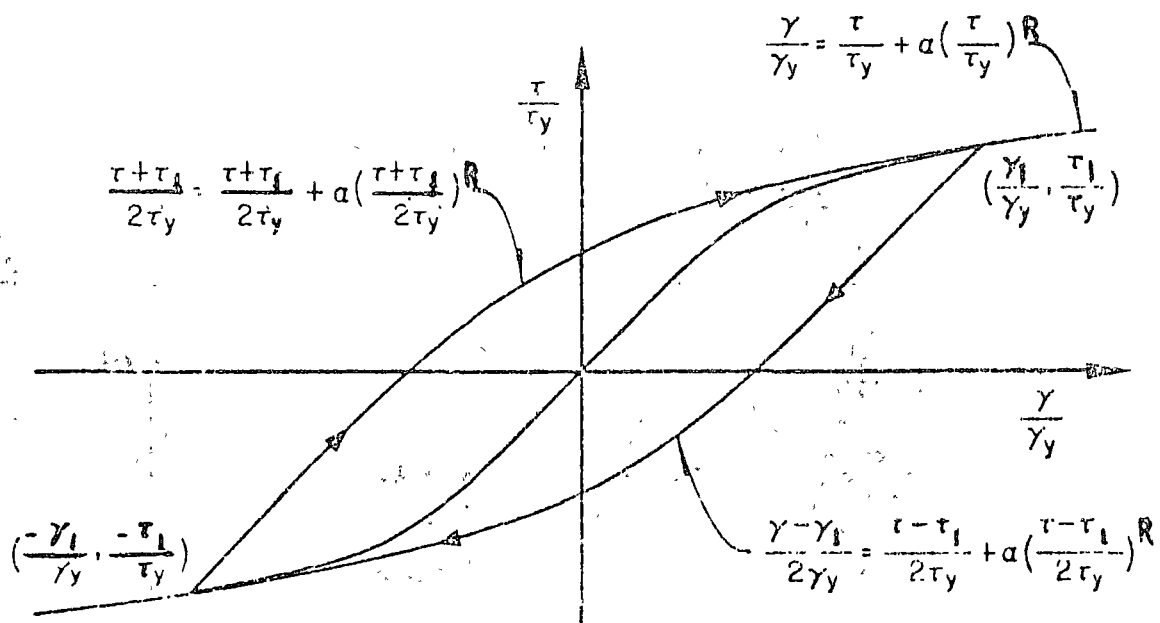
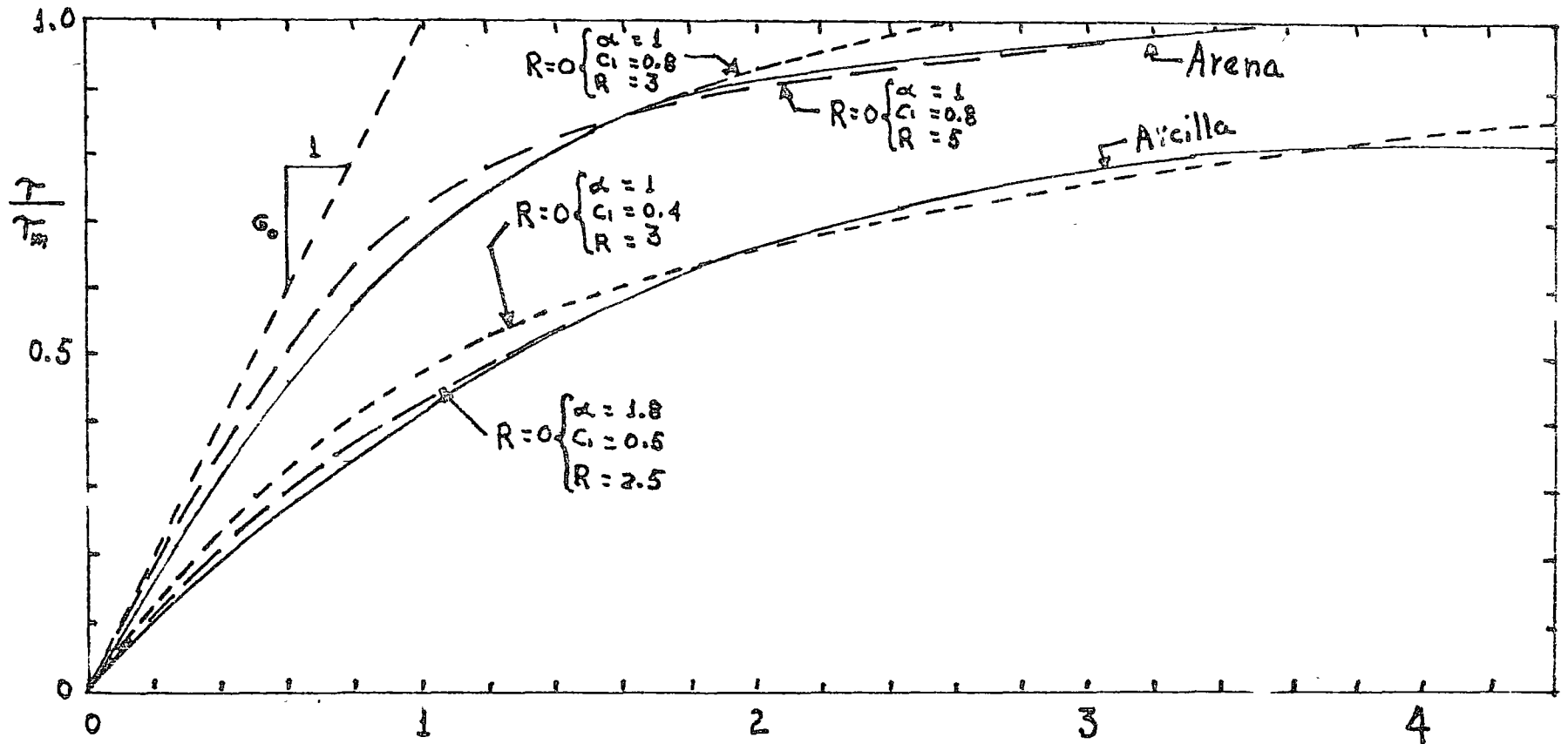
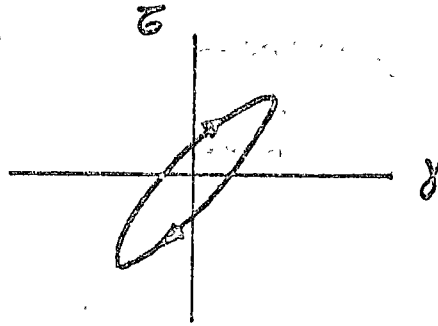
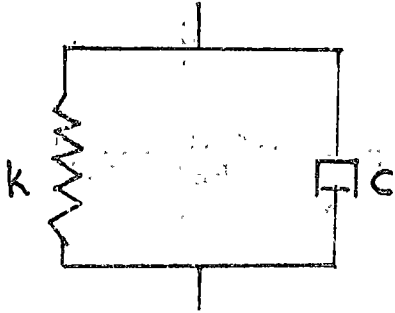


Fig 3.5 Modelo Constitutivo de Ramberg Osgood
(Ref. # 4)

Fig 3.6 Ajustamiento de las Curvas de Ramberg Osgood con las Curvas Experimentales
(Ref. #7)



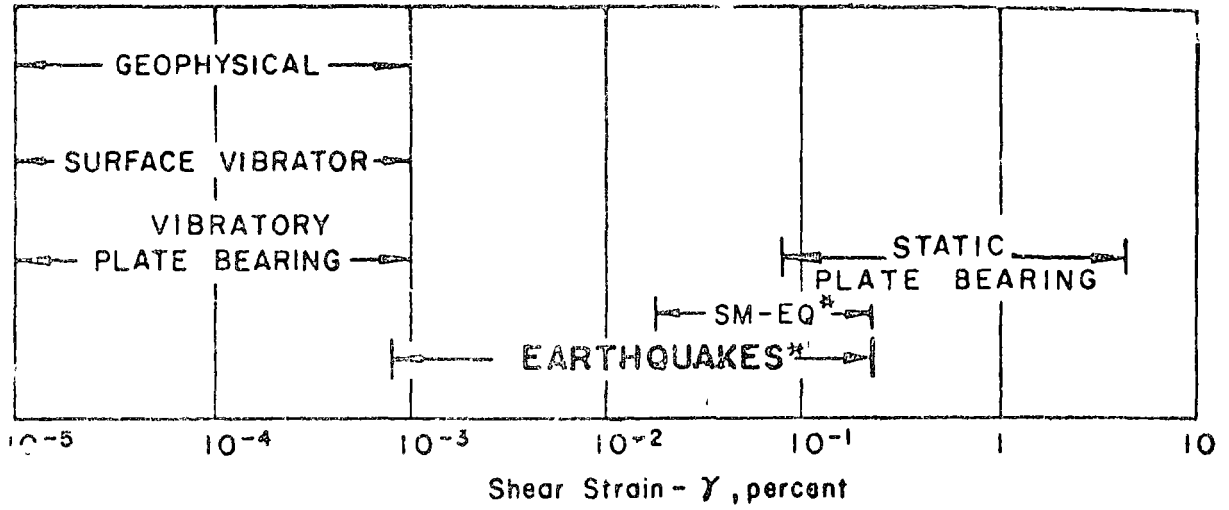
$$\frac{Y}{Y_r} \quad \text{ó} \quad \frac{Y G_0}{T_m}$$



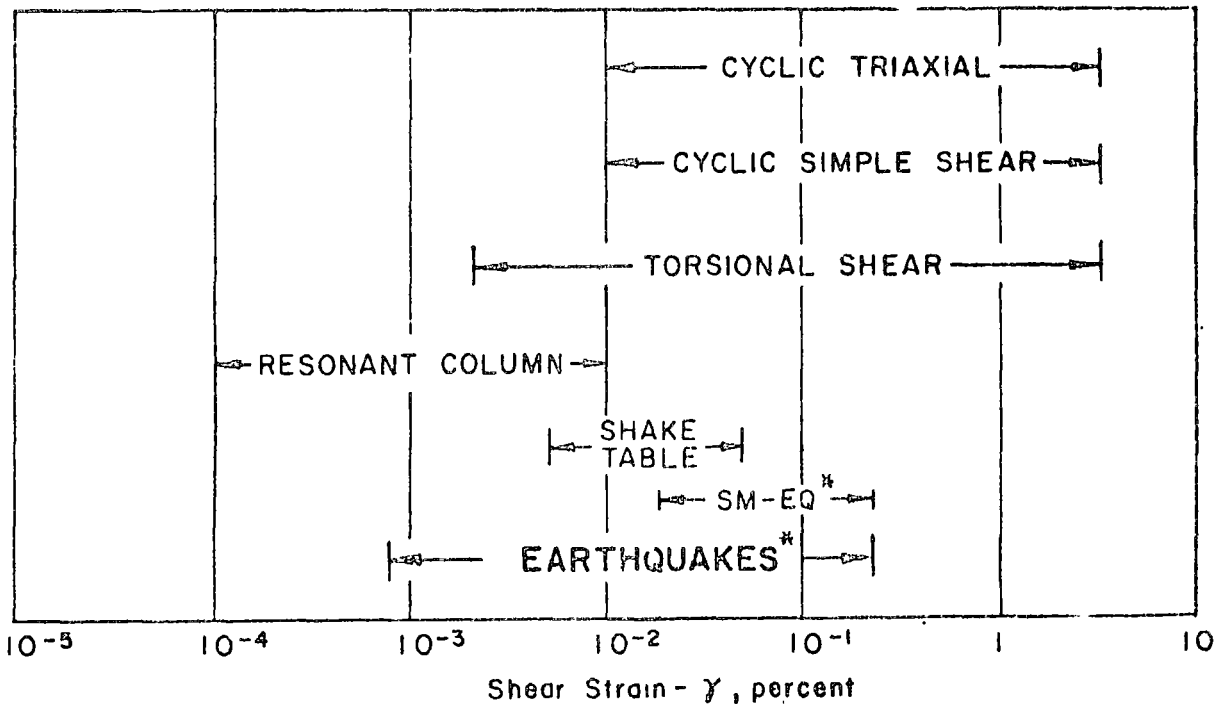
a) Representación del Modelo

b) Curva típica Real de Esfuerzo - Deformación

Fig 3.7 Modelo Viscoelástico Lineal



a. FIELD TESTS



b. LABORATORY TESTS

* Note: Range of shear strain denoted as "Earthquakes" represents an extreme range for most earthquakes. "SM-EQ" denotes strains induced by strong motion earthquakes.

Fig. 3.8 FIELD AND LABORATORY TESTS SHOWING APPROXIMATE STRAIN RANGES OF TEST PROCEDURES

(Ref # 14)

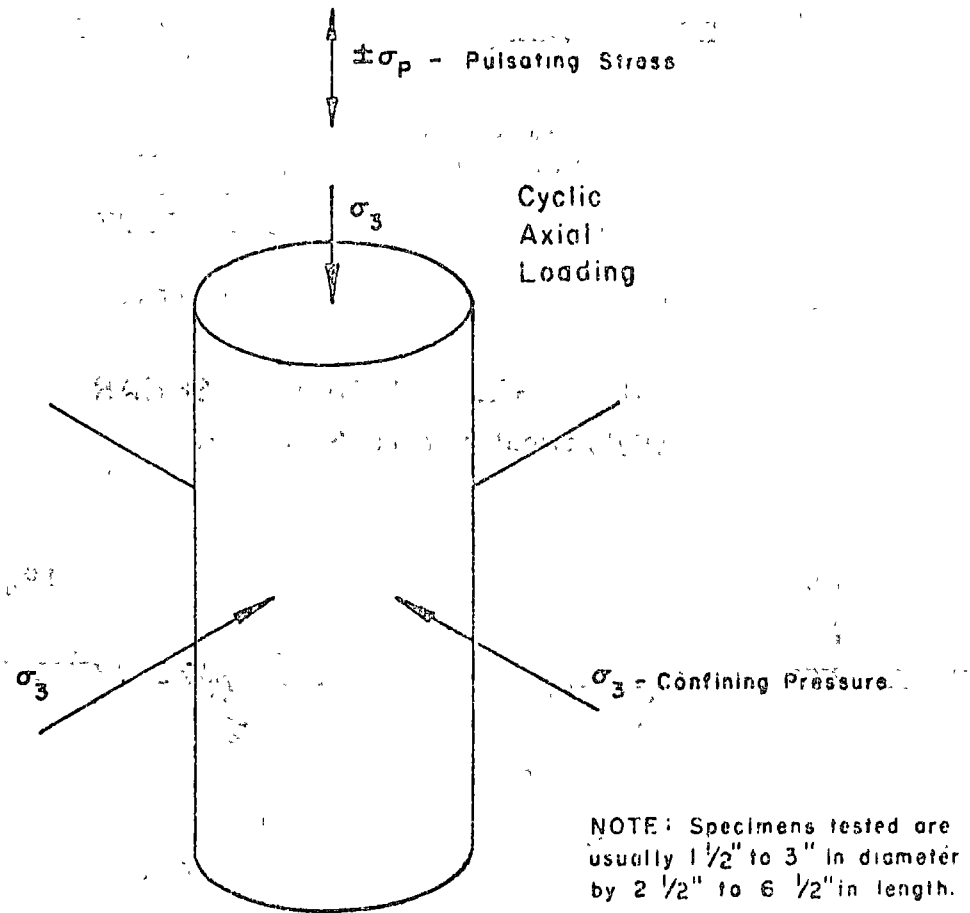
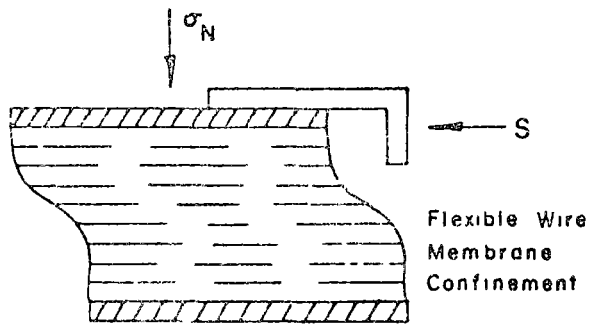


Fig. 3.9 CYCLIC TRIAXIAL TEST

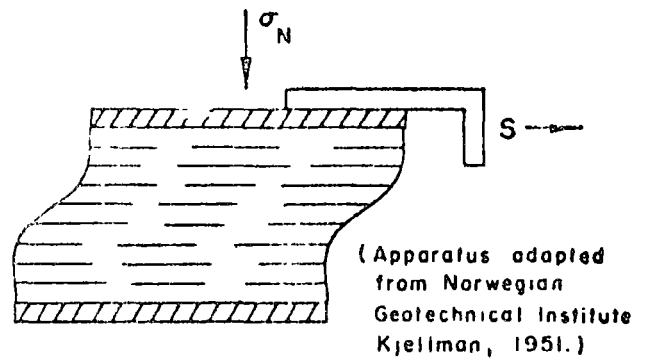
(Cyclic Axial Loading)

(Ref #14)

SPECIMENS APPROX.
3" diam. X 0.4" high

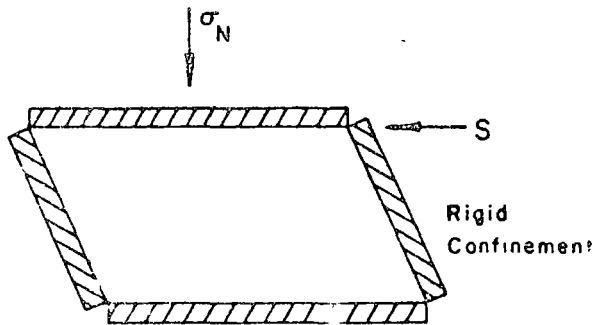


LOADING A

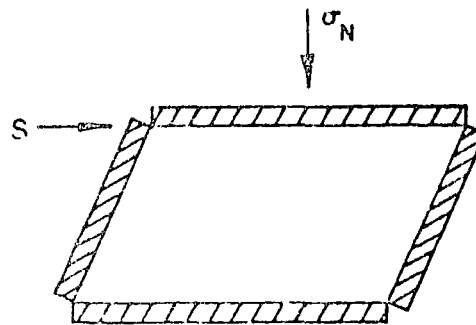


LOADING B

a. UNIFORM STRESS IN SIMPLE SHEAR
(Cylindrical Shaped Specimen)



LOADING A



LOADING B

(Apparatus adapted from the original design by Roscoe, 1953.)

b. UNIFORM STRAIN IN SIMPLE SHEAR
(Rectangular Shaped Specimen)

Fig. 3.10 CYCLIC SIMPLE SHEAR TESTS

(Cyclic Shear Loading)

(Ref #14)

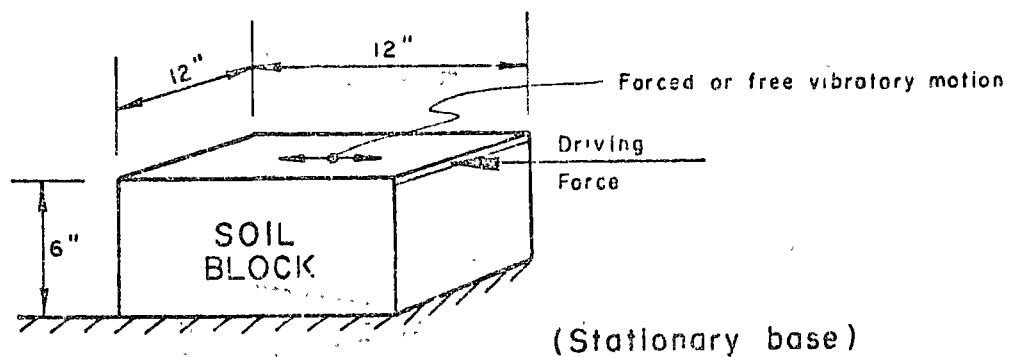


Fig. 3.11 LARGE SCALE SIMPLE SHEAR TEST
(Ref #6)

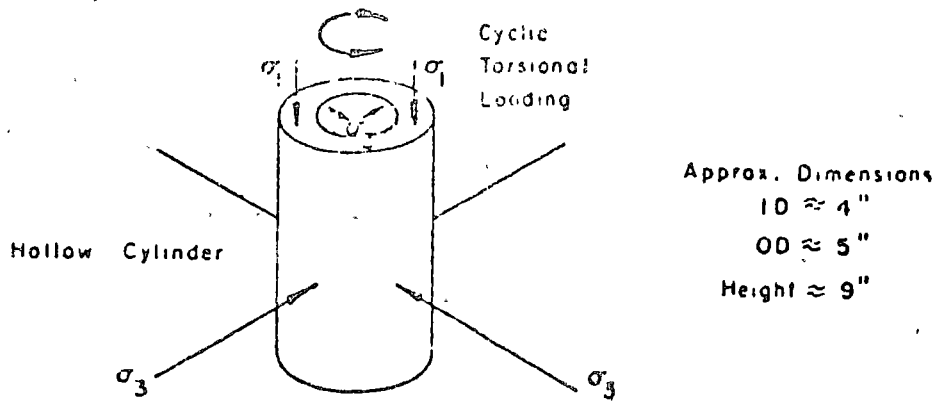


Fig 3.12 TORSIONAL COLUMN LOADING TEST
 (Torsional Cyclic Loading at Low Frequencies)

(Ref # 14)

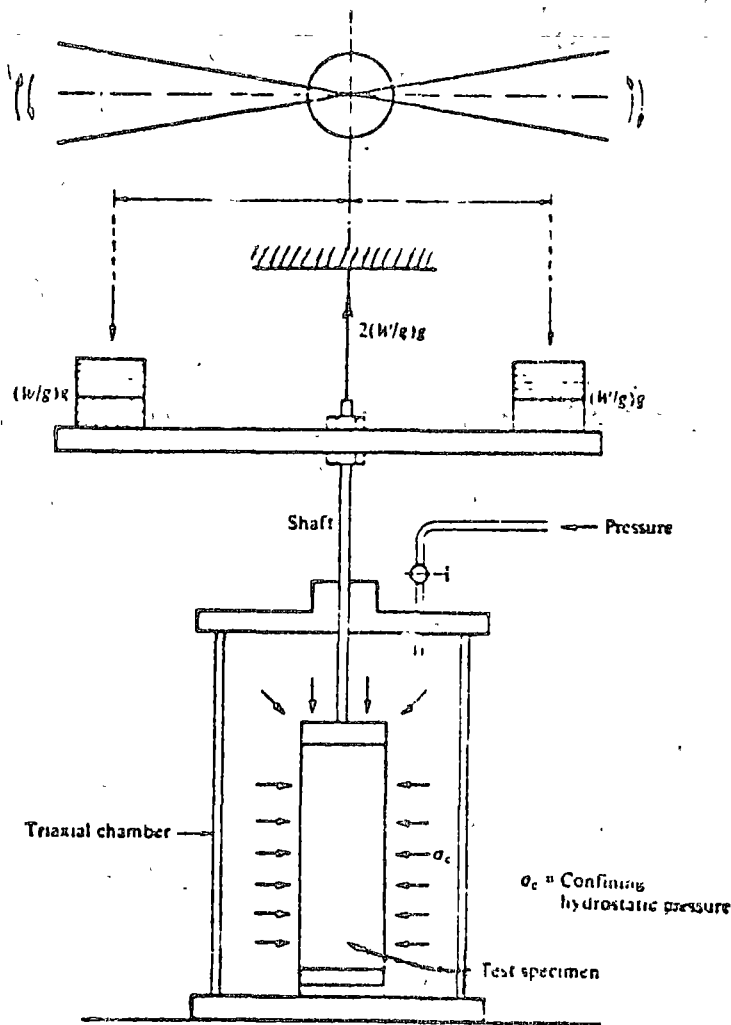
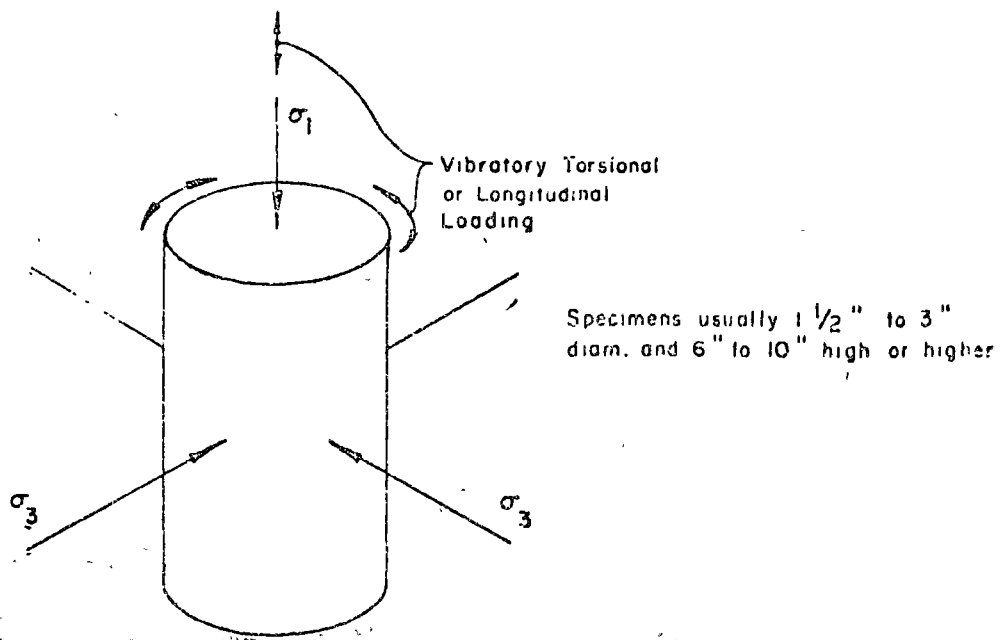
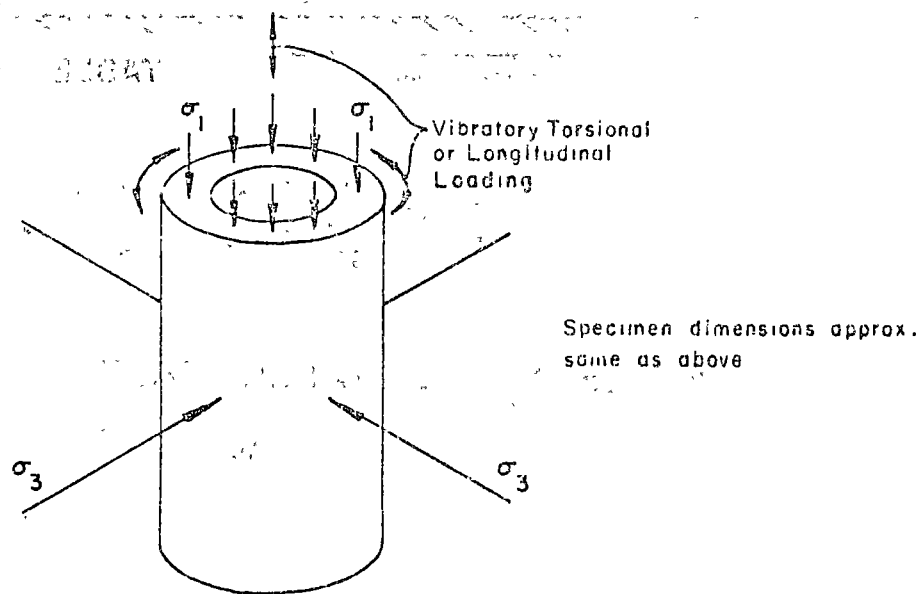


Fig. 3.13 Free torsion pendulum test under confined conditions.

(Ref # 16)



a. SOLID CYLINDER.



b. HOLLOW CYLINDER

Fig. 3.14 RESONANT COLUMN TESTS

(Ref. #14)

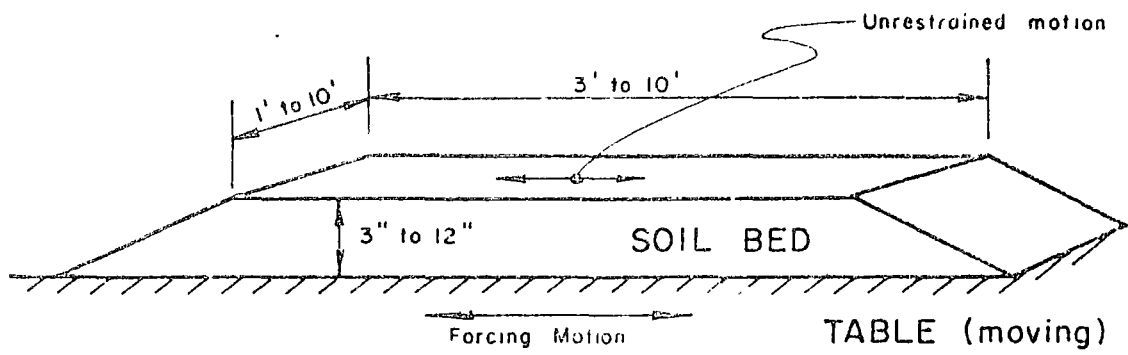


Fig. 3.15 SHAKE TABLE TEST
(Ref #14)

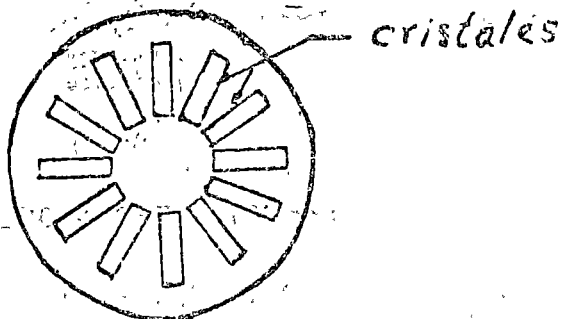
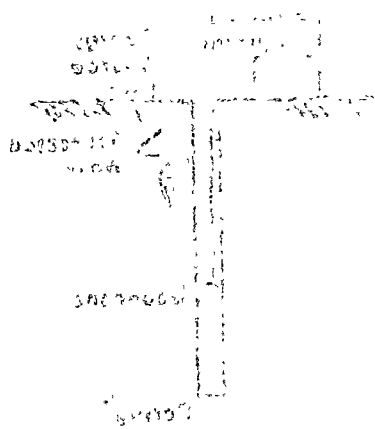


Fig 3.16 Disposición Radial de los Cristales Piezo-
eléctricos para Enviar o Recibir Ondas Cortan-
tes

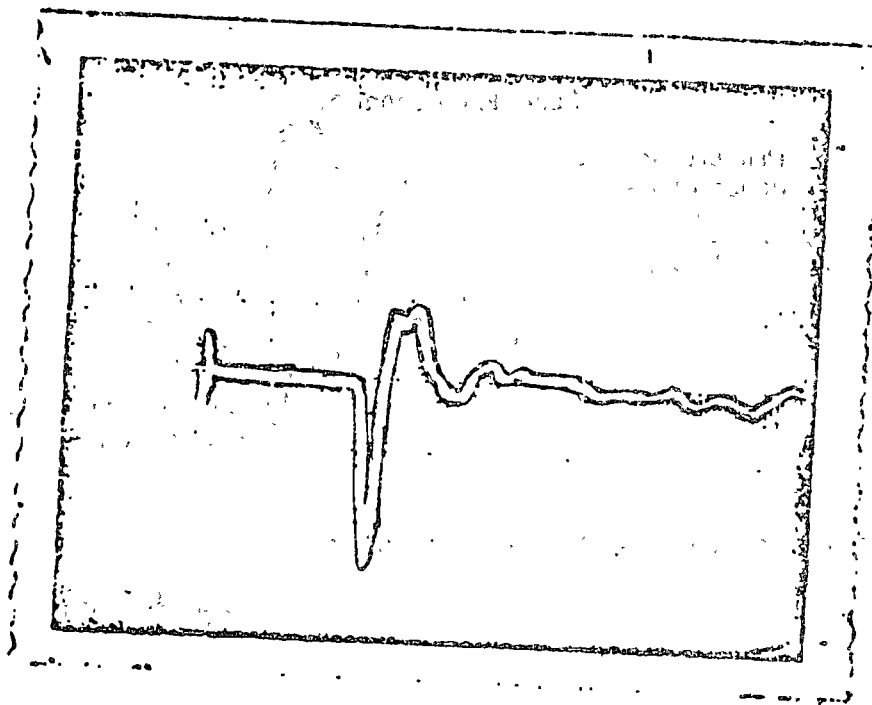


Fig. 3.17 Fotografía de una pantalla de Osciloscopio Indicando la Llegada de una Onda de Corte.

(Ref. # 15)

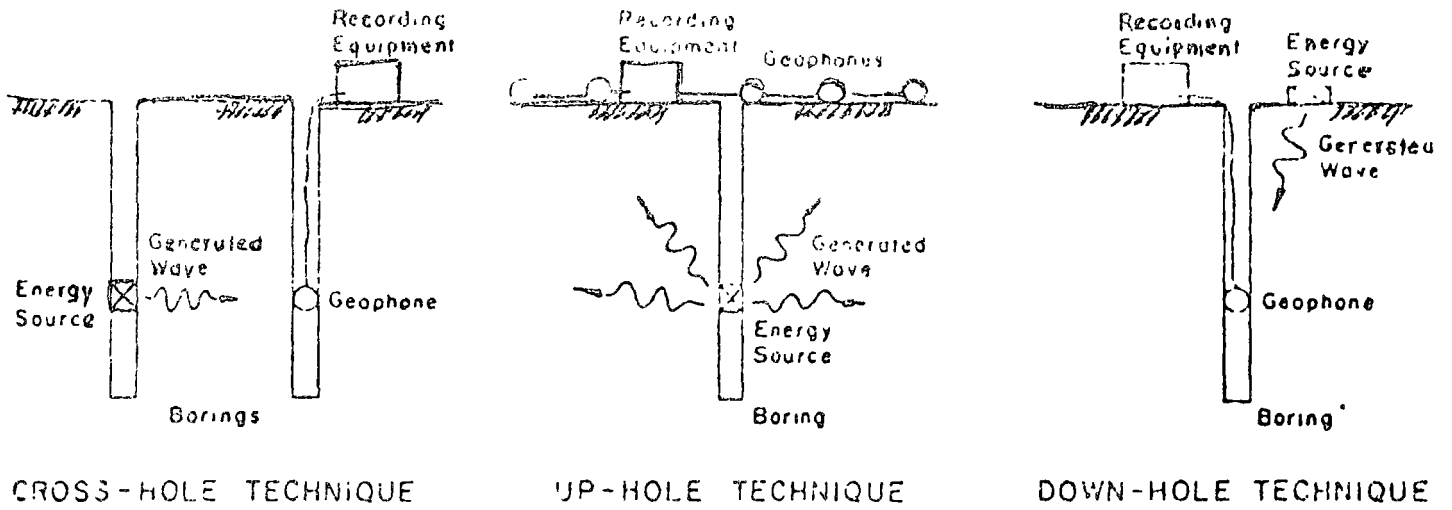


Fig 3.13 GEOPHYSICAL TESTS
(Ref. #14)

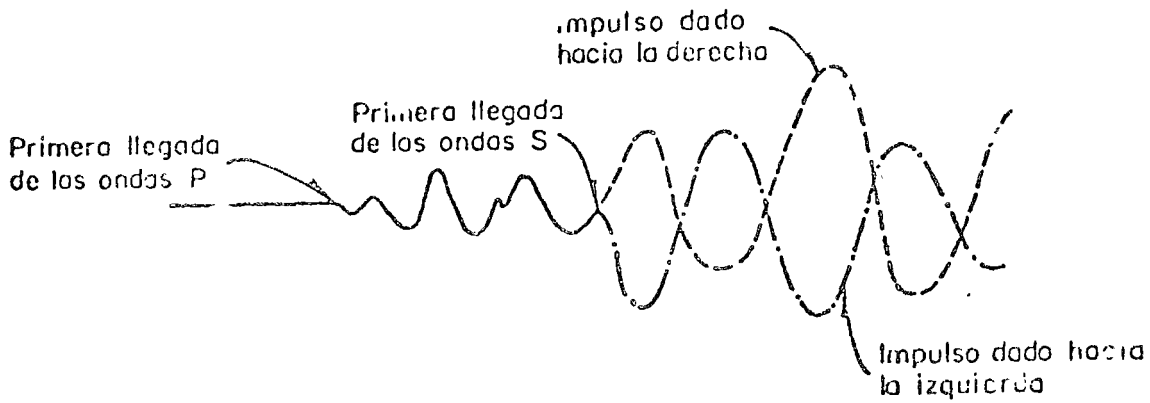
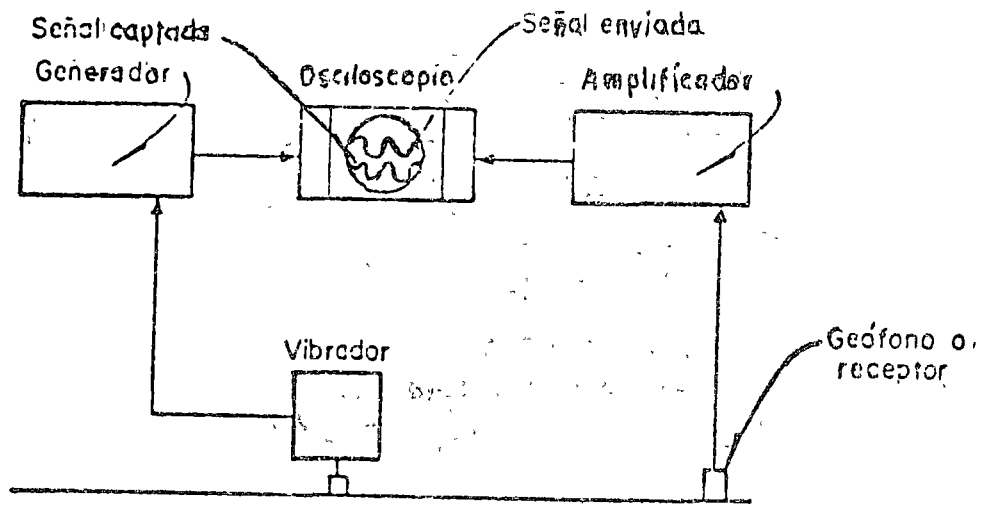


Fig 3.19 Efecto en las trazas al invertir el sentido del Impacto
(Ref # 7)



Disposición de los aparatos empleados para el registro de ondas

Fig. 3.20 a

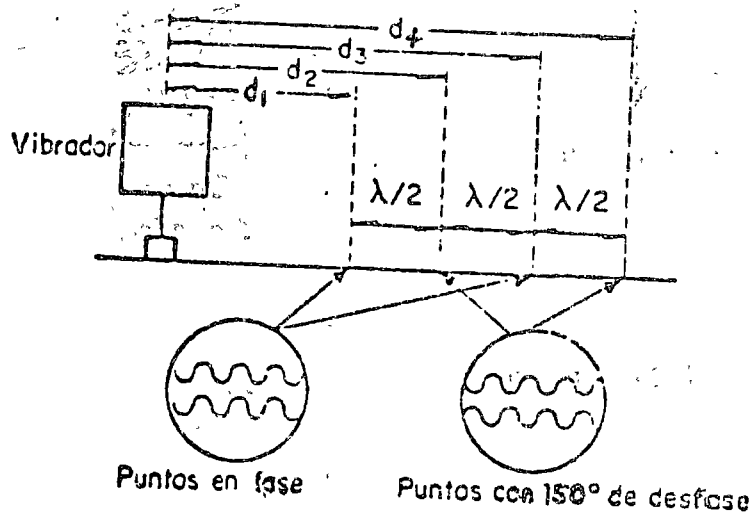
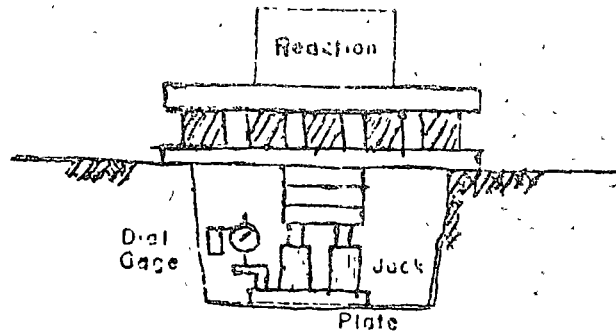


Fig. 3.20 b Determinación de la longitud de onda mediante las curvas observadas en el osciloscopio



STATIC TEST
 (Continuous Load & Unload Test)
 Fig 3.21 (Ref # 14)

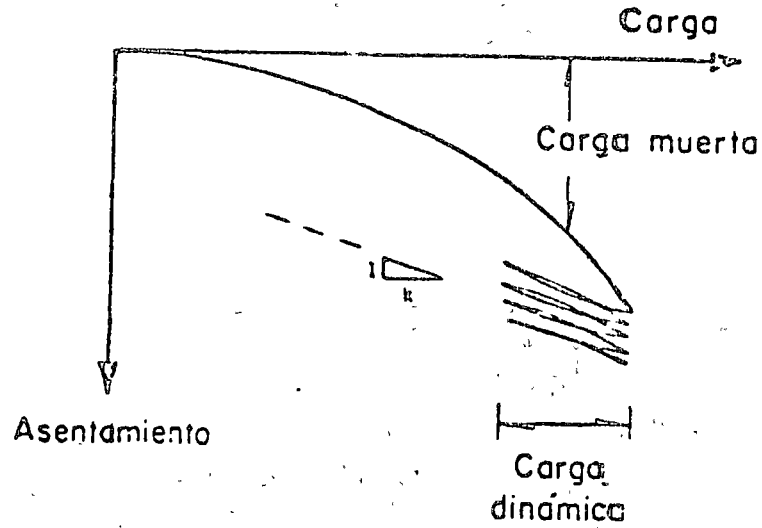
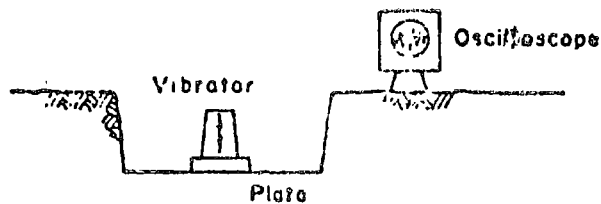


Fig 3.22 Determinación de k mediante pruebas de placa



VIBRATORY TEST

Fig 3.23 (Ref # 14)

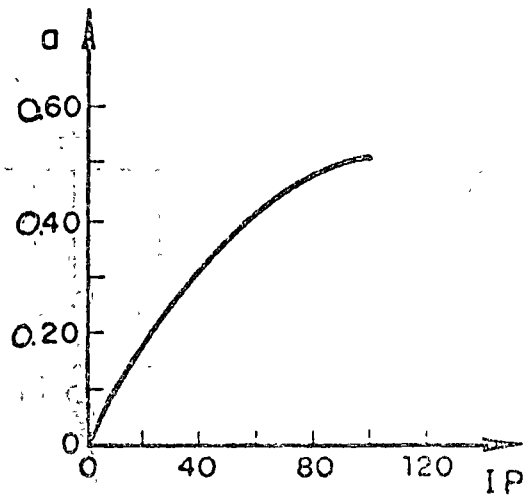
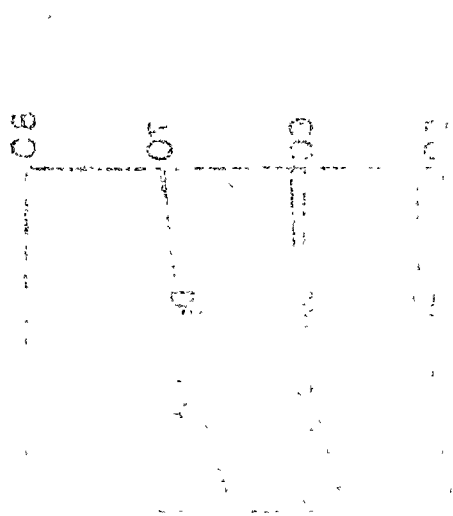


Fig 3.24 Parámetro "a" vs el índice de plasticidad (IP)

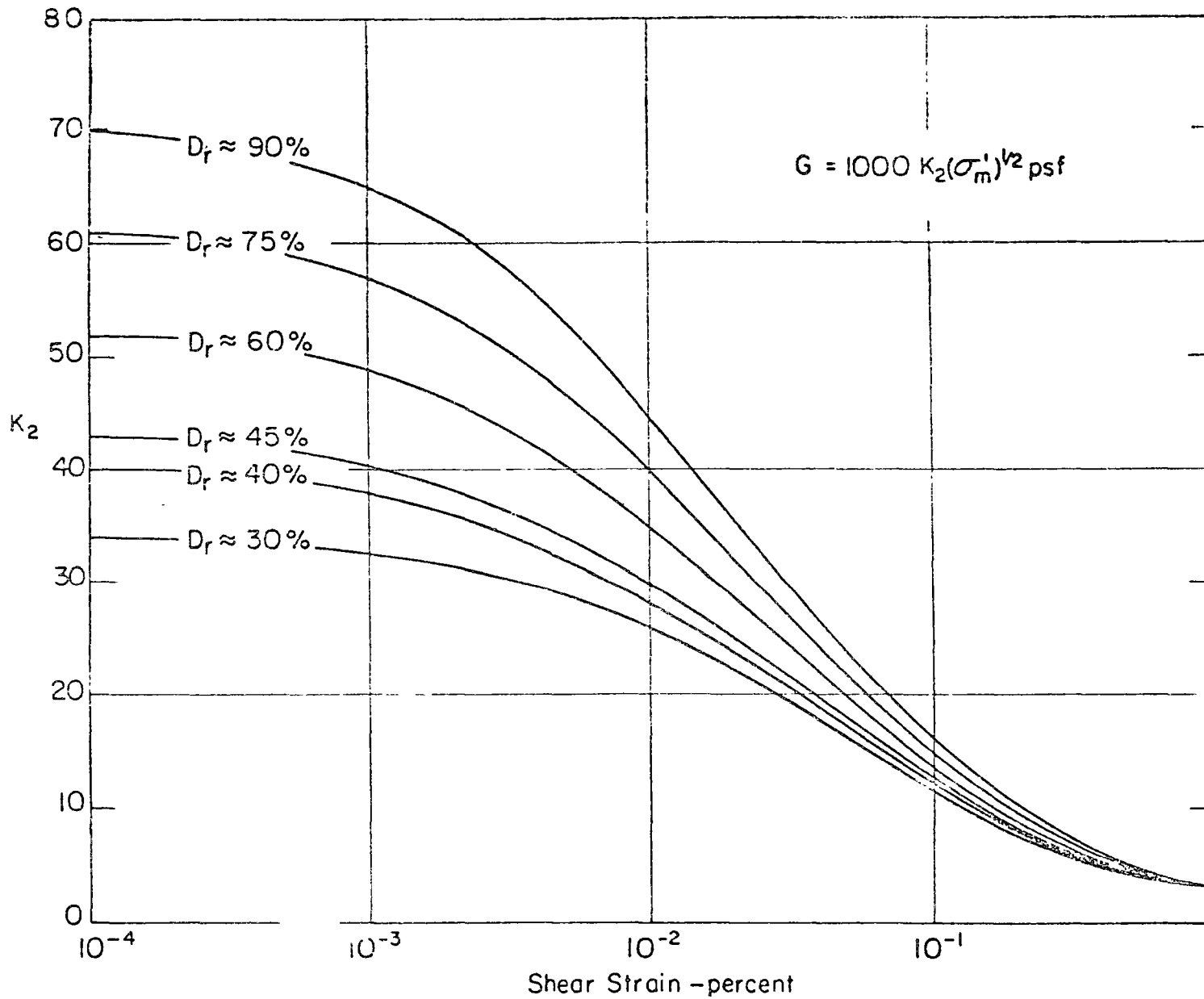


Fig. 3.25 SHEAR MODULI OF SANDS AT DIFFERENT RELATIVE DENSITIES.

(Ref #12)

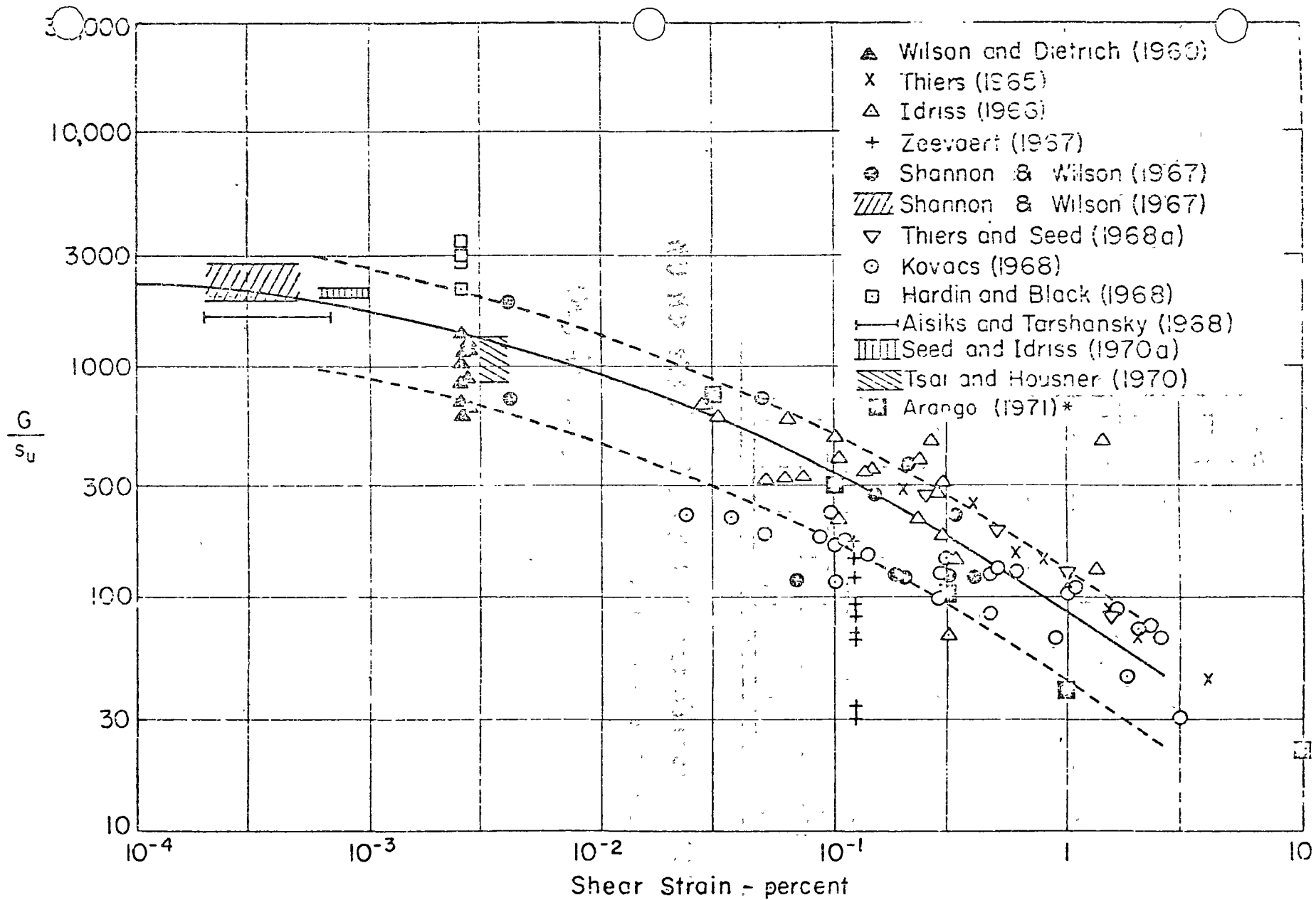


Fig. 3.2.6 IN-SITU SHEAR MODULI FOR SATURATED CLAYS.

(Ref #12)

* Data added subsequent to the referenced publication

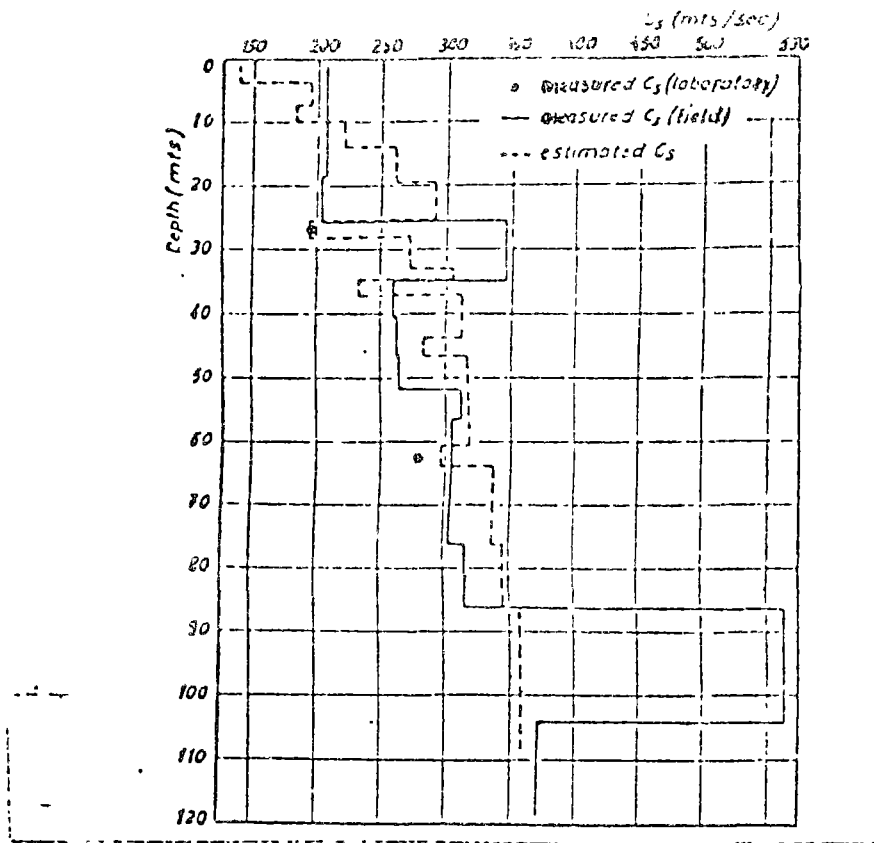
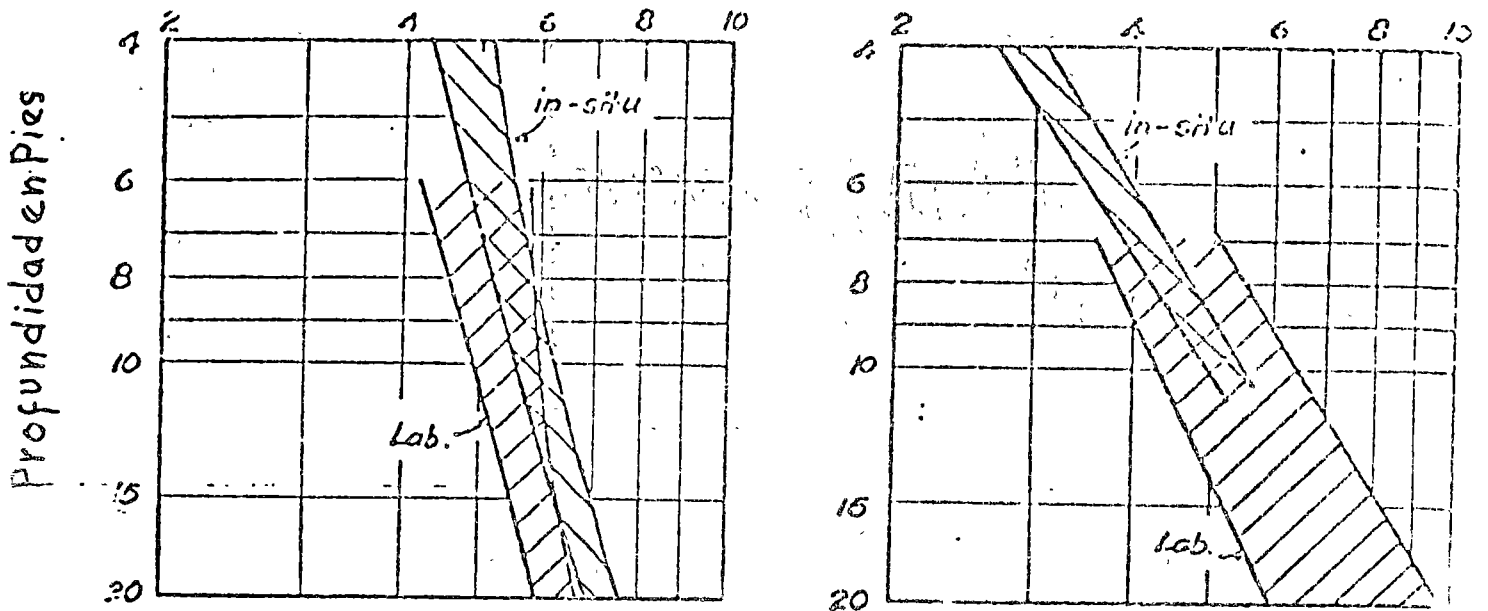


Fig. 3.27 Velocidades de Onda Cortante en un Depósito Fluvial Profundo

(Ref. # 15)

Módulo al Cortante en $\text{lb/pulg.}^2 \times 10^{-3}$



(a). Vicksburg site
Arena.

(b) Eglin site
Arcilla.

Fig. 3.28 Comparación de los Módulos Medidos en el Campo y en el Laboratorio

(Ref. # 15)

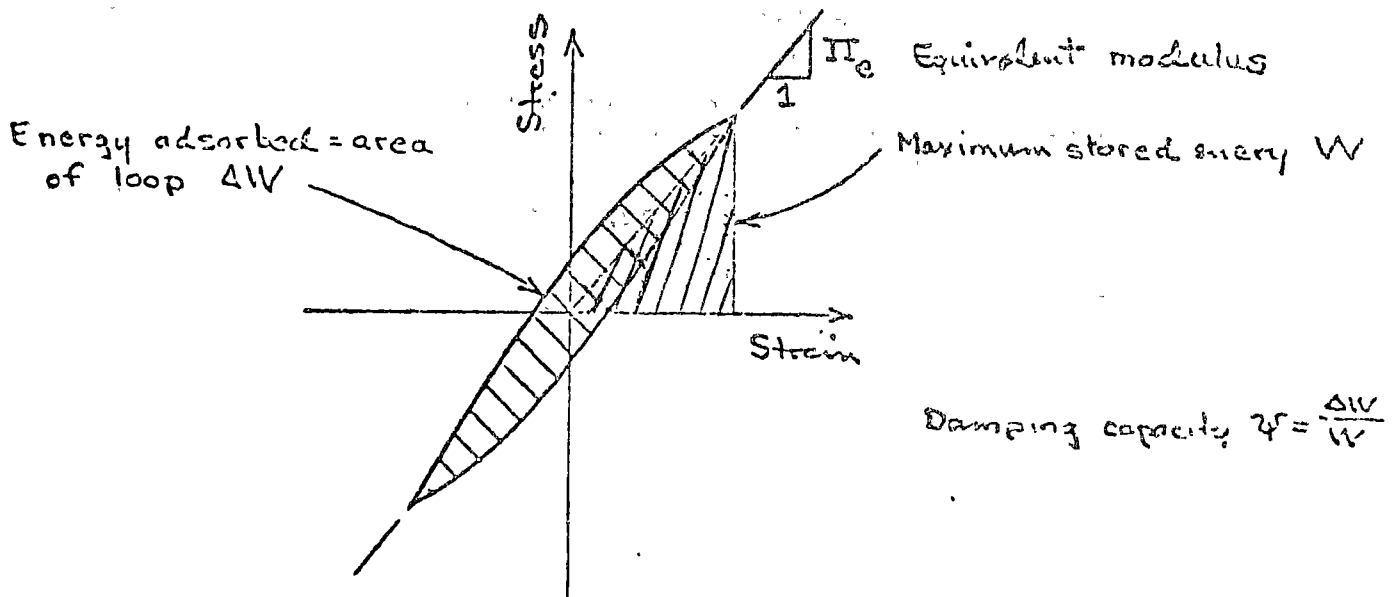
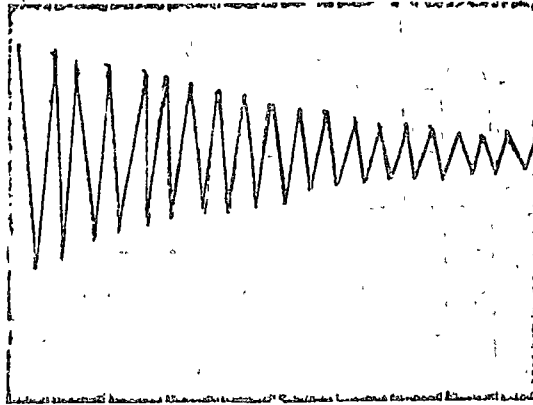
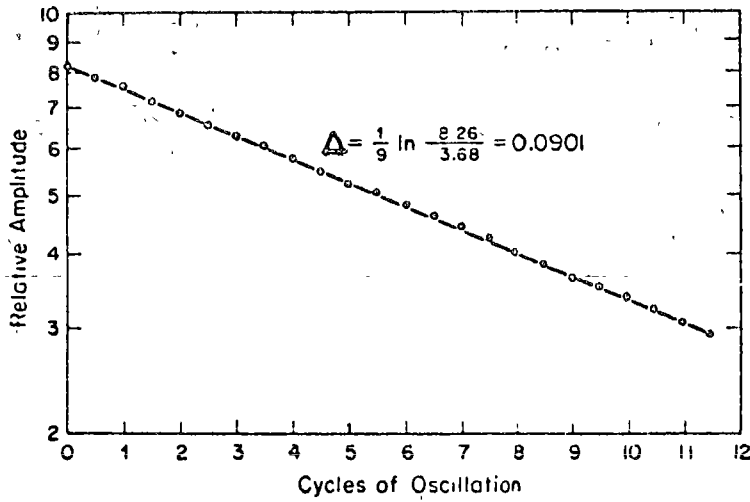


FIGURE 3.29 DEFINITION OF EFFECTIVE MODULUS AND DAMPING CAPACITY FOR CYCLIC LOADING OF HYSTERETIC MATERIAL

(Ref. # 15)



(a)



(b)

Figure 3.30 Typical free vibration-decay curves obtained from resonant-column tests of Ottawa sand (from Hall, 1952) (a) Amplitude-time decay curves (b) Amplitude vs. cycle number plot.

(Ref. # 8)

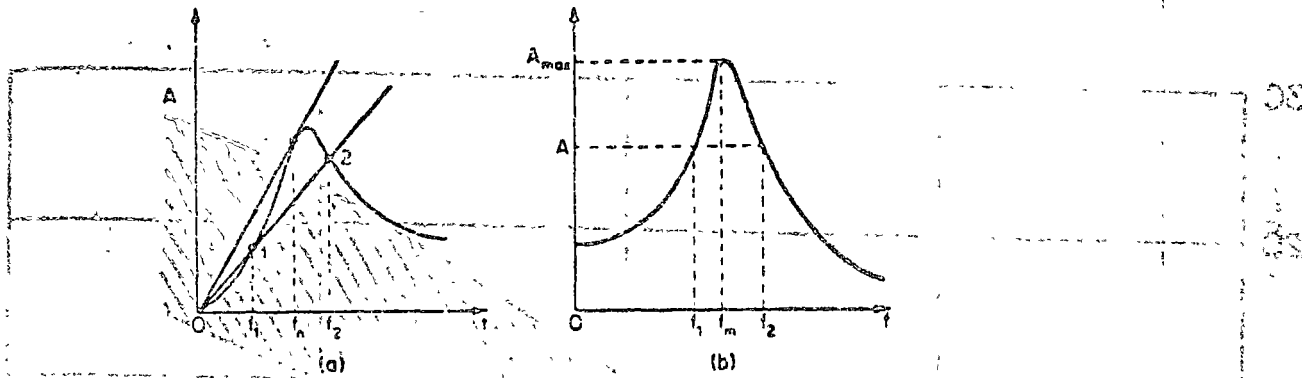
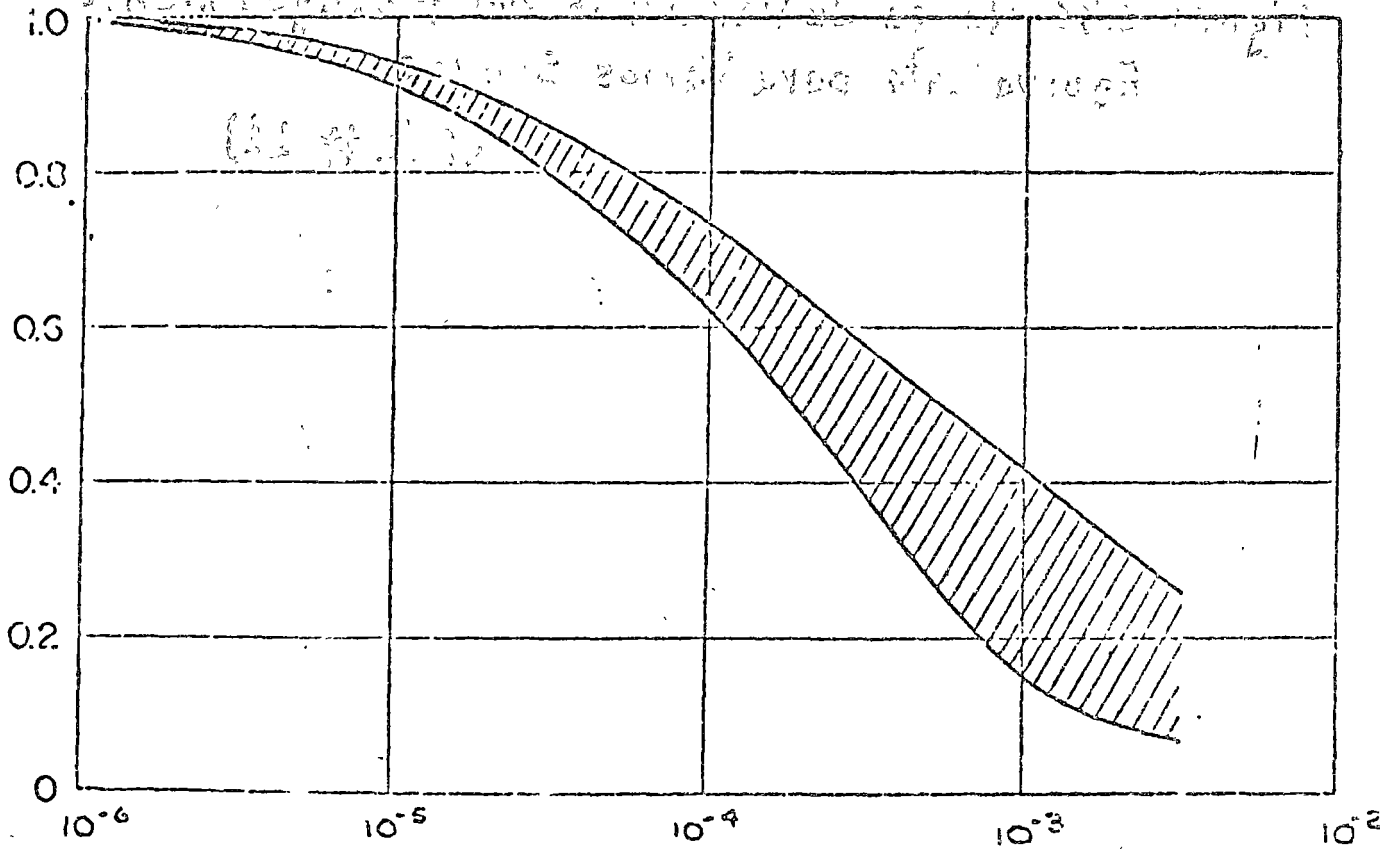


Figure 3.31 Geometric shapes of response curves for the determination of damping

(Ref. #8)

Relación: Mod equivalente a una Def. γ
Módulo para $\gamma = 10^{-6}$



Deformación al Corte

Fig. 3.32 Rango de Variación del Módulo Equivalente al Corte como Fracción del Módulo a una Deformación de 10^{-6}

(Ref. #11)

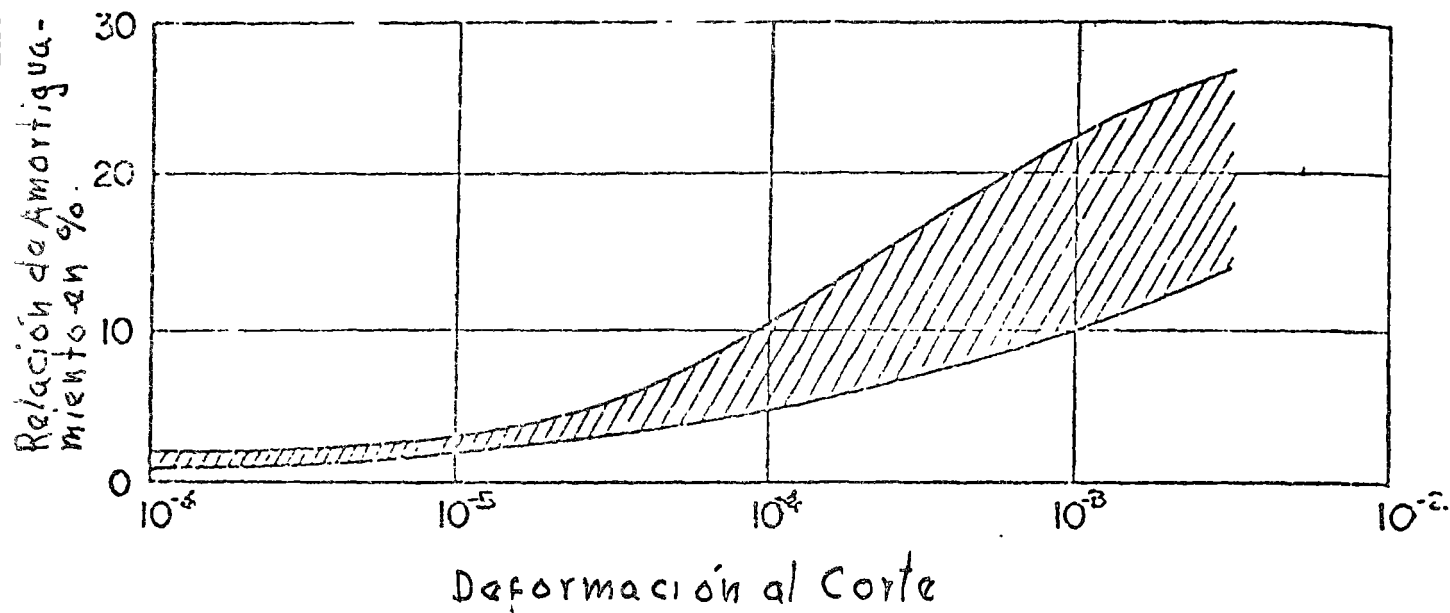
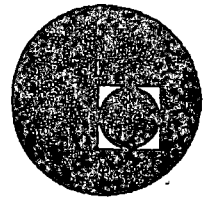


Figura 3.33 Rango de Variación del Amortiguamiento Equivalente para Varios Suelos

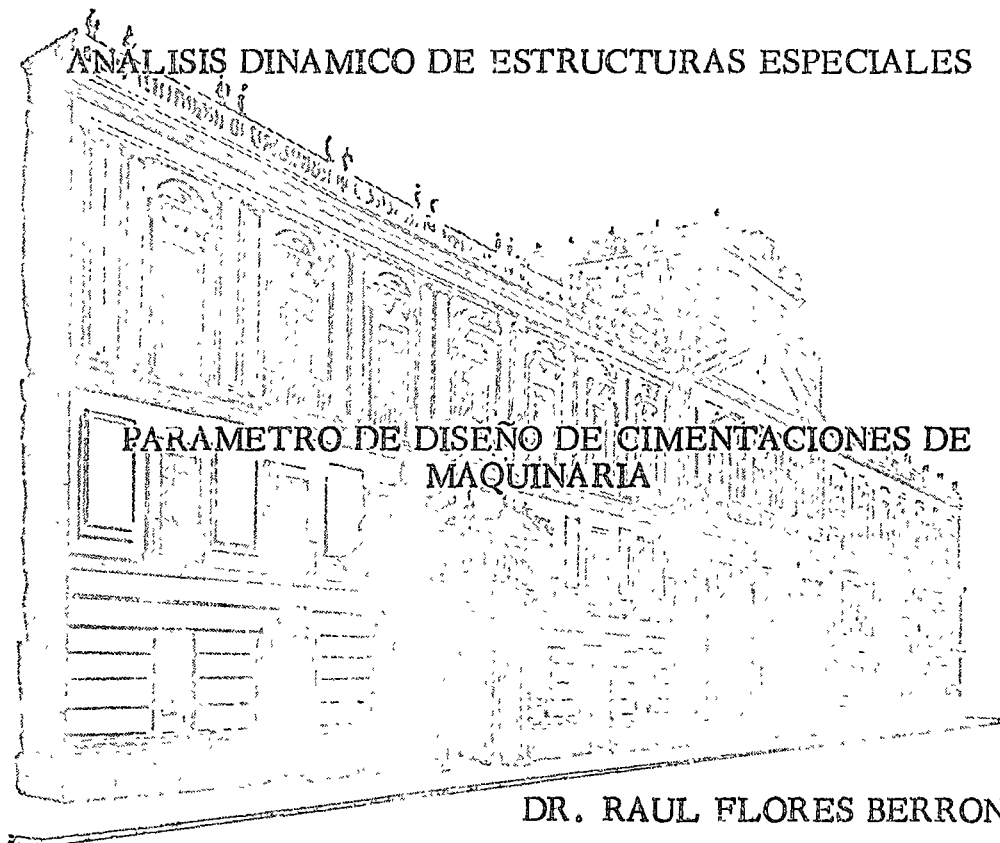
(Ref. # 11)



centro de educación continua
división de estudios superiores
facultad de ingeniería, unam



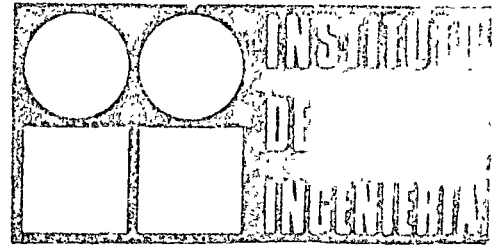
III CURSO INTERNACIONAL DE INGENIERIA SISMICA



JULIO-AGOSTO, 1977.

CONFIDENTIAL (mirrored text)
... ..
... ..





**PARAMETROS
DE DISEÑO
EN CIMENTACIONES
DE MAQUINARIA**

R FLORES BERRONES

**ELABORADO PARA
SECRETARIA DE ASENTAMIENTOS HUMANOS
Y OBRAS PUBLICAS**

AGOSTO 1977 389

UNIVERSIDAD NACIONAL AUTONOMA DE MEXICO



PARAMETROS
DE DISEÑO
EN CIMENTACIONES
DE MAQUINARIA

IR FLORES BERRONES *

* JEFE DE ESTUDIOS ESPECIALES E INVESTIGACIONES
DIRECCION GENERAL DE CAMINOS RURALES, SAHOP,
COMISIONADO AL INSTITUTO DE INGENIERIA



Faint, illegible text at the top of the page, possibly a header or title.



Faint, illegible text in the middle section of the page.

Faint, illegible text in the lower middle section of the page.

Faint, illegible text at the bottom of the page.



RESUMEN

NOTACION

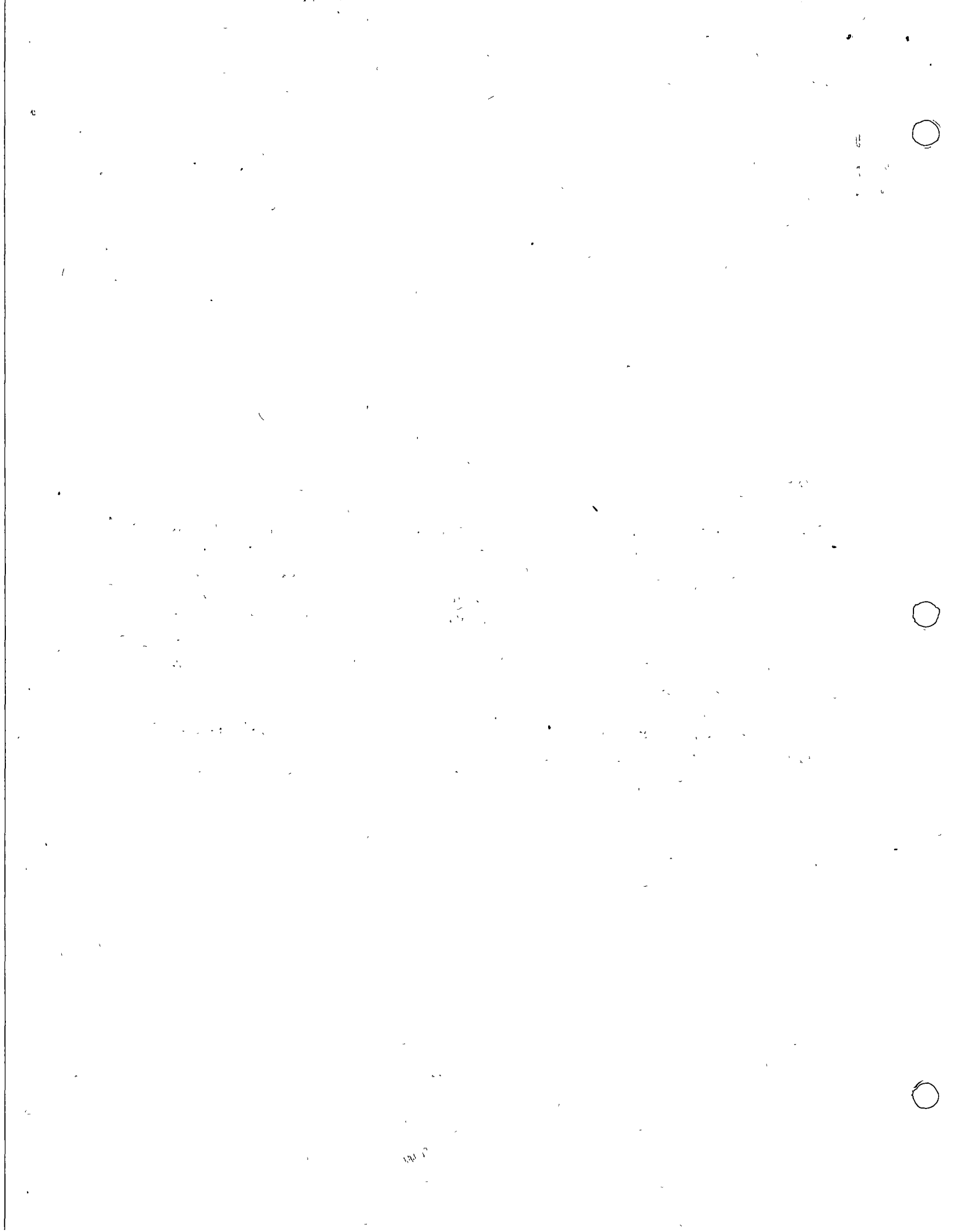
1.	INTRODUCCION	1
2.	SISTEMAS EQUIVALENTES	2
3.	SISTEMAS DE UN GRADO DE LIBERTAD	2
4.	TEORIA DEL SEMIESPACIO	5
4.1	<i>Antecedentes</i>	5
4.2	<i>Teoría de cuerpos rígidos en un medio elástico seminfinito</i>	6
4.3	<i>Evaluación de parámetros para el modo vertical</i>	9
4.4	<i>Parámetros para diferentes modos de vibración</i>	11
5.	EFFECTOS DE LA ESTRATIFICACION Y DEL ENCAJONAMIENTO	11
6.	RESPUESTA DE CIMENTACIONES EN UN MEDIO VISCOELASTICO	4
7.	CIMENTACIONES CUADRADAS O RECTANGULARES	14
8.	DETERMINACION DEL MODULO G	15
9.	ALGUNAS FORMAS PARA ESTIMAR DIRECTAMENTE k	19
9.1	<i>Cimentaciones piloteadas</i>	21
10.	CONCLUSIONES	24
11.	RECONOCIMIENTO	25
12.	REFERENCIAS	25
	TABLAS	31
	FIGURAS	37
	APENDICE. EJEMPLO DE APLICACION	53
	FIGURAS	59



ABSTRACT

The general approach for studying the vibrations of machine foundations, together with the methods for computing the behaviour of their equivalent lumped systems, is presented in this work. The elastic half-space theory for rigid bodies vibrating on the surface is summarized and formulae for obtaining the equivalent parameters on different modes of vibrations, and for different foundation shapes, are given. The most important factors that affect the numerical values of these parameters are found to be (besides the type of soil), the stress distribution at the contact area, the depth of embedment into the soil, and the depth to bedrock.

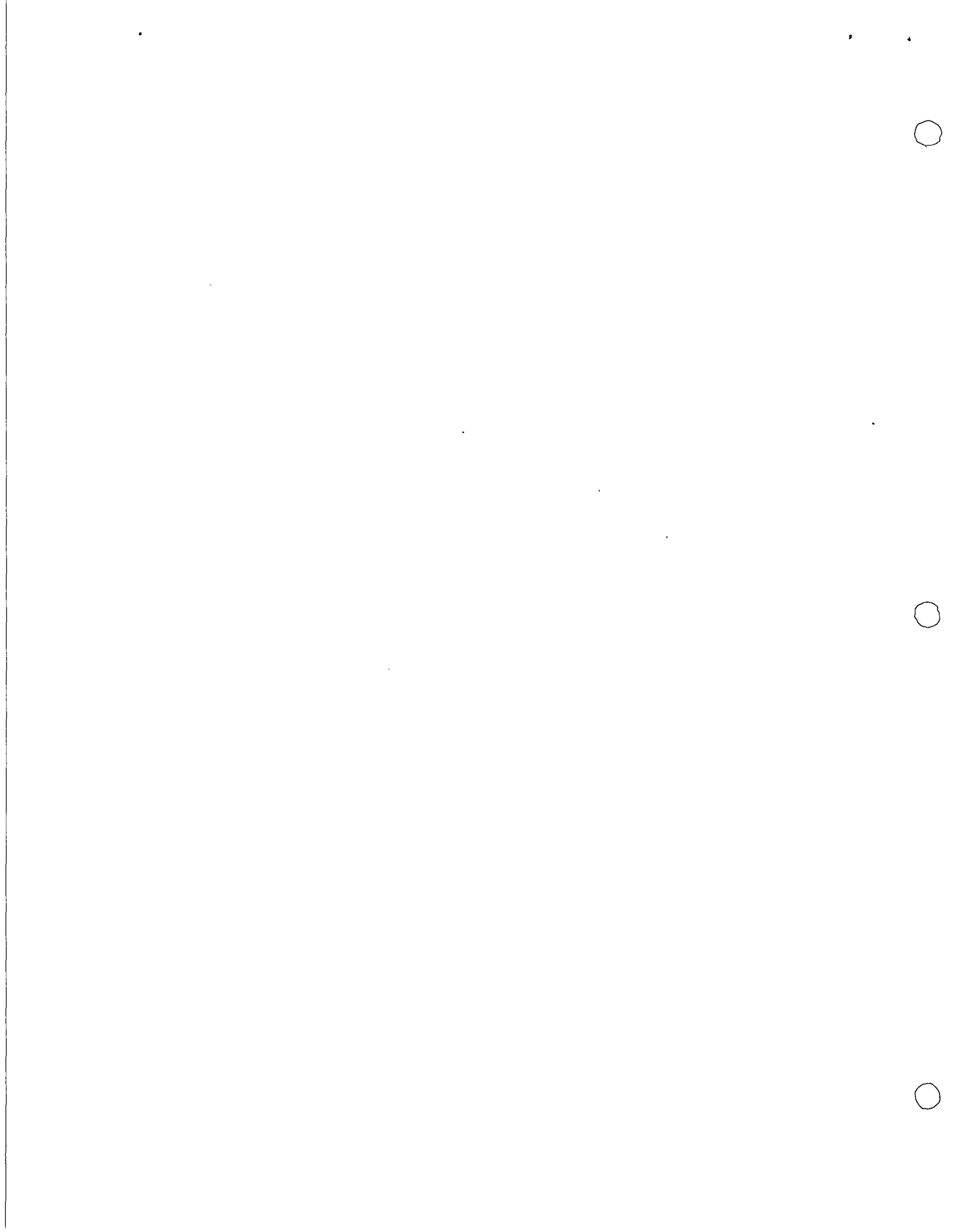
Several methods for computing the elastic shear modulus are given, and the use of the suggested criteria is illustrated through an example.



RESUMEN

Se presenta el enfoque general del análisis de las vibraciones de máquinas y se hace un repaso de los fundamentos que gobiernan el comportamiento de sistemas equivalentes constituidos por una masa, uno o varios resortes, y uno o varios amortiguadores. Se explica brevemente la teoría de cuerpos rígidos en un medio elástico seminfinite, y la forma cómo a partir de dicha teoría se obtienen los parámetros que rigen a los sistemas equivalentes. Se presentan las fórmulas con que se calculan estos parámetros en los distintos modos de vibración de zapatas circulares, cuadradas o rectangulares, y se mencionan los factores que influyen en sus valores numéricos. Entre dichos factores los más importantes son, además de la clase de suelo, el tipo de distribución de esfuerzos en el área de contacto, la profundidad de encajonamiento de la cimentación dentro del terreno, y la profundidad a la cual se encuentra la roca.

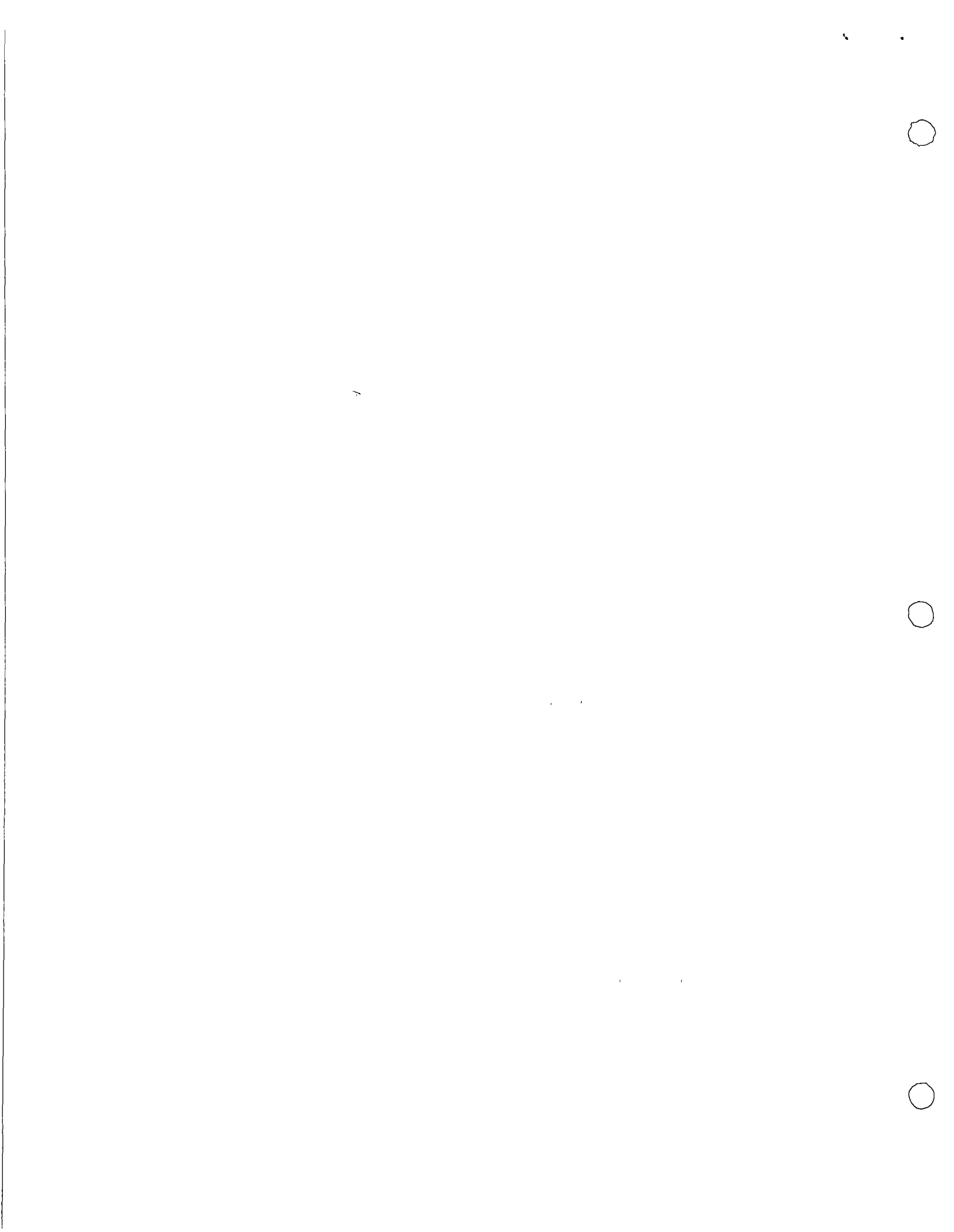
Finalmente, se incluyen varias formas para estimar el módulo elástico al cortante del suelo; dicho módulo constituye el factor más importante en la determinación de la constante, k , del resorte equivalente, y en forma de Apéndice se da un ejemplo donde se aplican varios de los conceptos expuestos en este trabajo.



NOTACION*

a	exponente empleado en la ec 13
a_0	$\Omega R/C_s$; relación de frecuencias
b	$M/\rho R^3$; relación de masas
B	ancho de cimentación
B_v, B_h, B_r	coeficientes para zapatas rectangulares (fig 11)
c	coeficiente de amortiguamiento
$c_{crítico}$	$2\sqrt{km}$
C_s	$\sqrt{G/\rho}$; velocidad de propagación de las ondas transversales
C_L	$\sqrt{E/\rho}$; velocidad de ondas dilatantes longitudinales
D	diámetro de la cimentación
D_0	$c/2\sqrt{kM}$; relación de amortiguamiento
E	módulo de Young del suelo
f_1, f_2	funciones empleadas en la teoría del semiespacio
f_n	frecuencia de resonancia
$F(t)$	fuerza que se aplica en la cimentación
FDC	factor dinámico de carga
G	$E/2(1 + \nu)$; módulo al cortante
h	profundidad equivalente
H	altura de probeta
I	momento de inercia

* Se incluyen todos los símbolos utilizados en este trabajo, excepto aquellos que se especifican en el texto



k	constante del resorte
k_v	$4GR/1-\nu$
L	largo de la cimentación (en el plano de cabeceo)
M	masa equivalente
P	fuerza aplicada directamente por la máquina a la cimentación
Q	fuerza aplicada por la cimentación al suelo
R	radio de la cimentación o radio equivalente
S_u	resistencia no drenada del suelo
T	$2\pi/\sqrt{k/M}$; periodo natural
w	desplazamiento vertical del suelo
x	desplazamiento del sistema equivalente
X_0	amplitud de desplazamiento
X_1	$\frac{1-\nu}{4} \frac{f_1}{f_1^2 + f_2^2}$
X_2	$\frac{1-\nu}{4} \frac{f_2/a_0}{f_1^2 + f_2^2}$
α	ángulo de desfaseamiento
γ_m	peso volumétrico del suelo
λ	longitud de onda
ν	relación de Poisson
ρ	masa específica del suelo
σ_0	esfuerzos de confinamiento
σ_v	esfuerzos verticales normales
ω	$\sqrt{k/M}$; frecuencia circular natural
Ω	frecuencia circular de excitación



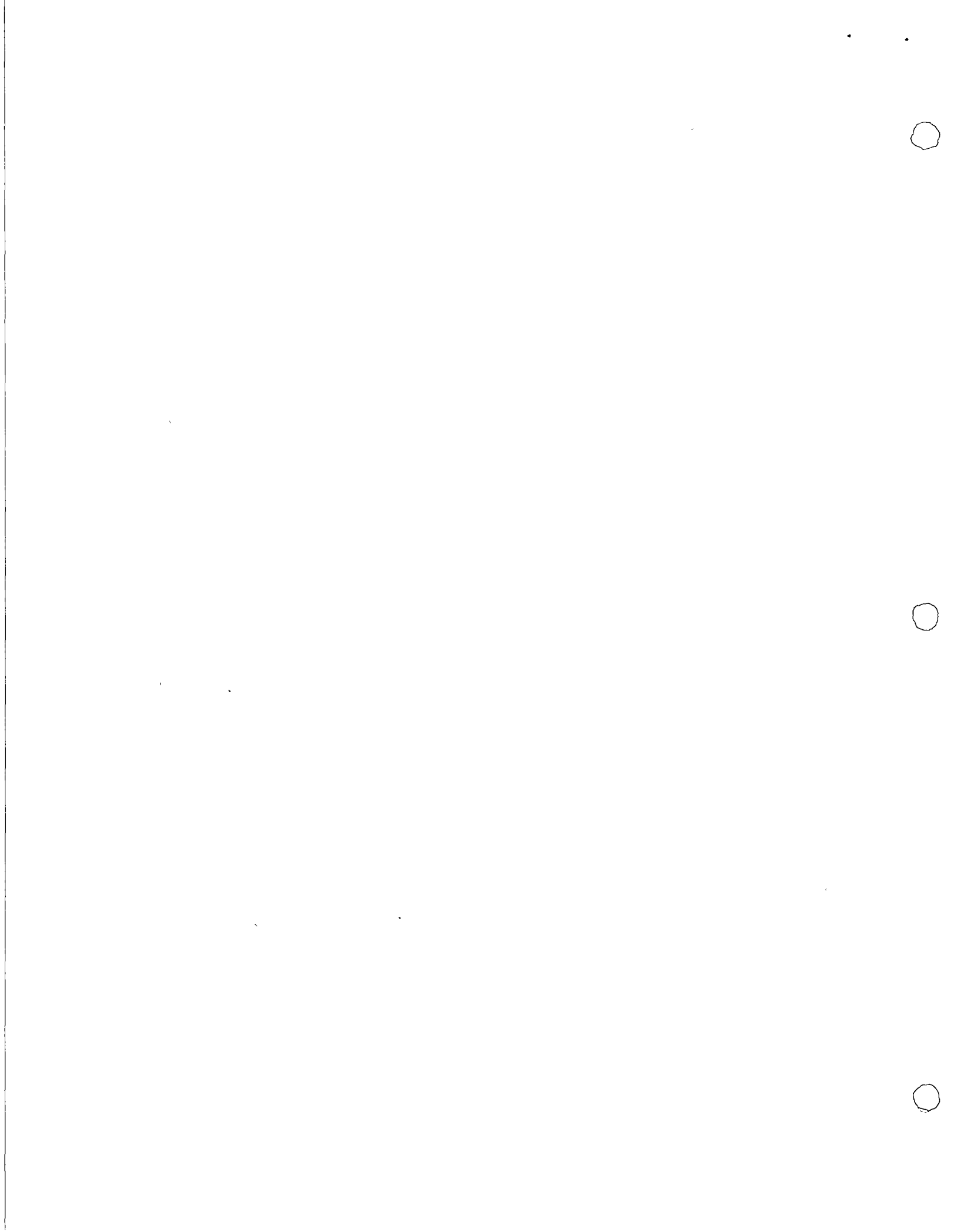
1. INTRODUCCION

Muchos ingenieros especializados en mecánica de suelos se han encontrado alguna vez con el problema de diseñar o dar recomendaciones para cimentar adecuadamente cierto tipo de maquinaria. Cuando el profesional no es experto en solucionar esta clase de problemas, al pasar a la literatura encontrará que generalmente la respuesta de sistemas reales se hace a través de sistemas simplificados equivalentes; los cuales están constituidos por masas concentradas, resortes y amortiguadores, que representan las masas, rigideces y amortiguamientos de los sistemas reales, respectivamente.

Al tratar de pasar de un sistema real a uno equivalente, necesariamente se debe responder a dos preguntas:

1. ¿Cuál es el sistema equivalente más adecuado para representar al sistema verdadero?
2. ¿Qué valor se debe aplicar a los parámetros del sistema equivalente para que la respuesta sea congruente con la realidad?

Mientras que la primera pregunta se puede contestar directamente en función del sentido en que se aplican las fuerzas y los desplazamientos que tienden a producirse (ref 1), la segunda involucra muchos factores que requieren de un cuidadoso estudio. Sin embargo, un análisis completo dinámico de cimentaciones deberá comprender estos dos aspectos y



sus objetivos estarán encaminados a: 1) establecer claramente las partes involucradas en el problema; 2) estudiar las alternativas que permitan cumplir con las especificaciones de comportamiento, y 3) dar las recomendaciones de cimentación.

El objeto del presente trabajo se limita a proporcionar un resumen de los procedimientos más comunes en la determinación de los parámetros mencionados, con el enfoque principal dirigido hacia la evaluación más racional que actualmente se emplea. Para mayor información sobre el análisis general de las cimentaciones de maquinaria se recomiendan las refs 2 y 3.

2. SISTEMAS EQUIVALENTES

La intención de representar un sistema real de máquina-cimentación-suelo mediante un sistema matemático equivalente, es obtener con cierta facilidad la respuesta del primero, para lo cual se emplean las curvas de amplificación y las ecuaciones que rigen el movimiento de los sistemas equivalentes.

La mayor parte de los sistemas reales que constituyen los problemas de cimentación, se pueden analizar mediante sistemas de un grado de libertad. En efecto, aun en los formados por más de un grado de libertad, generalmente se obtiene suficiente aproximación al analizar y superponer cada uno de sus modos de vibración mediante el llamado *método de superposición modal* (ref 4). La fig 1 muestra algunos de los sistemas más comunes en la práctica.

Por lo anterior, conviene hacer un breve repaso de los conceptos fundamentales sobre comportamiento de sistemas de un grado de libertad.

3. SISTEMAS DE UN GRADO DE LIBERTAD

La ecuación de equilibrio que gobierna el movimiento dinámico de estos sistemas es

$$M\ddot{x} + c\dot{x} + kx = F(t) \quad (1)$$

donde

- M masa del sistema
- c coeficiente de amortiguamiento
- k constante del resorte

- 1. ...
- 2. ...
- 3. ...

...

...

...

...

...

...

...

...

...

...

...

$F(t)$ fuerza exterior aplicada a la masa (fig 2)

\ddot{x} , \dot{x} , x aceleración, velocidad y desplazamiento del sistema, respectivamente

La derivación de la solución de la ec. 1, se encuentra en cualquier texto de dinámica básica (refs 4 y 5). Dicha solución está compuesta por dos términos: el correspondiente a las vibraciones libres que desaparecen después de cierto tiempo (como consecuencia del amortiguamiento), y el de las vibraciones forzadas que permanecen en el sistema mientras la fuerza, F , actúa. Solo se analizarán las vibraciones forzadas, por ser las que realmente interesan para el diseño.

La expresión que da respuesta a las vibraciones forzadas, cuando existe excitación armónica, es

$$x = \frac{F_0}{k} \sin(\Omega t + \alpha) \quad (2)$$

donde

F_0 amplitud de la fuerza aplicada

$$\alpha = \tan^{-1} \frac{2 D_0 \omega \Omega}{\omega^2 - \Omega^2}$$

Ω frecuencia circular de excitación, en rad/seg

$f = \frac{\Omega}{2\pi}$, frecuencia de excitación, en ciclos/seg

$D_0 = c/c_{\text{crítico}} = c/2\sqrt{kM}$, relación de amortiguamientos

$c_{\text{crítico}}$ amortiguamiento que suprime las vibraciones libres

$\omega = \sqrt{k/M}$, frecuencia circular natural, en rad/seg

$T = 2\pi/\omega$, periodo natural, en seg

t tiempo transcurrido

$f_n = \frac{\omega}{2\pi}$, frecuencia natural, en ciclos/seg

El factor

$$FDC = \frac{1}{\sqrt{\left[1 - \frac{\Omega^2}{\omega^2}\right]^2 + 4D_0^2 \left[\frac{\Omega}{\omega}\right]^2}} \quad (3)$$

se denomina *factor dinámico de carga* o de *amplificación*; representa la relación de la respuesta dinámica máxima respecto a la respuesta estática, es decir

$$X_0 = \frac{F_0}{k} FDC \quad (4)$$

donde X_0 es la amplitud de la respuesta dinámica, y F_0/k la respuesta estática.

Si se dibuja este factor como función de la relación de frecuencias Ω/ω , el tipo de gráficas que se obtiene es el de la fig 3, en la que se puede observar que el FDC es máximo para valores de Ω/ω (o f/f_n) cercanos a 1, mientras que cuando $\Omega/\omega \rightarrow \infty$, el $FDC \rightarrow 0$. Si no hay amortiguamiento, o en general si $3/2 \leq \Omega/\omega \leq 2/3$, el FDC es aproximadamente igual a

$$FDC \approx \frac{1}{\left|1 - \left(\frac{\Omega}{\omega}\right)^2\right|}$$

En caso de tener maquinaria con masas excéntricas, la amplitud de la fuerza aplicada varía con el cuadrado de la frecuencia de excitación, o sea

$$F(t) = M_e l \Omega^2 \text{sen } \Omega t$$

donde M_e es la masa excéntrica y l el brazo de palanca.

La ec 4 quedaría entonces:

$$x_0 = \frac{M_e l \Omega^2}{k} FDC = \frac{M_e l}{M} \left(\frac{\Omega}{\omega}\right)^2 FDC$$

Para este caso, la curva de FDC vs Ω/ω es también válida, pero resulta de mayor utilidad emplear curvas como las de la fig 4.

Conociendo la forma como responde un sistema de un grado de libertad a una excitación dinámica, el problema se reduce a la determinación correcta de los parámetros que lo constituyen. Quizá la forma más adecuada de efectuar esta determinación es mediante la teoría de cuerpos rígidos que vibran sobre un medio elástico seminfinito.

4. TEORIA DEL SEMIESPACIO

4.1 Antecedentes

Los primeros estudios sobre esta teoría fueron realizados por Reissner (ref 6), en 1936, quien analizó la respuesta dinámica de una zapata vibrando sobre una masa de suelo representada por un semiespacio homogéneo, isótropo y elástico; la zapata estaba representada por una masa oscilatoria que producía una presión vertical periódica, distribuida uniformemente, sobre un área circular en la superficie del semiespacio. Reissner obtuvo el desplazamiento vertical dinámico en el centro del área circular integrando la solución dada por Lamb (ref 7), quien determinó el desplazamiento debido a una fuerza oscilatoria o pulsativa actuando sobre un punto en la superficie o dentro del semiespacio.

En 1953 Quinlan (ref 8) y Sung (ref 9) extendieron, simultáneamente, la solución de Reissner para analizar el efecto del cambio en la presión de contacto sobre el área cargada; ambos consideraron la respuesta correspondiente a las distribuciones parabólica, uniforme y la que se produce en una base rígida bajo condiciones estáticas.

Más adelante, en 1956, Bycroft (ref 10) trató de mejorar los resultados de Sung, quien supuso que la distribución de presiones permanece constante en el intervalo de frecuencias considerado. (En realidad, la distribución de presiones correspondiente a una base rígida que bajo condiciones estáticas produce un desplazamiento uniforme, bajo condiciones dinámicas no produce desplazamiento uniforme, ref 5.) Para ello determinó el promedio pesado de los desplazamientos bajo la zapata y estableció mejores valores de las funciones que intervienen en el cálculo de los desplazamientos. De acuerdo con Bycroft, este promedio constituye el límite inferior del desplazamiento real que se tiene en un disco rígido.

Soluciones posteriores consideraron el problema matemático del valor frontera exacto mostrado en la fig 5. Ejemplo de esas soluciones son los presentados por Awojobi y Grootenhuis (ref 11) y Robertson (ref 12), quienes utilizaron métodos matemáticos exactos pero aproximaciones en el cálculo de las integrales. Al comparar los resultados obtenidos empleando dichos métodos exactos con los aproximados presentados por Sung y Bycroft, se observó que las diferencias eran prácticamente despreciables.

Trabajos más recientes de Veletsos y Wei (ref 13) y de Luco y Westmann (ref 14) permiten obtener, para un amplio intervalo de frecuencias, la respuesta dinámica de una zapata circular rígida para los modos vertical, horizontal, torsional y de cabeceo.

Actualmente existen estudios más prácticos que consideran el medio espacio como un medio viscoelástico (ref 15) o un medio estratificado (ref 16); en ambos casos se obtiene la respuesta de cimentaciones circulares rígidas, para los modos vertical, horizontal y de cabeceo.

En esta sección se explica primeramente, en términos generales, en qué consiste la teoría de un cuerpo circular rígido vibrando en la superficie de un medio elástico seminfinito, y se presenta la evaluación de los parámetros equivalentes en los modos vertical, horizontal y de cabeceo. Posteriormente, se muestran los efectos de la estratificación y el encajonamiento, así como la respuesta de cimentaciones en un medio viscoelástico. Finalmente, se analizan las cimentaciones de forma cuadrada o rectangular.

4.2 Teoría de cuerpos rígidos en un medio elástico seminfinito

Las suposiciones originales de esta teoría son:

1. La cimentación se apoya en la superficie de un medio seminfinito y es rígida, de radio R , y masa M .
2. El medio elástico es homogéneo, de profundidad infinita, y está caracterizado por las siguientes propiedades:

ρ densidad de masa

G módulo elástico al cortante, o E (módulo de Young) = $2G(1 + \nu)$

ν relación de Poisson

C_s velocidad de propagación de las ondas cortantes, función de G y ν

Bajo estas condiciones, el análisis se hace en dos partes. En la primera se obtiene la relación de la fuerza vertical Q , aplicada directamente en la superficie del medio espacio (figs 6a y b), y el desplazamiento vertical w . Dicha relación está dada por

$$w = \frac{Q_0 e^{i\Omega t}}{GR} (f_1 - if_2) \quad (5)$$

donde Q_0 es la amplitud de la carga, y f_1 y f_2 son funciones de:

1. $a_0 = \Omega R / C_s$
2. De la relación de Poisson
3. De la forma como los esfuerzos se distribuyen en el área cargada; si la cimentación es rígida la distribución queda dada por los otros parámetros.

La fig 7 muestra la forma en que varían f_1 y f_2 en función de a_0 , para una distribución dada de esfuerzos sobre un área circular.

La segunda parte consiste en considerar la ecuación que establece el equilibrio de la masa M de la cimentación

$$M\dot{w} + Q = P \quad (6)$$

A continuación se verá como puede expresarse el desplazamiento w directamente en términos de la fuerza P , mediante la combinación de las ecs 5 y 6. Para ello, despéjese Q de la ec 5 e inclúyase en la ec 6, considerándose además de que $\dot{w} = -\Omega^2 w$; es decir

$$-M\Omega^2 w + \frac{GR}{f_1 - if_2} w = P$$

Ahora, al despejar de esta expresión w se obtiene

$$w = P \frac{f_1 - if_2}{(GR - M\Omega^2 2f_1) + iM\Omega^2 f_2} = \frac{P}{GR} \frac{f_1 - if_2}{\left(1 - \frac{M\Omega^2}{GR} f_1\right) + i \frac{M\Omega^2}{GR} f_2}$$

puesto que

$$\frac{M\Omega^2}{GR} = \frac{\Omega^2 R^2 \rho}{G} \frac{M}{\rho R^3} = \frac{M}{\rho R^3} a_0^2$$

y llamando

$$b = \frac{M}{\rho R^3}$$

el valor del desplazamiento se puede escribir también como

$$w = \frac{P}{GR} \frac{f_1 - if_2}{(1 - a_0^2 bf_1) - ia_0^2 bf_2}$$

Si se considera que $P = P_0 e^{i\Omega t}$, la anterior ecuación puede escribirse

$$w = \frac{P_0 e^{i(\Omega t - \alpha)}}{GR} \frac{f_1^2 + f_2^2}{\sqrt{(1 - a_0^2 bf_1)^2 + (a_0^2 bf_2)^2}}$$

donde $\tan \alpha = \frac{f_2}{f_1 - a_0^2 b (f_1^2 + f_2^2)}$

Finalmente, el valor del desplazamiento se puede expresar de la siguiente manera

$$w = \underbrace{\left[\frac{P_0 (1-\nu)}{4GR} \right]}_I \underbrace{\left[\frac{4}{1-\nu} \frac{f_1^2 + f_2^2}{\sqrt{(1 - a_0^2 bf_1)^2 + (a_0^2 bf_2)^2}} \right]}_{II} \underbrace{\left[e^{i(\Omega t - \alpha)} \right]}_{III} \quad (7)$$

La ec 7 relaciona directamente a w y P ; en ella se aprecian tres componentes: el término I representa el desplazamiento estático, el II la amplificación dinámica, y el III el ángulo de desfase entre la fuerza aplicada y el desplazamiento w .

Al dibujar el factor de amplificación para diferentes valores de a_0 y b , se obtienen las curvas de la fig 8a, muy parecidas a las de la fig 3; es decir, en ambos casos se tiene un solo *peak* o valor máximo, y la forma general de las curvas es la misma. Mas aún, el semiespacio, aunque es totalmente elástico, se comporta como si fuera amortiguado debido a la energía por radiación es disipada; esta pérdida de energía es lo que se conoce como *amortiguamiento radial* del sistema.

Si se hace $P_0 = M_e I \Omega^2$, la ec 7 se puede escribir

$$w = \frac{M_e I}{M} \left[a_0^2 b \frac{f_1^2 + f_2^2}{\sqrt{(1 - a_0^2 bf_1)^2 + (a_0^2 bf_2)^2}} \right] e^{i(\Omega t - \alpha)} \quad (8)$$

Las curvas de amplificación correspondientes se muestran en la fig 8b, las cuales son muy similares a las obtenidas en la fig 4.

4.3. Evaluación de parámetros para el modo vertical

Al combinar nuevamente las ecs 5 y 6, se obtiene

$$M\ddot{w} + \frac{f_2/\Omega}{f_1^2 + f_2^2} GR\dot{w} + \frac{f_1}{f_1^2 + f_2^2} GRw = P \quad (9)$$

Del análisis de esta ecuación, se observa que es muy similar a la correspondiente a un sistema de un grado de libertad compuesto por una masa, un resorte y un amortiguador, la que se puede también escribir como

$$M\ddot{w} + c_v X_2 \dot{w} + k_v X_1 w = P \quad (10)$$

donde

$$c_v = \frac{4}{1-\nu} \sqrt{G} \rho R^2$$

$$X_2 = \frac{1-\nu}{4} \frac{f_2/a_0}{f_1^2 + f_2^2}$$

$$k_v = \frac{4GR}{1-\nu}$$

$$X_1 = \frac{1-\nu}{4} \frac{f_1}{f_1^2 + f_2^2}$$

Coefficientes relacionados con el amortiguamiento

Coefficientes relacionados con la rigidez del sistema

Los valores de k_v y c_v son independientes de la frecuencia de excitación, en cambio X_1 y X_2 sí dependen de ella, según se observa en la fig 9.

A fin de tener valores constantes de los coeficientes de \dot{w} y w , y obtener la equivalencia con sistema de masa-amortiguamiento-resorte de un grado de libertad, es necesario establecer el intervalo de frecuencias de interés y seleccionar en él los valores de estos coeficientes que, al usarse como constantes, den resultados aproximados a los que se obtendrían con los coeficientes reales.

Uno de los procedimientos más simplista y racional para efectuar esta selección de valores, es el propuesto por Lysmer (ref 18), con las siguientes sugerencias

- a) Para bajas frecuencias, $X_1 = 1$
- b) Para frecuencias altas, se considera solamente como masa equivalente la masa M , y se desprecia la llamada masa efectiva de suelo (concepto que se estudiará más adelante).
- c) Para frecuencias intermedias, usar un valor de $X_2 = 0.85$ (fig 9), o sea emplear una relación de amortiguamiento igual a

$$D_V = \frac{c}{c_{\text{crítico}}} = \frac{X_2 c_v}{2\sqrt{k_v M}} = \frac{0.85 c_v}{2\sqrt{k_v M}} = \frac{0.85}{\sqrt{b(1-\nu)}}$$

El error máximo con el procedimiento simplificado por Lysmer es de 30 por ciento, aun cuando en general es del orden de 10 por ciento. Sin embargo, la frecuencia de resonancia que se obtiene en el sistema de un grado de libertad equivalente es siempre menor que la obtenida directamente con la teoría del semiespacio.

A fin de mejorar la aproximación del método de Lysmer, Whitman (ref 19) sugiere introducir una masa adicional al sistema; el efecto de esta es hacer coincidir la frecuencia de resonancia del sistema equivalente con la que se obtiene directamente con la teoría del semiespacio. Para ello, se aproxima la curva de la función X_1 a la de una parábola de ecuación

$$X_1 = 1 - \xi a_0^2 \quad (11)$$

Al sustituir la ec 11 en la 10, se obtiene

$$\left(M + \frac{4\xi}{1-\nu} \rho R^3\right) \ddot{w} + cX_2 \dot{w} + k_v w = P \quad (12)$$

O sea, que el valor de la masa adicional está dado por

$$\frac{4\xi}{1-\nu} \rho R^3$$

Dicha masa es la que se conoce como *masa efectiva de suelo*.

4.4 Parámetros para diferentes modos de vibración

Para modos de vibración diferentes del vertical, el procedimiento que se sigue en la obtención de los parámetros equivalentes es similar al ya señalado. La tabla 1 contiene un resumen de los valores que se obtienen cuando la distribución de esfuerzos es la de una placa rígida en un medio elástico.

Dado que k y D_0 dependen de la distribución de esfuerzos (fig 10), la tabla 1 debe usarse con cierta precaución, por ejemplo, si se expresa el valor de k_v en términos de un coeficiente K , es decir, $k_v = \frac{KGR}{1-\nu}$, los valores de este coeficiente varían, según muestra la tabla 2.

5. EFECTOS DE LA ESTRATIFICACION Y DEL ENCAJONAMIENTO

Entre los efectos que influyen en el parámetro k están el del encajonamiento y el de la proximidad de la roca basal con el nivel de desplante. Al respecto, en la fig 11, H_1 es la distancia de la base de la cimentación a la roca, y H_2 la profundidad de encajonamiento; en todos los casos el coeficiente k está normalizado al k correspondiente a una profundidad infinita de la roca. En dicha figura se pueden hacer las siguientes observaciones:

1. Para el modo vertical, el valor de k es fuertemente influido por la presencia de la roca ($H_1/R < 4$) y por la profundidad del encajonamiento
2. Para el modo horizontal, el efecto del encajonamiento es mayor que en el caso vertical, y el efecto de la proximidad de la roca es un poco menor
3. Para el movimiento de cabeceo, el efecto de encajonamiento es más acentuado que en los demás tipos de movimiento; la influencia de la proximidad de la roca es, sin embargo, pequeña
4. Para la torsión, los coeficientes de rigidez son también influidos notablemente por efecto del encajonamiento, y muy poco por la proximidad de la roca. En la ref 20 se presenta un procedimiento para tomar en cuenta el caso de varios estratos en el cálculo de k .

Dos de los investigadores que más han analizado el caso de una masa sobre un estrato son Kobori (ref 21) y Luco (ref 16). De acuerdo con este último, los efectos principales de la estratificación, cuando el estrato superficial que se analiza es relativamente poco profundo y existe un contraste fuerte entre las velocidades de propagación de ondas de dicho

estrato y la roca basal, son un aumento del coeficiente de rigidez y una disminución en el coeficiente de amortiguamiento. Las gráficas que Luco presenta indican que ambos coeficientes son altamente dependientes de la frecuencia de excitación. La fig 12 ilustra esta dependencia para el caso del modo horizontal.

Kobori señala que para el caso de una zapata cuadrada de ancho B, sujeta a una fuerza horizontal periódica $P = P_0 e^{i\Omega t}$, la relación entre el desplazamiento u y la fuerza P es la misma que para el caso del medio espacio, esto es:

$$u = \frac{P_0 e^{i\Omega t}}{GB/2} (f_1 - i f_2)$$

solo que las funciones f_1 y f_2 dependen ahora de la relación H/B. La fig 13 presenta valores típicos de las dos funciones; las singularidades que se observan se deben a las frecuencias correspondientes a las vibraciones libres del estrato donde f_1 y f_2 tienden al infinito.

El encajonamiento de las cimentaciones dentro del suelo, además de un incremento en la rigidez (y por tanto en la frecuencia de resonancia) produce otro en el amortiguamiento. Desde el punto de vista de amortiguamiento, el criterio tradicional de desprestigiar el efecto del encajonamiento es siempre conservador; sin embargo, desde el punto de vista de la rigidez, esto no es cierto cuando la frecuencia de operación es mayor que la de resonancia calculada desprestigiar dicho efecto. Experimentalmente, se ha observado que el aumento del amortiguamiento varía en la misma proporción en que la frecuencia de resonancia se incrementa, por ejemplo, si k_v aumenta dos veces por efecto del encajonamiento, f_r y D lo hacen aproximadamente $\sqrt{2}$ veces (ref 19). Otra forma de estimar la variación del amortiguamiento con la profundidad de encajonamiento, es a través de la gráfica que Stoke y Richart presentan en uno de sus trabajos y que fue obtenida a partir de resultados experimentales realizados en modelos de zapatas (fig 14).

Girard y Picard (ref 22) sugieren el uso de las siguientes fórmulas empíricas, deducidas a partir de resultados experimentales obtenidos en zapatas cuadradas.

$$k = k_0 \sqrt[3]{1 + (4h/\bar{D})}$$

$$D = D_0 \sqrt[4]{[1 + (4h/\bar{D})]^3}$$

donde

\bar{D} Ancho o diámetro de la cimentación

D_0 constante del amortiguamiento para una cimentación superficial

h profundidad de encajonamiento

k_0 constante del resorte para una cimentación superficial

Con base en un trabajo realizado por Novak y Beredugo, Whitman (ref 23) obtuvo la siguiente tabla, que da las relaciones de k/k_0 y D/D_0 en los modos vertical, horizontal y de cabeceo. Posiblemente, las relaciones de la tabla 3 proporcionen los mejores valores de la rigidez y el amortiguamiento correspondiente a zapatas encajonadas.

El empleo de elementos finitos sirve también de gran auxiliar en el estudio del comportamiento dinámico de las cimentaciones y de los efectos producidos por la estratificación y el encajonamiento; algunos trabajos al respecto son los de Lysmer (ref 17), y Kausel (refs 24 a 26). Este último, mediante un modelo tridimensional axisimétrico, sometido a cargas dinámicas o desplazamientos no axisimétricos, obtuvo, para el caso de cimentaciones circulares apoyadas en la superficie de un medio elástico de profundidad infinita, valores de la rigidez y del amortiguamiento muy similares a los que se obtienen en el semiespacio elástico. En su análisis del efecto de la proximidad de la roca, Kausel encuentra que las rigideces estáticas para los modos horizontal y de cabeceo (los únicos que analizó), se pueden obtener mediante

a) Movimiento horizontal

$$k_h = \frac{8GR}{2-\nu} \left(1 + \frac{1}{2} \frac{R}{H}\right)$$

para $R/H \leq 1/2$

b) Movimiento de cabeceo

$$k_T = \frac{8GR^3}{3(1-\nu)} \left(1 + \frac{1}{6} \frac{R}{H}\right)$$

para $R/H \leq 1/2$

La limitación de $R/H \leq 1/2$ se debe a que para valores mayores que esta relación, las expresiones sobrestiman las rigideces estáticas.

En cuanto al estudio tridimensional del efecto de encajonamiento a través del elemento finito, Kausel presentó algunos resultados aunque no los suficientes para sacar

conclusiones prácticas. Sin embargo, es muy factible que en un futuro próximo sea el método de elementos finitos el que permita estudiar más convenientemente las distintas modalidades que existen en los casos reales.

6. RESPUESTA DE CIMENTACIONES EN UN MEDIO VISCOELASTICO

Para fines de diseño, es importante tomar en cuenta el amortiguamiento interno del sistema, es decir, el amortiguamiento histerético o viscoso. Para ello se pueden emplear los resultados de Veletsos y Verbic (ref 15) en su estudio sobre cimentaciones vibrando en un medio viscoelástico.

Una forma más simple de considerar el amortiguamiento interno, aunque desde luego menos aproximado, es aplicar el criterio sugerido por Whitman y Richart (ref 27); dicho criterio consiste en determinar los efectos combinados de los amortiguamientos radial e interno, suponiendo un valor típico de amortiguamiento interno de 0.05 y sumar este valor al amortiguamiento radial obtenido con la teoría elástica.

Este procedimiento simplificado de sumar directamente los amortiguamientos está basado en el estudio de los resultados obtenidos por Lee (ref 28) en su trabajo sobre cimentaciones en un medio viscoelástico, y en la comparación de los resultados que se obtienen, en las respuestas máximas, entre los valores exactos y los obtenidos de sumar los dos amortiguamientos; ambos valores resultaron muy parecidos (ref 23).

Para los modos vertical y horizontal, el amortiguamiento interno resulta relativamente poco importante con respecto al amortiguamiento radial; sin embargo, para los modos torsional y de cabeceo, el amortiguamiento radial es muy pequeño y el interno resulta importante. La tabla 4 presenta un resumen de algunos datos disponibles relacionados con el amortiguamiento interno en suelos al nivel de los esfuerzos que ocurren en cimentaciones de maquinaria.

Una forma de estudiar directamente el efecto del amortiguamiento interno es a través del método de elementos finitos. En uno de los trabajos de Kausel y Roesset (ref 26), se indica que el efecto principal de dicho amortiguamiento es la suavización de las curvas que señalan la variación que en realidad tienen los coeficientes de rigidez y amortiguamiento con la frecuencia de excitación; la fig 15 ilustra este efecto para los modos horizontal y cabeceo, y en ella se puede ver la gran dependencia que pueden tener estos coeficientes en el amortiguamiento interno, cuando la proximidad de la roca es relativamente pequeña.

7. CIMENTACIONES CUADRADAS O RECTANGULARES

Si la forma de la cimentación es cuadrada o rectangular, el valor de k se puede obtener en forma aproximada con la tabla 5 y la gráfica de la fig 16. Los valores con este método

semiempírico son prácticamente iguales a los calculados con la teoría exacta de Elorduy (refs 29 y 30). Existen también estudios de cimentaciones rectangulares sobre un medio viscoelástico (ref 31); aunque los resultados obtenidos no se han presentado en forma práctica.

En cuanto a los valores de amortiguamiento, D_0 , y la masa efectiva, M_{ef} , de cimientos cuadrados o rectangulares, estos se obtienen mediante una cimentación circular equivalente, la que debe tener la misma área (cuando los movimientos son verticales u horizontales) o el mismo momento de inercia (en el caso de cabeceo) que la cimentación rectangular; el radio de una base circular equivalente será

$$R = \frac{BL}{\pi} \quad \text{para movimiento horizontal o vertical}$$

$$R = \sqrt{\frac{4BL^2}{3\pi}} \quad \text{para cabeceo}$$

Una vez establecida la cimentación equivalente, se podrán emplear las tablas disponibles para bases circulares, por ejemplo, la tabla 1.

8. DETERMINACION DEL MODULO G

La rigidez k influye directamente en la determinación de la frecuencia de resonancia y la magnitud de los movimientos a frecuencias relativamente bajas y/o iguales a la de resonancia. Estas y algunas otras razones hacen que sea el parámetro más importante en el diseño de cimentación de máquinas. Dos de las características del suelo que influyen directamente en su valor, son G y ν .

En la mayoría de los suelos, el valor de ν varía en un intervalo relativamente estrecho: 0.35 y 0.4 en arenas, y cerca de 0.5 en arcillas saturadas; en cambio, el valor de G depende del nivel de deformaciones y es función fundamentalmente de ϵ y $\bar{\sigma}_0$. (Existen algunos otros factores que influyen en el valor de G , tales como los efectos de duración de la carga aplicada y el de la historia de esfuerzos que Richart (ref 32) menciona en uno de sus trabajos; sin embargo, dichos efectos son secundarios en comparación con ϵ y $\bar{\sigma}_0$.)

La determinación de G se puede hacer mediante los procedimientos que a continuación se indican:

Conjunto de formulas

Existen formulas semiempiricas que dan el valor de G para niveles de deformacion menores de 10^{-5} cm/cm (en dichos niveles el comportamiento del suelo es prácticamente elástico-lineal). Quizá la fórmula más común es la de Hardin y Drnevich (ref 33), que proporciona muy buenos resultados para valores pequeños de la relación de vacíos ($e \leq 2.0$), y es, además, válida tanto para suelos cohesivos como no cohesivos.

$$G = 1200 \frac{(3-e)^2}{1+e} (\text{OCR})^a (\bar{\sigma}_0)^{1/2} \quad (13)$$

donde σ_0 y G deben estar en lb/pulg²

$$\bar{\sigma}_0 = \frac{\bar{\sigma}_1 + \bar{\sigma}_2 + \bar{\sigma}_3}{3}$$

OCR es la relación de preconsolidación ($\sigma_{\text{máx}}/\bar{\sigma}_0$) y a depende del índice de plasticidad (fig 17).

Para el caso de arenas, Seed (ref 34) emplea la expresión

$$G = 1000K_2 (\bar{\sigma}_0)^{1/2}$$

donde K_2 depende de la densidad relativa (tabla 6).

Puesto que G es función de los esfuerzos efectivos que se tienen en el sitio, y la resistencia no drenada de suelos normalmente consolidados, S_u , también lo es, debe suponerse que G se puede obtener a partir de S_u ; al respecto, Whitman (ref 19) recomienda emplear

$$G = 1600 S_u$$

para valores de deformación angular entre 10^{-5} y 10^{-6} .

Pruebas de laboratorio

Resonancia en una columna de suelo. Este procedimiento consiste en aplicar un momento torsionante en la parte superior de una probeta cilíndrica de suelo, y obtener las frecuencias en las que ocurren los valores de respuesta máximos; es decir, las frecuencias de resonancia. Para el caso en que la probeta esté fija en su base y libre en su parte superior, las frecuencias de resonancia están dadas por:

$$f_n = (2n-1) \frac{C_s}{4H} \quad (14)$$

donde

n número entero (= 1 para el modo fundamental)

H altura de la probeta

C_s velocidad de onda al cortante

De la ec. 14 se obtiene C_s , y el valor de G mediante

$$G = \rho C_s^2 \quad (15)$$

Técnica pulsativa. Consiste en colocar varios cristales piezoeléctricos en cada extremo de una probeta de suelo, y aplicar un pulso eléctrico en los cristales de uno de los extremos (ref 19). Dichos cristales están manufacturados en forma tal que producen una distorsión al cortante cuando se aplica un pulso eléctrico, con lo que se origina una onda transversal de esfuerzos que pasa a través de la probeta de suelo. La onda es registrada en el otro extremo y su velocidad se determina directamente mediante

$$C_s = \frac{H}{\Delta t}$$

Donde Δt es el tiempo que tardó la onda en ir de un extremo al otro.

Pruebas de campo

Ejemplo de un pequeño vibrador. Esta técnica estriba en medir la longitud de onda superficial que genera un vibrador, trabajando a una determinada frecuencia, en la superficie del terreno (fig 18). La longitud de onda se determina moviendo un receptor a lo largo de una línea radial al eje del vibrador, y localizando los puntos que están en fase (refs 1 y 35). Al cambiar la frecuencia de excitación, se puede variar la longitud de onda y, por tanto, la profundidad de inspección. Una regla semiempírica es suponer que el módulo calculado mediante este procedimiento, corresponde al valor que dicho módulo tiene a una profundidad del suelo igual a $\lambda/2$ (λ , longitud de onda)

Métodos geofísicos. Se pueden utilizar en forma indirecta para calcular G. En efecto, mediante los procedimientos que se emplean para determinar las velocidades de propagación de ondas dilatantes, se puede hacer uso de las relaciones que existen entre C_D (velocidad de ondas dilatantes) y C_s . La relación está dada por

$$C_s = \sqrt{\frac{1-2\nu}{2(1-\nu)}} C_D$$

Teniendo C_s , el valor de G se obtiene mediante la ec 15.

Como se puede observar, la relación de Poisson, ν , debe conocerse para el empleo de esta técnica. Detalles de la forma como se realiza la medición de C_D mediante este procedimiento, pueden verse en las refs 5 y 36.

Método de hoyos en paralelo (cross-hole method). Este método (fig 19) consiste en determinar las velocidades de las ondas cortantes que se propagan y se detectan a diferentes profundidades en perforaciones hechas ex profeso. Cuando el transductor que capta la señal de salida se encuentra en la parte superior de la varilla de impulso (fig 19a), se debe hacer una corrección al tiempo de llegada a fin de considerar el tiempo que las ondas tardaron en viajar por dicha varilla. El proceso puede facilitarse en el osciloscopio si la dirección del impacto se cambia en el sentido opuesto; ello se debe a que las trazas generadas divergen en el momento en que las ondas cortantes llegan (fig 19b). Mayores detalles de este procedimiento, que es uno de los más empleados para determinar el módulo G a niveles pequeños de deformación, se pueden encontrar en las refs 5 y 37.

Ahora bien, tomando en cuenta que en general los esfuerzos efectivos y las características del suelo varían con la profundidad y, por tanto, el valor del módulo G también cambia, se presenta el problema de determinar la profundidad a la cual deberá escogerse el valor de G que se va a emplear en el cálculo de k . En general no existe un criterio único para la solución de este problema; se han propuesto varios procedimientos empíricos, algunos de los cuales se mencionan a continuación.

Quando se conoce C_s con la profundidad, Whitman (ref 19) recomienda usar la profundidad correspondiente al punto medio del bulbo de presiones; dicha profundidad está dada por

$$h = \frac{\bar{\sigma}_v}{\gamma_m} + \frac{3}{4} D$$

donde

- D diámetro (real o equivalente) de la cimentación
- $\bar{\sigma}_v$ 0.42 veces los esfuerzos estáticos aplicados en la superficie (o sea el esfuerzo vertical efectivo a la profundidad de $3/4 D$, originado por el peso de la cimentación y la maquinaria).

Si se emplea la fórmula de Hardin y Drnevich para el cálculo de G , es recomendable también determinar los esfuerzos efectivos a la mitad del bulbo de presiones ($3/4 D$); es decir, $\bar{\sigma}_0$ se calcula en función de

1. $\bar{\sigma}_v$ y $\bar{\sigma}_h$ debidas al sobrepeso del suelo a esa profundidad
2. $\bar{\sigma}_v$ y $\bar{\sigma}_h$ producidas por el peso de la cimentación.

Richart et al (ref 5) propone que la profundidad equivalente sea aquella donde el valor de $\bar{\sigma}_0$, calculado a la orilla de la cimentación, sea mínimo (fig. 20).

9. ALGUNAS FORMAS PARA ESTIMAR DIRECTAMENTE k

Pruebas de placa

La estimación de k mediante pruebas de placa, se hace aplicando cargas repetidas (fig. 21). La magnitud de las cargas estáticas y dinámicas debe ser similar a la esperada.

Barkan (ref 38) registra excelentes correlaciones entre los valores estimados de la frecuencia de resonancia (calculados con los resultados de pruebas de placa) y los determinados experimentalmente.

Para extrapolar las rigideces obtenidas usando las placas de áreas pequeñas a las áreas reales del prototipo, se pueden utilizar las recomendaciones de Terzaghi (ref 39) para cargas estáticas; es decir

$$\text{Suelo cohesivo} \quad k_{\text{prototipo}} = k_{\text{placa}} \cdot \text{diám}^C$$

$$\text{Suelo no cohesivo} \quad k_{\text{prototipo}} = k_{\text{placa}} \cdot \text{diám} \left(\frac{C+1}{2} \right)^2$$

donde

$$C = \frac{\text{tamaño menor de la cimentación}}{\text{tamaño menor de la placa}}$$

Pruebas a base de un vibrador

La prueba consiste en colocar un pequeño vibrador sobre una placa de 12 a 30 pulg de diámetro. La frecuencia de excitación se varía hasta alcanzar la condición de resonancia, y el valor de k se obtiene mediante

$$k = (f_r \cdot 2\pi)^2 M$$

donde

M masa del vibrador y placa + la masa efectiva del suelo

Los resultados que se obtienen con este procedimiento son muy similares a los de la prueba de placa, solo que la interpretación correcta de los datos resulta más complicada y difícil.

Correlaciones con el módulo de reacción

Para análisis preliminares de diseño, pueden emplearse las correlaciones que existen entre las constantes de resorte y el llamado módulo de reacción elástico. Dichas correlaciones son:

movimiento vertical $k_v = c_v A$

movimiento horizontal $k_h = c_h A$

movimiento de cabeceo $k_r = c_r I'$

movimiento torsionante $k_\phi = c_\phi I''$

donde

A área de contacto entre la cimentación y el suelo

I' segundo momento del área de contacto alrededor del eje horizontal que pasa por el centroide del área y es normal al plano de cabeceo

I'' segundo momento del área de contacto alrededor del eje vertical que pasa por el centroide del área

Los coeficientes c_u , c_h , c_r y c_ϕ son los módulos de reacción que dependen del tipo de suelo, así como del tamaño y geometría de la cimentación. Existen, sin embargo, tablas que relacionan dichos coeficientes solo en función del tipo de suelo; al respecto, Barkan (ref 38) proporciona la tabla 7.

9.1 Cimentaciones piloteadas

Desafortunadamente, esta parte de la dinámica de suelos no se ha desarrollado lo suficiente como para ofrecer métodos racionales aplicables a toda clase de problemas prácticos.

Dentro de los métodos más simples y más prácticos está el propuesto por Maxwell *et al* (ref 40), el cual se basa en los resultados que se obtienen a partir de pruebas dinámicas realizadas en pilotes prototipo, sobre los cuales se coloca un oscilador en el que varía la frecuencia de excitación (fig 22). Los parámetros del sistema equivalente de un grado de libertad obtenidos a partir de los datos observados y recomendados por estos investigadores para el modo vertical (el único que estudiaron), son:

$$k = \frac{Q_1}{W} \cos \alpha + M \Omega^2$$

$$c = \frac{Q_1}{\Omega W} \sin \alpha$$

donde

k constante del resorte

c coeficiente de amortiguamiento

- M masa sobre el terreno, que incluye la del oscilador, el cabezal y la carga estática
- Q fuerza de excitación periódica
- Q_1 amplitud de la fuerza de excitación
- t tiempo
- w desplazamiento periódico
- W amplitud del desplazamiento
- α ángulo de fase entre Q_1 y W
- Ω frecuencia circular, en rad/seg

En la resonancia α es aproximadamente 90° y la expresión anterior de la rigidez se reduce a la siguiente

$$k_0 = M\Omega_0^2$$

donde Ω_0 es la frecuencia observada de resonancia.

Considerando que el amortiguamiento crítico c_c vale $2M\Omega_0$, la relación de amortiguamiento

se obtiene mediante $D = \frac{c}{c_c}$, y el desplazamiento máximo por $W = \frac{Q_1}{2k_0 D}$

En pruebas experimentales realizadas por Maxwell *et al* en pilotes circulares de concreto y de acero con sección H, se encontró que los amortiguamientos a la frecuencia de resonancia eran relativamente pequeños (del orden de $D_0 = 0.06$) y que la rigidez dinámica aumentaba considerablemente si el cabezal se encontraba en contacto con el terreno natural, y ligeramente con el aumento de la carga estática.

Al considerar la variación de las frecuencias de excitación y definir como relación de rigideces a k/k_0 y de frecuencias a Ω/Ω_0 , los resultados experimentales de estos investigadores señalaron que, en general, la relación de rigideces disminuye y la del amortiguamiento se incrementa cuando la relación de frecuencias aumenta (fig 23). En lo que se refiere al grupo de pilotes, concluyen que se está del lado conservador si se considera como amortiguamiento para el grupo el obtenido a partir de pruebas en pilotes

individuales, y que la rigidez se puede considerar simplemente como la suma de las rigideces de cada pilote.

Boutwell y Saxema (ref 41) recomiendan, para el caso de pilotes de punta, utilizar el sistema de dos grados de libertad mostrado en la fig 24, donde:

m_f masa total del sistema cimentación-máquina

k_f rigidez de cada pilote; se obtiene mediante la teoría simple de columnas; por ejemplo, para el modo vertical $k_p = \frac{A_p E_p}{L_p}$, donde L_p , A_p y E_p son respectivamente longitud, área y módulo de elasticidad del pilote

K_f rigidez del grupo; es igual a la rigidez de cada pilote multiplicada por el número total de pilotes.

c_f amortiguamiento del sistema cimentación-máquina obtenido a través de vibraciones libres

m_s , c_s y k_s son los parámetros del suelo sobre el cual se apoyan los pilotes, y se obtienen mediante la teoría del semiespacio elástico (tabla 1). El problema principal en este procedimiento sugerido por Boutwell y Saxema estriba, precisamente, en la correcta determinación de estos últimos parámetros.

Para el movimiento vertical, la influencia que tiene la carga axial y la longitud del pilote sobre la frecuencia de resonancia en pilotes de punta se ilustra en la fig 25 obtenida por Richart (ref. 43). Dicha figura muestra que a medida que la carga axial se incrementa y/o la longitud del pilote aumenta, la frecuencia de resonancia disminuye. El mismo autor señala, en otro de sus trabajos (ref. 5), que la contribución de un pilote a la rigidez contra la torsión de una zapata, está dada por

$$k_t = K_h d^2 (EF)_m (EF)_F$$

donde

d diámetro del pilote

K_h módulo de reacción del suelo

- l longitud del pilote
- r radio de la zapata
- $(EF)_m$ factor de eficiencia para un pilote rígido que considera el efecto del movimiento del suelo
- $(EF)_F$ factor de eficiencia que considera la flexibilidad del pilote

Trabajos recientes realizados por Novak y Beredugo (refs 42,44 y 45) ofrecen resultados más realistas y por tanto más confiables. La tabla 8 señala los valores correspondientes a los coeficientes de rigidez y amortiguamiento para los distintos modos de vibración.

Las funciones $f_{11.1}$, $f_{11.2}$, etc, dependen de las características del suelo y del pilote y se obtienen a través de la tabla 9 y la fig 26.

De acuerdo con los resultados teóricos de Novak (ref 42), las cimentaciones piloteadas, en comparación con las cimentaciones por superficie, pueden tener mayores frecuencias naturales, menores amortiguamientos y mayores amplitudes en la resonancia. Como consecuencia de estos resultados, Novak establece que *"los pilotes pueden eliminar o reducir asentamientos permanentes, pero no pueden eliminar vibraciones"*.

10. CONCLUSIONES

La respuesta de cimentaciones superficiales de maquinaria se puede obtener a través de sistemas equivalentes de un grado de libertad, los que están constituidos por una masa concentrada que representa la masa de la maquinaria y la de la cimentación, uno o varios resortes que simulan la rigidez del suelo, y uno o varios amortiguadores que representan la pérdida de energía que ocurre en el sistema máquina-cimentación-suelo.

Los trabajos teóricos sobre la teoría del semiespacio elástico y viscoelástico que hasta la fecha se han desarrollado, permiten, desde el punto de vista matemático, evaluar correctamente los parámetros de diseño que rigen los sistemas equivalentes. Faltan, sin embargo, datos experimentales que permitan determinar la influencia que puedan tener otros factores en el verdadero comportamiento de los sistemas reales.

Para el caso de cimentaciones piloteadas, existen procedimientos que utilizan sistemas de uno o más grados de libertad; sin embargo, el método sugerido por Novak es el que hasta ahora ofrece mejores bases y es por tanto el más recomendable. El empleo de programas de elementos finitos puede ofrecer, en un futuro próximo, considerable auxilio en el análisis de esta clase de cimentaciones profundas.

Los efectos principales del encajonamiento de la cimentación es aumentar la rigidez y el amortiguamiento. En lo que se refiere a la estratificación, los efectos que se pueden tener por el hecho de permanecer la roca basal a relativa poca profundidad, es un aumento en el coeficiente de rigidez y una disminución en el coeficiente de amortiguamiento; dichos efectos resultan prácticamente despreciables cuando la relación H/R (profundidad de la roca/radio de la cimentación) es mayor de 5.

En comparación con las cimentaciones por superficie, las cimentaciones piloteadas pueden tener mayores frecuencias naturales (como consecuencia del aumento en la rigidez), menores amortiguamientos y mayores amplitudes en la resonancia.

11. RECONOCIMIENTO

Se agradece muy sinceramente al Dr. Jacobo Bidlak la revisión del manuscrito original y sus valiosas sugerencias. Este trabajo fue patrocinado por la Secretaría de Asentamientos Humanos y Obras Públicas, a la que el autor agradece profundamente las facilidades prestadas.

12. REFERENCIAS

1. Flores, J R, Técnicas vibratorias de evaluación en pavimentos, *Instituto de Ingeniería, UNAM, Informe interno (1975)*
2. Flores, J R, Lineamientos generales en el diseño de cimentaciones de maquinaria, *Ingeniería (1977), Próxima publicación*
3. Nieto, J A y Reséndiz, D, Criterios de diseño para cimentaciones de maquinaria, *Instituto de Ingeniería, UNAM, 131 (jul 1967)*
4. Biggs, J M, *Introduction to structural dynamics, Mc Graw-Hill Book Co, Nueva York (1964)*
5. Richart, F E, Jr, Hall, J R y Woods, R D, *Vibrations of soils and foundations, Prentice Hall, Inc, Englewood Cliffs, Nueva Jersey (1970)*
6. Reissner, E, Stationäre, axialsymmetrische durch eine schüttelnde masse erregte schwingungen eines homogen elastischen halbraumes, *Ingenieur Archiv, 7, Parte 6 (dic 1936), 381-96*

7. Lamb, H, On the propagation of tremors over the surface of an elastic solid, *Philosophical Transactions of the Royal Society, Serie A*, 203, Londres (1904), 1-42
8. Quinlan, P M, The elastic theory of soil dynamics, *Symposium on Dynamic Testing of Soil*, ASTM, STP-156 (1953), 3-34
9. Sunj, T Y, Vibrations in semi-infinite solids due to periodic surface loadings, *Symposium on Dynamic Testing of Soils*, ASTM, STP-156 (1953), 35-64
10. Lycroft, G N, Forced vibrations of a rigid circular plate on a semi-infinite elastic space and on an elastic stratum, *Philosophical Trans, Royal Society, Serie A*, 248, Londres (1956), 327-68
11. Avciobi, A O y Grootenbuis, P, Vibration of rigid bodies on semi-infinite elastic media, *Procs, Royal Society*, 287, Londres (1965), 27-63
12. Robertson, I A, Forced vertical vibration of a rigid circular disc on a semi-infinite elastic solid, *Procs, Cambridge Philosophical Society*, 62 (1966), 547-53
13. Veletsos, A S y Wei, Y T, Lateral and rocking vibration of footings, *Procs, ASCE*, 97, SM-9 (1971), 1227-48
4. Luco, J E y Westmann, R A, Dynamic response of circular footings, *Procs, ASCE*, 97 EM-5 (1971), 1381-95
15. Veletsos, A S y Verbic, B, Vibration of viscoelastic foundations, *Earthquake Engineering and Structural Dynamics*, 2 (1973), 87-102
16. Luco, J E, Impedance functions for a rigid foundation on a layered medium, *Nuclear Engineering and Design* 31, North-Holland Publishing Co (1974), 204-17
17. Lysmer, J y Kuhlemeyer, R L, "Finite dynamic model for infinite media"; *Procs, ASCE*, 95, EM-4 (1969), 859-77
18. Lysmer, J, "Vertical motion of rigid footings", Department of Civil Engineering, University of Michigan, Informe a WES Contract, 3-115 (1965)
19. Whitman, R V, "Notas de dinámica de suelos", Massachusetts Institute of Technology (1973)

20. Johnson, G R, Christiano, P y Howard, I, "Stiffness coefficients for embedded footings", *Journal of the Geotechnical Engineering Division, ASCE*, 101, GT-8 (1975), 789-800
21. Kobori et al, "Dynamic ground compliance of rectangular foundation on an elastic stratum over a semi-infinite rigid medium", *Institute for Preventing Failures, Universidad de Tokio, Japón* (mar 1968)
22. Girard, J y Picard, J, *Etude experimentale du dynamique de massifs de foundation de machine, Annales de L'Institute Technique et des Travaux Publics*, 273 (1970)
23. Whitman, R V, *Soil-Structure interaction and foundation design, Fundamentals of Soil Engineering for Buildings, Cap XIII, Massachusetts Institute of Technology* (1972)
24. Kausel, E, *Forced vibrations of circular foundations on layer media, Tesis Doctoral, MIT* (1974)
25. Kausel, E, Roesset, J M y Wass, G, *Dynamic analysis of footing on layered media, Procs, ASCE*, 101, EM-5 (1975), 679-95
26. Kausel, E y Roesset, J M, *Dynamic stiffness of circular foundation, Procs, ASCE*, 101, EM-6 (1975), 771-85
27. Whitman, R V y Richart, F E, Jr., *Design procedures for dynamically loaded foundations, Journal Soil Mechanical and Foundations Division, Procs, ASCE*, 93, SM-6 (nov 1967), 169-93
28. Lee, J M, *Dynamic surface loading on a viscoelastic half-space, School of Engineering, San Fernando Valley State College, California* (1968)
29. Elorduy, J, Nieto, J A y Szekely, M, *Dynamic response of bases of arbitrary shape subjected to periodic vertical loading, Procs, International Symposium on Wave Propagation and Dynamic Properties of Earth Material, Albuquerque* (ago 1967)
30. Flores, J R, *Validity of approximate rules for square and rectangular foundations, Soil Dynamics Terra Project, Department of Civil Engineering, MIT, Cambridge, Mass* (1968)

31. Kobori et al, Dynamic ground compliance of rectangular foundations on a semi-infinite viscoelastic medium, *Disaster Prevention Research Institute of Kyoto University, Informe anual, 11A (1968), 367-377*
32. Richart, F E, Jr., Some effects of dynamic soil properties on soil-structure interaction, *Journal of the Geotechnical Division, Proc, ASCE 101, GT12 (1975), 1197-240*
33. Hardin, B D y Drnevich, V P, Shear modulus and damping in soils II. Design equations and curves, *Journal of the Soil Mechanical and Foundations, Division, Proc, ASCE, 98, SM-7 (jul 1972), 667-92*
34. Seed, H B e Idress, I M, Soil moduli and damping factors for dynamic response analysis, EERC 70-10, *University of California, Berkeley (dic 1970)*
35. Blain, J, Generalite's sur le vibreur Goodman, *Bol des Laboratoires Routiers, Paris (1968)*
36. Mooney, H M, Seismic shear waves in engineering, *Journal of the Geotechnical Engineering Division, ASCE, 100 GT8, Paper 10745 (ago 1974), 905-23*
37. Richart, F E, Jr. y Whitman, R V, Comparison of footing vibration test with theory, *Journal Soil Mechanical and Foundations Engineering Division, ASCE, 93, SM-6 (nov 1967), 143-68*
38. Barkan, D D, "Dynamics of bases and foundations", *Mc Graw-Hill Book Co, Nueva York (1962)*
39. Terzaghi, K, Evaluation of coefficients of subgrade reaction *Geotechnique (1955), 297-326*
40. Maxwell, A A, Fry, Z V y Poplin, J K, Vibratory loading of pile foundations: Performance of Deep Foundations, *ASTM STP 444, American Society for Testing and Materials (1969), 338-61*
41. Boutwell, G P y Saxema, D S, Design method for dynamically loaded pile foundations, *ASCE Annual and National Environmental Engineering, Meeting Preprint No 1833 (oct 1972)*

42. Novak, M, Dynamic Stiffness and Damping of Piles, *Can. Geotech. J.*, 11 (1974) 574-98.
43. Richart, F E, Jr., Foundation Vibrations, *Trans. ASCE*, 127, Parte 1 (1962), 863-98
44. Beredugo, Y O y Novak M, Coupled horizontal and rocking-vibration of embedded footings, *Can. Geotech. J.*, 9, 4 (1972), 477-97
45. Novak, M y Beredugo, Y O, Vertical vibration of embedded footings, *J. Soil Mech. Found. Div. ASCE.*, 12 (1972), 1291-310
46. Lambe, T W y Whitman, R V, *Soil mechanics*, John Wiley & Sons Inc, Nueva York (1969), 228
47. Whitman, R V, Analysis of foundations vibrations, *Procs, Vibration in civil engineering*, Butterworths, Londres (1966)
48. Stokoe, K H y Richart, F E, Jr., Dynamic response of embedded machine foundations, *Procs. ASCE*, 98, SM-5, informe 8904 (may 1972), 443-60

TABLA 1. VALORES DE LOS PARAMETROS EQUIVALENTES EN CIMENTACIONES CIRCULARES* APOYADAS EN UN SEMIESPACIO ELASTICO (ref 19)

TIPO DE EXCITACION	RELACIONES DE MASAS MODIFICADAS	k	D ₀	M _{of}
Vertical	$B_v = \frac{1-\nu}{4} b$	$\frac{4GR}{1-\nu}$	$\frac{0.425}{\sqrt{B_v}}$	$0.27 \frac{M}{B_v}$
Horizontal	$B_h = \frac{2-\nu}{8} b$	$\frac{8GR}{2-\nu}$	$\frac{0.29}{\sqrt{B_h}}$	$0.095 \frac{M}{B_h}$
Cabeceo	$B_r = \frac{3(1-\nu)}{8} \frac{I}{R^3}$	$\frac{8GR^3}{3(1-\nu)}$	$\frac{0.15}{(1+B_r)\sqrt{B_r}}$	$0.24 \frac{1}{B_r}$

* Los valores se obtuvieron de igualar las amplitudes máximas determinadas con la teoría del semiespacio, con las determinadas con los sistemas equivalentes

I momento de inercia de la masa con respecto al eje de giro

TABLA 2. VALORES DE K PARA DISTINTOS TIPOS DE DISTRIBUCION DE ESFUERZOS (ref 19)

DISTRIBUCION DE ESFUERZOS	K	$\frac{(1-\nu)}{K}$, para $\nu = 1/4$
Base rígida	4	0.188
Uniforme	π	0.239
Parabólica	$(3/4)\pi$	0.319

TABLA 3. EXPRESIONES APROXIMADAS PARA CONSIDERAR EL EFECTO DE ENCAJONAMIENTO

MODO	k/k_0	D/D_0
Vertical	$1 + 0.6 (1-\nu) \frac{h}{R}$	$\frac{1 + 1.9 (1-\nu) h/R}{\sqrt{k/k_0}}$
Horizontal	$1 + 0.55 (2-\nu) \frac{h}{R}$	$\frac{1 + 1.9 (2-\nu) h/R}{\sqrt{k/k_0}}$
Cabeceo	$1 + 1.2 (1-\nu) \frac{h}{R} + 0.2 (2-\nu) \left(\frac{h}{R}\right)^3$	$\frac{1 + 0.7 (1-\nu) \frac{h}{R} + 0.6 (2-\nu) \left(\frac{h}{R}\right)^3}{\sqrt{k/k_0}}$

TABLA 4. AMORTIGUAMIENTO INTERNO EN SUELOS (ref 27)

TIPO DE SUELO	AMORTIGUAMIENTO EQUIVALENTE
Arenas y gravas secas	0.03 a 0.07
Arena saturada o seca	0.01 a 0.03
Arenas y gravas saturadas	0.05 a 0.06
Arcilla	0.02 a 0.05
Arena limosa	0.03 a 0.10

TABLA 5. CONSTANTES DE RESORTE PARA UNA BASE RECTANGULAR RIGIDA APOYADA EN EL SEMIESPACIO

MOVIMIENTO	CONSTANTE DE RESORTE*
Vertical	$k_v = \frac{G}{1-\nu} \beta_v \sqrt{BL}^{**}$
Horizontal	$k_h = 2(1+\nu) G \beta_h \sqrt{BL}$
Cabeceo	$k_r = \frac{G}{1-\nu} \beta_r BL^2$

* Los valores de β_v , β_h y β_r están dados por la fig 16

** B = ancho de la cimentación y L = longitud de la cimentación (en el plano de rotación en caso de cabeceo)

TABLA 6. VALORES DE K_2 VS DENSIDAD RELATIVA

DENSIDAD RELATIVA	K_2
30	34
40	40
60	52
75	62
90	70

TABLA 7. VALORES DE DISEÑO RECOMENDADOS POR BARKAN PARA c_v *

TIPO DE SUELO	CAPACIDAD DE CARGA ESTÁTICA PERMISIBLE, en kg/cm^2	COEFICIENTE c_v , en kg/cm^3
Suelos blandos	<1.5	<3
Suelos de resistencia media	1.5 - 3.5	3 - 5
Suelos resistentes (arcillas duras o arenas compactas)	3.5 - 5	5 - 10
Rocas	>5	>10

Los valores de c_h , c_r y c_ϕ se pueden estimar con las relaciones

$$c_h = c_v/2; c_r = 2c_v; c_\phi = \frac{3}{4} c_v$$

TABLA 8. COEFICIENTES DE RIGIDEZ Y AMORTIGUAMIENTO EN LA TEORIA DE NOVAK (ref 42)

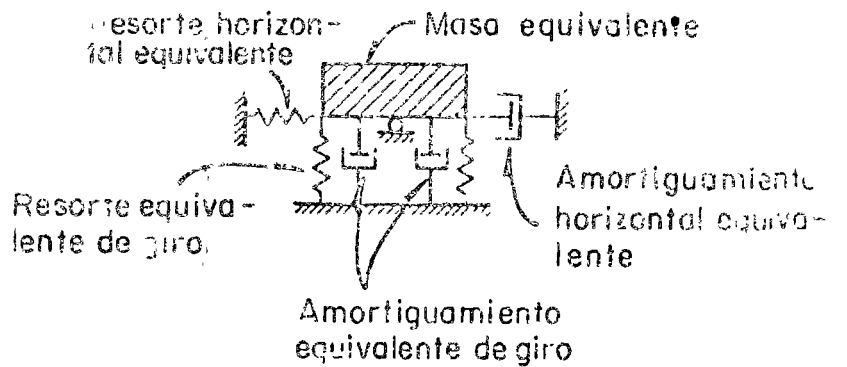
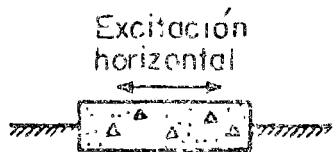
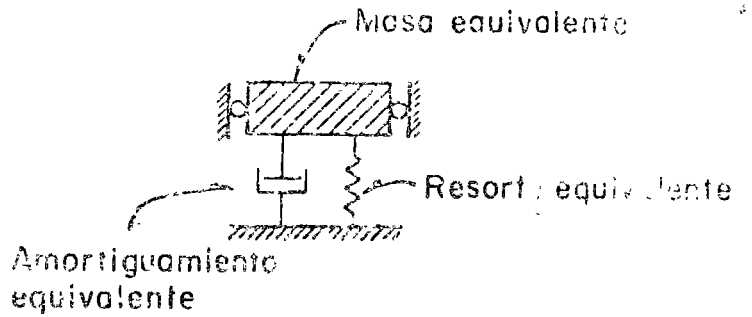
MODO	k	c
Vertical	$\frac{E_p A}{r_0} f_{18.1}$	$\frac{E_p A}{V_s} f_{18.2}$
Horizontal	$\frac{E_p I}{r_0^3} f_{11.1}$	$\frac{E_p I}{r_0^2 V_s} f_{11.2}$
Cabeceo	$\frac{E_p I}{r_0} f_{7.1}$	$\frac{E_p I}{V_s} f_{7.2}$
Acopladas (horizontal y de cabeceo)	$\frac{E_p I}{r_0^2} f_{9.1}$	$\frac{E_p I}{r_0 V_s} f_{9.2}$

- A. área de la sección transversal del pilote
- E_p módulo de Young del pilote
- I momento de inercia de la sección transversal
- r_0 radio del pilote
- V_s velocidad de ondas cortantes en el suelo

Las funciones $f_{11.1}$, $f_{11.2}$ etc, dependen de las características del suelo y del pilote, y se obtienen a través de la tabla 9 y la fig 26.

TABLA 9. PARAMETROS DE RIGIDEZ Y AMORTIGUAMIENTO f_7 , f_9 y f_{11} PARA
 PILOTES DE MADERA Y DE CONCRETO CON $l/r_0 > 5$ (ref 42)

ν	$\frac{\rho}{\rho_p}$	$\frac{V_s}{V_c}$	PARAMETROS DE RIGIDEZ			PARAMETROS DE AMORTIGUAMIENTO		
			$f_{7,1}$	$f_{9,1}$	$f_{11,1}$	$f_{7,2}$	$f_{9,2}$	$f_{11,2}$
0.4	0.7 (Concreto)	0.01	0.202	-0.0194	0.0036	0.139	-0.0280	0.0084
		0.02	0.285	-0.0388	0.0100	0.200	-0.0566	0.0238
		0.03	0.349	-0.0582	0.0185	0.243	-0.0848	0.0438
		0.04	0.403	-0.0776	0.0284	0.281	-0.1130	0.0674
		0.05	0.450	-0.0970	0.0397	0.314	-0.1410	0.0942
0.4	2.0 (Madera)	0.01	0.265	-0.0336	0.0082	0.176	-0.0466	0.0183
		0.02	0.374	-0.0673	0.0231	0.249	-0.0932	0.0516
		0.03	0.459	-0.1010	0.0425	0.305	-0.1400	0.0949
		0.04	0.529	-0.1350	0.0654	0.352	-0.1860	0.1460
		0.05	0.592	-0.1680	0.0914	0.394	-0.2330	0.2040
0.25	0.7 (Concreto)	0.01	0.195	-0.0181	0.0032	0.135	-0.0262	0.0076
		0.02	0.275	-0.0362	0.0090	0.192	-0.0529	0.0215
		0.03	0.337	-0.0543	0.0166	0.235	-0.0793	0.0395
		0.04	0.389	-0.0724	0.0256	0.272	-0.1057	0.0608
		0.05	0.435	-0.0905	0.0358	0.304	-0.1321	0.0850
0.25	2.0 (Madera)	0.01	0.256	-0.0315	0.0074	0.169	-0.0434	0.0165
		0.02	0.362	-0.0630	0.0209	0.240	-0.0868	0.0465
		0.03	0.444	-0.0945	0.0385	0.293	-0.1301	0.0854
		0.04	0.512	-0.1260	0.0593	0.339	-0.1735	0.1315
		0.05	0.573	-0.1575	0.0828	0.379	-0.2168	0.1838



Excitación torsional



PLANTA

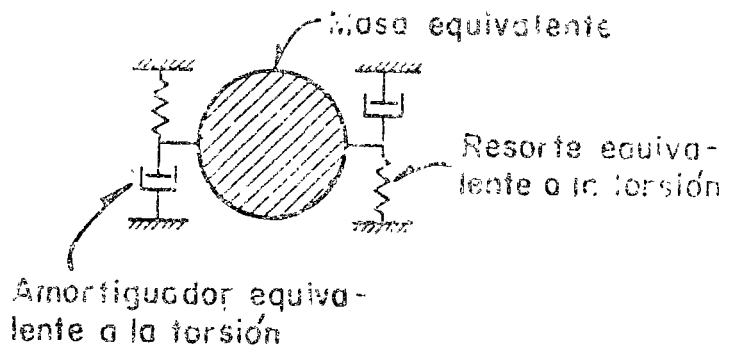


Fig 1 - Sistemas equivalentes típicos (ref 46)

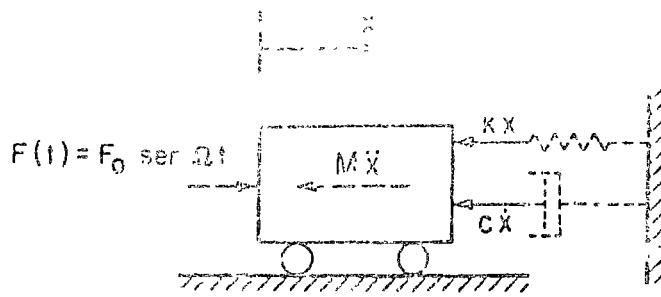


Fig 2. Fuerzas que actúan sobre un sistema de un grado de libertad

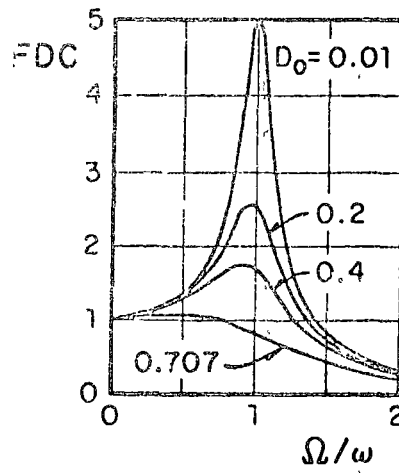


Fig 3. Curvas de amplificación

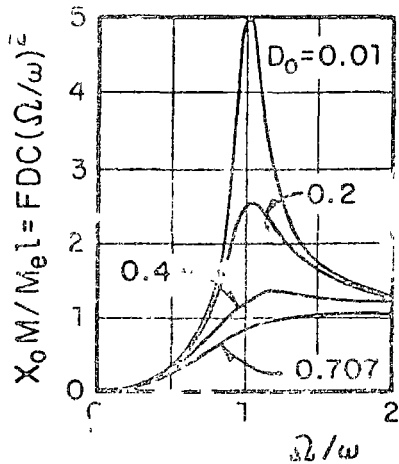
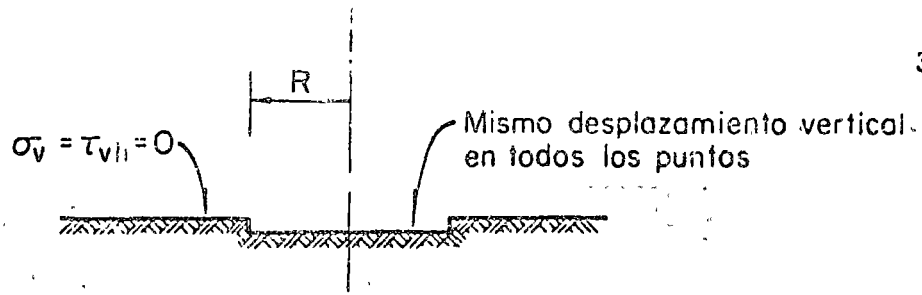
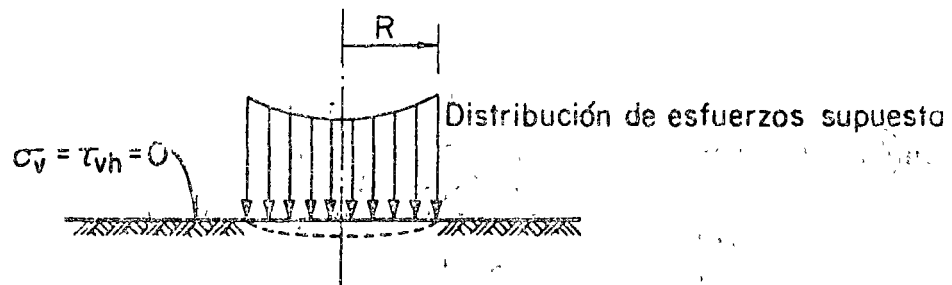


Fig 4. Curvas de respuesta en sistemas con masas excéntricas



a) Correcto establecimiento de las condiciones de frontera



b) Establecimiento aproximado de las condiciones de frontera

Fig 5. Condiciones de frontera (ref 19)

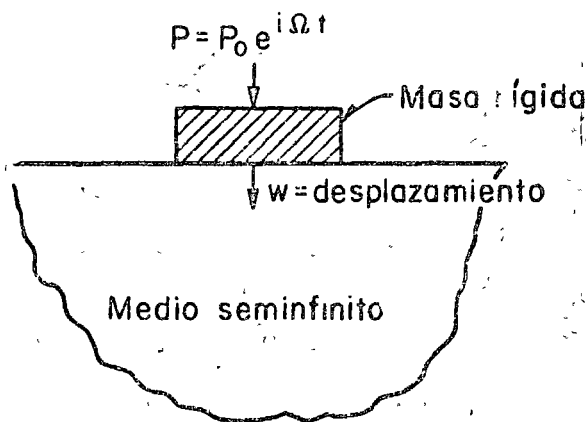


Fig 6a. Sistema de masa rígida en medio seminfinito (ref 19)

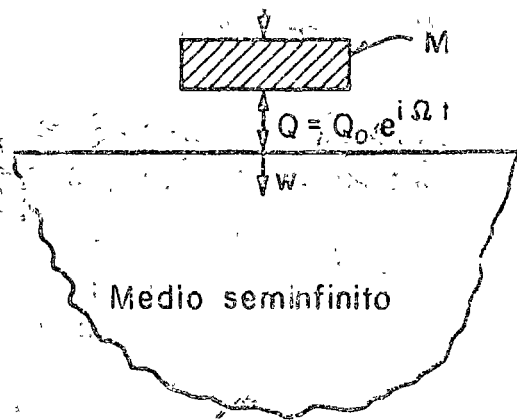


Fig 6b. Separación de las fuerzas que obran en el sistema (ref 19)

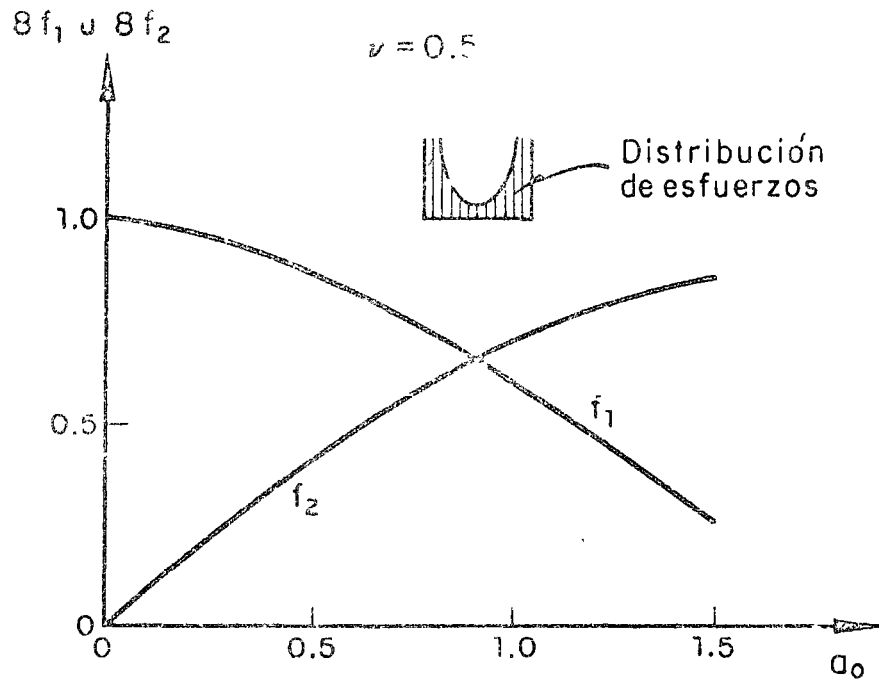
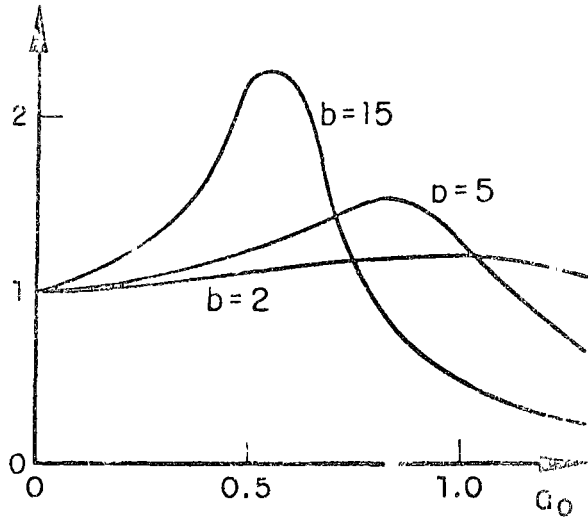


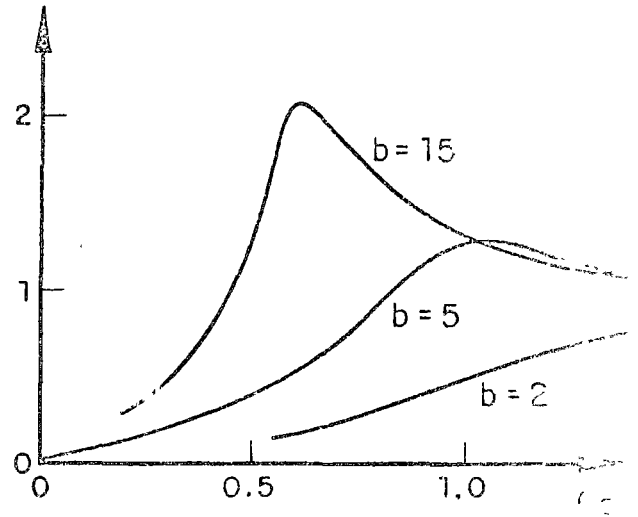
Fig 7. Valores de f_1 y f_2 en función de $a_0 = aR/C_s$

$$\frac{4GRW_0}{P_0(1-\nu)} = FDC_{m\acute{a}x}$$



(a)

$$\frac{W_0 M}{Me l}$$



(b)

Fig 8. Curvas de amplificación dinámica en el semiesfuerzo elástico

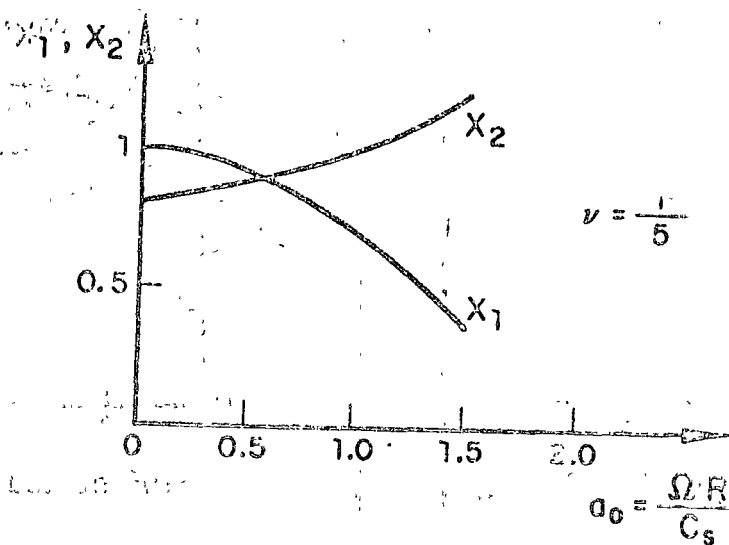


Fig 9. Variación de X_1 y X_2 en función de la relación adimensional de frecuencias α_0

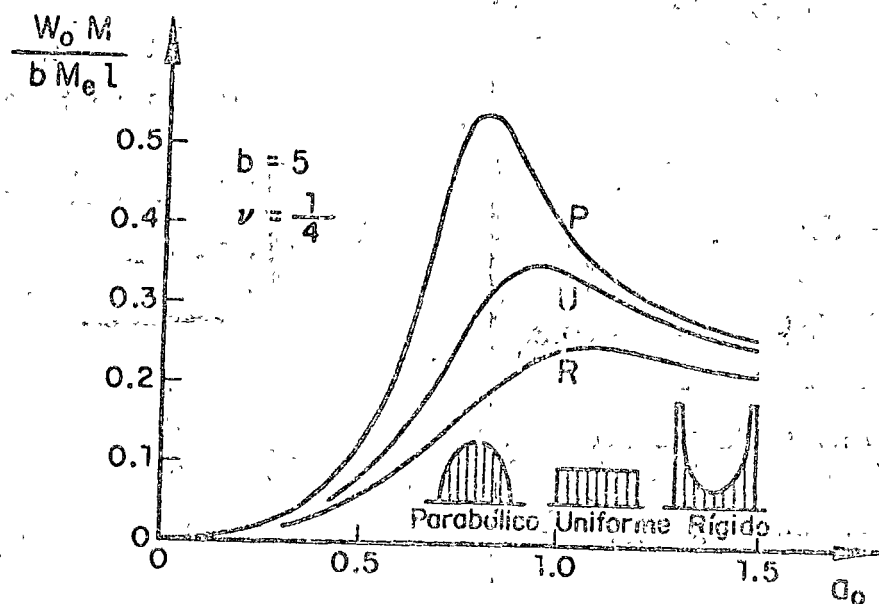
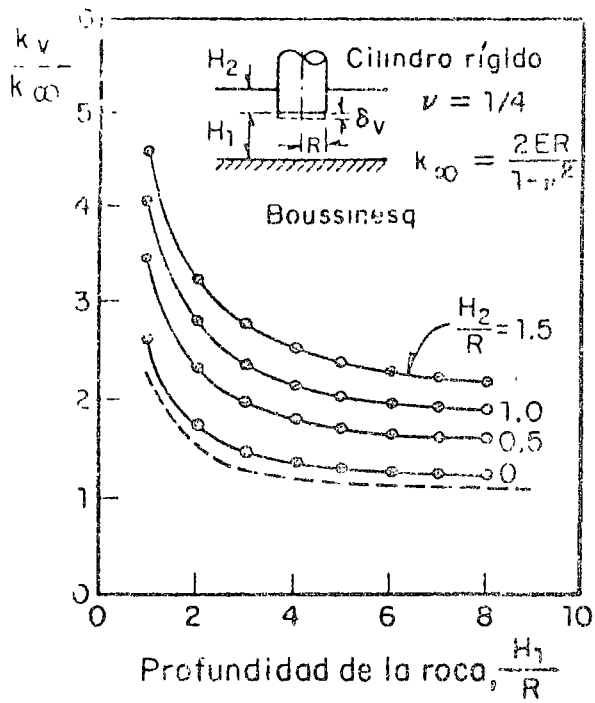
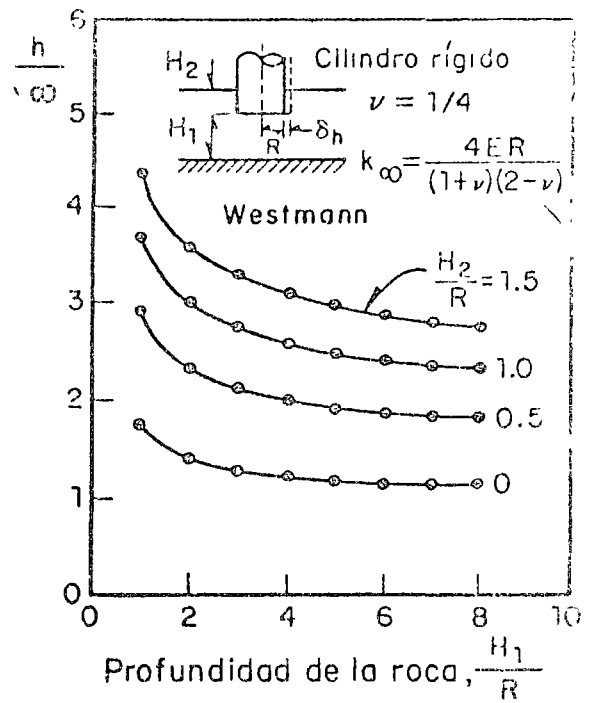


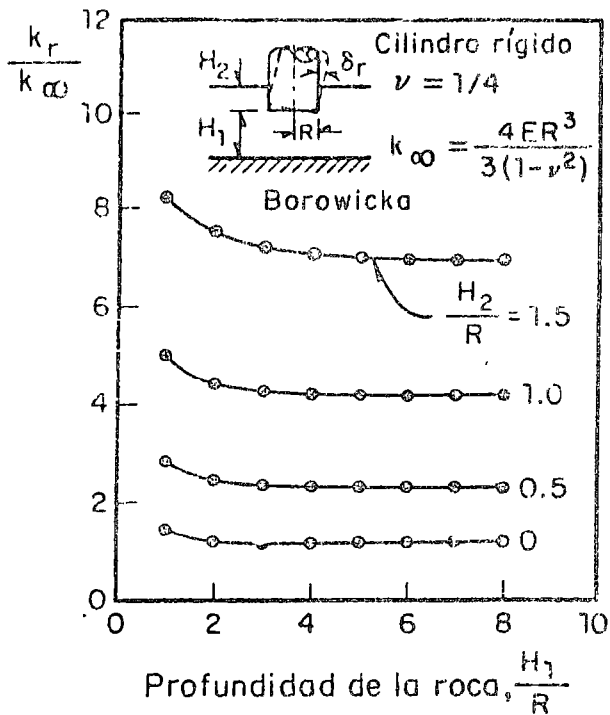
Fig 10. Efecto del tipo de distribución de esfuerzos en las curvas de respuesta (ref 3)



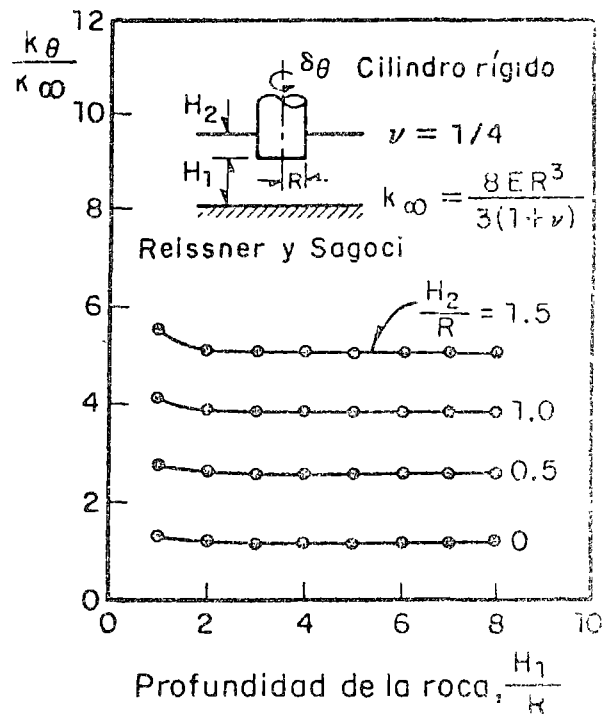
a) Modo vertical



b) Modo horizontal



c) Cabeceo



d) Modo torsional

Fig 11. Efecto del encajonamiento y la proximidad de la roca en el coeficiente k (ref 20)

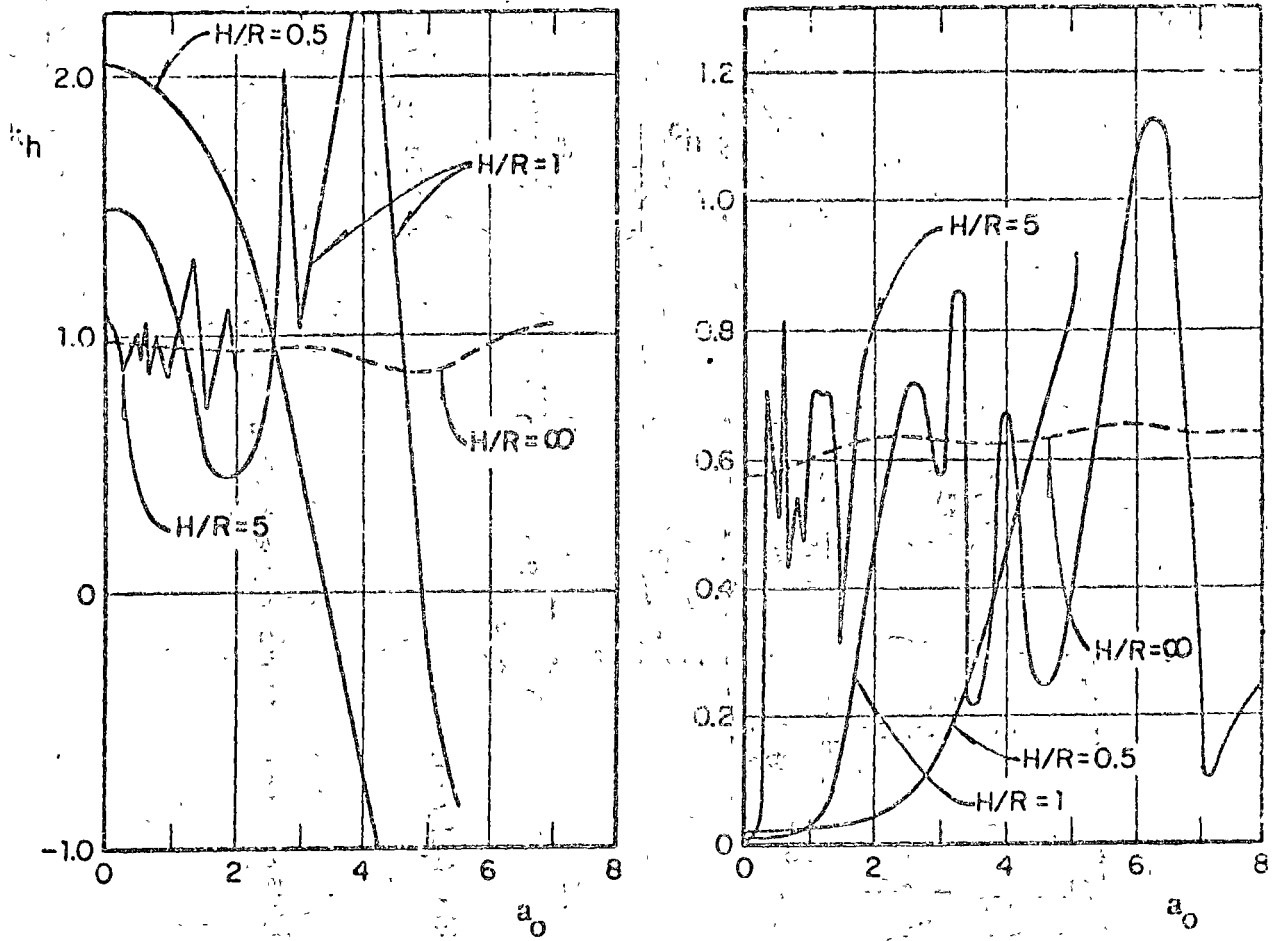
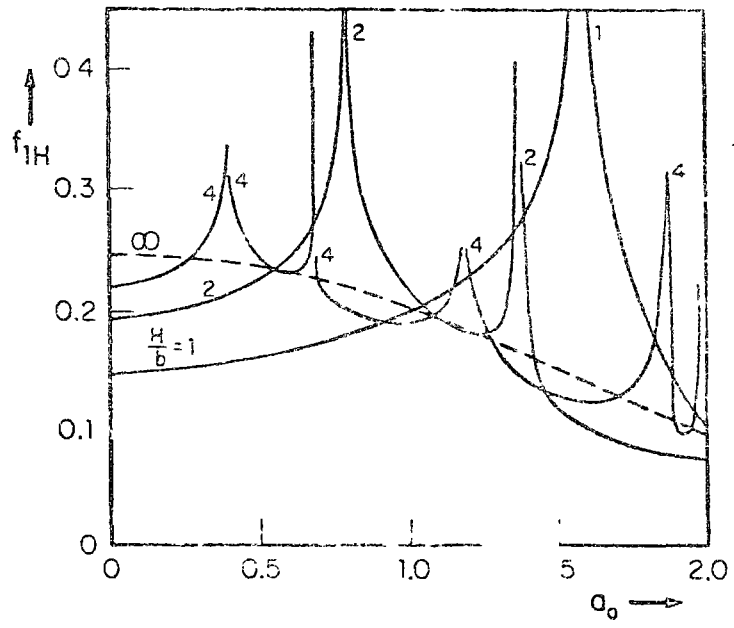
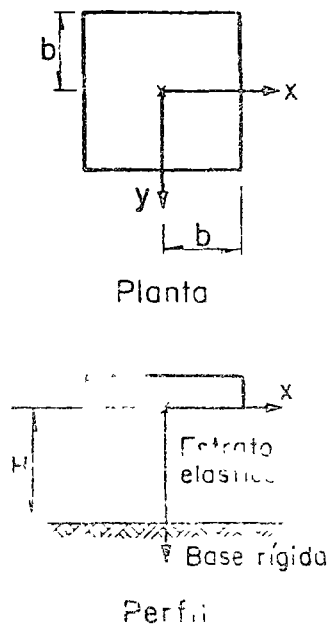
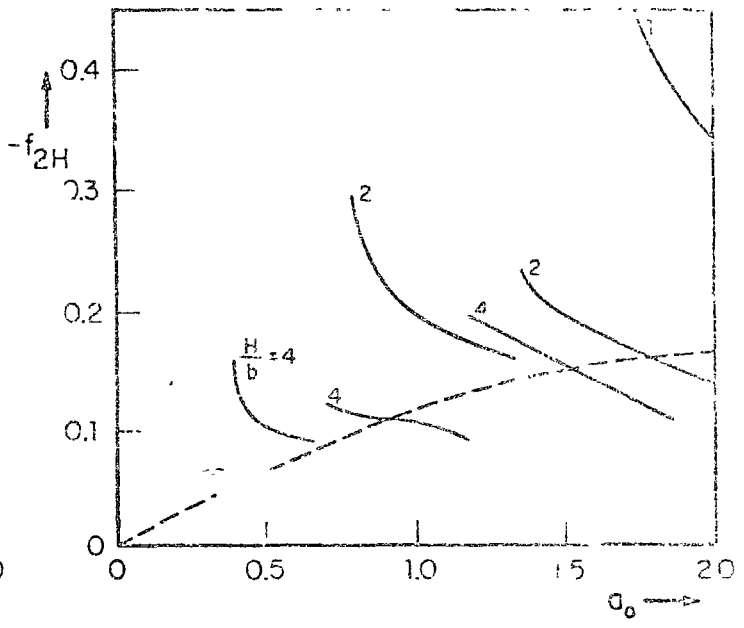


Fig 12. Coeficientes de rigidez y amortiguamiento, según Luco (ref 16)

Cimentación cuadrada



a) Función f_1 ($\nu = 1/4$)



b) Función f_2 ($\nu = 1/4$)

Fig 13. Funciones f_1 y f_2 para una cimentación cuadrada sujeta a una fuerza vertical horizontal dinámica, apoyada en un estrato elástico (ref 21)

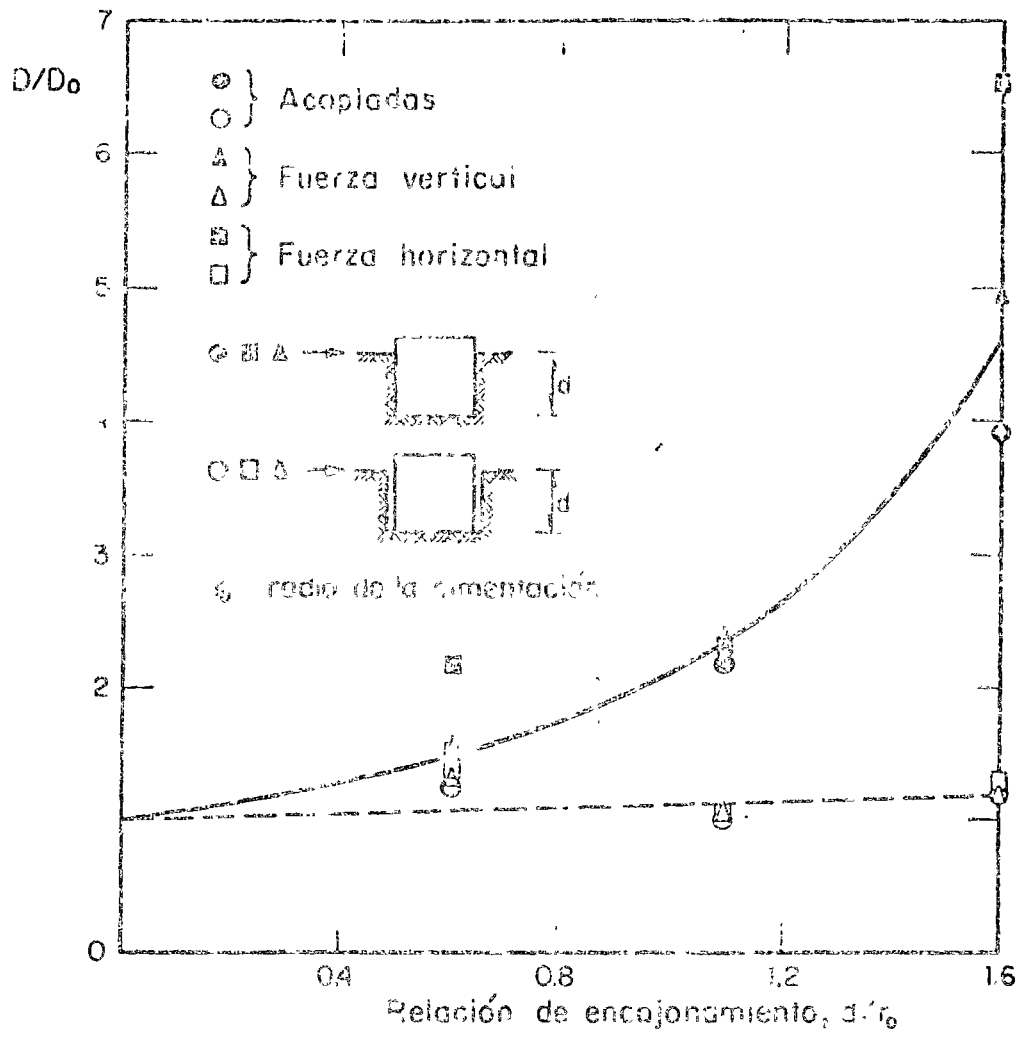
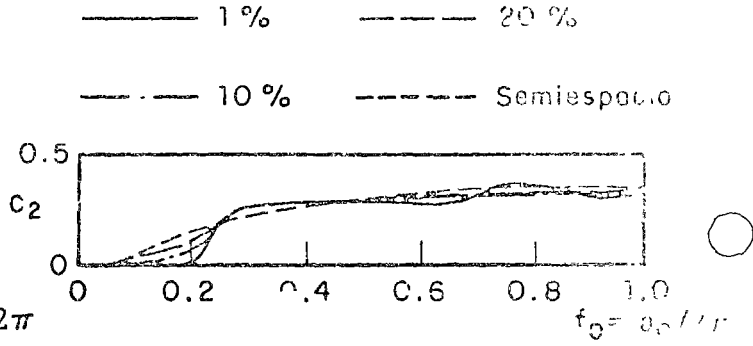
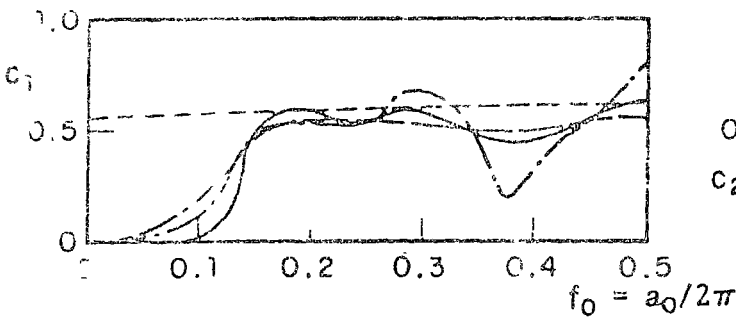
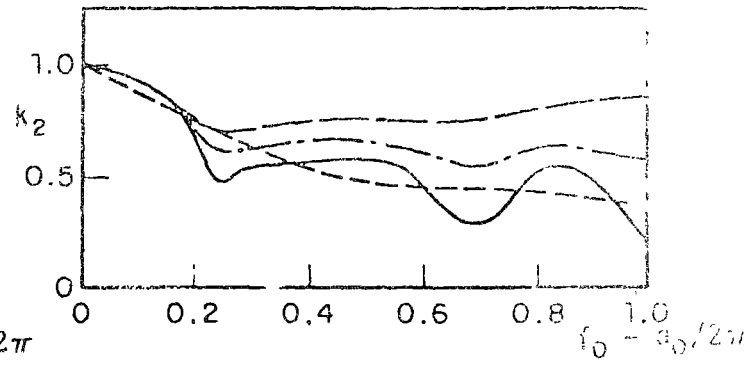
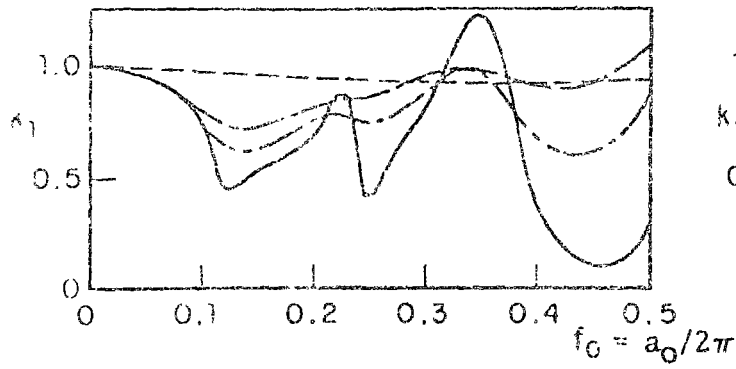


Fig 14. Variación de la relación de amortiguamiento con la profundidad de encajonamiento (ref 48)



——— 1% - - - - 20%
 - · - · - 10% - - - - Semiespacio

a) Movimiento horizontal

b) Cabeceo

Fig 15. Efecto del amortiguamiento interno. $H_1/R = 2$, $\nu = 0.33$ (ref 26)

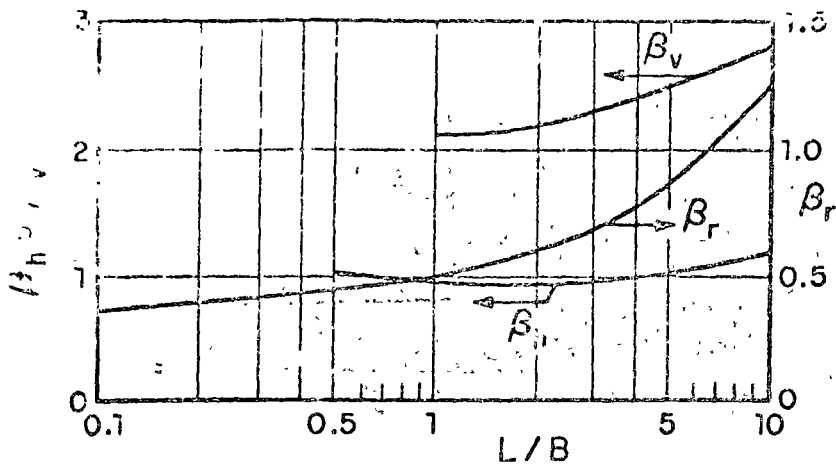


Fig 16. Coeficientes β_v , β_h y β_r para zapatas rectangulares (ref 27)

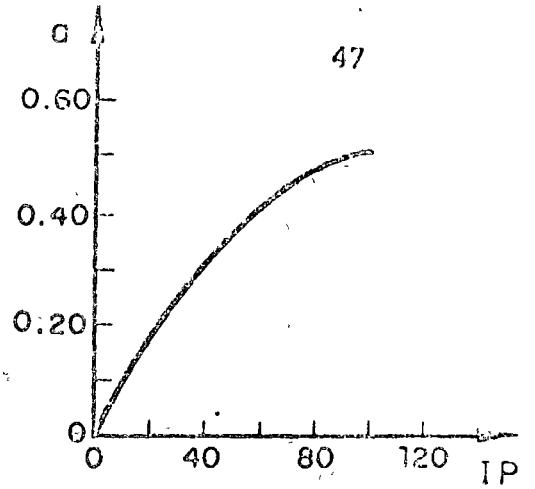
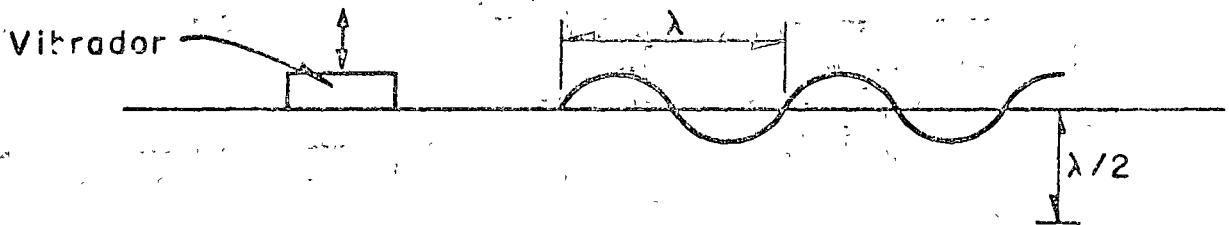


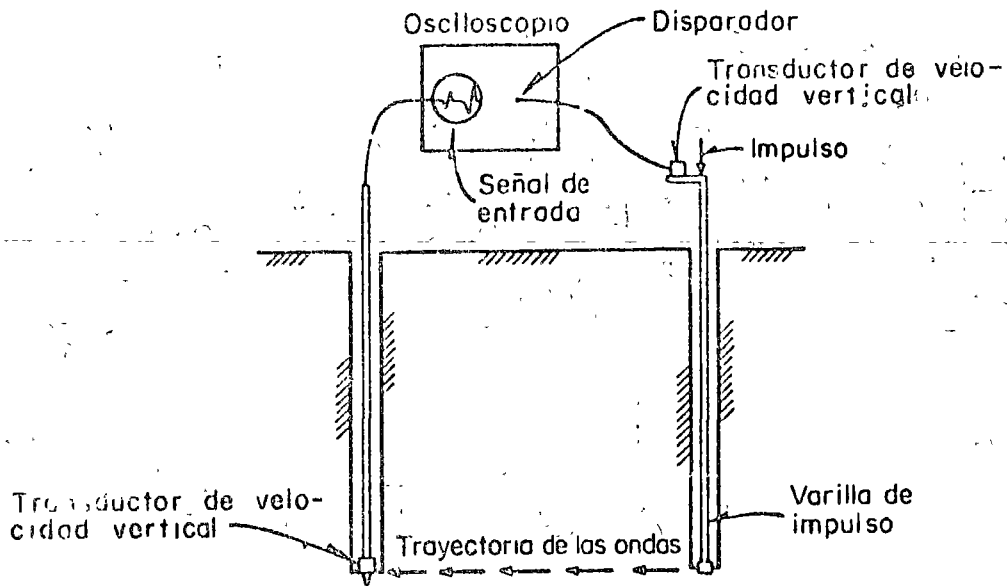
Fig 17. Parámetro a vs índice de plasticidad (IP)



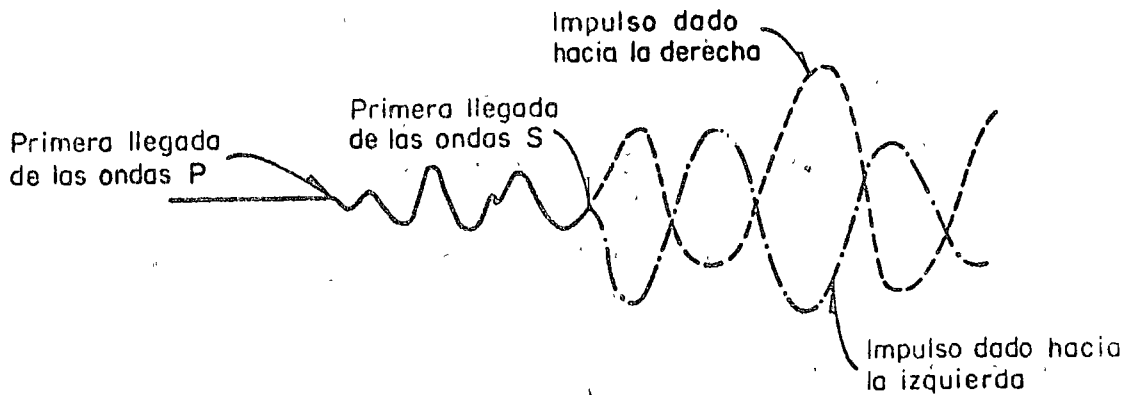
- G módulo al cortante = ρC_s^2
- C_s^* velocidad de ondas transversales = $f\lambda$
- ρ densidad del suelo
- f frecuencia de excitación
- λ longitud de onda

• Se desprecia la diferencia entre las velocidades de onda Rayleigh y las transversales

Fig 18. Determinación del módulo al cortante mediante el uso de pequeños vibradores



a) Corte esquemático que ilustra la disposición de los elementos



b) Efecto en las trazas al invertir el sentido del impacto

Fig 19. Método de hoyos en paralelo (cross-hole method) (ref 32)

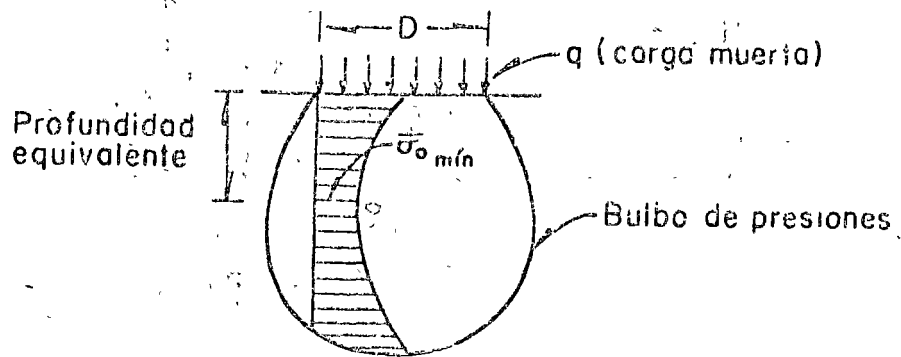


Fig 20. Determinación de la profundidad equivalente usando el procedimiento de Richart

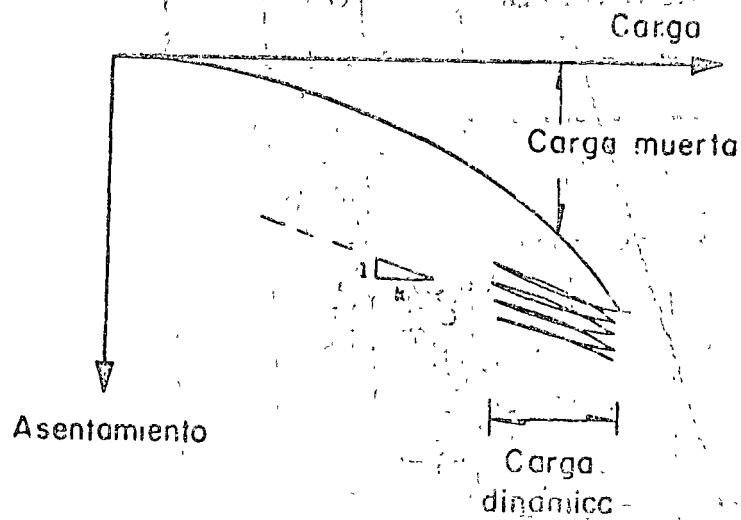


Fig 21. Determinación de k mediante pruebas de placa

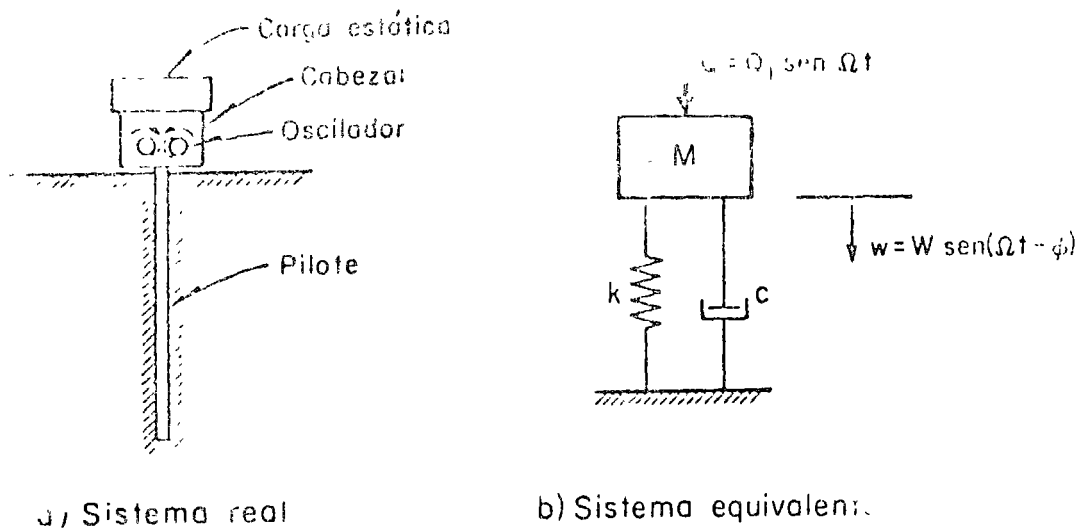


Fig 22. Sistema analítico de Maxwell et al (ref 40)

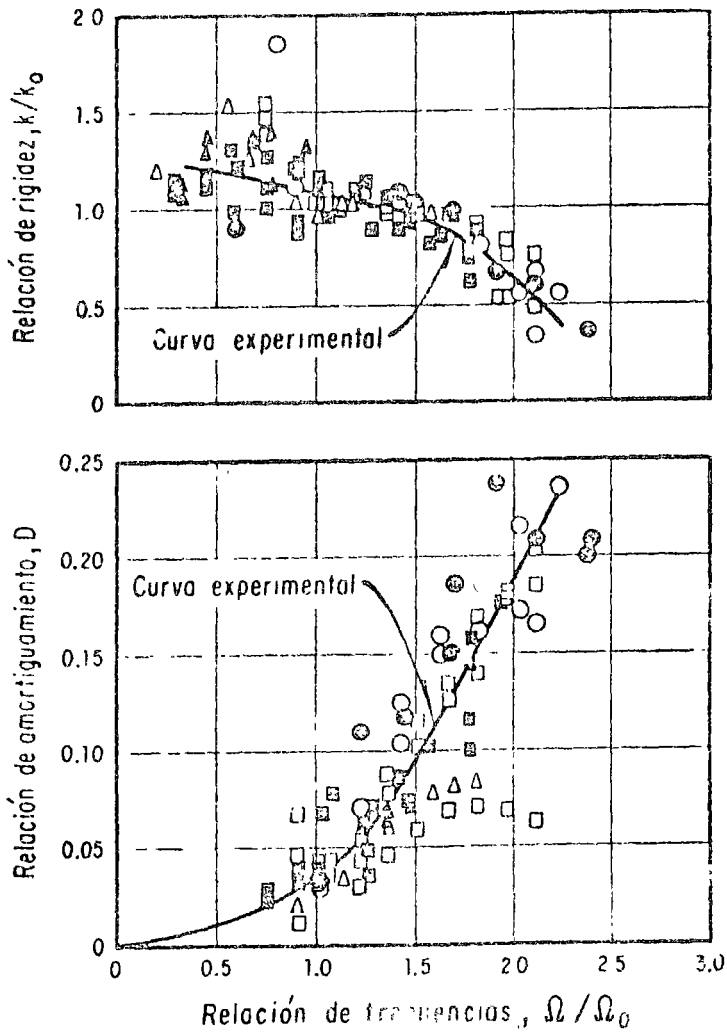


Fig 23. Relación de rigideces y amortiguamiento vs relación de frecuencias (ref 40)

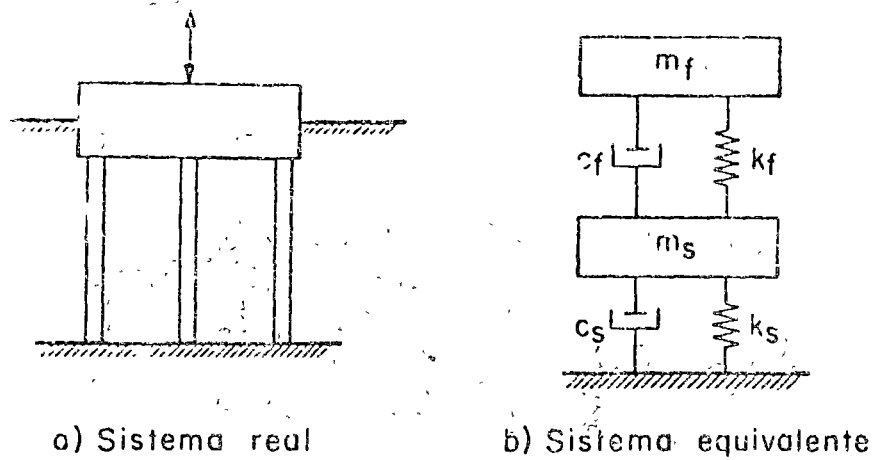
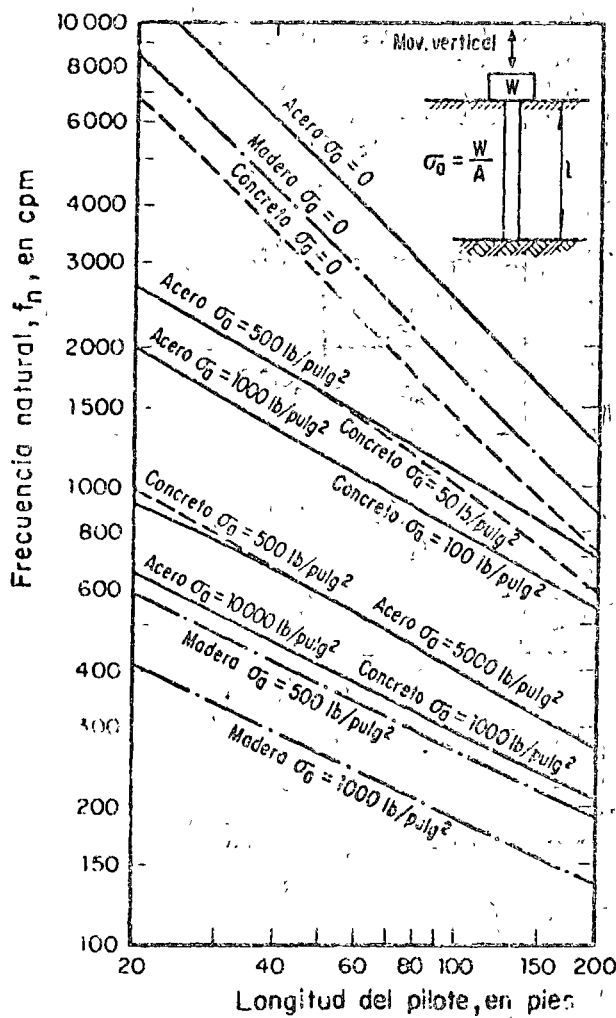
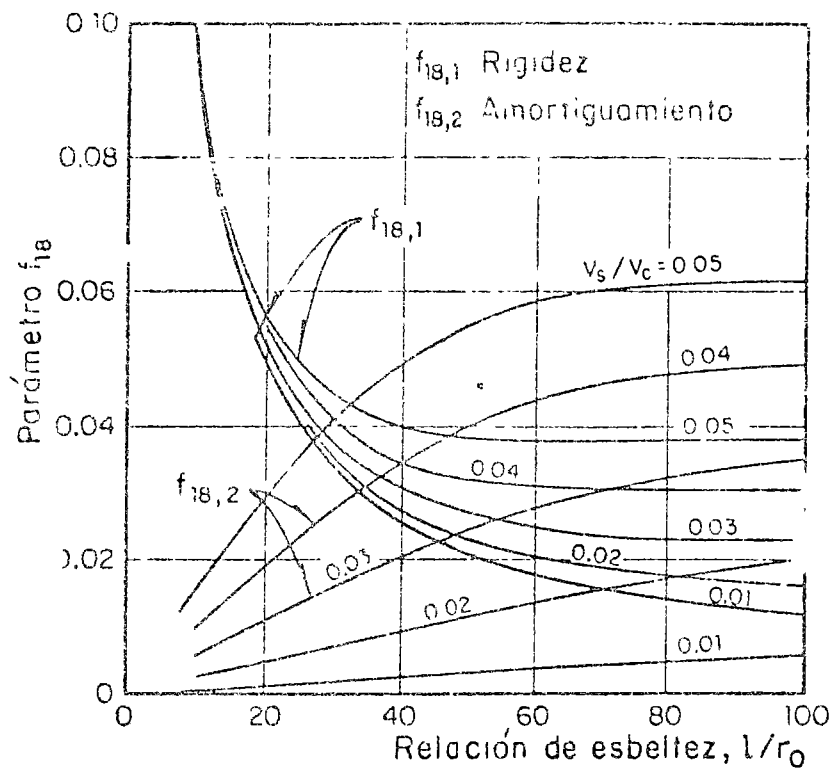


Fig 24. Sistema de dos grados de libertad (ref 41)

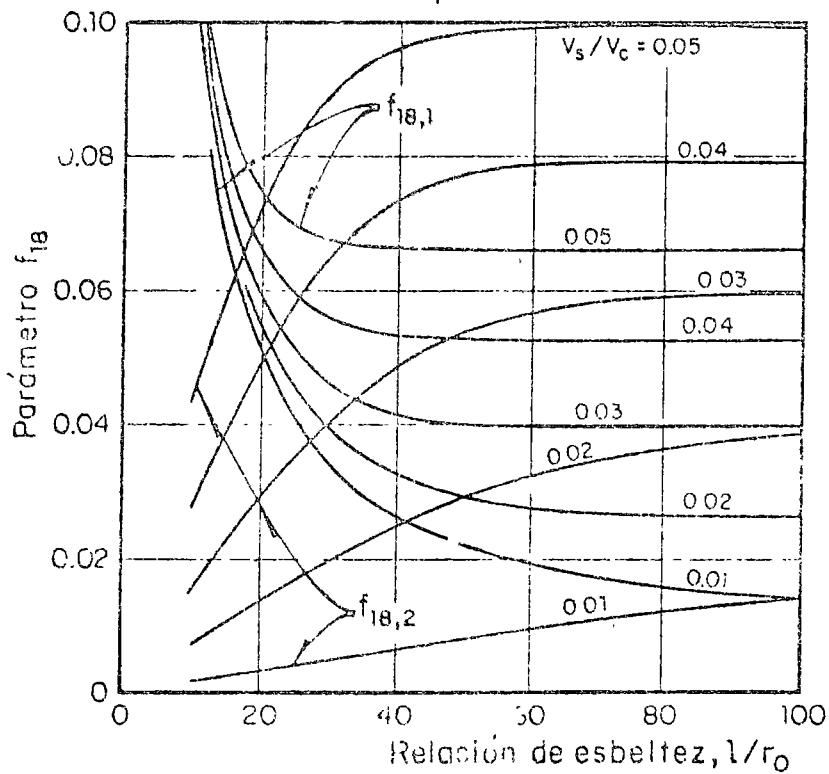


Material	E, lb/pulg ²	γ , lb/pie ³
Acero	29.4×10^6	480
Concreto	3.0×10^6	150
Madera	1.2×10^6	40

Fig 25. Frecuencia de resonancia en pilotes de punta sujetos a vibraciones verticales que soportan carga estática (ref 43)



a) Pilotes de concreto, $\rho/\rho_p = 0.7$



b) Pilotes de madera, $\rho/\rho_p = 2.0$

ρ densidad de masa del suelo
 ρ_p densidad de masa del pilote

Fig 26. Parámetros de rigidez y amortiguamiento para el nodo vertical (ref 42)

APENDICE. EJEMPLO DE APLICACION*

Se requiere determinar las dimensiones de la cimentación cuadrada de una máquina que pesa 2 700 kg, sujeta a una fuerza dinámica de 680 kg, que opera con una frecuencia de 10 cps. Los requisitos que debe cumplir la cimentación son: 1) la máquina necesita quedar a 2 m sobre el nivel natural del terreno, y 2) la velocidad de las partículas debe ser menor de 0.075 cm/seg.

Datos del terreno de cimentación. Se trata de un suelo limoarcilloarenoso duro, con un peso volumétrico igual a 1.92 ton/m³. Los valores de la velocidad de onda al cortante, medidos *in situ*, están dados por la fig A1.

Los resultados de una prueba de placa cuadrada, de 1' x 1', son los de la fig A.2.

Cálculo de G

El valor de k, con los datos de la prueba de placa, es

$$k = \frac{2\,000 \times 12}{0.003} = 8 \times 10^6 \text{ lb/pie} = 12 \times 10^6 \text{ kg/m}$$

* El ejemplo que se presenta fue adaptado del original que aparece en la ref 13

De la tabla 5 y de la fig 16 para una cimentación cuadrada, al asignar un valor de $\nu = 0.35$, se tiene

$$C_s = \frac{k_v(1-\nu)}{2.16B} = \frac{8 \times 10^6 (1-0.35)}{2.16 \times 1} = 2.4 \times 10^6 \text{ lb/pie}^2$$

o sea

$$G = 1.187 \times 10^3 \text{ kg/cm}^2 \quad (\text{A.1})$$

El siguiente paso es comprobar el valor de G con las mediciones de C_s obtenidas *in situ*, para lo cual se determina el valor del esfuerzo a mitad del bulbo de presiones en la placa. El radio equivalente para este caso sería

$$r = \sqrt{1/\pi} = 0.564 \text{ pies}$$

$$D = 1.12 \text{ pies}$$

$$3/4 D = 0.85 \text{ pies}$$

y los esfuerzos verticales a la mitad del bulbo

$$\sigma_v = 0.42^* \times 4000 \text{ lb/pie}^2 + 0.85 \times 120 \text{ lb/pie}^2 = 1782 \text{ lb/pie}^2$$

$$\sigma_v = .8815 \text{ kg/cm}^2$$

$$\text{Profundidad equivalente} = \frac{0.8910}{1.92 \times 10^{-3}} = 460 \text{ cm} = 4.6 \text{ m.}$$

De la fig A.1 se deduce que $C_s = 240$ n/seg, o sea

$$G = \rho C_s \frac{1920}{g} \times 240 = 1.13 \times 10^7 \text{ kg/cm}^2$$

* Factor de esfuerzos correspondiente a una profundidad de $\frac{3}{4} D$

lo que equivale a

$$G = 1.13 \times 10^3 \text{ kg/cm}^2 \quad (\text{A.2})$$

Como los valores de las ecs A.1 y A.2 son prácticamente iguales, se usará el valor dado por esta última en el diseño preliminar.

Diseño preliminar. Conforme la tabla 5, el valor de k para cimentaciones cuadradas está dado por

$$k_v = \frac{G}{1-\nu} 2.16B$$

por lo que al sustituir valores se obtiene

$$k_v = \frac{1.13 \times 10^7}{0.65} \times 2.16 \times B = 3.75 \times 10^7 B \quad (B, \text{ en metros}) \quad (\text{A.3})$$

Si se supone que la frecuencia de operación es relativamente pequeña con respecto a la de resonancia, se puede aplicar la simplificación:

$$V_{\text{máx}} = \Omega X_e = \Omega \frac{P_0}{k} \left| \frac{1}{1 - (\Omega/\omega)^2} \right| \approx \Omega \frac{P_0}{k}$$

o sea que el valor requerido de k será

$$k = \frac{P_0 \Omega}{\text{velocidad de diseño/factor de seguridad}} = \frac{680 \times (2. \times 10)}{0.075/2} \text{ kg/cm}$$

$$k = 1.14 \times 10^3$$

De las ecs A.3 y A.4 se obtiene que $B = 3$ m, por tanto, la cimentación mostrada en la fig A.3 puede suponerse como diseño preliminar.

Revisión del diseño preliminar

Para un análisis más detallado del diseño, se calculará la masa total del sistema

a) Masa de la máquina (M_m)

$$M_m = \frac{2720}{9.8} = 278 \frac{\text{kg}}{\text{m/seg}^2}$$

b) Masa de la cimentación (M_c)

$$M_c = \frac{\text{vol} \times \gamma_{\text{concreto}}}{9.8} = \frac{3 \times 6 + 2.6 \times 2400}{9.8} = \frac{56160}{9.8}$$

$$M_c = 5730 \text{ kg/m/seg}^2$$

c) Masa efectiva de suelo (M_{ef})

$$\text{Radio equivalente} = \sqrt{9/\pi} = 1.69 \text{ m}; R^3 = 4.85 \text{ m}^3$$

$$b = \frac{M}{\rho R^3} = \frac{5730 + 278}{\frac{1920}{9.8} \times 4.85}$$

$$B_v = \frac{1-\nu}{4} b = \frac{0.65 \times 6}{4} = 0.975$$

De la tabla 5

$$M_{ef} = 0.27 \frac{M}{B_v} = \frac{0.27(5730)}{0.975} = 1663 \frac{\text{kg}}{\text{m/seg}^2}$$

d) Masa total

Esta masa está dada por

$$M_m + M_c + M_{ef} = 278 + 5730 + 1663 = 7671 \text{ kg/m/seg}^2$$

Profundidad equivalente

Se estima ahora el punto medio del bulbo de presiones; para ello primero se calcularán los esfuerzos por peso propio al nivel de desplante:

$$= \frac{56\,160 + 2\,720}{9} = 6.54 \text{ ton/m}^2$$

A la mitad del bulbo de presiones, los esfuerzos totales son

$$\sigma_v \left(@ \frac{3}{4} D \right) = 0.42 \times 6.54 + \frac{3}{4} \times 3.38 \times 1.92 = 7.6$$

$$\text{Profundidad equivalente} = \frac{7.6}{1.92} = 4 \text{ m}$$

De la gráfica de la fig. A.10 se deduce un valor de $C_s = 230 \text{ m/seg}$. Calculando el valor de G , se tiene

$$G = 230^2 \times \frac{1920}{9.8} = 1.03 \times 10^7 \text{ kg/m}^2 = 1.03 \times 10^3 \text{ kg/cm}^2$$

y

$$k = 1.03 \times 10^7 \times 2.16 \times 3 = 1.03 \times 10^8 \frac{\text{kg}}{\text{m}}$$

ótese que en el cálculo de k se ha estado despreciando la profundidad de encajonamiento de 0.6 m; ello se debe a que dicha profundidad es relativamente pequeña y que al despreciarla se está dentro del lado de la seguridad. Sin embargo, si se deseara utilizar la influencia del encajonamiento en k , se podría utilizar alguno de los criterios señalados en el cap 5.

Por tanto, la frecuencia natural del sistema es

$$f_n = \frac{1}{2\pi} \sqrt{\frac{1.03 \times 10^8}{7671}} = 18.4 \text{ c/s}$$

Cálculo de la velocidad máxima:

$$V_{m\acute{a}x} = \Omega \frac{P_0}{k} \frac{1}{1 - (\Omega/\omega)^2} = 62.8 \times \frac{680}{1.03 \times 10^8} \frac{1}{1 - \left(\frac{10}{18.4}\right)^2}$$

$$V_{m\acute{a}x} = 5.8 \times 10^{-4} \text{ m/seg} = 0.058 \text{ cm/seg} < 0.075$$

Si se quiere tener un factor de seguridad mayor de $0.075/0.058 = 1.29$, deberá procurarse aumentar k sin que M aumente, lo que se consigue, por ejemplo, al ampliar la base de la cimentación, pero reduciendo las dimensiones superiores. Para la cimentación de la fig. A.4, los resultados que se obtienen son:

M_m	=	278 kg/m/seg ²
M_c	=	4 861 kg/m/seg ²
M_{ef}	=	2 504 kg/m/seg ²
M_{TOT}	=	7 643 kg/m/seg ²
C_s	=	250 m/seg
G	=	1.22×10^7 kg/m ²
k	=	1.42×10^8 kg/m
f_n	=	21.7 cps
$V_{m\acute{a}x}$	=	0.038 cm/seg
FS	≈	2

Se recomienda al lector verificar, a manera de ejercicio, estos resultados.

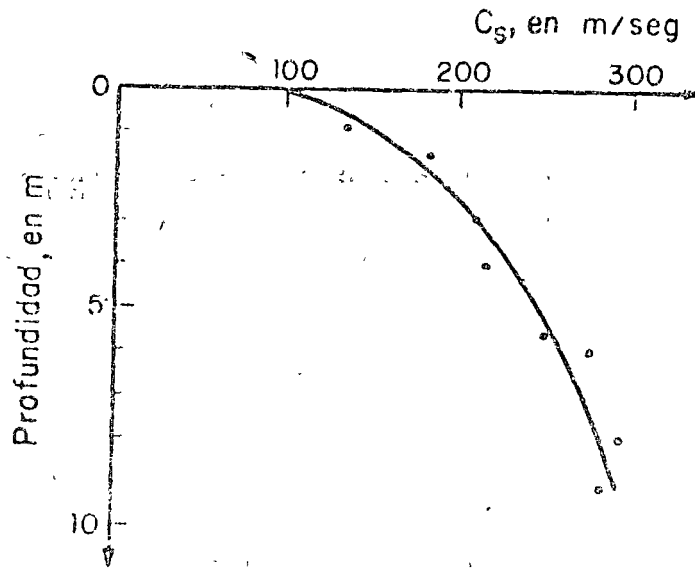


Fig A.1. Valores in situ de c_s vs profundidad

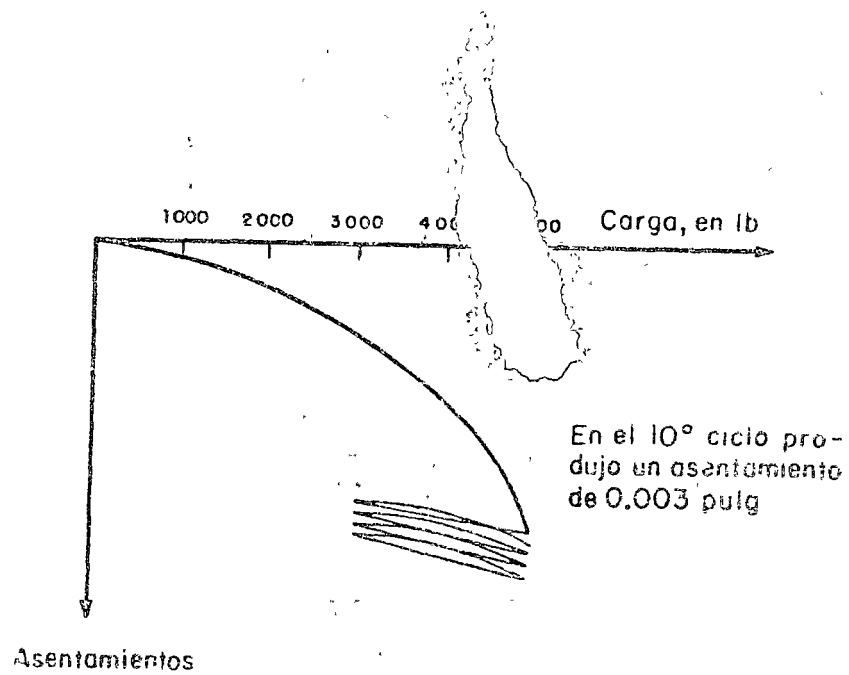


Fig A.2. Datos de la prueba de palanca

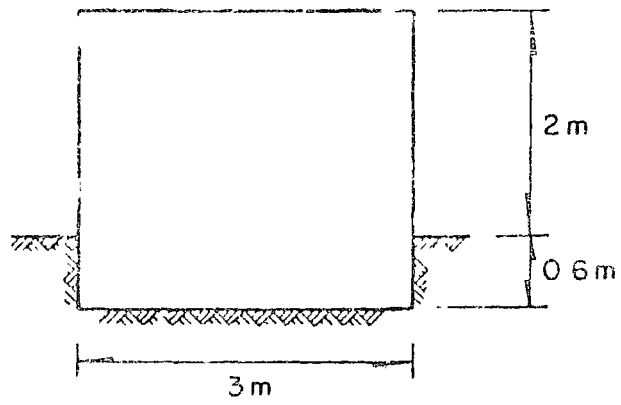


Fig A.3. Dimensiones preliminares del diseño de cimentación

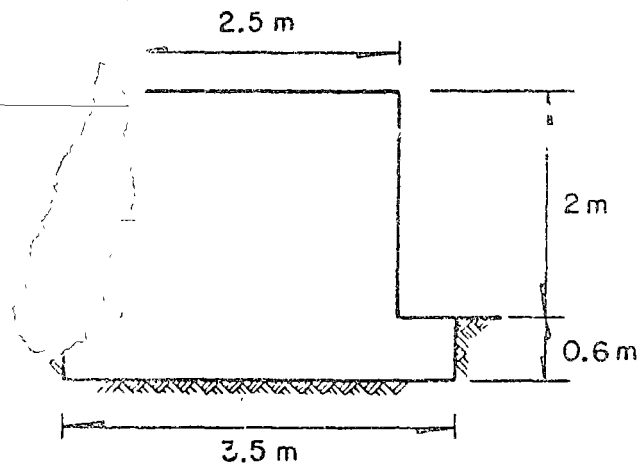
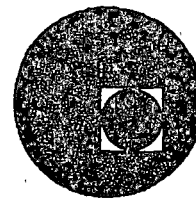


Fig A.4. Dimensiones definitivas de la cimentación

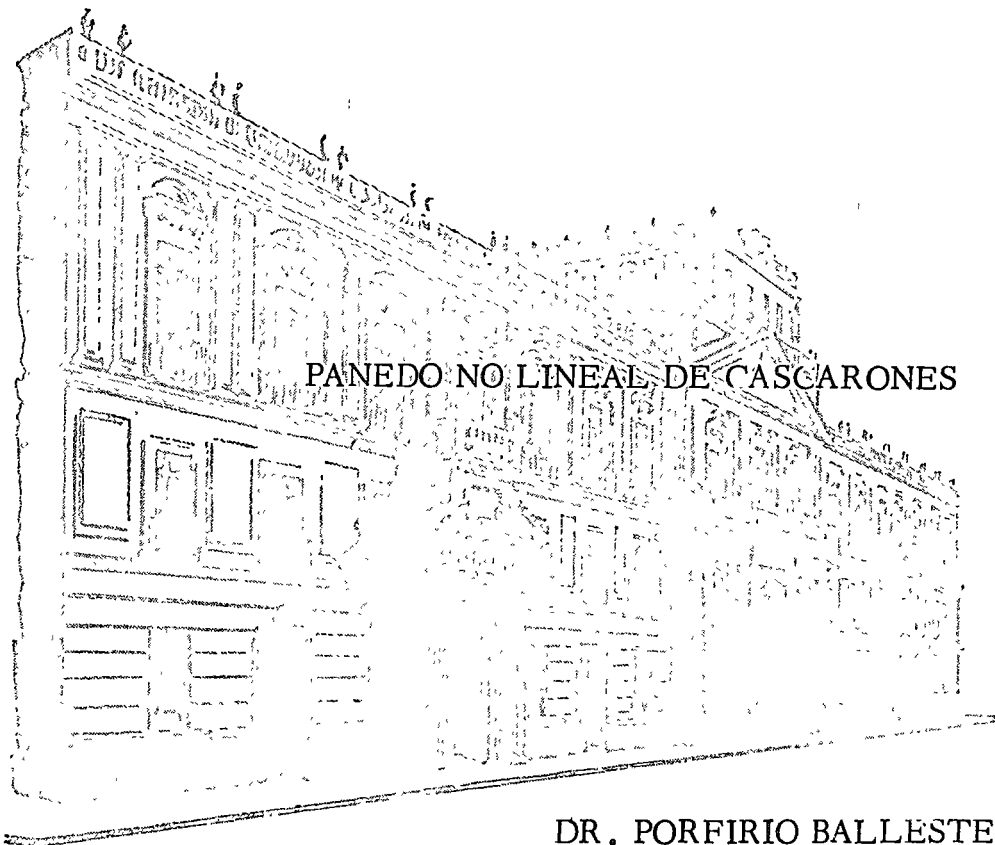


centro de educación continua
división de estudios superiores
facultad de ingeniería, unam



III CURSO INTERNACIONAL DE INGENIERIA SISMICA

ANALISIS DINAMICO DE ESTRUCTURAS ESPECIALES



DR. PORFIRIO BALLESTEROS BAROCIO

JULIO-AGOSTO, 77.

UNITED STATES DEPARTMENT OF JUSTICE
FEDERAL BUREAU OF INVESTIGATION
WASHINGTON, D. C. 20535



CONFIDENTIAL - SECURITY INFORMATION

ALL INFORMATION CONTAINED HEREIN IS UNCLASSIFIED

DATE 08-15-01 BY 60322/UC/STP

EXEMPT FROM AUTOMATIC DOWNGRADING AND DECLASSIFICATION

NONLINEAR DYNAMICS

"INCREMENTAL STIFFNESS METHOD

FOR FINITE ELEMENT ANALYSIS"

I. INTRODUCTION

Many advances have been made in finite element theory which account for both nonlinear geometric and material behavior. These advances have recently been summarized in the literature [e.g., 1-3]. This nonlinear theory is in principle applicable to problems in both the static and dynamic regime. The research effort directed to investigating the use of the finite element method in the analysis of structures under dynamic loads compares rather unfavorably with its rapid development in the static regime.

Following the development of a nonlinear static finite element program a companion program was started to study nonlinear dynamic problems. Parallel formulations were made for the latter problem, with some expectations that the dynamic problem would yield to a similar approach. In the event it turned out that there were sufficient shortcomings in the convergence properties of the element used, and in the numerical procedures adopted for the integration of the equations in time and space, to cause considerable delays in the progress of the study. This paper presents a synopsis of the results obtained to date which are described more completely in [4]. As in the static problem [2], the writers set out to develop a base on which a general purpose finite element program could be built for analyzing nonlinear dynamic problems. This procedure seemed the most expedient approach since much common programming could be utilized from the static program.

II. REVIEW OF LITERATURE

It is interesting to note that the original development of the finite element method was directed to the solution of dynamic problems [5]. The emphasis rapidly switched to static solutions and it is only recently that its potential for solving complex dynamic problems is being realized. The earliest

examples in the literature of the solution of a dynamic problem using the finite element method are those given in [6] and [7] where the linear solution for a shallow shell cap under a step pressure load was given. A more recent and more general application of the method to linear problems was illustrated in [8] where a nuclear containment vessel, an earth dam, and other complex structures are examined.

Although the geometrically nonlinear static problem was formulated using the finite element method by Turner et al. [9] over a decade ago, it was not until one year ago that results were obtained for the corresponding elastic dynamic problem by Stricklin et al. [10]. In [9] the equations were solved in an incremental form where the behavior was assumed to be linear for each increment and the problem was reduced to a series of linear solutions. In this method a new set of equations was formulated for each increment. The method adopted in [10] used the total form of the governing equations and transformed the nonlinear terms into pseudo forces which were then treated as additional loads on the structure. The difficulty arises in that these forces depend on the unknown current displacements and must then be found by extrapolation or iteration techniques. In [10] it is concluded, after comparisons with parabolic and cubic extrapolation schemes, that a linear procedure is sufficient for determining these forces. The results given in [10] apply to a shell of revolution only with certain asymmetries of the applied load allowed. The approach used in [10] has been extended by Klein [11] to include other asymmetric properties of the shell structure and the loading.

The other nonlinearity we wish to discuss is material nonlinearity due to nonlinear constitutive laws as used in modeling the behavior of an elastic-plastic solid. Two general methods for incorporating this behavior into a finite element analysis have been developed, based on the Prandtl-Reuss equation [12] for an elastic-plastic solid, viz. the initial strain method and the tangent modulus method. The tangent modulus approach corresponds to the incremental method adopted for nonlinear geometry and therefore is the most convenient and direct manner of accounting for both the geometric and material nonlinearities. The only references known to the writers for dynamic finite element analysis with nonlinear material behavior are [13,14] where elastic-plastic wave problems were studied.

The paucity of nonlinear dynamic results is in contrast with those obtained using the finite difference approach together with numerical integration in time. There is a large body of literature surveyed in [15] covering the area of nonlinear elastic deformations, and which is primarily directed to the solution of dynamic elastic deformations, and which is primarily directed to the solution of dynamic elastic shell buckling problems. The works cited in [15] are concerned with solving numerically the coupled differential equations of motion of the structure. However, a method which is closer to the finite element approximation was developed initially by Witmer et al. [16]. In this approach the structure is discretized initially and equilibrium equations are written for each separate division resulting in an uncoupled system which may be solved directly. Solutions which include large displacements and plastic deformations have been obtained by this method for a variety of problems. It has also been extended to cover general shell structures undergoing three-dimensional deformations [17]. Many experimental programs have been carried out with the purpose of validating this method and good agreement has been shown between the theory and experiment [15-18]. The drawback with the above solutions is that they are special purpose solutions restricted to certain geometric shapes divided into a regular grid pattern, whereas the finite element approach allows irregular structural shapes and grids. Approximate techniques for solving dynamic problems which include large plastic deformations have been developed and are based on the assumption that elastic deformations may be neglected. These methods are described in an extensive review by Symonds [19] where the relative accuracy and merit of the various approximations are discussed. There are also the mode approximation methods [20] based on the bound theorems of Martin [21,22]. A criterion adopted for the purpose of deciding when these approximate methods may be useful is that the energy applied by the external loading on the structure should be about ten times the amount of energy which could be absorbed elastically by the structure [19].

III. THEORETICAL CONSIDERATIONS

The basic equations for nonlinear finite element analysis are well understood and will not be derived here. Instead, we shall quote the equations as our point of departure. By the principle of virtual work we obtain in terms of initial geometry:

$$\int_{V^0} [N]^T [\rho] [N] \{\ddot{u}\} dV^0 = \int_{V^0} [B] \{\sigma\} dV^0 + P \quad (2)$$

where $[N]$ is an interpolation function that transforms displacements at the nodes to displacement at any point within an element.

$[B]$ is the transformation matrix that transforms displacement rates at the nodes to strain rates at any point in an element.

$\{\sigma\}$ is the generalized stress vector.

$[\rho]$ is the density matrix (the density takes on its matrix form in problems of beams and shells).

$\{P\}$ is the applied load.

We may now linearize the equation by writing it in incremental form:

$$\int_{V^0} [N]^T [\rho] [N] dV^0 \Delta \{\ddot{u}\} = - \int_{V^0} \Delta [B] \{\sigma\} dV^0 - \int_{V^0} [B] \Delta \{\sigma\} dV^0 + \Delta \{P\} + O(I) + O(t^m)$$

In the above Equation $\Delta\{P\}$ should be understood to include the effects of following loads. The two error terms $O(t^m)$ and $O(I)$ are also included to show that the solution in incremental form contains a discretization error due to the current increment as well as an inherited error due to all previous increments. The error due to discretization in time is shown as a function of time raised to the power m .

We now make use of the linearized incremental stress strain relations which are written as

$$\Delta \{\sigma\} = [D] \Delta \{e\} \quad (3)$$

This equation is appropriate for elastic plastic behavior and has been outlined for small strain in [24] and for large strains in [25].

Substituting (3) in (2) results in a linearized incremental equation

$$- [M] \Delta \{\ddot{u}\} = - [K] \Delta \{u\} + \Delta \{P\} + O(t^m) + O(I) \quad (4)$$

This equation can be specialized to the static case by neglecting the term on the left. In the static case convergence to the true solution may be achieved by applying the load in increasingly smaller increments. A parallel procedure was investigated for the dynamic case where the rate of convergence with decrease in time step was examined. The results of this analysis are discussed later.

We now consider the error term $O(I)$ which will be called the residual load correction [26] and consists of writing the residual equation for (1)

$$O(I) = -[M] \{u\} - \int_{V_0} [B] \{\sigma\} dV^0 + P \quad (5)$$

It is noted that this error term consists of evaluating the terms at the state before the current increment and that if no numerical errors had been introduced by previous increments the error would be equal to zero. It was shown in [4] that, by including the residual load correction in the dynamic equations, one may obtain convergent solutions using time increments relatively large in comparison with the solutions obtained without the correction.

IV. SOLUTION PROCEDURE

The selection of an integration scheme for the solution of the incremental equations in the time domain is critical with respect to computational efficiency. A suitable solution scheme which allows a large time step and yet gives an accurate solution is that developed by Houbolt [27]. The Houbolt scheme is based on the third order backwards difference expression

$$\Delta\{u\}_n = \frac{1}{\Delta t^2} (2\Delta u_{n-5} + 4\Delta u_{n-2} - \Delta u_{n-3})$$

Applying this to the condition for incremental equilibrium (4), we have

$$(2[M] + \Delta t^2 [K_n]) \Delta\{u_{n+1}\} = \Delta\{P_{n+1}\} \Delta t^2 + [M] (5\Delta\{u_n\} - 4\Delta\{u_{n-1}\} + \Delta\{u_{n-2}\}) + O(I_n) \Delta t^2$$

where n is a subscript denoting the time at which the increment is taken.

This equation is solved for the displacement increment $\Delta\{u_{n+1}\}$ at each step except the first where a special starting procedure must be employed [27]

Haisler et al. [23] have reported on studies of numerical integration schemes and their convergence properties in the nonlinear static case. It was there shown that the incremental finite element formulation gave satisfactory results when the load increments used were small as compared with those adopted in the solutions using the residual load correction term. The nature of the correction procedure was illustrated in [4] where the order of the error for the corrected and uncorrected equations are examined. The result was given for a one-dimensional model and serves to give an order of magnitude estimate of the error.

In the static case for the solution without the residual load correction and a slowly varying stiffness K , the total discretization error is the sum of the truncation errors for each increment of the incremental approximation. This error may be expressed as

$$u_N - u_N^* = -\frac{1}{2} \sum_{n=2}^N K_{n-1}^{-1} \frac{dK_{n-1}}{du} \Delta u_n^2 + O(\Delta u^3) \quad (6)$$

where u_n is the correct total displacement after N load increments and u_N^* is the displacement obtained by the incremental approach. It is noted that the error is $O(\Delta u^2)$ in the displacement increment. When the residual load correction is included we find that

$$u_N - u_N^c = -\frac{1}{2} K_{N-1}^{-1} \sum_{n=2}^{\frac{N}{2}+1} \frac{dK_{\ell}}{du} \Delta u_k^2 + O(\Delta u^3) \quad (7)$$

where for N even $\ell = m - 1$, $k = m$

N odd $\ell = m$, $k = m + 1$,

$m = 2\left(\frac{2n-1}{2}\right)$, and fractions are discarded in the computation of the indices. Equation (7) may be described by stating that for even N only the terms involving even displacement increments remain in the series and likewise for odd N and odd displacement increments. In comparing (6) and (7) we see that the inclusion of the residual load correction reduces the number of terms in the series by a half. One could state that, approximately speaking, the error is halved in the

corrected equations except for the fact that the stiffness quantity is inside the summation sign in [6]. The assumption of a slowly varying stiffness K in [6] means the neglect of errors caused by the inherited error terms.

In the dynamic case the expressions for the discretization errors of the uncorrected and corrected equations at time $N\Delta t$ are, respectively,

$$u_N - u_N^* = \frac{\Delta t^2}{4} M^{-1} \left\{ \sum_{n=2}^N R_{n-1} \frac{dK_{n-1}}{du} \Delta u_n^2 + E^* \right\} + o(\Delta u^3) + o(\Delta t^4) \quad (8)$$

$$u_N - u_N^c = -\frac{\Delta t^2}{4} M^{-1} \left\{ R_{N-1} \sum_{n=2}^{\frac{N}{2} + 1} \frac{dK_n}{du} \Delta u_k^2 + E^c \right\} + o(\Delta u^3) + o(\Delta t^4) \quad (9)$$

where $R_n = (1 - \frac{\Delta t^2}{2} M^{-1} K_n)$. In the above equations E^* and E^c are the truncation errors inherited from the inertia terms and, for the current integration scheme in time, do not appear to be expressible in a general form. However, they are of the same order as the first terms in the brackets in (8) and (9), and it is interesting to speculate that a similar reduction in the error occurs in E^c as compared with E^* .

It has been demonstrated in [23] that the static solutions given by the corrected and uncorrected equations tend to converge as the number of load increments in the uncorrected case are increased. A particular example given in [23] is a spherical shell cap under a point load at the apex where the uncorrected solution converged using an increment one eighth that required for convergence in the corrected solution. One would expect that judging from (8) and (9) the convergence rate in the dynamic case would be more rapid both for the corrected and uncorrected solutions considering the presence of the factor Δt^2 , and the fact that the truncation errors for the static and dynamic solu-

tions are approximately of the same order. In the sample problems given later, it is shown for the example of a beam under a half-sine wave impulse over the span, that the uncorrected solution converges rapidly with the variation in the time increment. On the other hand, the corrected solution changes very little over a range of time increments. It appears that with the reduced truncation error of the corrected equations the effect of Δt^2 on the convergence of the solution is diminished.

The advantage in using the corrected dynamic equations is that one may obtain practically convergent results with large time increments. In the numerical examples given later it is shown that convergent solutions to dynamic problems using the corrected incremental equations may be obtained using time increments an order of magnitude greater than those used by other investigators. The other solutions were obtained by using the Houbolt scheme and the total form of the finite element equations so the comparisons are direct. This fact has important consequences in terms of doing nonlinear problems economically.

Computer Program

The system of equations for the dynamic elastic-plastic analysis with large displacement have been incorporated in a pilot program. A program previously developed at Brown University [2] was used as the basis. Figure 1 gives a flow diagram for the program. The various stiffness and the mass matrices are assembled by the program from stored information which enables certain element types to be generated. Presently, there are four such elements available in the library, two for beams and two for axisymmetric shells. Controls have been introduced to avoid the generation of the stiffness matrix every time step and thus uncouple the physical modeling from the small time steps required for numerical accuracy.

VI. CASE STUDIES

In the following section, examples have been selected from [4] in

order a) to make comparisons with results in the literature, b) to investigate the limits of numerical approximations in terms of the frequency of reassembly and residual load correction, and c) to observe the effect of geometric imperfections in a dynamically loaded sphere. The one-dimensional element used in the following examples is of the isoparametric type and has a rapid rate of convergence even for small numbers of elements. This is due to the fact that it can represent exactly all the rigid body modes of the interpolated surface which is arbitrarily close to the actual structural shape. It has proved to be a very accurate and economic element for use in analyzing dynamic problems. All the current results were obtained on a CDC-6600 using a 60-bit word and the effects of rotary inertia have been included in the equations although the response is not changed noticeably by this term.

1. Shallow Spherical Cap Under A Step Pressure Load

A linear example is illustrated in Figure 2 for the case of a shallow spherical cap under a constant dynamic pressure. The solution using the finite element method was first given in [6] and later in [10]. It is noted from Figure 2 that all three solutions agree even though different elements and different numbers of elements were used in each case. The current values shown and those from [10] agree more closely in that both used curved elements whereas [6] approximated the shell by straight segments. A solution [7] based on modal analysis also follows the current results closely.

2. Nonlinear Elastic Analysis of a Simply-Supported Beam Under A Half-Sine Initial Velocity Distribution

The problem illustrated in Figure 3 was analyzed in order to check the elastic large displacement portion of the method. This problem has been treated theoretically in [28] and [29] where the differential equations of motion for a beam under an initial displacement condition were solved using perturbation techniques. In [28] more general equations were written which included the effects

of large strain, rotary inertia, and transverse shear, whereas [29] neglects these effects and solves simpler equations which consider large rotations but small strains. The final solutions in terms of the variation of the ratio of the nonlinear to the linear period of vibration of the beam with a perturbation parameter are identical for both approaches.

A finite difference method is used in [30] to solve the same problem with the initial velocity distribution given in Figure 3. The numerical values computed for deflections and generalized forces were found to agree with values found from expressions given in [29]. In this case a time step of one microsecond was used and the beam was divided into twenty meshes.

Since rather exact results are known for this problem, it was chosen as an example for testing the various solution schemes available with the current formulation of the finite element method. Five isoparametric elements were used and the most exact finite element solution is shown by the small circles in Figure 3. The equations were reassembled at each time increment and stresses were computed at three integration points per element. The period of vibration agrees with the theoretical result as shown in Figure 3 and the value for the maximum displacement agrees with that given in [30].

Shown in Figure 3 are solutions which were obtained using the corrected and uncorrected equations for a series of time increments. In all cases the equations were reassembled at each increment and corrected at each increment as required. As mentioned previously, the uncorrected equations converge rapidly while the solutions for the corrected cases change very little with the change in time step. A feature of the dynamic behavior is the convergence of all solutions over the first half-period whereas in static nonlinear solutions the uncorrected solution diverges rapidly from the corrected solution for reasonably sized load increments. This phenomenon bears out the conclusions of the error analysis which indicated the more rapid convergence of the dynamic equations. If we assume that the corrected solution has converged at $\Delta t = 2.5 \times 10^{-6}$ sec. we note that the uncorrected solution for the same time increment has converged

over practically all the response but still only compares with the corrected solution for $\Delta t = 1 \times 10^{-5}$ sec.

A procedure which results in a great economy of solution time is to reassemble the equations at certain multiples of the basic time step. For the example under consideration, as illustrated in Figure 3a, the reassembly operation was performed at every increment, every tenth increment, and every twentieth increment with no apparent change in the response. However, the load correction was applied at each step. The effect of varying the latter parameter was also investigated and as shown in Figure 3a the solution is much more sensitive to changes in correction frequency as compared with changes in reassembly frequency.

An approximation which is used frequently in the static analysis of structures is to consider the stress at the center of the element as being the average stress in the element and to use this value alone in computing the stiffness matrix. The results are shown in Figure 3a where it is noted that with the load correction, the response compares very favorably with the most exact solution shown. This procedure is very economical with respect to storage requirements and solution times and could be usefully employed as an economic first run designed to investigate the probable response of the structure. It would appear unwise, however, to use this approximation without the load correction as evidenced by the response shown in Figure 3a.

An attempt was made to rate the solution procedures just described with respect to cost in computer time and accuracy as compared with the solution which requires the equations to be corrected and reassembled at each step. For the sake of comparison the accuracy is determined by the minimum displacement value as a percentage of the absolute minimum. The most efficient solution scheme, judging from the table given in Figure 3a, appears to be the case where the equations are reassembled every tenth increment and corrected

every second increment. It will be demonstrated by other examples how effective and accurate this procedure may be.

3. Nonlinear Elastic Analysis of a Spherical Shell Cap Under a Point Load at the Apex

In order to determine whether the solution scheme chosen as the most efficient for the previous problem is of general use, it was applied to the problem of an axisymmetric spherical shell cap under a concentrated load of infinite durations applied at the apex. The equations were assembled every tenth time increment and the correction term was applied as indicated in Fig. 4. It is noted that the form of the plot does not change but the maximum deflection begins to drop off with the decrease in frequency of application of the correction term. These results give an indication of how often the correction should be applied, but it may be deduced that for an accurate solution the correction should be applied at every step.

The sensitivity of the solution to the correction term may be explained as follows. The correction is computed as an unbalanced force at the end of an increment. Theoretically a correction to the current displacement should be computed by using this force and the equations applying at the beginning of the increment. In the present formulation because of the computational difficulties and expense involved in doing this displacement correction, the unbalanced force is added on as a load over the next increment. This in effect means that the correction will be computed using the current equations rather than the equation at the beginning of the increment. We may assume that over one time increment the equations governing the structure will not change appreciable and the method just described for applying the correction will be suitable but it becomes less accurate as the number of intervals between corrections is increased.

Also shown on Fig. 4 is the effect of doubling the time increment where the equations are still reassembled every ten increments and corrected at every increment. Finally a plot is shown of a result obtained with the parameters jus

described but using the element of [31]. It is noted that this element has one less degree of freedom per node but in terms of computational efficiency the isoparametric element takes only approximately 15 per cent more time for an equal number of elements. The element in [31] gave good comparisons with the current results when thirty elements were used.

The solution arrived at by reassembling every ten steps and correcting every step with a time increment of 1×10^{-6} seconds is compared with the results of a finite element solution given in [10]. This solution was obtained using the total form of the equations which necessitates extrapolating for displacements over an increment and computing the nonlinear portion of the equations as pseudo forces on the right-hand side of the equations. The equations were solved using iteration or Newton-Raphson for the more nonlinear problems and the time integration was performed using the Houbolt scheme.

As shown in Fig. 5 the present solution using fifteen elements agrees substantially with the results of [10] for thirty elements. This agreement is interesting in that the approaches used to solve the problem, such as the element type, the time increment (the present increment is eight times that used in [10]), the assembly of the nonlinear terms, and the solution scheme (incremental versus total equations), are quite different in each case.

4. Elastic-Plastic Beam Under a Uniform Initial Velocity Over a Portion of the Span

The essentials of the example are given in Fig. 6 where a beam of span 10" is given an impulse of 2172 in./sec. over the central 2" of the span. The material of the beam is elastic-plastic work-hardening and is modeled by a piecewise linear stress-strain curve as shown in Fig. 6. The results for the finite element case were obtained using ten isoparametric elements with three integration points per element. The reassembly of the equations and the correction term were computed every fifth and every time increment respectively, and a time increment of 2.5×10^{-6} sec. was used.

The results are compared in Fig. 6 with a finite difference solution and with experimental data given in [32]. The finite difference solution was computed using twentieth mesh points on the beam and a time increment of $1/3$ micro-second, which is 20 per cent of the step size necessary for the stability of the solution. The finite element solution using Houbolt's scheme was unstable only for a time increment greater than 2.5 micro-seconds. A check was made on the solution by running the problem with a time step equal to 1 micro-second, reassembling every ten steps, and correcting every step, but no significant change occurred.

Since the elastic large-displacement results already presented are in perfect agreement with other finite difference and finite element results, the slight discrepancy between the numerical results in Fig. 6 must be attributed to the elastic-plastic portion of the problem. A further check was made on the finite element solution by using five Gaussian integration points per element as opposed to the three used originally but no change was reflected in the result, and so it is assumed that the solution has converged. The differences between the numerical solutions may be accounted for by the fact that in the current solution scheme the elastic-plastic constitutive law is weighted for stress states going from elastic to plastic over an increment. The discrepancy between both numerical results and the experimental values may be accounted for by the fact that the effect of strain rate sensitivity on the yield stress of the steel used in the experiments is neglected in the numerical solutions.

Results obtained by various investigators on the variation of the yield stress of structural materials with increase in strain rate are reviewed in [19] and it is mentioned there that for the steel used in the experiments in question the increase in yield is about twenty per cent at a strain rate of 100 sec.^{-1} . The inclusion in the numerical analysis of this factor on the yield stress would tend to improve the agreement between theory and experiment.

5. Elastic-Plastic Buckling of an Imperfect Sphere Under a Uniform Constant External Pressure

The geometry of the sphere is shown in Fig. 7 where the imperfection is given as a flat section of the shell of radius R_{imp} , which is taken to be the mean radius of the oblate portion of the sphere. For the more simple elements, where only displacement continuity is required at the nodes, as in [31] and [6],

the junction of the imperfect portion with the rest of the shell presents no special problem. But for the higher order isoparametric element, the displacements and their first derivatives are incompatible. The combination of these higher order elements across the junction is achieved by applying a constraint relating the displacements at two hypothetical nodes, in the manner of Hibbitt and Marcal [33]. Preliminary analysis of a linear hemispherical shell suggested that a solution with twenty elements and a time increment of 0.1 micro-seconds would be sufficient to cover the response.

Inserted in Fig. 8 are the expressions for the geometric parameter λ and the critical static buckling pressure $P_{crit.}$ for the sphere. Also shown is the model of the stress-strain behavior of the shell material which corresponds to that of an aluminum alloy (7075-T6).

The shell was analyzed both elastically and elastic-plastically and the results for the parameter $\lambda = 2.12$ are shown in Fig. 8, where the deflection at the apex is plotted against time. It is noted that there is a great difference between the elastic and the elastic-plastic values for the ratio of the pressure required to cause dynamic buckling to $P_{crit.}$ in the imperfect shell. The form of the response history also is quite different for each material idealization. The structure is deemed to have buckled when the deflection profile increases drastically for a small increment in pressure. As an example of this, consider the divergence between the deflection profiles for the elastic response to the nondimensional pressure values given by $P/P_{crit.} = 0.575$ and $P/P_{crit.} = 0.55$. Nearly all of the curves point to the fact that the response must be traced over a number of oscillations before it is decided whether buckling will occur or not. This is especially true for the elastic example with $P/P_{crit.} = 0.55$ which appears to be just below the buckling pressure threshold.

To illustrate the different response characteristics of this shell with the variation of the parameter λ , results are shown in Fig. 9 for $\lambda = 3.42$. In this case the response is mainly elastic and this is reflected in the proximity of the elastic and elastic-plastic buckling values for $P/P_{crit.}$ given in Fig. 9. However, the overall response history is very different from that of Fig. 8 in that buckling occurs after the first maximum and not after a number of oscillations.

The problem under discussion was first solved by Bushnell [34] for the static elastic case, and also by Marcal [2] for the elastic-plastic case. These results are now compared with the present elastic and elastic-plastic dynamic results in Fig. 10. Values of the pressure parameters P/P_{crit} , which initiate buckling are plotted against the geometric parameter λ . The main feature of the results is the manner in which the dynamic elastic-plastic curve resembles the form of the corresponding static result from [2]. In both the static and dynamic cases, for $\lambda < 3$, the buckling pressure is governed very strongly by the plastic flow of the material. For these values of λ any analysis neglecting nonlinear material behavior would be meaningless. This problem is a good example of a strong interaction between large displacements and nonlinear material behavior.

As observed in Fig. 8 and 9, two different manners of collapse take place for different shell parameters, namely collapse on the first maximum displacement and collapse on subsequent maxima. It is noted from Fig. 10 that, compared to the penalty due to the imperfection, dynamic loading does not impose too large a penalty.

In computing the results just described the equations were reassembled every ten increments and corrected every second increment. It was felt that these values were sufficiently accurate in that the time increment used of 1/10 micro-second was very small, and in that the final buckling value taken was computed as the average of two close values, one of which caused buckling while the other did not.

VII. DISCUSSION AND CONCLUSIONS

A numerical procedure has been developed whereby the finite element method may be used to analyze large elastic-plastic deformations of structures under a variety of dynamic loadings. It has been determined that the standard incremental equations are not totally sufficient in the dynamic case and that a correction should be applied to the system in the form of an equilibrium check. The error in the simple incremental method is shown to be of the order of the displacement increment squared coupled with a factor equal to the time increment squared. It is this factor which causes the incremental method to converge

rapidly as the time increment is made smaller and smaller. On the other hand, it has been found that the corrected incremental equations give stable and accurate solutions with time increments approximately one order of magnitude greater than corresponding time steps used in finite difference, and other finite element work. In this case the reduction of the truncation error of the solution by the correction process favors the convergence of the solution, and makes the incremental approach competitive economically with other methods which require extrapolation, and therefore small time steps, in order to handle the nonlinear terms.

Many approximate procedures, which are often employed in static finite element analysis, were tested with the purpose of gauging their suitability for use in dynamic work. It was shown for the example in Fig. 3b that computing the stress at one representative point only in the element gives results which agree substantially with the analysis which includes all stress points. This approximation saves time and storage in the computer, and is useful as a first step in an analysis, but it should be used only with the corrected form of the incremental equations. A point to remember about nonlinear analysis, such as demonstrated in the example given for the elastic and elastic-plastic buckling of a sphere, is that it is difficult to estimate the probable response in order to plan a numerical solution. An inexpensive way of investigating the problem, used frequently in this research as a preliminary step, is to reassemble the equations at very wide intervals and likewise with respect to applying the correction terms. Cases in point are the beam example in Fig. 3b and the shell example in Fig. 4 where the reassembly and correction operations were performed every tenth and every fifth increment, respectively, without any great change in the frequency or amplitude. Since most of the solution time is used in the updating procedure, the savings in execution time increase substantially with the frequency of the updating. A word of caution is inserted here to the effect that, while the reassembly of the equations may be performed at will, the correction terms should be computed more frequently as pointed out in the example of the spherical cap under a point load at the apex. This is especially true for the elastic-plastic case where the solution tends to be unstable for too low a frequency of the application of the correction terms. As an example, the solution of the elastic-plastic buckling of the sphere was unstable when the correction was applied every

f n increment, but gave a stable solution when the computation was made every second increment. This is to be expected in a solution where the response varies widely and serves as a built-in indicator of such a response. An added advantage of the incremental method, as opposed to using the total form of the equations and extrapolating for the nonlinear forces, is that the above approximate and inexpensive solutions may be obtained.

A useful development of this research is the general purpose computer program from which the results described here have been obtained. This forms a versatile research tool due to its modular and flexible construction. Especially important is that any element may be used in this program, and conversely any improvements made in the solution scheme in the body of the program apply to all elements. The capability for node-typing is also available and would be suitable for problems involving combined element analysis where linear constraints must be imposed on the interfaces between the different element types. The solution scheme used, the incremental method, also allows one to add other constitutive relations to the program directly. In using the total form of the equations it is not clear how one would separate the pseudo forces due to material and geometric behavior even for the simplest nonlinear constitutive relation.

In summary, some progress has been made in the solution of nonlinear dynamic problems. Useful approximations have been found to yield economic solution times. The effect of geometric imperfections on the dynamic buckling of an elastic-plastic shell has been observed. Future work will be concerned with extending the analysis to other structure types and to the inclusion of visco-plastic behavior.

R E F E R E N C E S

1. Hibbitt, H. D., Levy, N. J. and Marcal, P. V., "On General Purpose Programs for Nonlinear Finite Element Analysis," Proc. ASME Seminar on General Purpose Finite Element Programs, ASME Winter Annual Meeting, N.Y., December 1970.
2. Marcal, P.V., "Finite Element Analysis of Combined Problems of Nonlinear Material and Geometric Behavior," Proc. ASME Joint Computer Conference on Computational Approach to Applied Mechanics, Chicago 1969.
3. Oden, J. T., "General Theory of Finite Elements," *Int. J. Numerical Methods in Engineering*, Parts I and II, 1, 1969, p. 205 and p. 247.
4. McNamara, J. F., "Incremental Stiffness Method for Finite Element Analysis of the Nonlinear Dynamic Problem," Ph.D. Thesis, submitted August 1971.
5. Turner, M. J., Clough, R. W., Martin, H. C. and Topp, L. J., "Stiffness and Deflection Analysis of Complex Structures," *Journal of Aerospace Sciences*, 23, (1956), pp. 805-823.
6. Klein, S. and Sylvester, R.J., "The Linear Elastic Dynamic Analysis of Shells of Revolution by the Matrix Displacement Method," Air Force Flight Dynamics Laboratory, TR-66-80, 1966, pp. 299-329.
7. Popov, P. V. and Chow, Y. C., Addendum to the above paper.
8. Clough, R. W., "Analysis of Structural Vibrations and Dynamic Response," Japan-U. S. Seminar on Matrix Methods of Structural Analysis and Design, Tokyo, Japan, August 1969.
9. Turner, M. J., Dill, E. H., Martin, H. C. and Melosh, R. J., "Large Deflection Analysis of Complex Structures Subjected to Heating and External Loads," *Journal of Aerospace Sciences*, 27, February 1960, pp. 97-106.
10. Stricklin, J. A., Martinez, J. E., Tillerson, J. R. Hong, J. H. and Haisler, W. E., "Nonlinear Dynamic Analysis of Shells of Revolution by Matrix Displacement Method," Report 69-77, Texas Engineering Experiment Station, Texas A&M University, February 1970.
11. Klein, S., "The Nonlinear Dynamic Analysis of Shells of Revolution with Asymmetric Properties by the Finite Element Method," The Aerospace Corporation, San Bernardino, California ATR-71(S-9900)-7, April 1971.
12. Hill, R., "Mathematical Theory of Plasticity," Oxford (1950).
13. Chang, G. C. and Gilbert, F. S., "Finite Element Approach to Wave Motions in Elastic-Plastic Continua," Proceedings of the AIAA 6th Aerospace Sciences Meeting," paper 68-145, New York, January 1962.

14. Costantino, C. J., "Two Dimensional Wave Propagation Through Nonlinear Media," *Journal of Computational Physics*, 4, No. 2, August 1969, pp. 147-170.
15. Fulton, R. E., "Numerical Analysis of Shells of Revolution," paper presented at the IUTAM Symposium on High-Speed Computing of Elastic Structures at Liege, Belgium August 29- September 6, 1970.
16. Witmer, E. A., Balmer, H. A., Leach, J. W. and Pian, T. H. H., "Large Dynamic Deformations of Beams, Rings, Plates, and Shells," *AIAA Journal*, 1, No. 8, August 1963, pp. 1848-1857.
17. Leach, J. W., Witmer, E. A. and Pian, T. H. H., "A Numerical Calculation Technique for Large Elastic-Plastic Dynamically-Induced Deformations of General Thin Shells," *AIAA Journal*, 6, No. 1, December 1968, pp. 2352-2359.
18. Witmer, E. A., Clark, E. N. and Balmer, H. A., "Experimental and Theoretical Studies of Explosive-Induced Large Dynamic and Permanent Deformations of Simple Structures," *Experimental Mechanics*, February 1967, pp. 56-66.
19. Symonds, P. S., "Survey of Methods of Analysis for Plastic Deformation of Structures under Dynamic Loading," Brown University Report, BU/NSRDS/1-67, June 1967.
20. Martin, J. B. and Symonds, P. S., "Mode Approximations for Impulsively Loaded Rigid-Plastic Structures," *Proceedings of the American Society of Civil Engineers*, 92, pp. 43-66, 1966.
21. Martin, J. B., "Impulsive Loading Theorems for Rigid-Plastic Continua," *Proceedings of the American Society of Civil Engineers*, 90, pp. 27-42, 1964.
22. Martin, J. B., "A Displacement Bound Principle for Inelastic Continua Subjected to Certain Classes of Dynamic Loading," *Journal of Applied Mechanics*, 32, No. 1, pp. 1-6, 1965.
23. Haisler, W. E., Stricklin, J. A. and Stebbins, F. J., "Development and Evaluation of Solution Procedures for Geometrically Nonlinear Structural Analysis by the Direct Stiffness Method," paper presented at the AIAA/ASME 12th Structures, Structural Dynamics and Material Conference, Anaheim, California, April 19-21, 1971.
24. Marcal, P. V. and King, I. P., "Elastic-Plastic Analysis of Two-Dimensional Stress Systems by the Finite Element Method," *International Journal of Mechanical Science*, 9, No. 3, 1967, pp. 143-155.

25. Hibbitt, H. D., Marcal, P. V. and Rice, J. R., "A Finite Element Formulation for Problems of Large Strain and Large Displacement," *International Journal of Solids and Structures*, 6, pp. 1069-1086, 1970.
26. Hofmeister, L. D., Greenbaum, G. A. and Evensen, D. A., "Large Strain, Elasto-Plastic Finite Element Analysis," to be published in the *AIAA Journal*.
27. Houbolt, J. C., "A Recurrence Matrix Solution for the Dynamic Response of Elastic Aircraft," *Journal of Aerospace Sciences*, 17, 1950, pp. 540-550.
28. Eringen, C. A., "On the Nonlinear Vibration of Elastic Bars," *Quantum Applied Mathematics*, 10, No. 4, 1952.
29. Chu, Hu-Nan, and Herrman, G., "Influence of Large Amplitudes on Free Flexural Vibrations of Rectangular Elastic Plates," *Journal of Applied Mechanics*, Paper No. 56-APM-27, December 1956.
30. Krieg, R. D. and Key, S. W., "Univalve, A Computer Code for Analyzing Dynamic Large Deflection Elastic-Plastic Response of Beams and Rings," SC-RR-66-2682, Sandia Laboratories, Albuquerque, New Mexico, January 1968.
31. Khojasteh-Bakht, M., "Analysis of Elastic-Plastic Shells of Revolution under Axisymmetric Loading by the Finite Element Method," Ph.D. Dissertation, University of California at Berkeley, SESM 67-68, April 1969.
32. Krieg, R. D., Duffey, T. A. and Key, S. W., "The Large Deflection Elastic-Plastic Response of Impulsively Loaded Beam: A Comparison Between Computations and Experiment," SC-RR-88-226, Sandia Laboratories, Albuquerque, New Mexico, July 1968.
33. Hibbitt, H. D. and Marcal, P. V., "Hybrid Finite Element Analysis with Particular Reference to Axisymmetric Structures," Proc. AIAA 8th Aerospace Sciences Meeting, New York, January 19-21, 1970.
34. Bushnell, D., "Nonlinear Axisymmetric Behavior of Shells of Revolution," *AIAA Journal*, 5, No. 3, 1967, pp. 432-439.

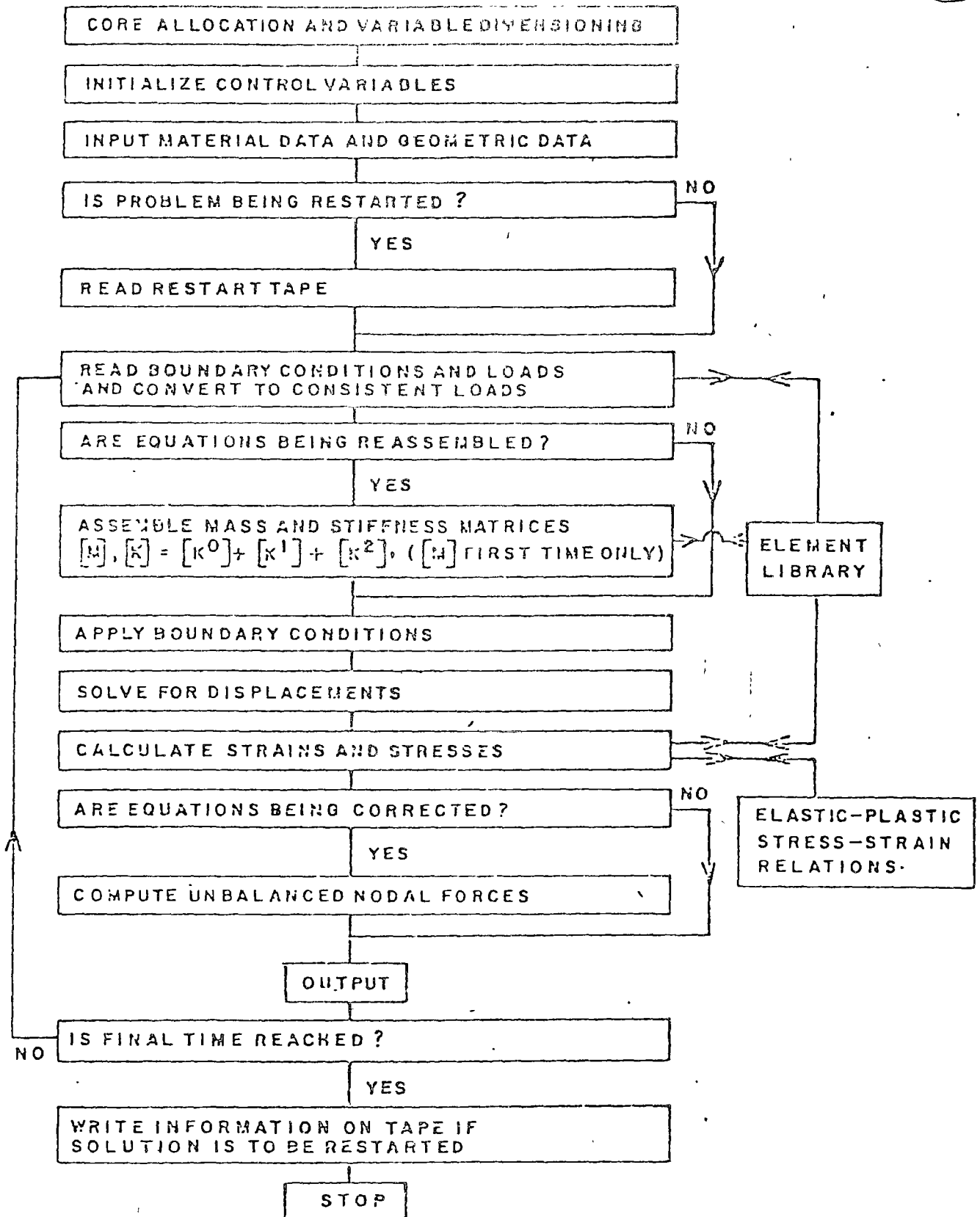


FIG. 1 FLOW CHART FOR COMPUTER PROGRAM.

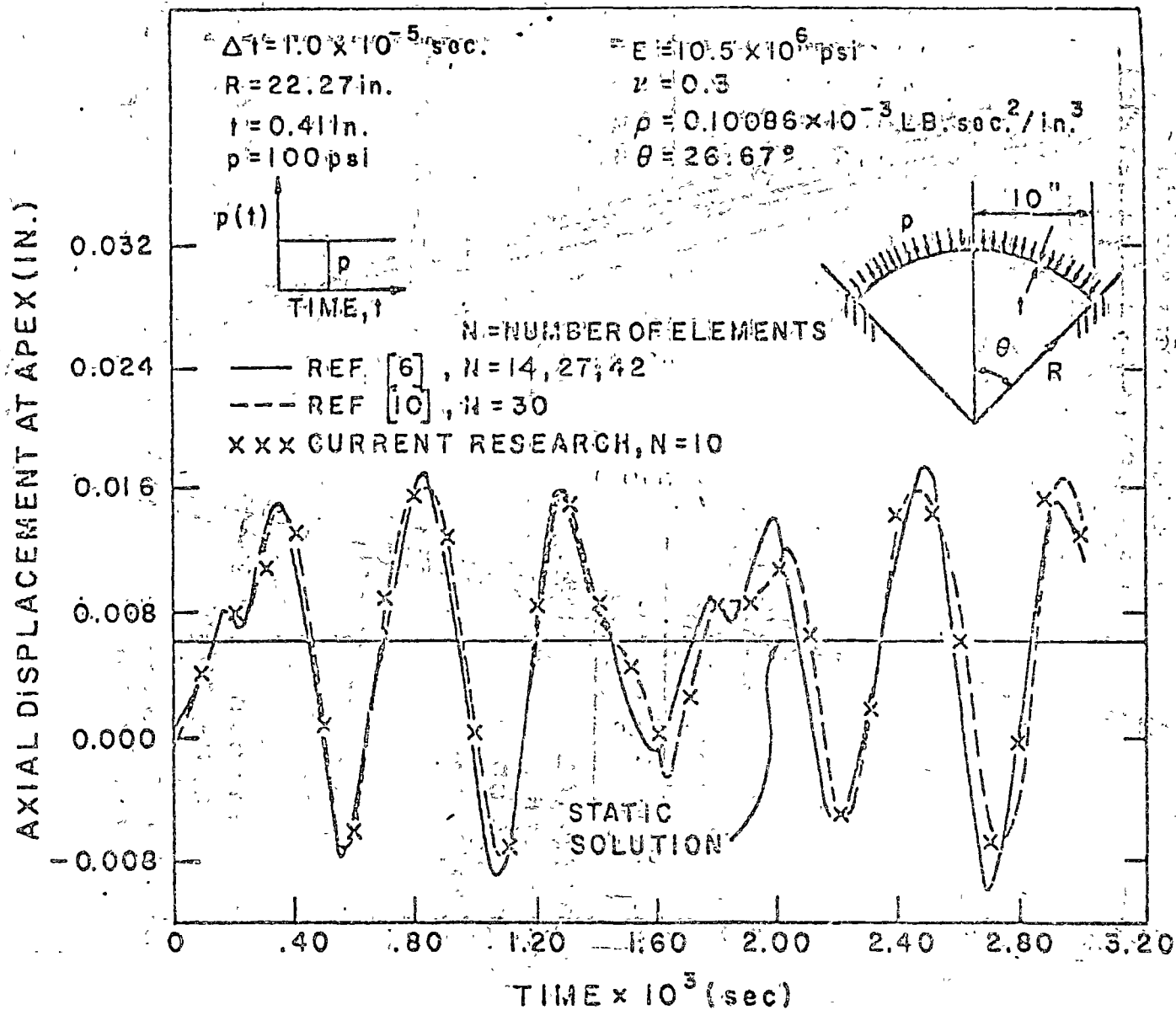
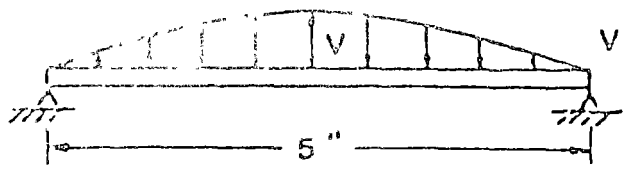


FIG. 2 SHALLOW SPHERICAL CAP UNDER AXISYMMETRIC DYNAMIC LOADING.



$V = 1000 \text{ in/80}$

$h = .125 \text{''}$

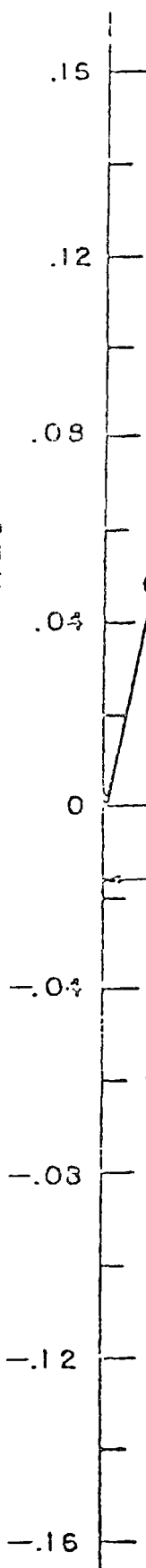
$b = 1.0 \text{''}$

$E = 10.605 \times 10^6 \text{ lbs./in}^2$

$\rho = 2.508 \times 10^{-4} \text{ lbs. sec}^2/\text{in}^4$

5 ELEMENTS (ISOPARAMETRIC)

CENTRAL DEFLECTION IN INCHES



THEORETICAL
NONLINEAR
HALF-PERIOD
[28, 29]

--- NO LOAD
CORRECTION
— INCLUDES LOAD
CORRECTION
○ $\Delta T = 2.5 \times 10^{-6}$

$\Delta T = 1 \times 10^{-5} \text{ sec}$

$\Delta T = 2.5 \times 10^{-5} \text{ sec}$

$\Delta T = 5 \times 10^{-6} \text{ sec}$

TIME $\times 10^4 \text{ sec}$

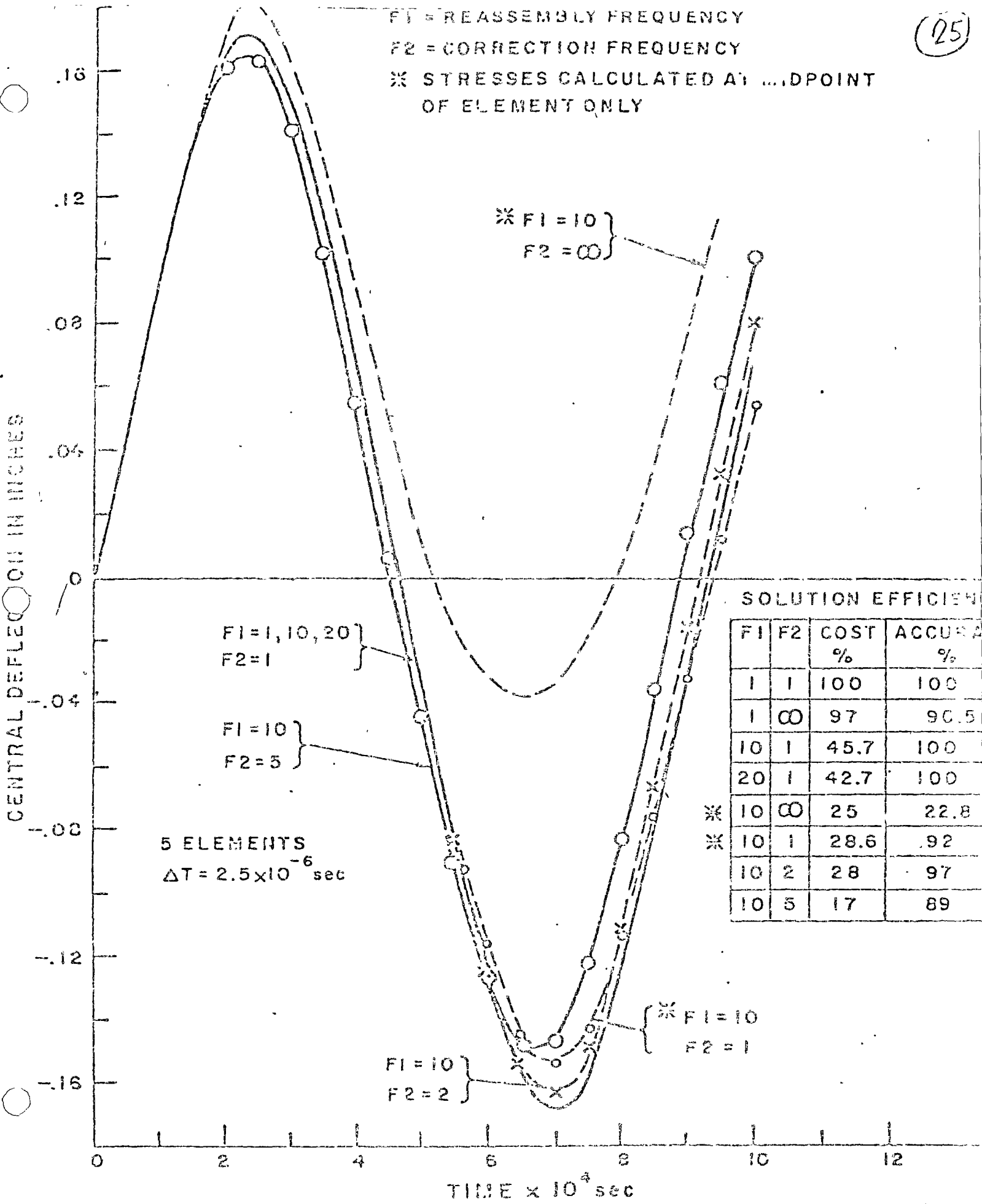


FIG. 3. APPROXIMATE SOLUTION SCHEMES

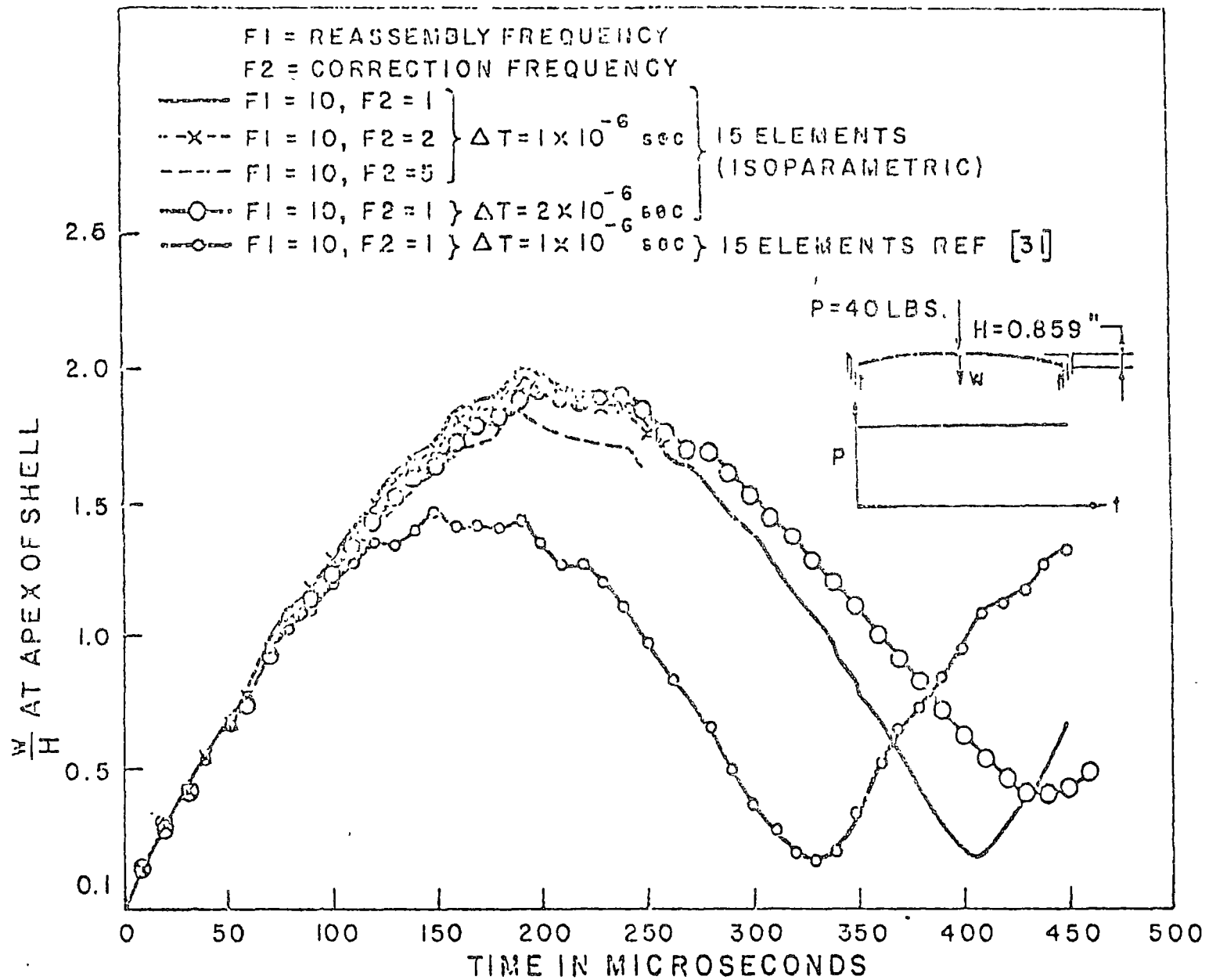


FIG. 4 EFFECT OF VARIOUS PARAMETERS ON SOLUTION CONVERGENCE

LIBRARY
UNIVERSITY OF MICHIGAN

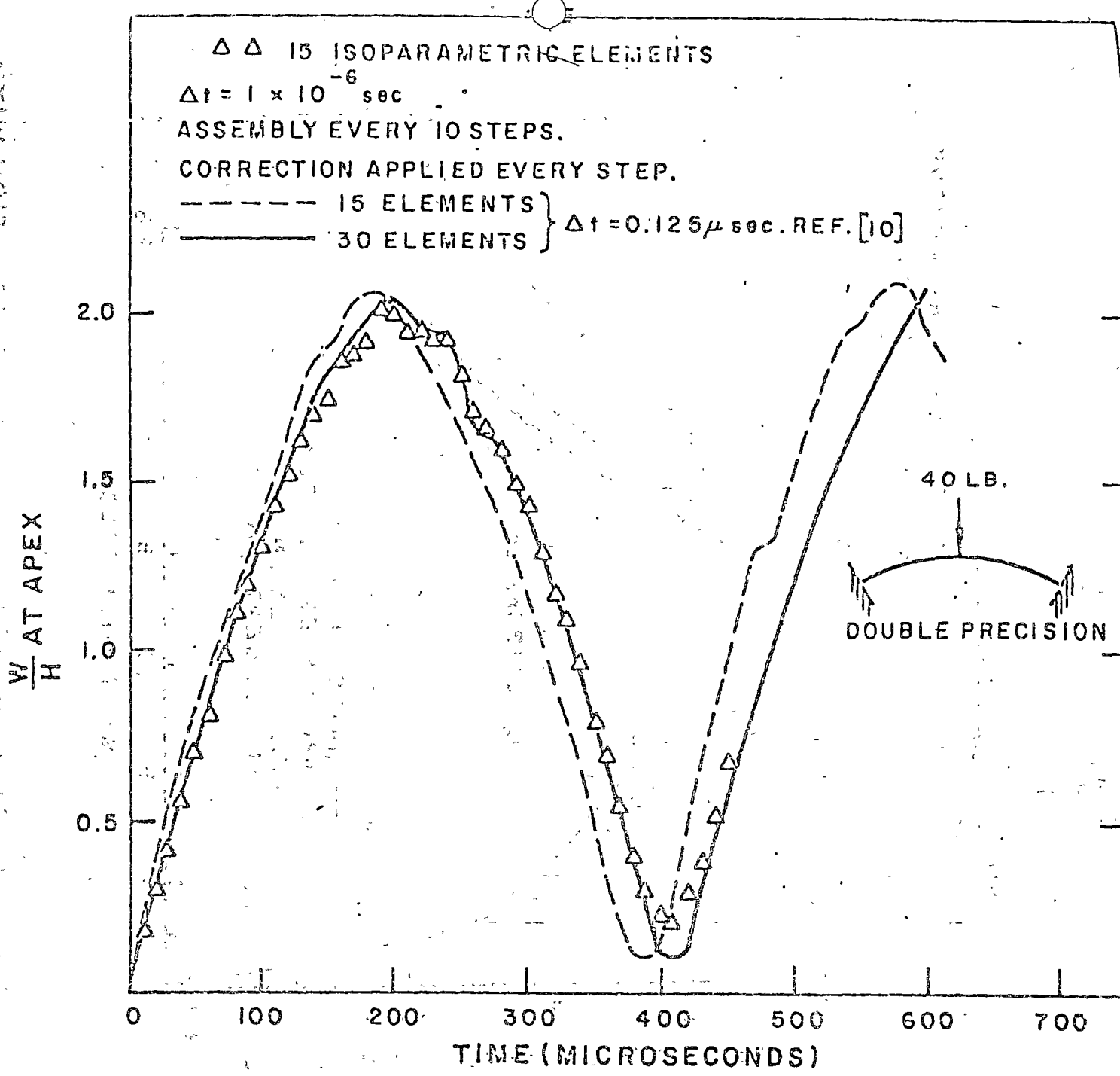


FIG. 5 SOLUTION CONVERGENCE

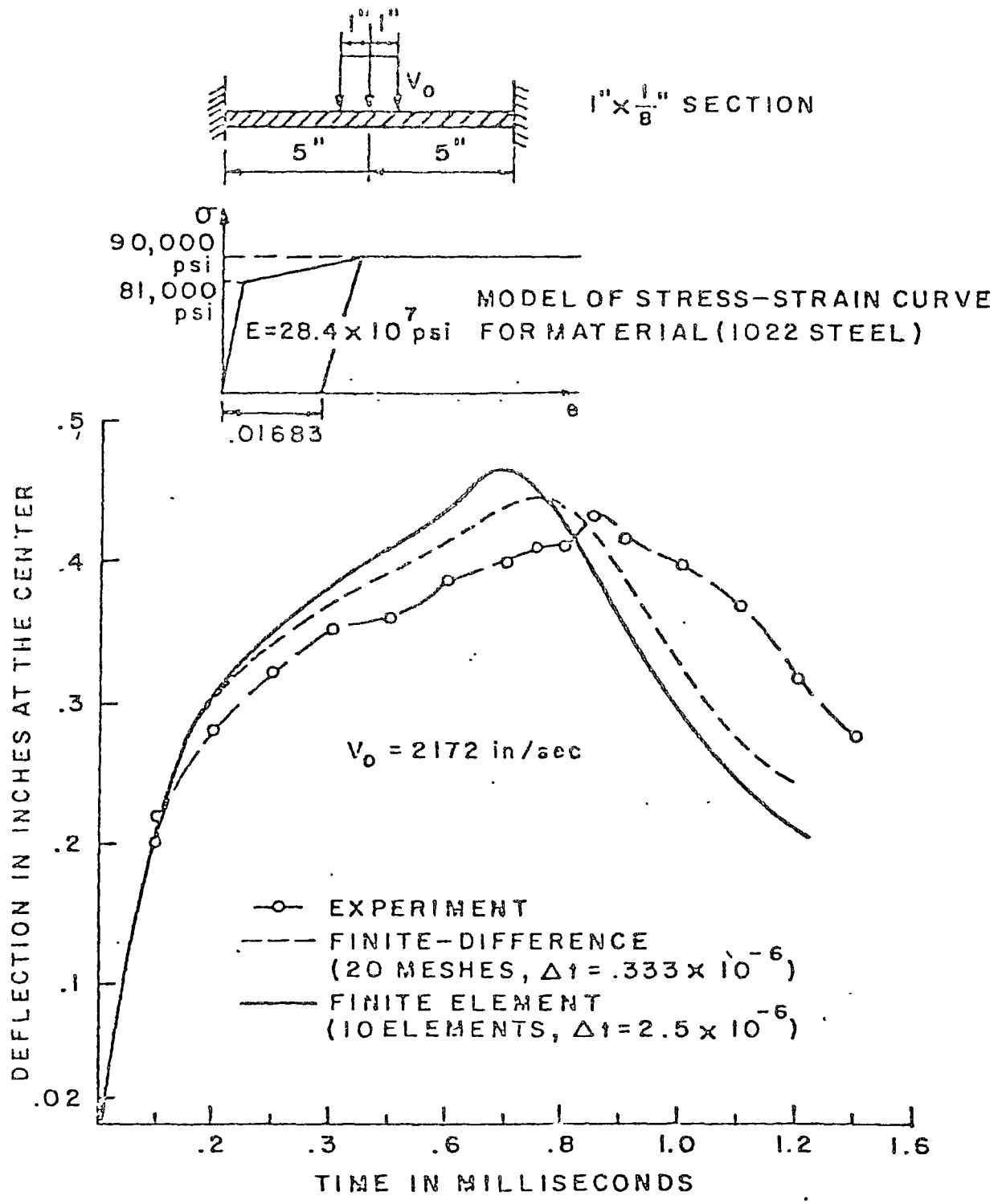
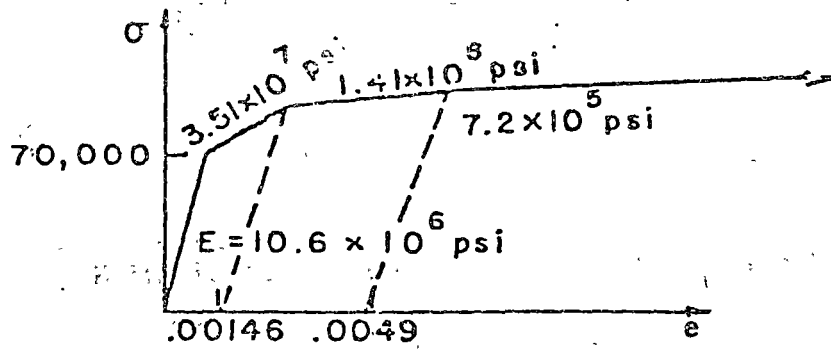


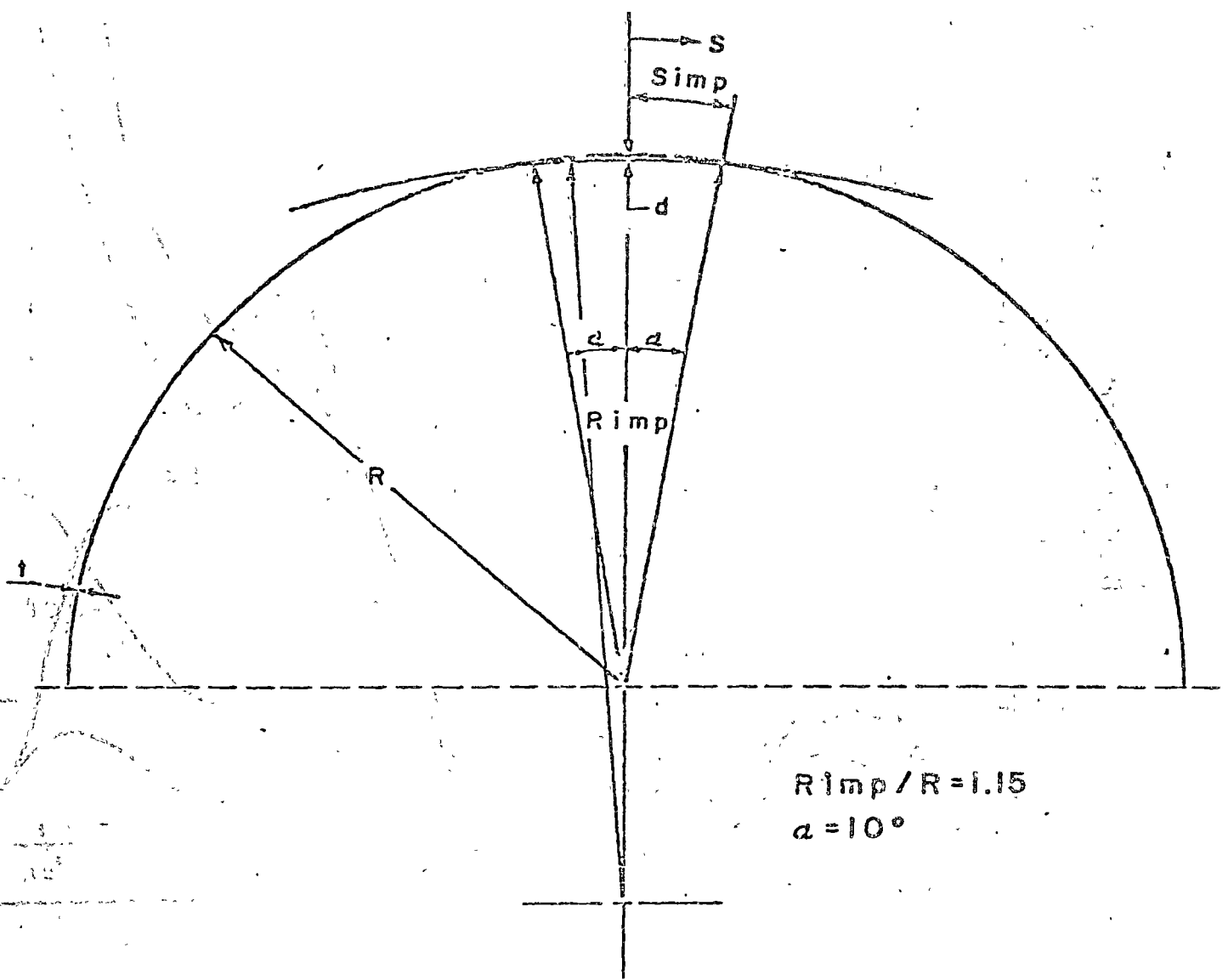
FIG.6 COMPARISON OF FINITE ELEMENT SOLUTION WITH FINITE DIFFERENCE SOLUTION FOR BEAM PROBLEM



MODEL OF STRESS-STRAIN CURVE

$$\lambda = [12(1-\nu^2)]^{1/4} \left(\frac{R}{t}\right)^{1/2} \left(\frac{R}{R_{imp}}\right)^{1/2} \alpha$$

$$P_{cr} = \frac{2E}{[3(1-\nu^2)]^{1/2}} \left(\frac{t}{R}\right)^2$$



$R_{imp}/R = 1.15$
 $\alpha = 10^\circ$

FIG. 7 EXTERNALLY PRESSURIZED IMPERFECT HEMISPHERE AND MATERIAL CONSTANTS

$R = .812 \quad \epsilon = .0159$

$P_{cr} = 4,880 \text{ psi} \quad \lambda = 2.12$

$\frac{P}{P_{cr}} = .563$ FOR ELASTIC BUCKLING

$\frac{P}{P_{cr}} = .340$ FOR ELASTIC-PLASTIC BUCKLING

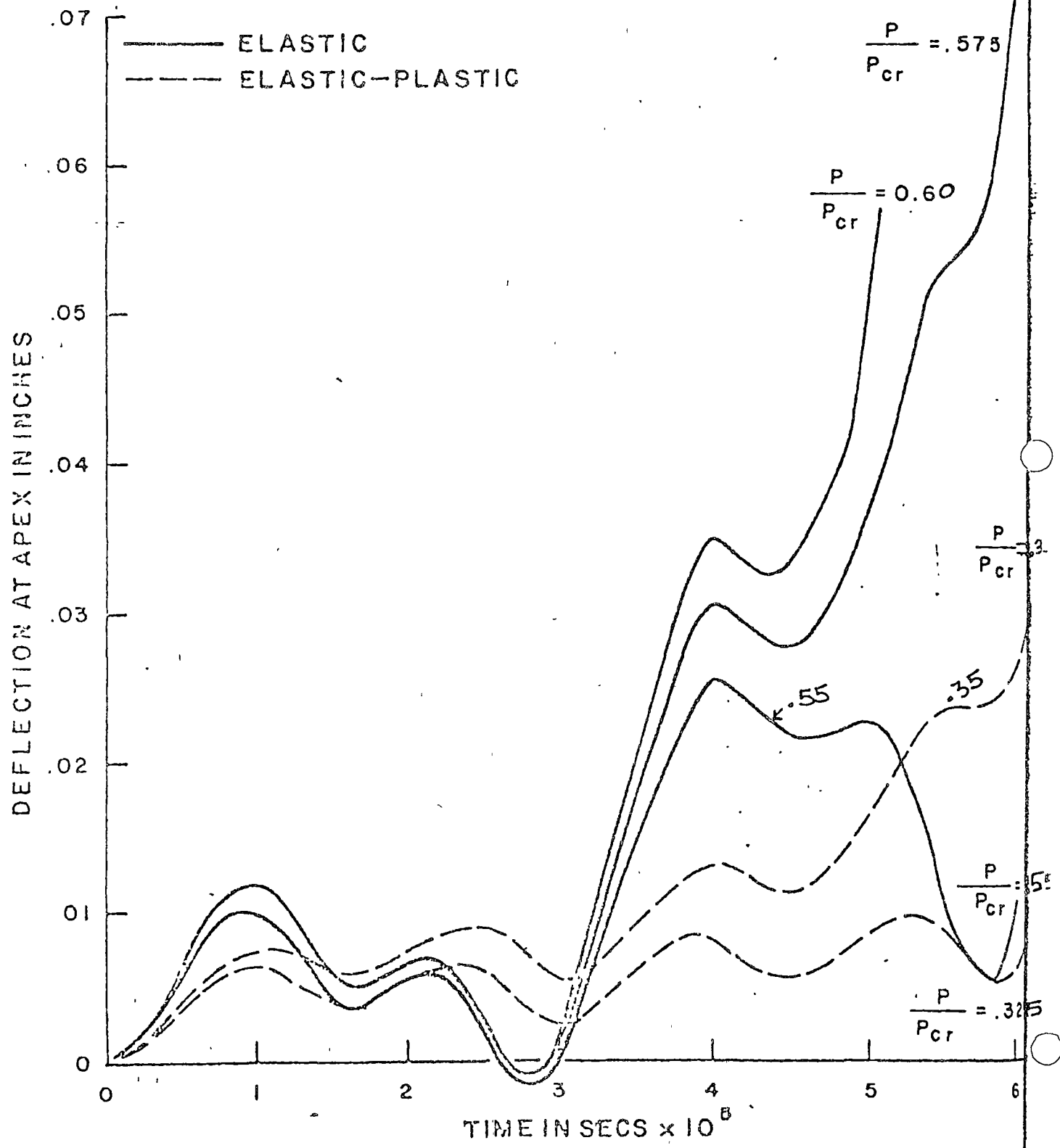


FIG. 8 DEFLECTION PROFILES FOR ELASTIC AND ELASTIC-PLASTIC BUCKLING OF IMPERFECT SPHERE, $\lambda = 2.12$

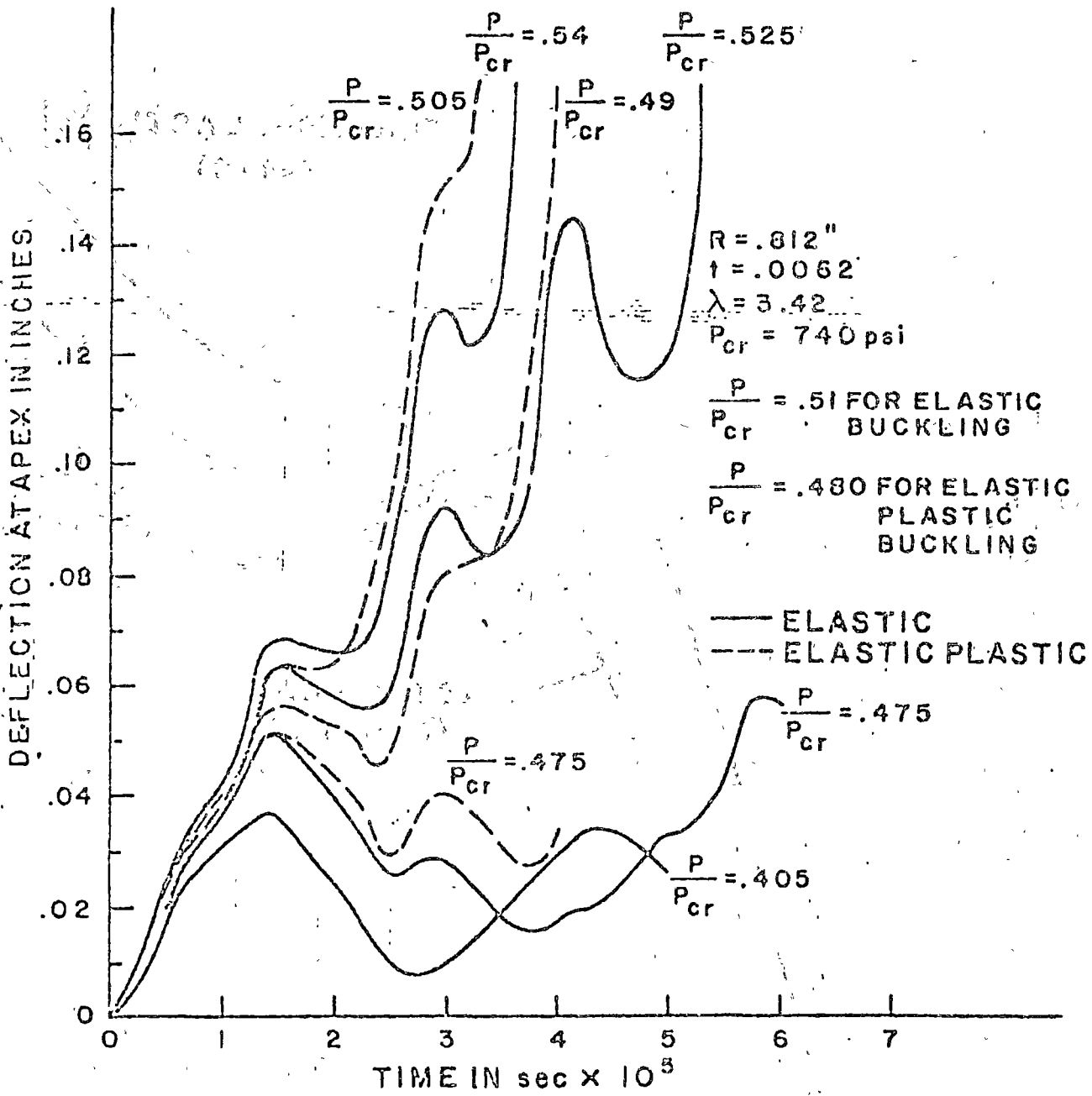


FIG. 9 DEFLECTION PROFILES FOR ELASTIC AND ELASTIC-PLASTIC BUCKLING OF IMPERFECT SPHERE, $\lambda = 3.42$

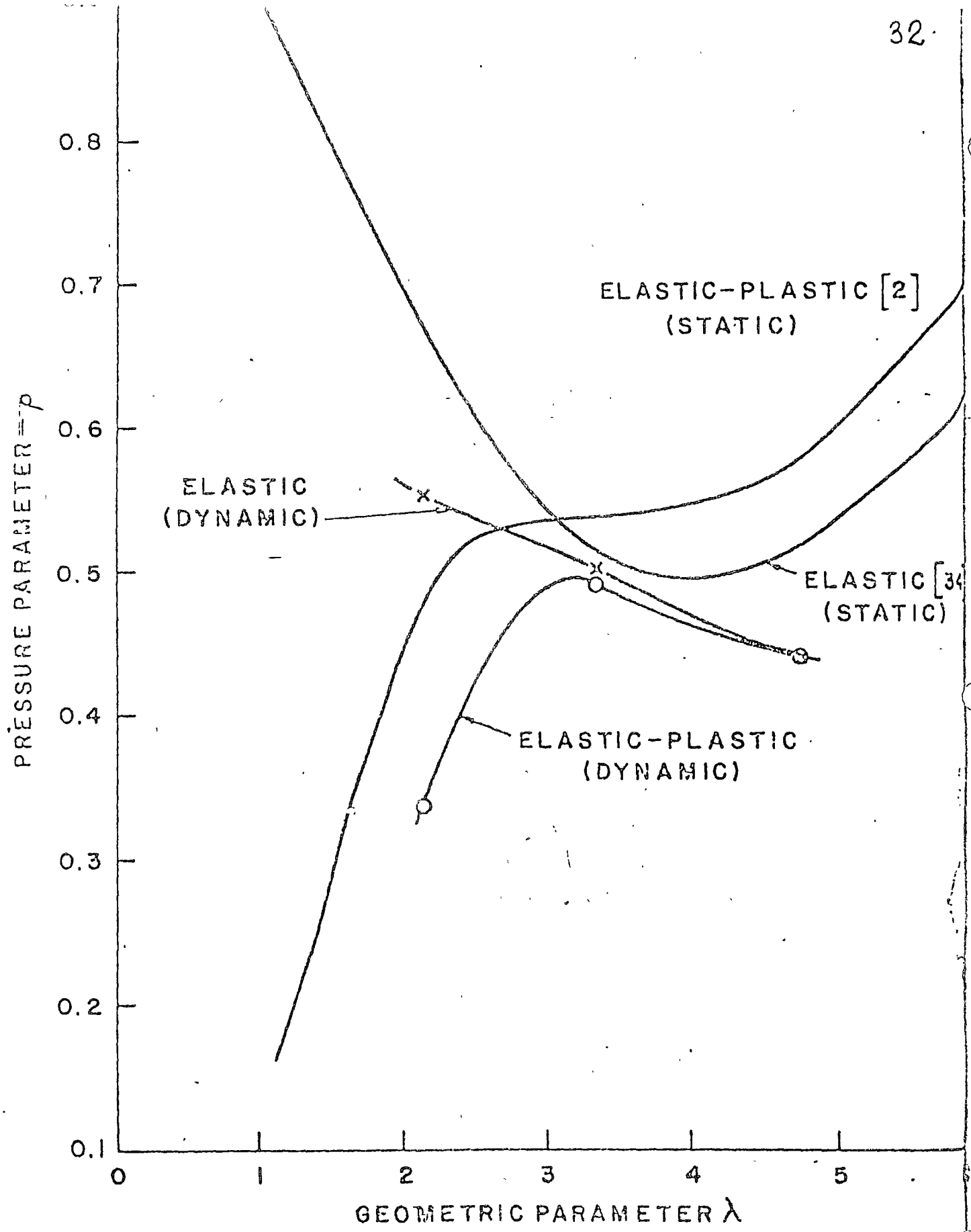


FIG. 10 BUCKLING PRESSURES FOR OBLATE SHELLS, $R_{imp}/R=1.1$

The solution of the dynamic finite element equations involve a step-by-step integration. To-date workers have only pursued the implicit methods. The writer thinks that this is due to interest in the structural dynamics regime of behavior where there is less penalty for adopting the implicit integration schemes. There is every evidence that in the shock regimes the explicit equations will prove useful. Similar work by finite differences (e.g. the Pisce code) use explicit integration schemes to the fullest.

In the use of the implicit schemes, the user should be aware of two possible types of errors. The integration scheme introduces their stability by 'averaging' or 'damping' with past values. This results in a distortion of the amplitude as well as the phase.

DIRECT INTEGRATION OPERATORS

Two direct integration operators are commonly used. The first is the Newmark β method, with $\gamma = 1/2$, $\beta = 1/4$ (trapezoidal rule), while the second is the Houbolt operator (displacement approximated over 3 time-steps by a cubic). Both of these operators are implicit (i.e., matrix solution is required to step the solution forward) and both are unconditionally stable with respect to time step size for linear problems. The Houbolt operator introduced artificial damping, the amount of such damping increasing with the ratio of time step to period of the natural modes of the system. Thus the Houbolt operator effectively removes higher mode response from the system. The usual recommendation is to extract the Eigen modes and frequencies of the system and then decide on which modes are important to the response. The time step should then be chosen as 1/15 to 1/30 of the period of the highest such mode. However, in nonlinear problems, the mode shapes and frequencies are strong functions of time, through plasticity and large displacement effects, so that the above guideline may be quite a coarse approximation. A more general rule would be to repeat a part of the analysis with a significantly different time step (1/5 to 1/10 of the original), and compare response. This is easily achieved through the use of restart.

Both the Newmark and the Houbolt operators introduce periodicity errors, again reversing with the ratio of time step to period of the natural mode involved. With the above guideline, minor errors would occur for the modes below that used for time step estimates.

The derivations below show the equations used in MARC to solve the system, based on the Newmark and Houbolt operators:

NEWMARK β OPERATOR

The generalized form of the Newmark β operator is

$$u^{n+1} = u^n + \Delta t v^n + \left(\frac{1}{2} - \beta\right) \Delta t^2 a^n + \beta \Delta t^2 a^{n+1}$$

$$v^{n+1} = v^n + (1-\gamma) \Delta t a^n + \gamma \Delta t a^{n+1}$$

The particular form corresponding to the trapezoidal rule is $\gamma = \frac{1}{2}$, $\beta = \frac{1}{4}$:

$$u^{n+1} = u^n + \Delta t v^n + \frac{\Delta t^2}{4} a^n + \frac{\Delta t^2}{4} a^{n+1} \tag{1}$$

$$v^{n+1} = v^n + \frac{\Delta t}{2} a^n + \frac{\Delta t}{2} a^{n+1}$$

The equation of motion at time t^{n+1} is

$$M a^{n+1} + C^{n+1} v^{n+1} + I^{n+1} = F^{n+1}, \quad I = \int \int \beta^T \sigma \, dV \tag{2}$$

Rearranging (1) gives

$$a^{n+1} = \frac{4}{\Delta t^2} u^{n+1} - \frac{4}{\Delta t^2} u^n - \frac{4}{\Delta t} v^n - a^n$$

and

$$v^{n+1} = \frac{2}{\Delta t} u^{n+1} - \frac{2}{\Delta t} u^n - v^n$$

Substituting in (2):

$$\left(\frac{4}{\Delta t^2} M + \frac{2}{\Delta t} C^{n+1}\right) u^{n+1} + I^{n+1} = F^{n+1} + M \left(a^n + \frac{4}{\Delta t} v^n + \frac{4}{\Delta t^2} u^n\right) + C \left(v^n + \frac{2}{\Delta t} u^n\right)$$

Now approximate $I^{n+1} = I^n + K \Delta u$

$$C^{n+1} = C^n$$

and subtract

$$\left(\frac{4}{\Delta t^2} M + \frac{2}{\Delta t} C\right) u^n$$

from both sides, to give:

$$\left(\frac{4}{\Delta t^2} M + \frac{2}{\Delta t} C + K\right) \Delta u = F^{n+1} - I^n + M \left(a^n + \frac{4}{\Delta t} v^n\right) + C v^n \quad (3)$$

Equation (3) allows implicit solution of the system: $u^{n+1} = u^n + \Delta u$ and then (1) gives a^{n+1} and v^{n+1} .

Note that (3) contains residual load correction implicitly. To remove the correction, we use

$$F^n = I_n + C^n v^n + M a^n$$

to remove I^n ,
so that (3) becomes

$$\left(\frac{4}{\Delta t^2} M + \frac{2}{\Delta t} C + K\right) \Delta u = \Delta F + M \left(2a^n + \frac{4}{\Delta t} v^n\right) + 2 C v^n \quad (4)$$

DAMPING

Making the assumption

$$C = \alpha M + \beta K \quad (\alpha, \beta \text{ scalars})$$

gives (3) as

$$\left[\left(\frac{4}{\Delta t^2} + \frac{2\alpha}{\Delta t}\right) M + \left(\frac{2\beta}{\Delta t} + 1\right) K\right] \Delta u = F^{n+1} - I^n + \beta K v^n + M \left(a^n + \left(\frac{4}{\Delta t} + \alpha\right) v^n\right) \quad (3a)$$

and (4) as

$$\left[\left(\frac{4}{\Delta t^2} + \frac{2\alpha}{\Delta t}\right) M + \left(\frac{2\beta}{\Delta t} + 1\right) K\right] \Delta u = \Delta F + M \left(2a^n + \left(\frac{4}{\Delta t} + 2\alpha\right) v^n\right) + 2 \beta K v^n \quad (4a)$$

The Houbolt operator is based on the use of a cubic fitted through three previous points and the current (unknown) point in time. Let t^{n+1} be the new time: then the operator is based on assuming:

$$\begin{aligned}
 u = & \frac{(t-t^n)(t-t^{n-1})(t-t^{n-2})}{(t^{n+1}-t^n)(t^{n+1}-t^{n-1})(t^{n+1}-t^{n-2})} & u_{n+1} \\
 & + \frac{(t-t^{n+1})(t-t^{n-1})(t-t^{n-2})}{(t^n-t^{n+1})(t^n-t^{n-1})(t^n-t^{n-2})} & u_n \\
 & + \frac{(t-t^{n+1})(t-t^n)(t-t^{n-2})}{(t^{n-1}-t^{n+1})(t^{n-1}-t^n)(t^{n-1}-t^{n-2})} & u_{n-1} \\
 & + \frac{(t-t^{n+1})(t-t^n)(t-t^{n-1})}{(t^{n-2}-t^{n+1})(t^{n-2}-t^n)(t^{n-2}-t^{n-1})} & u_{n-2}
 \end{aligned}$$

Now writing $f = (t-t^a)(t-t^b)(t-t^c)$,

we have $\frac{df}{dt} = (t-t^b)(t-t^c) + (t-t^a)(t-t^c) + (t-t^a)(t-t^b)$

and $\frac{d^2f}{dt^2} = 2 \{ (t-t^a) + (t-t^b) + (t-t^c) \}$

Thus, if we assume $t^{n+1} = t^n + \Delta t = t^{n-1} + 2\Delta t = t^{n-2} + 3\Delta t$ (i.e. uniform time steps), we obtain v^{n+1} and a^{n+1} as

$$v^{n+1} = \left\{ \frac{1}{\Delta t} \left[\frac{11}{6} u^{n+1} - 3 u^n + \frac{3}{2} u^{n-1} - \frac{1}{3} u^{n-2} \right] \right\} \quad (2)$$

$$\text{and } a^{n+1} = \frac{1}{t^2} \left\{ 2 u^{n+1} - 5 u^n + 4 u^{n-1} - u^{n-2} \right\}$$

The equation of motion of tire t^{n+1} is

$$M a^{n+1} + C^{n+1} v^{n+1} + I^{n+1} = F^{n+1}, \quad I^{n+1} = \int B^T dv \quad (3)$$

Substituting (2) in (3) to remove a^{n+1} and v^{n+1} gives

$$\begin{aligned} \left(\frac{2}{\Delta t^2} M + \frac{11}{6\Delta t} C^{n+1}\right) u^{n+1} + I^{n+1} &= F^{n+1} \\ &+ \frac{1}{\Delta t^2} (5 u^n - 4 u^{n-1} + t u^{n-2}) M \\ &+ \frac{1}{\Delta t} \left(3 u^n - \frac{3}{2} u^{n-1} + \frac{1}{3} u^{n-2}\right) C \end{aligned} \quad (4)$$

Now assume we can approximate $I^{n+1} = I^n + \frac{dI}{du} \Delta u$

$$I^{n+1} = I^n + K \Delta u$$

$$(\Delta u = u^{n+1} - u^n)$$

and assume $C^{n+1} = C^n$, since C is never accurately known.

Then (4) becomes

$$\begin{aligned} \left(\frac{2}{\Delta t^2} M + \frac{11}{6\Delta t} C^n\right) u^{n+1} + K^n \Delta u &= F^{n+1} - I^n \\ &+ \frac{1}{\Delta t^2} (t u^n - 4 u^{n-1} + u^{n-2}) M \\ &+ \frac{1}{\Delta t} \left(3 u^n - \frac{3}{2} u^{n-1} + \frac{1}{3} u^{n-2}\right) C \end{aligned}$$

Subtract $\left(\frac{2}{\Delta t^2} M + \frac{11}{6\Delta t} C^n\right) u^n$ from both sides to obtain an incremental form:

$$\begin{aligned} \left(\frac{2}{\Delta t^2} M + \frac{11}{6\Delta t} C^n + K^n\right) \Delta u &= F^{n+1} - I^n + \frac{1}{\Delta t^2} (3 u^n - 4 u^{n-1} + u^{n-2}) M \\ &+ \frac{1}{\Delta t} \left(\frac{7}{6} u^n - \frac{3}{2} u^{n-1} + \frac{1}{3} u^{n-2}\right) C \end{aligned} \quad (5)$$

This equation provides an implicit solution scheme: Solve (5) for Δu , hence obtain $u^{n+1} = u^n + \Delta u$ and so, using (2), obtain v^{n+1} and a^{n+1} . Two points should be kept in mind -

- (1) (5) is based on uniform time steps and so must be modified when time step size is changed.
- (2) A special starting procedure is necessary since u^n , u^{n-1} and u^{n-2} appear in (5).

Recasting of Houbolt in terms of accelerations and velocities, $a^n + v^n$...

From (1) and its derivatives, again assuming uniform time steps,

$$v^n = \frac{1}{\Delta t} \left(\frac{1}{3} u^{n+1} + \frac{1}{2} u^n - u^{n-1} + \frac{1}{6} u^{n-2} \right)$$

and
$$a^n = \frac{1}{\Delta t^2} (u^{n+1} - 2u^n + u^{n-1})$$

Rearranging,

$$u^{n-1} = \Delta t^2 a^n - u^{n+1} + 2u^n$$

and so

$$u^{n-2} = 6\Delta t^2 a^n + 6\Delta t v^n - 8u^{n+1} + 9u^n$$

Thus (2) may be re-written as

$$v^{n+1} = \frac{1}{\Delta t} \left\{ 3u^{n+1} - 3u^n - 2\Delta t v^n - \frac{1}{2} \Delta t^2 a^n \right\} \quad (6)$$

and

$$a^{n+1} = \frac{1}{\Delta t^2} \left\{ 6u^{n+1} - 6u^n - 6\Delta t v^n - 2\Delta t^2 a^n \right\}$$

Substituting in the equation of motion (3) gives

$$\begin{aligned} \left(\frac{6}{\Delta t^2} M + \frac{3}{\Delta t} c \right) u^{n+1} + I^{n+1} &= F^{n+1} + \frac{1}{\Delta t^2} M (6u^n + 6\Delta t v^n + 2\Delta t^2 a^n) \\ &+ \frac{1}{\Delta t} c (3u^n + 2\Delta t v^n + \frac{1}{2} \Delta t^2 a^n) \end{aligned}$$

So that approximating

$$I^{n+1} = I^n + K\Delta u,$$

We have

$$\begin{aligned}
\left(\frac{6}{\Delta t^2} M + \frac{3}{\Delta t} C + K\right) \Delta u &= F^{n+1} - I^n \\
&+ \frac{1}{\Delta t} M (6 v^n + 2\Delta t a^n) \\
&+ C (2 v^n + \frac{1}{2} \Delta t a^n)
\end{aligned}
\tag{7}$$

Note that with this technique, no special starting procedure (other than computing the accelerations at $t = 0$ from the total equations of motion) is necessary.

Equation (7) may be solved for the Δu , hence $u^{n+1} = u^n + \Delta u$ and equations (6) complete the step to time $(n+1)$. Note that uniformity of time step was assumed throughout the derivation.

Equation (7) contains residual load correction implicitly. To remove this, we assume

$$F^n = I^n + C^n v^n + Ma^n$$

So that (7) becomes

$$\begin{aligned}
\left(\frac{6}{\Delta t^2} M + \frac{3}{\Delta t} C + K\right) \Delta u &= \Delta F + \frac{1}{\Delta t} M (6v^n + 3\Delta t a^n) \\
&+ c (3v^n + \frac{1}{2} \Delta t a^n)
\end{aligned}
\tag{8}$$

DAMPING

With the assumption

$$C = \alpha M + \beta K \quad (\alpha, \beta \text{ scalars})$$

$$\begin{aligned}
 & \left[\left(\frac{6}{\Delta t^2} + \frac{3\beta}{\Delta t} \right) + \left(\frac{3\beta}{\Delta t} + 1 \right) K \right] \Delta u = F^{n+1} - Y^n \\
 & + M \left[\left(\frac{6}{\Delta t} + 2\alpha \right) v^n + \left(2 + \frac{\Delta t}{2} \alpha \right) a^n \right] \\
 & + \beta K \left[2v^n + \frac{1}{2} \Delta t a^n \right]
 \end{aligned}
 \tag{7a}$$

With residual load correction,

and

$$\begin{aligned}
 & \left[\left(\frac{6}{\Delta t^2} + \frac{3\alpha}{\Delta t} \right) M + \left(\frac{3\beta}{\Delta t} + 1 \right) K \right] \Delta u = \Delta F \\
 & + M \left[\left(\frac{6}{\Delta t} + 3\alpha \right) v^n + \left(3 + \frac{\Delta t}{2} \alpha \right) a^n \right] \\
 & + \beta K \left(3v^n + \frac{1}{2} \Delta t a^n \right)
 \end{aligned}$$

TERCER CURSO INTERNACIONAL DE INGENIERIA SISMICA
CENTRO DE EDUCACION CONTINUA
DIVISION DE ESTUDIOS SUPERIORES,
FACULTAD DE INGENIERIA, UNAM, MEXICO

TEMA : PROSPECCION SISMICA
FECHA: 28 DE JULIO DE 1977
M. EN I. BELZAY MARTINEZ R.
INSTITUTO DE INGENIERIA, UNAM

BIBLIOGRAFIA

A) TEORIA SOBRE ONDAS ELASTICAS Y METODOS SISMICOS

1. Heiland, C.A., Geophysical Exploration, Hafner Publishing, Co. (1963)
2. Jakosky, J.J., Exploration Geophysics, Trija Publishing Co. (1961)
3. Dobrin, M.B., Introduction to Geophysical Prospecting, International Student Edition. (1960)
4. Griffiths, D.H., King, R.F., Applied Geophysics for Engineers and Geologists, Pergamon Press Ltd (1972)
5. Gurvich, I., Seismic Prospecting, MIR Publishing, Moscow (1972)
6. Hvorslev, M.J., Subsurface Exploration and Sampling of Soils for Civil Engineering Purposes, ASCE. (1965)
7. Fung, Y.C., A First Course in Continuum Mechanics, Prentice-Hall Inc (1969)
8. Richart, F.E., Hall, J.R.Jr. and Woods, R.D., Vibration of Soils and Foundations, Prentice-Hall Inc (1970)
9. Knopoff, L., On Rayleigh Wave Velocities, Bull. Seis. Soc. Amer., v 42, pp 307-308 (1952)
10. Ewing, W.M., W.S. Jardetzky. and F. Press, Elastic Waves in Layered Media, McGraw-Hill, (1957)
11. Kolsky, H., Stress Waves in Solids, Dover, New York, (1963)
12. White, J.E., Seismic Waves, McGraw-Hill, (1965)
13. Miller, G.F. and H. Pursey, On the Partition of Energy Between Elastic Waves in a Semi-infinite Solid, Proc. Royal Society, v 233, pp 55-69 (1955)

B) APLICACIONES DE LOS METODOS TRANSITORIOS

14. Jolly, R.N., Investigation of Shear Waves, Geophysics, v 21, no 4, pp 905-938 (oct 1956)
15. Ohta, Y. and Shima, E., Experimental Study on Generation and Propagation of S-waves: II. Preliminary Experiments on Generation of SV-waves, Bull. Earthq. Res. Inst., v 45, pp 33-42 (1967)

TERCER CURSO INTERNACIONAL DE INGENIERIA SISTEMICA
CENTRO DE INVESTIGACIONES Y ESTUDIOS AVANZADOS
FACULTAD DE INGENIERIA, UNAM, MEXICO

TEMA: PROPOSICION SISTEMICA
RECONSTRUCCION DE UN SISTEMA

BIBLIOGRAFIA

(A) FORMA PARA LA ECUACION Y LOS SISTEMAS

1. Forma para la Ecuacion y los Sistemas, (1981)

2. Forma para la Ecuacion y los Sistemas, (1981)

3. Forma para la Ecuacion y los Sistemas, (1981)

4. Forma para la Ecuacion y los Sistemas, (1981)

5. Forma para la Ecuacion y los Sistemas, (1981)

6. Forma para la Ecuacion y los Sistemas, (1981)

7. Forma para la Ecuacion y los Sistemas, (1981)

8. Forma para la Ecuacion y los Sistemas, (1981)

9. Forma para la Ecuacion y los Sistemas, (1981)

10. Forma para la Ecuacion y los Sistemas, (1981)

11. Forma para la Ecuacion y los Sistemas, (1981)

12. Forma para la Ecuacion y los Sistemas, (1981)

13. Forma para la Ecuacion y los Sistemas, (1981)

14. Forma para la Ecuacion y los Sistemas, (1981)

15. Forma para la Ecuacion y los Sistemas, (1981)

16. Forma para la Ecuacion y los Sistemas, (1981)

17. Forma para la Ecuacion y los Sistemas, (1981)

18. Forma para la Ecuacion y los Sistemas, (1981)

16. Shima, E. and Ohta, Y., Experimental Study on Generation and Propagation of S-waves: I. Designing of SH-wave Generator and Its Field Tests, Bull. Earthq. Res. Inst., v 45 pp 19-32 (1967)
17. S. Hattori, Investigation of Seismic Waves Generated by Small Explosions, Bull. Earthq. Res. Inst., v 9, pp 27-105 (1972)
18. White, J.E., S.N. Heaps and P.L. Lawrence, Seismic Waves from a Horizontal Source, Geophysics, v 21, pp 715-723 (1956)
19. Duke, M.C., Techniques for Field Measurement of Shear Wave Velocity in Soils, Proc. 4th. World Conf. on Earthq. Engng., Santiago, pp 39-54 (ene 1969)
20. White, J.E. and R.L. Sengbush, Shear Waves from Explosive Sources, Geophysics, v 28, pp 1001-1019 (dic 1963)
21. Martínez, B., Frontana de la Cruz, B., Shima, E., Rascón, O., Palencia, V.J., Prospección Sísmica en el area donde se Planea instalar una mesa vibradora, Bol. Soc. Mex. de Ing. Sísmica, Vol 9, pp 11-37 (1973)
22. Martínez, B., León, J.L., Rascón, O., Villarreal, A., Determinación de las propiedades dinámicas de la arcilla en el Vaso de Texcoco, Revista Ingeniería, Vol 44, No 2, pp 182-203 (abr-jun 1974)
23. Martínez, B., Villarreal, A., Rascón, O., Estudios de prospección sísmica en los sitios de las cimentaciones principales de la Planta Siderúrgica Lázaro Cárdenas-Las Truchas, informe del Instituto de Ingeniería, UNAM, a SICARTSA (abr 1974)
24. Martínez, B., Estudios de Prospección Sísmica en dos sitios de la Cuenca del Río Balsas, informe del Instituto de Ingeniería, UNAM, a la SRH (oct 1974)
25. Martínez, B., Estudio del subsuelo de Managua mediante prospección geosísmica, informe del Instituto de Ingeniería, UNAM, a SOP (oct 1975)
26. Figueroa, J., Determinación de las constantes de la arcilla del Valle de México por prospección sísmica, Boletín SMIS, Vol. II, No 2, pp 57-66 (sep 1964)
27. Manual for Dynametric Seismic Timer Model 117-C, DynaMetric Inc.(nov 1971)
28. White, J.E., Sengbush, R.L., Velocity Measurements in Near Surface Formations, Geophysics, Vol 18, pp 54-70 (1953)
29. Asano, S., Nozumu, D., Mikumo, T., Shima, E., and Usami, T., On the travel Times of S-Waves, Derived From Explosion Seismic Observations, Bull. of ERI, Vol 37, pp 279-306 (1959)
30. Shima, E., Modifications of Seismic Waves in Superficial Soil Layers as Verified by Comparative Observations on and beneath the Surface, Bull. of ERI, Vol 40, pp 187-259 (1962)
31. Shima, E., Yanagisawa, M. and Allam, A., Experimental Study on Generation and Propagation of S-wave Prospecting by Means of Well Shooting, Bull. of ERI, Vol 46, pp 517-528 (1968)

16. Shimizu, E. and Chiba, Y. Experimental Study on Generation and Propagation of 2-Wave Gravity Waves and Its Field Velocity in the Troposphere. J. Geophys. Res., Vol. 72, pp. 18-22 (1967).

17. Shimizu, E. and Chiba, Y. Experimental Study on Generation and Propagation of 2-Wave Gravity Waves and Its Field Velocity in the Troposphere. J. Geophys. Res., Vol. 72, pp. 18-22 (1967).

18. Shimizu, E. and Chiba, Y. Experimental Study on Generation and Propagation of 2-Wave Gravity Waves and Its Field Velocity in the Troposphere. J. Geophys. Res., Vol. 72, pp. 18-22 (1967).

19. Duke, M.C. Laboratory Field Measurement of Gravity Wave Velocity in the Troposphere. J. Geophys. Res., Vol. 72, pp. 39-54 (1967).

20. Shimizu, E. and Chiba, Y. Experimental Study on Generation and Propagation of 2-Wave Gravity Waves and Its Field Velocity in the Troposphere. J. Geophys. Res., Vol. 72, pp. 18-22 (1967).

21. Shimizu, E. and Chiba, Y. Experimental Study on Generation and Propagation of 2-Wave Gravity Waves and Its Field Velocity in the Troposphere. J. Geophys. Res., Vol. 72, pp. 18-22 (1967).

22. Shimizu, E. and Chiba, Y. Experimental Study on Generation and Propagation of 2-Wave Gravity Waves and Its Field Velocity in the Troposphere. J. Geophys. Res., Vol. 72, pp. 18-22 (1967).

23. Shimizu, E. and Chiba, Y. Experimental Study on Generation and Propagation of 2-Wave Gravity Waves and Its Field Velocity in the Troposphere. J. Geophys. Res., Vol. 72, pp. 18-22 (1967).

24. Shimizu, E. and Chiba, Y. Experimental Study on Generation and Propagation of 2-Wave Gravity Waves and Its Field Velocity in the Troposphere. J. Geophys. Res., Vol. 72, pp. 18-22 (1967).

25. Shimizu, E. and Chiba, Y. Experimental Study on Generation and Propagation of 2-Wave Gravity Waves and Its Field Velocity in the Troposphere. J. Geophys. Res., Vol. 72, pp. 18-22 (1967).

26. Shimizu, E. and Chiba, Y. Experimental Study on Generation and Propagation of 2-Wave Gravity Waves and Its Field Velocity in the Troposphere. J. Geophys. Res., Vol. 72, pp. 18-22 (1967).

27. Shimizu, E. and Chiba, Y. Experimental Study on Generation and Propagation of 2-Wave Gravity Waves and Its Field Velocity in the Troposphere. J. Geophys. Res., Vol. 72, pp. 18-22 (1967).

28. Shimizu, E. and Chiba, Y. Experimental Study on Generation and Propagation of 2-Wave Gravity Waves and Its Field Velocity in the Troposphere. J. Geophys. Res., Vol. 72, pp. 18-22 (1967).

29. Shimizu, E. and Chiba, Y. Experimental Study on Generation and Propagation of 2-Wave Gravity Waves and Its Field Velocity in the Troposphere. J. Geophys. Res., Vol. 72, pp. 18-22 (1967).

30. Shimizu, E. and Chiba, Y. Experimental Study on Generation and Propagation of 2-Wave Gravity Waves and Its Field Velocity in the Troposphere. J. Geophys. Res., Vol. 72, pp. 18-22 (1967).

C) APLICACIONES DE LOS METODOS ESTACIONARIOS

32. Arnold, R.N., Bycroft y G.B. Warburton, Forced Vibration of a Body on an Infinite Elastic Solid, Jour. Appl. Mech., v 77, no 3, pp 391-400 (sept 1955)
33. Barkan, D.D., Dynamics of Bases and Foundations, McGraw-Hill, (1962)
34. Cherry, J.T. y K.H. Waters, Shear-Wave Recording Using Continuous Signal Methods, Part I - Early Development, Geophysics, v 33, no 2, pp 229-239 (abr 1968)
35. Jones, R., In Situ Measurements of the Dynamic Properties of Soil by Vibration Methods, Geotechnique, v VIII, no 1, pp 1-21 (mar 1958)
36. Kanai, K., An Explanation for the Ground Vibration Caused by Periodically Exerted Force, Bull. Earthq. Res. Inst., v 33, pp 283-286 (sep 1955)
37. Maxwell, A.A. y Z.B. Fry, A Procedure for Determining Elastic Moduli of In Situ by Dynamic Techniques, Symposium on Wave Propagation and Dynamic Properties of Earth Materials, Univ. of New Mexico, Albuquerque, N.M., (jun 1967)
38. Richart, F.E.Jr., y Whitman, R.V., Comparison of Footing Vibration Tests with Theory, Jour. Soil Mech. Fndns, Div. ASCE, v 93, no SM6, pp 143-168 (nov 1967)
39. Richart, F.E.Jr., Foundation Vibrations, Transactions ASCE, v 127, part I, pp 863-898 (1962)
40. Warburton, G.B., Forced Vibration of a Body upon an Elastic Stratum, Jour. Appl. Mech., v 24, pp 55-58 (1957)
41. Whitman, R.V. y Richart, F.E.Jr., Design Procedures For Dynamically Loaded Foundations, Jour. Soil Mech. Fndns. Div. ASCE, v 93, no SM6, pp 169-193 (nov 1967)

32. Arnold, R.W. & G. W. ... Journal of Applied Mechanics, v. 52, no. 2, pp. 291-295, 1985.

33. Barkan, D.P. ... Journal of Applied Mechanics, v. 52, no. 2, pp. 291-295, 1985.

34. ... Journal of Applied Mechanics, v. 52, no. 2, pp. 291-295, 1985.

35. Jones, R. ... Journal of Applied Mechanics, v. 52, no. 2, pp. 291-295, 1985.

36. Kanai, K. ... Journal of Applied Mechanics, v. 52, no. 2, pp. 291-295, 1985.

37. Maxwell, J.C. ... Journal of Applied Mechanics, v. 52, no. 2, pp. 291-295, 1985.

38. ... Journal of Applied Mechanics, v. 52, no. 2, pp. 291-295, 1985.

39. ... Journal of Applied Mechanics, v. 52, no. 2, pp. 291-295, 1985.

40. ... Journal of Applied Mechanics, v. 52, no. 2, pp. 291-295, 1985.

41. ... Journal of Applied Mechanics, v. 52, no. 2, pp. 291-295, 1985.